Asymptotic Analysis of Wave Propagation through Periodic Arrays and Layers

Department of Mathematical Sciences

Loughborough University

Asymptotic Analysis of Wave Propagation through Periodic Arrays and Layers

by

Shiyan Guo

A doctoral thesis
submitted in partial fulfillment of the requirements
for the award of the degree of
Doctor of Philosophy
of Loughborough University,
16th September 2011

Author Shiyan GUO

Programme Applied Mathematics

Supervisor Professor Phil MCIVER

Abstract

In this thesis, we use asymptotic methods to solve problems of wave propagation through infinite and finite (only consider those that are finite in one direction) arrays of scatterers. Both two- and three-dimensional arrays are considered. We always assume the scatterer size is much smaller than both the wavelength and array periodicity. Therefore a small parameter is involved and then the method of matched asymptotic expansions is applicable.

When the array is infinite, the elastic wave scattering in doubly-periodic arrays of cavity cylinders and acoustic wave scattering in triply-periodic arrays of arbitrary shape rigid scatterers are considered. In both cases, eigenvalue problems are obtained to give perturbed dispersion approximations explicitly. With the help of the computer-algebra package Mathematica, examples of explicit approximations to the dispersion relation for perturbed waves are given.

In the case of finite arrays, we consider the multiple resonant wave scattering problems for both acoustic and elastic waves. We use the methods of multiple scales and matched asymptotic expansions to obtain envelope equations for infinite arrays and then apply them to a strip of doubly or triply periodic arrays of scatterers. Numerical results are given to compare the transmission wave intensity for different shape scatterers for acoustic case. For elastic case, where the strip is an elastic medium with arrays of cavity cylinders bounded by acoustic media on both sides, we first give numerical results when there is one dilatational and one shear wave in the array and then compare the transmission coefficients when one dilatational wave is resonated in the array for normal incidence.

Key words: matched asymptotic expansions, multiple scales, acoustic scattering, elastic scattering, periodic structures, dispersion relation.

Acknowledgment

It is a pleasure to thank the many people who made this thesis possible.

First, I would like to express my deep and sincere gratitude to my supervisor, Professor Phil McIver for his continuous support of my PhD study and research, for his patience, motivation and immense knowledge. His guidance helped me in all the time of research and writing of this thesis. I could not have imagined having a better supervisor for my PhD study.

Besides, I would like to thank the other members in the Wave Group: Professor Chris Linton, Dr Maureen McIver, Dr Ian Thompson, Dr Victor Zalipaev and Dr Karima Khusnutdinova, for their encouragement and insightful comments. Further thanks to Ian for allowing me to use his Fortran code and helping me with other computing issues.

I am grateful to all the support staff in the Department for helping me in many different ways, in particular to Dr Keith Watling for assisting me in dealing with any issues related to computer and programming.

Last but not least, I would like to give my special gratitude to my beloved husband, Fajin Wei, and my parents and brothers for their extraordinary support and patience during this period.

Contents

Chapter 1

Introduction

The propagation of waves in periodic media has been a problem of increasing interest in recent years. These waves include acoustic, elastic, electromagnetic or water waves. The main interest is focused on the question of the existence or not of band gaps for these periodic media. Band gaps are those regions of frequency where plane waves cannot propagate through the array. A comprehensive bibliography about photonic and sonic band-gaps (analysis of filtering properties of composite structures in the theory of electromagnetic and acoustic scattering) can be found on a website compiled by Dowling [19]. The research on phononic band gaps (filtering properties for acoustic and elastic composites) has also attracted much interest. Various methods have been developed to investigate the band structures of waves propagation in phononic crystals, for example, the plane-wave method [84], the finite difference time domain method [23], the multiple scattering theory method [54, 35] and multipole expansion method [77, 105] etc. In these methods, the phononic band gaps are all obtained numerically. The method of homogenisation can approximate dispersion relation (the relation between frequency and wavenumber) explicitly [21], but only for low-frequencies. This method requires the wavelength to be much bigger than both the scatterer size and the array periodicity, which makes it impossible to assess the phenomenon related with the array periodicity, such as band gaps. In this thesis, we mainly use the perturbation method of matched asymptotic expansions to consider the wave (acoustic and elastic) propagation through periodic arrays under the assumption that the scatterer size is much smaller than both the wavelength and the array periodicity. One advantage of this method over the method of homogenisation is

that the array periodicity can be as large as the wavelength, therefore the phenomena associated with the periodicity of the array (such as band gaps) may be described. In particular, explicit expressions for the perturbed dispersion relation are given to show the appearance of the local band gaps for infinite arrays. This method can be used to solve those singular perturbation problems involving several different length scales and two subdomains on which no single asymptotic expansion in a series of gauge functions (functions of the small parameter) can hold uniformly over the whole space. Thus separate expansions must be developed in those two subdomains, where they must have a overlapping area in which the two expansions hold simultaneously. Then any indeterminacy in the expansions is solved by the matching. These two subdomains are usually named the inner region (near the scatterer) and the outer region (far from the scatterer), and the expansions in them are named the inner expansion and the outer expansion respectively. This method was developed in the 1950s and was then applied to a variety of problems in fluid mechanics in 1960s. Most of the earlier applications were to viscous flows. But since the 1960, applications of the method have proliferated in some other fields of fluid mechanics, as well as in other branches of applied mathematics, see [102, page 77] for more details.

Recently, this method was used to consider the problem of acoustic wave propagation through a doubly-periodic array of rigid cylinders by McIver [60]. Following this, we first apply the same method to the two-dimensional elastic wave scattering problem. The main difference between the acoustic case and elastic case is that in the former only dilatational waves are present, while in the latter, both dilatational and shear waves are involved. A notable feature of the modified matching procedure for the elastic case is that certain eigenfunctions must be included in the inner solution ahead of any obvious need for them. The method of matched asymptotic expansions is also used by Datta and his colleagues to solve the elastic wave scattering problem for both one scatterer [17] and composite materials containing multiple scatterers [16]. They also showed that feature about the eigenfunctions but didn't give the explicit form. Acoustic wave propagation through three-dimensional infinite arrays of arbitrary shape rigid scatterers are also considered in this thesis using the same method. For general shaped inclusions in acoustic problems (i.e. the Neumann or Dirichlet boundary conditions), this method could also work by

using conformal mappings in the inner problem as the leading order solution is harmonic and the boundary conditions will not change after the conformal mappings. For these infinite arrays, their periodicity requires that the solutions satisfy the Bloch theorem: the eigenfunctions of a system whose wavefunction of a particle is placed in a periodic potential (Bloch wave) can be written into the form of a plane wave times a function with the periodicity of the Bravais lattice. Bravais lattice is an infinite array of discrete points generated by a set of discrete translation operations for some primitive vectors. The method of matched asymptotic expansions we use here is based on the assumption that the material is isotropic. When the material is anisotropic the outer solutions will change their forms because they are on the assumption that every cell of the lattice is exactly the same. Therefore more complicated outer solutions need to be developed for the anisotropic materials.

With the help of the solutions in problems of infinite arrays, we then consider the multiple resonant scattering problems using the method of multiple scales. Multiple resonant scattering, or Bragg resonance, means intense peaks of scattered waves are produced for specific wavelength and/or incident angles. The method of multiple scales is also used to solve singular perturbation problems. The idea is to introduce a number of different scales, each one (measured in terms of the small parameter) associated with some property of the solution. This problem is motivated by the paper by Li and Mei [49], in which they considered the Bragg resonance of surface water waves by a two-dimensional array of vertical cylinders as a model for the support of an off-shore airport. Fast and slow variables are defined to describe fast and slow variation of the envelope (the outline of the variation in amplitude). The scattered wave from each scatterer is in higher order of the small parameter compared to the incident wave. But the cumulative effects of the scattered waves are no longer weak after scattering by a large number of cylinders, that is why the slow variations must be counted in. As Li and Mei [49] assumed the water depth is constant and the array is composed of vertical cylinders, this problem is actually equivalent to a two-dimensional acoustic problem with an array of rigid cylinders. Therefore we first reproduce their results for the corresponding acoustic case and then generalise it to arbitrary cross section cylinder arrays. A generalization to the elastic resonant scattering is also obtained in this thesis by the consideration of providing theoretical

support for the design of efficient soundproof materials. Further, the acoustic resonant scattering by a three-dimensional array of arbitrary shape scatterers is also considered. In all these problems about resonant scattering, the envelope equations are first derived in infinite arrays using Bloch theorem and they are then used to a strip of array with finite width in one direction (the array in other directions are infinite). The width of the strip is assumed to be large enough to make sure the resonance occurs.

The structure of this thesis is as follows. Chapter 2 is an introductory part to give the governing equations and boundary equations of the wave propagation in elastic medium. The corresponding equations in an acoustic medium can be obtained by setting the shear modulus of the elastic medium to be zero (as no shear stress exists in an acoustic medium).

The elastic wave propagation through doubly-periodic arrays of cavity cylinders is considered in chapter 3. As the exact solution of this problem has already been obtained by Poulton *et al.* [77] and Zalipaev *et al.* [105], we first give a brief introduction of their method and results and also make a correction about the quasi-static limit (the dispersion relation in low frequency as the wavenumber goes to zero) Zalipaev *et al.* [105] obtained. The problem is then solved by matched asymptotic expansions and an eigenvalue problem is obtained to give the perturbed dispersion relations and the size of the local band gaps explicitly. The results are then illustrated in diagrams to show the splits and interactions of multipoles caused by the presence of the scatterers. Comparisons of the results by these two methods are also given and it is shown our method is more accurate when the cylinder size is smaller.

Chapter 4 is about the two-dimensional resonant scattering. Li and Mei's result [49] is first reproduced by considering the corresponding acoustic problem and then generalised to arrays of arbitrary shape cross-section cylinders. The comparison among four different types of cylinders are given for the transmission wave intensity. The envelope equations are also used to solve the resonant scattering by a semi-infinite array. In this chapter, another generalization to the elastic wave resonant scattering is also achieved .

In chapter 5, we consider the acoustic wave propagation through triply-periodic arrays of arbitrary shape scatterers using matched asymptotic expansions. As in the two-dimensional case, eigenvalue problems are obtained to give the perturbed dispersion

relation and illustrate the appearance of the local band gaps. Comparisons for the perturbation of multipoles are made between two types of scatterers (sphere and prolate spheroid).

Chapter 6 is about the acoustic resonant scattering by a three-dimensional finite width strip (only finite in one direction) array of arbitrary shape scatterers, which is also a generalization of Li and Mei's method [49]. We also make comparisons of the transmission wave intensities among three different types scatterers (sphere, prolate spheroid and oblate spheroid).

A summary of this thesis and some future work are given in the last chapter 7.

Chapter 2

The equations of wave motion

In this chapter, we introduce the governing equations and boundary conditions for wave motions in elastic medium [9, chapter 5], where both of dilatational and shear waves exist simultaneously. The elastic medium can be characterised through two parameters, named Lamé constants, λ and μ, where μ is called the shear modulus. For wave propagation in acoustic media, as no shear stress exists the corresponding governing equations can be deduced by setting $\mu = 0$.

2.1 Wave equations

Given Cartesian coordinates x, y, z with origin O, the governing equation for wave motion in an elastic medium is

$$\rho \frac{\partial^2 \mathbf{u}}{\partial t^2} = (\lambda + \mu)\nabla(\nabla \cdot \mathbf{u}) + \mu \nabla^2 \mathbf{u}, \tag{2.1}$$

where $\mathbf{u} = (u_1, u_2, u_3)$ is the displacement, ρ is the mass density, λ and μ are the Lamé constants of the medium and ∇^2 is the Laplace operator. This equation (generally referred to as **Navier's equation**) can be written as

$$\rho \frac{\partial^2 \mathbf{u}}{\partial t^2} = (\lambda + 2\mu)\nabla(\nabla \cdot \mathbf{u}) - \mu \nabla \times (\nabla \times \mathbf{u}), \tag{2.2}$$

by using $\nabla^2 \mathbf{u} = \nabla(\nabla \cdot \mathbf{u}) - \nabla \times (\nabla \times \mathbf{u})$.

The divergence of (2.2) gives

$$\rho \frac{\partial^2}{\partial t^2}(\nabla \cdot \mathbf{u}) = (\lambda + 2\mu)\nabla^2(\nabla \cdot \mathbf{u}),$$

so the dilatation $D = \nabla \cdot \mathbf{u}$ satisfies

$$\nabla^2 D = \frac{1}{c_1^2}\frac{\partial^2 D}{\partial t^2}, \quad c_1^2 = \frac{\lambda + 2\mu}{\rho}, \tag{2.3}$$

which shows that volume changes within the elastic body propagate as solutions of the three-dimensional wave equation with speed $c_1 = \sqrt{(\lambda + 2\mu)/\rho}$. These are known as **dilatational waves** (also called **primary waves** or **compressional waves**).

The curl of (2.2) gives

$$\rho\frac{\partial^2}{\partial t^2}(\nabla \times \mathbf{u}) = -\mu\nabla \times \{\nabla \times (\nabla \times \mathbf{u})\},$$

and we get

$$\nabla^2 \mathbf{r} = \frac{1}{c_2^2}\frac{\partial^2 \mathbf{r}}{\partial t^2}, \quad c_2^2 = \frac{\mu}{\rho}, \tag{2.4}$$

if we use the notation $\mathbf{r} = \frac{1}{2}\nabla \times \mathbf{u}$. The vector, $\mathbf{r}$, of infinitesimal rotations of the body therefore propagates as a solution of the three-dimensional vector wave equation with speed $\sqrt{\mu/\rho}$. These are known as **shear waves** (also called **secondary waves** or **rotational waves**).

By the Helmholtz representation, we can write $\mathbf{u} = \nabla\Phi + \nabla \times \mathbf{\Psi}$, where Φ is known as the Lamé scalar potential and $\mathbf{\Psi}$ as the Lamé vector potential, along with the constraint $\nabla \cdot \mathbf{\Psi} = 0$. Substituting for $\mathbf{u}$ in (2.2) we get two equations

$$\frac{\partial^2 \Phi}{\partial t^2} = c_1^2 \nabla^2 \Phi, \tag{2.5}$$

$$\frac{\partial^2 \mathbf{\Psi}}{\partial t^2} = c_2^2 \nabla^2 \mathbf{\Psi}. \tag{2.6}$$

General plane wave solutions of these two equations are

$$\Phi = f(\mathbf{k} \cdot \mathbf{x} - c_1 t), \tag{2.7}$$

and

$$\mathbf{\Psi} = \mathbf{A}g(\mathbf{k} \cdot \mathbf{x} - c_2 t), \tag{2.8}$$

where f and g are arbitrary scalar functions, $\mathbf{k}$ is the propagation vector and $\mathbf{A}$ is any constant vector normal to $\mathbf{k}$ (in order to satisfy the constraint $\nabla \cdot \mathbf{\Psi} = 0$). So the dilatational wave displacement $\mathbf{u}_c$ derived from the scalar potential of equation (2.7) is

$$\mathbf{u}_c = \nabla\Phi = \mathbf{k}f'(\mathbf{k} \cdot \mathbf{x} - c_1 t). \tag{2.9}$$

Because $\mathbf{A}$ is normal to the wave vector $\mathbf{k}$, we can choose $\mathbf{A}$ to be $\mathbf{A} = \mathbf{p} \times \mathbf{k}$, where $\mathbf{p}$ is the unit polarization vector. Then the shear wave particle displacement $\mathbf{u}_s$ is

$$\begin{aligned} \mathbf{u}_s &= \nabla \times \mathbf{\Psi} = \nabla \times (\mathbf{A}g) = \nabla g \times \mathbf{A} \\ &= (\mathbf{k}g') \times \mathbf{A} = (\mathbf{k}g') \times (\mathbf{p} \times \mathbf{k}) = (\mathbf{k} \cdot \mathbf{k})\mathbf{p}g'(\mathbf{k} \cdot \mathbf{x} - c_2 t). \end{aligned}$$

Suppose Φ and $\mathbf{\Psi}$ are time harmonic so that

$$\Phi(\mathbf{r}, t) = \phi(\mathbf{r})\mathrm{e}^{-\mathrm{i}\omega t}, \tag{2.10}$$

$$\mathbf{\Psi}(\mathbf{r}, t) = \boldsymbol{\psi}(\mathbf{r})\mathrm{e}^{-\mathrm{i}\omega t}. \tag{2.11}$$

Substituting these into the wave equations (2.5) and (2.6) and then simplifying, we obtain two Helmholtz equations

$$(\nabla^2 + k_1^2)\phi = 0, \tag{2.12}$$

$$(\nabla^2 + k_2^2)\boldsymbol{\psi} = 0, \tag{2.13}$$

where $k_i = \omega/c_i, i = 1, 2$ are the wavenumbers of the dilatational and shear wave, respectively. For time harmonic waves, we usually omit the time factor $\mathrm{e}^{-\mathrm{i}\omega t}$ in the following.

Since three functions are needed to describe the displacement vector field $\mathbf{u}$, only three of the four scalar solutions of the Helmholtz equations are independent. Specifically two components of the vector potential are needed to define the vector potential $\boldsymbol{\psi}$ uniquely. We decompose the shear displacement vector $\mathbf{u}_s$ into two orthogonal vectors: $\mathbf{u}_s = (\mathbf{u}_{s1}, \mathbf{u}_{s2})$ where $\mathbf{u}_{s1}$ lying in the plane parallel to the (x, y) plane, and the other $\mathbf{u}_{s2}$ in the plane perpendicular to the (x, y) plane. Both of them should satisfy the Helmholtz equations

$$\nabla^2 \mathbf{u}_{s(1,2)} + k_2^2 \mathbf{u}_{s(1,2)} = \nabla(\nabla \cdot \mathbf{u}_{s(1,2)}) - \nabla \times \nabla \times \mathbf{u}_{s(1,2)} + k_2^2 \mathbf{u}_{s(1,2)} = 0. \tag{2.14}$$

For a cylindrical coordinate system (r, θ, z) we can write [30]

$$\mathbf{u}_{s1} = \nabla \times (\psi_{s1}\mathbf{e}_z), \quad \mathbf{u}_{s2} = \nabla \times \nabla \times (\psi_{s2}\mathbf{e}_z)/k_2, \tag{2.15}$$

such that the two scalar potentials ψ_{s1} and ψ_{s2} satisfy the scalar Helmholtz wave equations

$$(\nabla^2 + k_2^2)\psi_{s1} = 0, \tag{2.16}$$

$$(\nabla^2 + k_2^2)\psi_{s2} = 0. \tag{2.17}$$

Then we can prove that $\mathbf{u}_{s1}$ and $\mathbf{u}_{s2}$ satisfy Helmholtz equations:

$$(\nabla^2 + k_2^2)\mathbf{u}_{s1} = 0,\ (\nabla^2 + k_2^2)\mathbf{u}_{s2} = 0. \tag{2.18}$$

First of all, we consider $\mathbf{u}_{s1}$:

$$\begin{aligned}
\nabla^2\mathbf{u}_{s1} &= \nabla(\nabla\cdot\mathbf{u}_{s1}) - \nabla\times(\nabla\times\mathbf{u}_{s1}) \\
&= -\nabla\times(\nabla\times\mathbf{u}_{s1}) \\
&= -\nabla\times\{\nabla\times[\nabla\times(\psi_{s1}\mathbf{e}_z)]\} \\
&= -\nabla\times[\nabla(\nabla\cdot\psi_{s1}\mathbf{e}_z) - \nabla^2(\psi_{s1}\mathbf{e}_z)] \\
&= -\nabla\times\left[\nabla\left(\frac{\partial\psi_{s1}}{\partial z}\right)\right] + \nabla\times[\nabla^2(\psi_{s1}\mathbf{e}_z)] \\
&= \nabla\times(-k_2^2\psi_{s1}\mathbf{e}_z) \\
&= -k_2^2\nabla\times(\psi_{s1}\mathbf{e}_z) \\
&= -k_2^2\mathbf{u}_{s1}.
\end{aligned} \tag{2.19}$$

So we have $\nabla^2\mathbf{u}_{s1} = -k_2^2\mathbf{u}_{s1}$, that is $(\nabla^2 + k_2^2)\mathbf{u}_{s1} = 0$, i. e. $\mathbf{u}_{s1}$ defined by (2.15) satisfies the Helmholtz equation.

Similarly for the second shear vector field $\mathbf{u}_{s2}$:

$$-\nabla^2\mathbf{u}_{s2} = \nabla\times\nabla\mathbf{u}_{s2}, \tag{2.20}$$

$$\begin{aligned}
\mathbf{u}_{s2} &= \frac{1}{k_2}\nabla\times\nabla\times(\psi_{s2}\mathbf{e}_z) \\
&= \frac{1}{k_2}\left[\nabla\left(\frac{\partial\psi_{s2}}{\partial z}\right) - \nabla^2(\psi_{s2}\mathbf{e}_z)\right] \\
&= \frac{1}{k_2}\left[\nabla\left(\frac{\partial\psi_{s2}}{\partial z}\right) + k_2^2(\psi_{s2}\mathbf{e}_z)\right].
\end{aligned} \tag{2.21}$$

Applying $\nabla\times\nabla\times$ to (2.21) and using (2.20) one has

$$-\nabla^2\mathbf{u}_{s2} = k_2^2\nabla\times\nabla\times(\psi_{s2}\mathbf{e}_z) = k_2^2\mathbf{u}_{s2}, \tag{2.22}$$

thus $\mathbf{u}_{s2}$ satisfies the Helmholtz equation as well.

Therefore the complete displacement vector field $\mathbf{u}$ can be found from three scalar potentials ϕ, ψ_{s1} and ψ_{s2}, each of which satisfies the scalar Helmholtz equations (2.12), (2.16) and (2.17) respectively.

2.2 Stress tensor

Stress is an important element when we deal with the elastic waves. So it is necessary to give some explanations about it.

Stress is the internal distribution of force per unit area in the body caused by the permanent deformation or external loads etc. It is a vector and is related to the position of the point and direction of the cross-section we considered. We can define the stress on a point M as follows [18, page 287]:

$$\boldsymbol{\sigma}_j = \lim_{\Delta S_j \to 0} \frac{\Delta \mathbf{F}}{\Delta S_j}, \tag{2.23}$$

where the $\Delta\mathbf{F}$ is the force acting on one of the cross sections, ΔS_j, of the point M. Its normal component which is perpendicular to ΔS_j is called **normal stress** and parallel components are called **shear stresses**. In the limit, when ΔS_j approaches zero, the stresses become those at the point M. All the stresses on a point are called the **stress state** on that point which can be described by the stresses on three cross sections perpendicular to each other. That is to say, the stress on any cross section of that point can be denoted by those three stresses (nine components altogether), which is called the **stress tensor**. Usually, we take those three perpendicular cross sections parallel to the coordinate planes and the nine components are $\sigma_{ij}, i, j = 1, 2, 3$, so the stress tensor $\boldsymbol{\sigma} = (\boldsymbol{\sigma}_1, \boldsymbol{\sigma}_2, \boldsymbol{\sigma}_3)^T$, see Figure 1. The equilibrium requires that the summation of moments with respect to an arbitrary point is zero, which leads to the conclusion that the stress tensor is symmetric, i.e. $\sigma_{ij} = \sigma_{ji}$ for all i and j. So only six of them are independent. The stress tensor can be written as

$$\boldsymbol{\sigma} = \begin{pmatrix} \sigma_{11} & \sigma_{12} & \sigma_{13} \\ \sigma_{21} & \sigma_{22} & \sigma_{23} \\ \sigma_{31} & \sigma_{32} & \sigma_{33} \end{pmatrix}.$$

By the generalised Hooke's law for isotropic materials we have

$$\sigma_{ij} = \lambda e_{kk} \delta_{ij} + 2\mu e_{ij}, \tag{2.24}$$

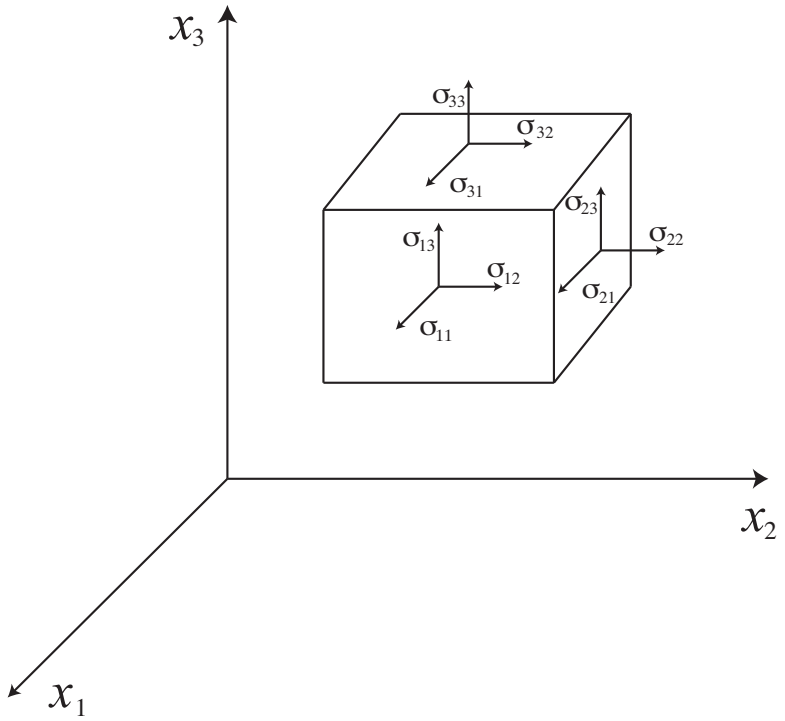

Figure 2.1: Stress tensor

where λ and μ are the Lamé constants, $e_{kk} = \nabla \cdot \mathbf{u} = \frac{\partial u_1}{\partial x_1} + \frac{\partial u_2}{\partial x_2} + \frac{\partial u_3}{\partial x_3} = D$ is the dilatation, ∇ is the gradient operator, $\mathbf{u}$ is a displacement vector, δ_{ij} is Kronecker delta function and $e_{ij} = \frac{1}{2}(u_{i,j} + u_{j,i})$ is the strain tensor.

2.3 Wave equations and stress tensor in cylindrical coordinates

The components of Navier's equation in cylindrical polar coordinates (r, θ, z) are [9, page 149]

$$\nabla^2 u_r - \frac{u_r}{r^2} - \frac{2}{r^2}\frac{\partial u_\theta}{\partial \theta} + \frac{1}{1-2\nu}\frac{\partial D}{\partial r} = \frac{1}{c_2^2}\frac{\partial^2 u_r}{\partial t^2}, \tag{2.25}$$

$$\nabla^2 u_\theta - \frac{u_\theta}{r^2} + \frac{2}{r^2}\frac{\partial u_r}{\partial \theta} + \frac{1}{1-2\nu}\frac{1}{r}\frac{\partial D}{\partial \theta} = \frac{1}{c_2^2}\frac{\partial^2 u_\theta}{\partial t^2}, \tag{2.26}$$

$$\nabla^2 u_z + \frac{1}{1-2\nu}\frac{\partial D}{\partial z} = \frac{1}{c_2^2}\frac{\partial^2 u_z}{\partial t^2}, \tag{2.27}$$

where ν is Poisson's ratio, the displacement $\mathbf{u} = u_r\mathbf{e}_r + u_\theta\mathbf{e}_\theta + u_z\mathbf{e}_z$, the Laplace operator is

$$\nabla^2 = \frac{\partial^2}{\partial r^2} + \frac{1}{r}\frac{\partial}{\partial r} + \frac{1}{r^2}\frac{\partial^2}{\partial \theta^2} + \frac{\partial^2}{\partial z^2}, \tag{2.28}$$

and the dilatation is

$$D = \frac{\partial u_r}{\partial r} + \frac{u_r}{r} + \frac{1}{r}\frac{\partial u_\theta}{\partial \theta} + \frac{\partial u_z}{\partial z}. \tag{2.29}$$

The components of the stress tensor that we shall use most frequently are [9, page 150]

$$\sigma_{rr} = \lambda D + 2\mu\frac{\partial u_r}{\partial r}, \tag{2.30}$$

$$\sigma_{r\theta} = \mu\left(\frac{1}{r}\frac{\partial u_r}{\partial \theta} - \frac{u_\theta}{r} + \frac{\partial u_\theta}{\partial r}\right), \tag{2.31}$$

$$\sigma_{\theta z} = \mu\left(\frac{\partial u_\theta}{\partial z} + \frac{1}{r}\frac{\partial u_z}{\partial \theta}\right), \tag{2.32}$$

$$\sigma_{rz} = \mu\left(\frac{\partial u_r}{\partial z} + \frac{\partial u_z}{\partial r}\right). \tag{2.33}$$

By the Helmholtz representation, we can write $\mathbf{u} = \nabla\phi + \nabla \times \boldsymbol{\psi}$. If we take $\boldsymbol{\psi} = \psi_r\mathbf{e}_r + \psi_\theta\mathbf{e}_\theta + \psi_z\mathbf{e}_z$ and suppress the time dependence then

$$\nabla \times \boldsymbol{\psi} = \left(\frac{1}{r}\frac{\partial \psi_z}{\partial \theta} - \frac{\partial \psi_\theta}{\partial z}\right)\mathbf{e}_r + \left(\frac{\partial \psi_r}{\partial z} - \frac{\partial \psi_z}{\partial r}\right)\mathbf{e}_\theta + \left(\frac{\psi_\theta}{r} + \frac{\partial \psi_\theta}{\partial r} - \frac{1}{r}\frac{\partial \psi_r}{\partial \theta}\right)\mathbf{e}_z, \tag{2.34}$$

and

$$\nabla\phi = \frac{\partial \phi}{\partial r}\mathbf{e}_r + \frac{1}{r}\frac{\partial \phi}{\partial \theta}\mathbf{e}_\theta + \frac{\partial \phi}{\partial z}\mathbf{e}_z, \tag{2.35}$$

so we have

$$u_r = \frac{\partial \phi}{\partial r} + \frac{1}{r}\frac{\partial \psi_z}{\partial \theta} - \frac{\partial \psi_\theta}{\partial z}, \tag{2.36}$$

$$u_\theta = \frac{1}{r}\frac{\partial \phi}{\partial \theta} + \frac{\partial \psi_r}{\partial z} - \frac{\partial \psi_z}{\partial r}, \tag{2.37}$$

$$u_z = \frac{\partial \phi}{\partial z} + \frac{\psi_\theta}{r} + \frac{\partial \psi_\theta}{\partial r} - \frac{1}{r}\frac{\partial \psi_r}{\partial \theta}. \tag{2.38}$$

Substituting for u_r, u_θ, u_z in (2.30) – (2.33) we get

$$\sigma_{rr} = \lambda \nabla^2 \phi + 2\mu \left(\frac{\partial^2 \phi}{\partial r^2} - \frac{1}{r^2}\frac{\partial \psi_z}{\partial \theta} + \frac{1}{r}\frac{\partial^2 \psi_z}{\partial r \partial \theta} - \frac{\partial^2 \psi_\theta}{\partial r \partial z} \right), \tag{2.39}$$

$$\begin{aligned} \sigma_{r\theta} = \mu \Bigg(& \frac{2}{r}\frac{\partial^2 \phi}{\partial r \partial \theta} - \frac{2}{r^2}\frac{\partial \phi}{\partial \theta} + \frac{\partial^2 \psi_r}{\partial z \partial r} - \frac{1}{r}\frac{\partial^2 \psi_\theta}{\partial \theta \partial z} - \frac{1}{r}\frac{\partial \psi_r}{\partial z} \\ & + \frac{1}{r^2}\frac{\partial^2 \psi_z}{\partial \theta^2} - \frac{\partial^2 \psi_z}{\partial r^2} + \frac{1}{r}\frac{\partial \psi_z}{\partial r} \Bigg), \end{aligned} \tag{2.40}$$

$$\sigma_{\theta z} = \mu \left(\frac{2}{r}\frac{\partial^2 \phi}{\partial \theta \partial z} + \frac{\partial^2 \psi_r}{\partial z^2} - \frac{1}{r}\frac{\partial^2 \psi_r}{\partial \theta^2} + \frac{1}{r}\frac{\partial \psi_\theta}{\partial \theta} + \frac{\partial^2 \psi_\theta}{\partial \theta \partial r} - \frac{\partial^2 \psi_z}{\partial r \partial z} \right), \tag{2.41}$$

$$\begin{aligned} \sigma_{rz} = \mu \Bigg(& 2\frac{\partial^2 \phi}{\partial r \partial z} + \frac{1}{r^2}\frac{\partial \psi_r}{\partial \theta} - \frac{1}{r}\frac{\partial^2 \psi_r}{\partial r \partial \theta} + \frac{\partial^2 \psi_\theta}{\partial r^2} + \frac{1}{r}\frac{\partial \psi_\theta}{\partial r} \\ & - \frac{\psi_\theta}{r^2} - \frac{\partial^2 \psi_\theta}{\partial z^2} + \frac{1}{r}\frac{\partial^2 \psi_z}{\partial z \partial \theta} \Bigg). \end{aligned} \tag{2.42}$$

2.4 The boundary conditions in scattering problems

In the elastic scattering problems, if we consider the scattering by a cavity scatterer, there is no stress acted on the boundary of the scatterer. Therefore they satisfy the stress free boundary conditions

$$\sigma_{rr} = 0, \quad \sigma_{r\theta} = 0, \quad \sigma_{rz} = 0. \tag{2.43}$$

When the scatterers are made from another different elastic material from the host material, the boundary conditions will become the continuity of the displacement and stresses.

When considering the acoustic scattering by rigid scatterers, as we assume the wave cannot propagate in the scatterer, i.e. the velocity has no normal component on the

scatterer, so the wave potential ϕ satisfies the Neumann boundary condition

$$\frac{\partial \phi}{\partial n} = 0, \tag{2.44}$$

where n is a coordinate measured normal to the scatterer.

Chapter 3

Two-dimensional elastic wave scattering by arrays

In this chapter, we consider the elastic wave scattering by circular cylindrical cavities in an elastic medium using the method of matched asymptotic expansions. To introduce the method and make preparations for the more complicated case of elastic wave propagation through an infinite array, we first consider scattering by one circular cylindrical cavity in an elastic medium. The theory for scattering of elastic waves by circular cylinders is given by White [101]. He considered the scattering of dilatational and shear waves incident obliquely on one infinitely long circular cylindrical obstacle in a solid medium. The cylindrical obstacles could be fluid-filled, a cavity or another different solid medium. He obtained boundary condition equations whose unknowns are coefficients in infinite series expressions for the scattered waves, then the scattered wave displacements and stresses are determined by these coefficients. Using White's theory Lewis and Kraft [46] considered normal incidence and gave explicit approximate expressions for the coefficients and the scattering cross sections (the scattered power per unit length divided by the incident intensity) valid for long waves. In another paper by Lewis *et al.* [47], numerical computations of the scattering cross sections are made for a cavity cylinder.

In the first section of this chapter, we consider the one cylinder case. Both the exact solutions and approximations by method of matched asymptotic expansions are given in order to validate the latter. The exact solutions are obtained using White's theory [101] and after expanding the coefficients for the leading terms we find the approximations

exactly agree with them. The applicability of matched asymptotic expansions involves a small parameter $\epsilon = k_1 a$, which requires that the radius a of the cylinder must be much smaller than the incident wavelength k_1^{-1}.

In the second section, we consider the wave propagation through a doubly-periodic array of cavity cylinders in an isotropic elastic medium. Accurate solution methods for this problem are provided by Poulton *et al.* [77] for square lattice, Zalipaev *et al.* [105] for hexagonal and rhombic lattices using the multipole expansions and Mei *et al.* [57] using the multiple scattering theory. Then the multipole expansions are used to consider the oblique wave incidence searching for the phononic band gaps [24] or both phononic and photonic band gaps [26] for cylindrical inclusion arrays. Guenneau & Movchan [25] considered the elliptical inclusions to explore the elastic band gaps by the finite element method. Low-frequency approximations to dispersion relation for circular inclusions are obtained directly from their multipole formulation by Zalipaev *et al.* [105], while other authors, for example Parnell & Abrahams [72, 73], Parnell & Grimal [74] and Andrianov *et al.* [5], have used asymptotic homogenisation to obtain low-frequency approximations to elastic wave propagation through periodic materials. Wide complete band gaps were founded for both photonic and phononic materials. For example, Nicorovici and McPhedran [67] used a generalized Rayleigh identity method to obtain the photonic band gaps for a square array of perfectly conducting cylinders in air. Vasseur *et al.* [103] used the same method and obtained very wide phononic band gaps for a square lattice of carbon cylinders in epoxy.

The method we use is the matched asymptotic expansions, which is based on the assumptions that the scatterer size is much smaller than both the wavelength and the array periodicity. This follows that of McIver [60] who investigates acoustic wave propagation through a lattice of rigid scatterers. The main difference between the acoustic case and elastic case is that in the former only dilatational waves are present, while in the later, both the dilatational and shear waves are involved which arises from the boundary conditions. A notable feature of the modified matching procedure for the elastic case is that certain eigenfunctions must be included in the inner solution ahead of any obvious need for them. The same method is used by Datta and his colleagues to solve the elastic wave scattering problem for both one scatterer [17] and composite materials containing finite

scatterers [16], but not for infinite arrays. Krynkin and McIver [39] also used matched asymptotic expansions to consider wave propagation through a lattice of arbitrary shape Dirichlet scatterers to obtain approximations to the dispersion relation.

The main idea of our method is to obtain perturbations of the quasi-periodic plane wave solutions that exist in the absence of the scatterers. Here there is no restriction on the wavelength relative to the array periodicity, and hence the method yields explicit approximations that can describe the phenomena associated with periodic media, such as band gaps. The disadvantage of the method of matched asymptotic expansions is that only small volume fractions can be considered. Explicit expressions to the perturbed dispersion relation (between the angular frequency and wavenumber) and explicit formulas are obtained for the size of local band gaps that show how they depend on the geometry of the lattice and the size of the cylinder. This is illustrated by reference to square and hexagonal lattices. Craster *et al.* [13] describe a multiple scales approach to obtain results valid outside the low-frequency regime and near the edges of the Brillouin zone (although they do not apply their method to elastic waves). In contrast to the present work, application of the method of Craster *et al.* [13] would require the numerical solution of a single-cell problem but, on the other hand, there would be no restriction on the size of an inclusion.

3.1 Scattering by one circular cylindrical cavity

3.1.1 Exact solution

We assume the cylinder is infinitely long and of radius a. Cartesian coordinates are chosen with origin O on the axis of the cylinder, and with the z axis directed along the axis of the cylinder. Polar coordinates in the x-y plane are denoted by (r, θ), then the cylinder surface is denoted by $r = a$. A time harmonic incident dilatational wave (see (2.10) in chapter 2 for the origin of ϕ) defined by

$$\phi^i = \mathrm{e}^{\mathrm{i}k_1 x} \tag{3.1}$$

propagates in the positive x-direction with constant velocity c_1 and angular frequency $\omega = k_1 c_1$, so the boundary condition only involves plane strain, i.e. $\sigma_{rz} = 0$. Here we assume the amplitude of the incident wave is one. For a stress free cavity the boundary

conditions are

$$\sigma_{rr} = \sigma_{r\theta} = 0, \qquad r = a. \tag{3.2}$$

As the incident wave impinge upon the cavity, a dilatational wave ϕ^s and a shear wave ψ^s is scattered from the boundary. In this case the vector potential $\boldsymbol{\psi} = \psi_s \mathbf{e}_z = (0, 0, \psi_s)$. Then the total wave potentials $\phi = \phi^i + \phi^s$ and $\psi = \psi^s$ satisfy the Helmholtz equations

$$(\nabla^2 + k_1^2)\phi = 0, \tag{3.3}$$

$$(\nabla^2 + k_2^2)\psi = 0, \tag{3.4}$$

and the stress free boundary conditions on the cylinder surface $r = a$ obtained from (2.39) and (2.40)

$$\left.\begin{aligned} \sigma_{rr} &= 2\mu\left(\frac{1}{r}\frac{\partial^2\psi}{\partial\theta\partial r} - \frac{1}{r^2}\frac{\partial\psi}{\partial\theta} - \frac{1}{r}\frac{\partial\phi}{\partial r} - \frac{1}{r^2}\frac{\partial^2\phi}{\partial\theta^2}\right) - k_1^2(\lambda + 2\mu)\phi = 0, \\ \sigma_{r\theta} &= -\frac{2}{r^2}\frac{\partial\phi}{\partial\theta} + \frac{2}{r}\frac{\partial^2\phi}{\partial\theta\partial r} + \frac{2}{r}\frac{\partial\psi}{\partial r} + \frac{2}{r^2}\frac{\partial^2\psi}{\partial\theta^2} + k_2^2\psi = 0, \end{aligned}\right\} \tag{3.5}$$

where the dilatational and shear wavenumbers are related by

$$k_2 = Pk_1, \quad P = \sqrt{\frac{\lambda + 2\mu}{\mu}}. \tag{3.6}$$

To ensure the scattered waves are outgoing, they must satisfy the radiation conditions so that

$$\phi^s \sim \frac{1}{\sqrt{k_1 r}} \mathrm{e}^{\mathrm{i}k_1 r} f_1(\theta), \ \psi^s \sim \frac{1}{\sqrt{k_2 r}} \mathrm{e}^{\mathrm{i}k_2 r} f_2(\theta) \quad \text{as } k_i r \to \infty. \tag{3.7}$$

The scattered potentials are in forms of the outgoing cylindrical wave functions [55, page 40]

$$\phi^s = \sum_{n=0}^{\infty} \left(A_n H_n^{(1)}(k_1 r)\cos n\theta + B_n H_n^{(1)}(k_1 r)\sin n\theta \right), \tag{3.8}$$

$$\psi^s = \sum_{n=0}^{\infty} \left(C_n H_n^{(1)}(k_2 r)\cos n\theta + D_n H_n^{(1)}(k_2 r)\sin n\theta \right), \tag{3.9}$$

where the Hankel function of the first kind $H_n^{(1)}(z) = J_n(z) + \mathrm{i}Y_n(z)$ (for simplicity we use H_n rather than $H_n^{(1)}$ in the following), $J_n(z)$ and $Y_n(z)$ are the first and second kind Bessel functions and A_n, B_n, C_n, D_n are unknowns that need to be determined by the boundary conditions.

First of all, we expand the incident wave in terms of the regular cylindrical wave functions as

$$\phi^i = \sum_{n=0}^{\infty} \epsilon_n \mathrm{i}^n J_n(k_1 r) \cos n\theta, \tag{3.10}$$

where

$$\epsilon_n = \begin{cases} 1, & n = 0, \\ 2, & n \geqslant 1. \end{cases}$$

Then the total wave fields are

$$\phi = \sum_{n=0}^{\infty} \left\{ \left[\epsilon_n \mathrm{i}^n J_n(k_1 r) + A_n H_n(k_1 r) \right] \cos n\theta + B_n H_n(k_1 r) \sin n\theta \right\}, \tag{3.11}$$

$$\psi = \sum_{n=0}^{\infty} \left(C_n \cos n\theta + D_n \sin n\theta \right) H_n(k_2 r). \tag{3.12}$$

Substituting for ϕ and ψ from (3.11) and (3.12) into (3.5) we get

$$\left.\begin{aligned} \sigma_{rr}|_{r=a} &= \frac{2\mu}{a^2} \sum_{n=0}^{\infty} \left\{ (a_{n1} A_n + d_{n1} D_n + e_{n1}) \cos n\theta + (b_{n1} B_n + c_{n1} C_n) \sin n\theta \right\} = 0, \\ \sigma_{r\theta}|_{r=a} &= \frac{1}{a^2} \sum_{n=0}^{\infty} \left\{ (a_{n2} A_n + d_{n2} D_n + e_{n2}) \sin n\theta + (b_{n2} B_n + c_{n2} C_n) \cos n\theta \right\} = 0, \end{aligned}\right\} \tag{3.13}$$

where

$$a_{n1} = b_{n1} = \left(n^2 - \frac{1}{2} P^2 k_1^2 a^2 \right) H_n(k_1 a) - k_1 a H_n'(k_1 a),$$

$$c_{n1} = -d_{n1} = n H_n(P k_1 a) - n P k_1 a H_n'(P k_1 a),$$

$$e_{n1} = \left(n^2 - \frac{1}{2} P^2 k_1^2 a^2 \right) \epsilon_n \mathrm{i}^n J_n(k_1 a) - k_1 a \epsilon_n \mathrm{i}^n J_n'(k_1 a),$$

$$a_{n2} = -b_{n2} = 2n H_n(k_1 a) - 2n k_1 a H_n'(k_1 a),$$

$$c_{n2} = d_{n2} = (P^2 k_1^2 a^2 - 2n^2) H_n(P k_1 a) + 2 P k_1 a H_n'(P k_1 a),$$

$$e_{n2} = 2n \epsilon_n \mathrm{i}^n (J_n(k_1 a) - k_1 a J_n'(k_1 a)).$$

Because of the orthogonality of $\cos n\theta$ and $\sin n\theta$ in $(0, 2\pi)$ for all n, the coefficients in each term of the series (3.13) must vanish. It then follows that

$$\left.\begin{aligned} a_{n1} A_n + d_{n1} D_n + e_{n1} &= 0, \\ a_{n2} A_n + d_{n2} D_n + e_{n2} &= 0, \end{aligned}\right\} \tag{3.14}$$

and

$$\left.\begin{aligned} b_{n1}B_n + c_{n1}C_n = 0, \\ b_{n2}B_n + c_{n2}C_n = 0. \end{aligned}\right\} \tag{3.15}$$

It is easy to see that only zero coefficients can satisfy (3.15) (because the determinant of the coefficient matrix is nonzero). The solutions of (3.14) are

$$A_n = \frac{\begin{vmatrix} -e_{n1} & d_{n1} \\ -e_{n2} & d_{n2} \end{vmatrix}}{\begin{vmatrix} a_{n1} & d_{n1} \\ a_{n2} & d_{n2} \end{vmatrix}} = \frac{-e_{n1}d_{n2} + e_{n2}d_{n1}}{a_{n1}d_{n2} - a_{n2}d_{n1}}, \tag{3.16}$$

$$D_n = \frac{\begin{vmatrix} a_{n1} & -e_{n1} \\ a_{n2} & -e_{n2} \end{vmatrix}}{\begin{vmatrix} a_{n1} & d_{n1} \\ a_{n2} & d_{n2} \end{vmatrix}} = \frac{-a_{n1}e_{n2} + a_{n2}e_{n1}}{a_{n1}d_{n2} - a_{n2}d_{n1}}. \tag{3.17}$$

Using Mathematica, we expand the coefficients A_n and D_n to the order of ϵ^2 and find the leading terms are the first three coefficients for both of dilatational and shear waves, specifically

$$A_0 = \frac{P^2 - 1}{4}\pi\mathrm{i}\epsilon^2 + O(\epsilon^4),$$

$$A_1 = \frac{\pi}{4}\epsilon^2 + O(\epsilon^3),$$

$$A_2 = \frac{\pi\mathrm{i}}{2 - 2P^2}\epsilon^2 + O(\epsilon^3),$$

$$D_0 = 0,$$

$$D_1 = \frac{\pi}{4}P\epsilon^2 + O(\epsilon^3),$$

$$D_2 = \frac{\pi\mathrm{i}}{2 - 2P^2}P^2\epsilon^2 + O(\epsilon^3).$$

The scattering of an anti-plane shear wave by a vertical cavity cylinder can be solved in a same way but more simply because when the incident wave is horizontally polarised (in x-y plane), only shear wave is scattered [71, page 113].

3.1.2 Solutions by matched asymptotic expansions

In this section, we obtain approximate solutions of the plane wave scattering by a cavity cylinder using the method of matched asymptotic expansions. This method is a very useful way to solve singular perturbation problems which involve a small parameter ϵ that is a ratio of lengths. In this problem we take $\epsilon = k_1 a$, where a and the wave length $2\pi/k_1$ will become disparate as $\epsilon \to 0$, so displaying the hallmark of a singular perturbation problem. Because there will be no single perturbation series valid both in the near field and in the far field, separate expansions must be developed to describe the near and far fields, and these must have an overlap to effect the matching. Then, any indeterminacy in the expansions will be resolved in the matching of the two expansions in the overlap domain in which they hold simultaneously.

When solving the problems with Neumann boundary condition by the method of matched asymptotic expansions [15, page 193], the leading order term in the inner solution can be easily obtained from the boundary condition, which is the order of the term related to the incident wave in the boundary condition when written in inner coordinates. But in the current problem, the leading order term in the inner solutions cannot be obtained in the same way. If doing so, the order ϵ^2 terms in inner solutions would not satisfy the boundary conditions if they are chosen to match with the outer solutions, and vice versa. This will be shown later.

We separate the whole region into two, the inner region around the cylinder $r \ll 1/k_1$ and the outer region far away from the cylinder $r \gg a$. In these two regions, dimensionless variables are needed to assess the smallness of various terms as $\epsilon \to 0$. The potentials are already dimensionless, and either a or k_1^{-1} can be used to normalize lengths. We define $\rho = r/a$ and $R = k_1 r$ as the inner and outer radial coordinates and rewrite the scattered potentials ϕ^s and ψ^s in inner and outer coordinates separately, which are denoted by $\phi(\rho, \theta, \epsilon)$, $\psi(\rho, \theta, \epsilon)$ and $\Phi(R, \theta, \epsilon)$, $\Psi(R, \theta, \epsilon)$. Our aim is to find the valid approximate solutions for the scattered wave ϕ^s and ψ^s in the whole domain $r > a$.

The scattered fields ϕ^s and ψ^s satisfy the Helmholtz equations

$$(\nabla^2 + k_1^2)\phi^s = 0, \tag{3.18}$$

$$(\nabla^2 + k_2^2)\psi^s = 0, \tag{3.19}$$

and the boundary conditions

$$\left.\begin{aligned} a\frac{\partial\phi^s}{\partial r}+a^2\frac{\partial^2\phi^s}{\partial r^2}+\frac{\partial^2\phi^s}{\partial\theta^2}+\frac{2\mu}{\lambda}\left(a^2\frac{\partial^2\phi^s}{\partial r^2}+a\frac{\partial^2\psi^s}{\partial\theta\partial r}-\frac{\partial\psi^s}{\partial\theta}\right)& \\ =\left(1+\frac{\mu}{\lambda}(1+\cos 2\theta)\right)k_1^2a^2\mathrm{e}^{\mathrm{i}k_1a\cos\theta},& \\ 2a\frac{\partial^2\phi^s}{\partial r\partial\theta}-2\frac{\partial\phi^s}{\partial\theta}+\frac{\partial^2\psi^s}{\partial\theta^2}-a^2\frac{\partial^2\psi^s}{\partial r^2}+a\frac{\partial\psi^s}{\partial r}=-\sin 2\theta k_1^2a^2\mathrm{e}^{\mathrm{i}k_1a\cos\theta},& \end{aligned}\right\} \tag{3.20}$$

on $r=a$, where the right side parts are from the incident wave and we can see their orders are ϵ^2. Because the scattered waves must be outgoing, they should also satisfy the radiation conditions

$$\phi^s\sim\frac{1}{\sqrt{k_1r}}\mathrm{e}^{\mathrm{i}k_1r}f_1(\theta),\ \psi^s\sim\frac{1}{\sqrt{k_2r}}\mathrm{e}^{\mathrm{i}k_2r}f_2(\theta)\quad\text{as } r\to\infty. \tag{3.21}$$

In terms of the outer coordinate $R=k_1r$, we have

$$(\nabla_R^2+1)\Phi=0, \tag{3.22}$$

$$(\nabla_R^2+P^2)\Psi=0,\ P=O(1), \tag{3.23}$$

$$\Phi\sim\frac{1}{\sqrt{R}}\mathrm{e}^{\mathrm{i}R}g_1(\theta),\ \Psi\sim\frac{1}{\sqrt{PR}}\mathrm{e}^{\mathrm{i}PR}g_2(\theta)\text{ as } r\to\infty, \tag{3.24}$$

and the boundary conditions on the cavity are not relevant to the outer region. In terms of the inner coordinate $\rho=r/a$, we define the Laplace operator

$$\nabla_\rho=\frac{\partial^2}{\partial\rho^2}+\frac{1}{\rho}\frac{\partial}{\partial\rho}+\frac{1}{\rho^2}\frac{\partial^2}{\partial\theta^2}$$

and then have

$$(\nabla_\rho^2+\epsilon^2)\phi=0, \tag{3.25}$$

$$(\nabla_\rho^2+P^2\epsilon^2)\psi=0, \tag{3.26}$$

and the boundary conditions

$$\left.\begin{aligned} \frac{\partial\phi}{\partial\rho}+\frac{\partial^2\phi}{\partial\rho^2}+\frac{\partial^2\phi}{\partial\theta^2}+\frac{2\mu}{\lambda}\left(\frac{\partial^2\phi}{\partial\rho^2}+\frac{\partial^2\psi}{\partial\rho\partial\theta}-\frac{\partial\psi}{\partial\theta}\right)& \\ =\epsilon^2\left[1+\frac{\mu}{\lambda}(1+\cos 2\theta)\right][1+\mathrm{i}\epsilon\cos\theta+O(\epsilon^2)],& \\ 2\frac{\partial^2\phi}{\partial\rho\partial\theta}-2\frac{\partial\phi}{\partial\theta}+\frac{\partial^2\psi}{\partial\theta^2}-\frac{\partial^2\psi}{\partial\rho^2}+\frac{\partial\psi}{\partial\rho}=-\epsilon^2\sin 2\theta[1+\mathrm{i}\epsilon\cos\theta+O(\epsilon^2)],& \end{aligned}\right\} \tag{3.27}$$

on $\rho = 1$; the radiation conditions are not relevant to the inner region.

In the inner region, the term inner eigensolution is used for any solutions of

$$\nabla_\rho^2 \phi = 0, \ \nabla_\rho^2 \psi = 0,$$

and the homogeneous boundary conditions

$$\left.\begin{aligned} &\frac{\partial \phi}{\partial \rho} + \frac{\partial^2 \phi}{\partial \rho^2} + \frac{\partial^2 \phi}{\partial \theta^2} + \frac{2\mu}{\lambda}\left(\frac{\partial^2 \phi}{\partial \rho^2} + \frac{\partial^2 \psi}{\partial \rho \partial \theta} - \frac{\partial \psi}{\partial \theta}\right) = 0, \\ &2\frac{\partial^2 \phi}{\partial \rho \partial \theta} - 2\frac{\partial \phi}{\partial \theta} + \frac{\partial^2 \psi}{\partial \theta^2} - \frac{\partial^2 \psi}{\partial \rho^2} + \frac{\partial \psi}{\partial \rho} = 0, \end{aligned}\right\} \tag{3.28}$$

on $\rho = 1$. Therefore the inner eigensolutions are (the barred terms refer to the dilatational wave and the hatted terms to the shear wave)

$$\left\{\begin{aligned} &\overline{E}_n(\rho,\theta) = \rho^n \cos n\theta, \\ &\widehat{E}_n(\rho,\theta) = -\rho^n \sin n\theta, \end{aligned}\right. \qquad n \in \mathbb{Z}, \quad n \neq 1,$$

$$\left\{\begin{aligned} &\overline{E}_1(\rho,\theta) = \rho\cos\theta, \\ &\widehat{E}_1(\rho,\theta) = 0, \end{aligned}\right. \qquad \left\{\begin{aligned} &\overline{E}_1(\rho,\theta) = 0, \\ &\widehat{E}_1(\rho,\theta) = \rho\sin\theta, \end{aligned}\right.$$

where $\overline{E}_n(\rho,\theta)$ is symmetric in θ, $\widehat{E}_n(\rho,\theta)$ is antisymmetric in θ and both of them are continuous functions of θ.

In the outer region $r \gg a$, the cylinder appears as a singularity at the origin, so that we seek solutions of the Helmholtz equation, satisfying the radiation condition, with singular behavior at $k_1 r = 0$. Such solutions are in terms of a sum of Hankel functions of the first kind and of integral orders:

$$\Phi^s = \sum_{n=0}^{\infty} a_n H_n^{(1)}(k_1 r)\cos n\theta, \quad \Psi^s = \sum_{n=0}^{\infty} b_n H_n^{(1)}(k_2 r)\sin n\theta,$$

the typical terms of which vary with r like $\mathrm{e}^{\mathrm{i}k_1 r}/\sqrt{k_1 r}$ or $\mathrm{e}^{\mathrm{i}k_2 r}/\sqrt{k_2 r}$ for large r and so satisfy the radiation conditions.

Following [14, page 177], we introduce the notations $\phi^{(m)}$ and $\psi^{(m)}$ for the asymptotic expansion of the inner solutions $\phi(\rho,\epsilon)$ and $\psi(\rho,\epsilon)$ up to and including all terms of order ϵ^m for fixed inner coordinate ρ; and we write $\phi^{(m,n)}$ and $\psi^{(m,n)}$ for the result of rewriting

$\phi^{(m)}$ and $\psi^{(m)}$ in terms of the outer coordinate R and expanding up to and including all terms of or order ϵ^n for fixed R. Similarly $\Phi^{(n)}$ and $\Psi^{(n)}$ will denote the asymptotic expansion of the outer solutions $\Phi(R,\epsilon)$ and $\Psi(R,\epsilon)$ up to and including all terms of order ϵ^n as $\epsilon \to 0$ for fixed outer coordinate R, and $\Phi^{(n,m)}$ and $\Psi^{(n,m)}$ will denote the result of expressing $\Phi^{(n)}$ and $\Psi^{(n)}$ in inner coordinates ρ, which is then held fixed as $\epsilon \to 0$ and expanding that expression through order ϵ^m. All logarithmic terms must be grouped with their algebraic multipliers in these expansions. For example, terms that are strictly order $\epsilon \log \epsilon$ and order ϵ are here both regarded as order ϵ.

With these notations, the matching rules are expressed as [14]

$$\phi^{(m,n)} \equiv \Phi^{(n,m)}, \ \psi^{(m,n)} \equiv \Psi^{(n,m)}, \tag{3.29}$$

and these identifications will be performed after transformation of one or other of these expressions back into the coordinates in which the other is written.

In the case of the Neumann boundary condition, the order of the inner solutions can be obtained directly by the boundary condition. But in the current problem, we can not get the order of the inner solution by the same way. Assume we can, then the boundary conditions (3.27) suggest that the inner solutions have the form

$$\phi = \epsilon^2 \phi_2 + \ldots, \quad \psi = \epsilon^2 \psi_2 + \ldots. \tag{3.30}$$

Substituting for ϕ and ψ in the inner problem (3.25) – (3.27) with (3.30) then equating like powers of ϵ we find ϕ_2 and ψ_2 satisfy Laplace equations and the boundary conditions

$$\left.\begin{aligned} &\frac{2}{P^2-2}\left(\frac{\partial^2\phi_2}{\partial\rho^2}+\frac{\partial^2\psi_2}{\partial\rho\partial\theta}-\frac{\partial\psi_2}{\partial\theta}\right)=1+\frac{1}{P^2-2}(1+\cos 2\theta),\\ &2\frac{\partial^2\phi_2}{\partial\rho\partial\theta}-2\frac{\partial\phi_2}{\partial\theta}+\frac{\partial^2\psi_2}{\partial\theta^2}-\frac{\partial^2\psi_2}{\partial\rho^2}+\frac{\partial\psi_2}{\partial\rho}=-\sin 2\theta. \end{aligned}\right\} \tag{3.31}$$

To match with the leading terms in the inner expansion of outer solutions, these inner solutions must decay as $r \to \infty$, and from the boundary conditions (3.27), whose first terms on right sides are in 2θ, we should take ϕ_2 and ψ_2 as

$$\phi_2 = a_2^{(2)} \frac{\cos 2\theta}{\rho^2}, \quad \psi_2 = b_2^{(2)} \frac{\sin 2\theta}{\rho^2}. \tag{3.32}$$

To satisfy the boundary conditions (3.27), substituting for ϕ_2 and ψ_2 in (3.31), we get

$$\left.\begin{aligned} &12(a_2^{(2)} - b_2^{(2)}) = 1\\ &12(a_2^{(2)} - b_2^{(2)}) = -1 \end{aligned}\right\}. \tag{3.33}$$

Obviously, this system has no solution. Therefore we cannot start the inner solutions with order ϵ^2. Similarly, if we started the inner solutions with order ϵ, the same problem would happen. The correct procedure is to start the inner solutions with strictly order one term, which include eigenfunctions in 2θ. These terms then generate further terms at order ϵ^2 in ϕ and ψ through particular solutions of the field equations (3.25)-(3.26). We take the inner expansions as

$$\phi = \phi_0 + \nu_{11}(\epsilon)\phi_{11} + \epsilon\phi_1 + \nu_{21}(\epsilon)\phi_{21} + \epsilon^2\phi_2 \ldots, \tag{3.34}$$

$$\psi = \psi_0 + \mu_{11}(\epsilon)\psi_{11} + \epsilon\psi_1 + \mu_{21}(\epsilon)\psi_{21} + \epsilon^2\psi_2 \ldots, \tag{3.35}$$

where the terms $\nu_{11}(\epsilon)$, $\nu_{21}(\epsilon)$, $\mu_{11}(\epsilon)$, $\mu_{21}(\epsilon)$ are possible intermediate terms that might arise. Substituting for (3.34) and (3.35) in (3.25) and (3.26) and collect the like terms in ϵ, we find ϕ_0 and ψ_0 satisfy Laplace equations and the homogeneous boundary conditions. ϕ_2 and ψ_2 satisfy Poisson equations whose inhomogeneous parts are obtained from ϕ_0 and ψ_0. With the help of the particular solutions of the Poisson equations the inhomogeneous boundary conditions (3.31) can be satisfied. From the boundary conditions (3.27), whose first terms on right sides having terms are in 2θ, we take

$$\phi_0 = a_2^{(0)}\frac{\cos 2\theta}{\rho^2}, \quad \psi_0 = a_2^{(0)}\frac{\sin 2\theta}{\rho^2}, \quad (n = -2), \tag{3.36}$$

which are eigenfunctions and must be singular by the need to match with the outer solutions. Here the 2θ terms in ϕ_0 and ψ_0 generate further terms at order ϵ^2 in ϕ and ψ through particular solutions of the field equations (3.25)-(3.26) to satisfy the boundary conditions. In general, in order to satisfy the boundary conditions at order ϵ^{n+2}, the inner solution at order ϵ^n must contain singular eigenfunctions up to and including those in $(n+2)\theta$. The outer expansions of the inner solutions are

$$\phi^{(0)}\left(\frac{R}{\epsilon}\right) = \phi_0\left(\frac{R}{\epsilon}\right) = a_2^{(0)}\frac{\cos 2\theta}{R^2}\epsilon^2 = \phi^{(0,2)},$$

$$\psi^{(0)}\left(\frac{R}{\epsilon}\right) = \psi_0\left(\frac{R}{\epsilon}\right) = a_2^{(0)}\frac{\sin 2\theta}{R^2}\epsilon^2 = \psi^{(0,2)},$$

which shows that the leading terms in the outer solutions must be in order ϵ^2, so that

$$\Phi = \epsilon^2\Phi_2 + \ldots, \quad \Psi = \epsilon^2\Psi_2 + \ldots.$$

Because the leading inner term is strictly order one, $\epsilon^2\Phi(\epsilon\rho)$ and $\epsilon^2\Psi(\epsilon\rho)$ cannot be larger than that (if more singular terms are included in the outer solutions and appropriate terms are added in inner solutions to effect matching, an unsolvable difficulty would arise later) and so

$$\Phi_2 = A_0^{(2)}H_0(R) + A_1^{(2)}H_1(R)\cos\theta + A_2^{(2)}H_2(R)\cos 2\theta,$$
$$\Psi_2 = B_0^{(2)}H_0(PR) + B_1^{(2)}H_1(PR)\sin\theta + B_2^{(2)}H_2(PR)\sin 2\theta,$$

and the inner expansions of the outer solutions are

$$\Phi^{(2)} = \epsilon^2\Phi_2(\epsilon\rho)$$
$$= \epsilon^2 A_0^{(2)}\frac{2\mathrm{i}}{\pi}\left(\log\epsilon\rho + \gamma_E - \log 2 - \frac{\pi\mathrm{i}}{2}\right) + \epsilon A_1^{(2)}\frac{2\cos\theta}{\pi\mathrm{i}\rho} + A_2^{(2)}\frac{4\cos 2\theta}{\pi\mathrm{i}\rho^2}, \tag{3.37}$$

$$\Psi^{(2)} = \epsilon^2\Psi_2(\epsilon\rho)$$
$$= \epsilon^2 B_0^{(2)}\frac{2\mathrm{i}}{\pi}\left(\log P\epsilon\rho + \gamma_E - \log 2 - \frac{\pi\mathrm{i}}{2}\right) + \epsilon B_1^{(2)}\frac{2\sin\theta}{\pi\mathrm{i}P\rho} + B_2^{(2)}\frac{4\sin 2\theta}{\pi\mathrm{i}P^2\rho^2}. \tag{3.38}$$

So

$$\Phi^{(2,0)} = A_2^{(2)}\frac{4\cos 2\theta}{\pi\mathrm{i}\rho^2}, \quad \Psi^{(2,0)} = B_2^{(2)}\frac{4\sin 2\theta}{\pi\mathrm{i}P^2\rho^2}, \tag{3.39}$$

$$\Phi^{(2,1)} = A_2^{(2)}\frac{4\cos 2\theta}{\pi\mathrm{i}\rho^2} + \epsilon A_1^{(2)}\frac{2\cos\theta}{\pi\mathrm{i}\rho}, \quad \Psi^{(2,1)} = B_2^{(2)}\frac{4\sin 2\theta}{\pi\mathrm{i}P^2\rho^2} + \epsilon B_1^{(2)}\frac{2\cos\theta}{\pi\mathrm{i}P\rho}. \tag{3.40}$$

Applying the matching rules

$$\phi^{(0,2)} \equiv \Phi^{(2,0)}, \quad \psi^{(0,2)} \equiv \Psi^{(2,0)},$$

give

$$A_2^{(2)} = \frac{\pi\mathrm{i}}{4}a_2^{(0)}, \quad B_2^{(2)} = \frac{\pi\mathrm{i}}{4}P^2 a_2^{(0)}. \tag{3.41}$$

The inner expansions of the outer solutions (3.37), (3.38) suggest that there are not any intermediate terms between the order one terms and order ϵ terms, so the inner solutions should be continued with order ϵ terms

$$\phi = \phi_0 + \epsilon\phi_1 + \ldots, \quad \psi = \psi_0 + \epsilon\psi_1 + \ldots. \tag{3.42}$$

Then similar to ϕ_0 and ψ_0, ϕ_1 and ψ_1 also satisfy Laplace equations and the homogeneous boundary conditions and so they are inner eigensolutions as well. To effect the matching

$$\phi_1 = a_1^{(1)}\frac{\cos\theta}{\rho} + a_3^{(1)}\frac{\cos 3\theta}{\rho^3}, \quad \psi_1 = a_1^{(1)}\frac{\sin\theta}{\rho} + a_3^{(1)}\frac{\sin 3\theta}{\rho^3}. \tag{3.43}$$

We put $\cos 3\theta$ and $\sin 3\theta$ here as the corresponding terms that will be needed when we search for particular solutions of Poisson equations later to satisfy the boundary conditions for order ϵ^3 terms of the inner solutions because of the reason we state before. In terms of the outer coordinates

$$\phi^{(1)} = \phi_0 + \epsilon\phi_1 = a_2^{(0)}\frac{\cos 2\theta}{R^2}\epsilon^2 + a_1^{(1)}\frac{\cos\theta}{R}\epsilon^2 + a_3^{(1)}\frac{\cos 3\theta}{R^3}\epsilon^4, \tag{3.44}$$

$$\psi^{(1)} = \psi_0 + \epsilon\psi_1 = a_2^{(0)}\frac{\sin 2\theta}{R^2}\epsilon^2 + a_1^{(1)}\frac{\sin\theta}{R}\epsilon^2 + a_3^{(1)}\frac{\sin 3\theta}{R^3}\epsilon^4, \tag{3.45}$$

which give

$$\phi^{(1,2)} = a_2^{(0)}\frac{\cos 2\theta}{R^2}\epsilon^2 + a_1^{(1)}\frac{\cos\theta}{R}\epsilon^2, \tag{3.46}$$

$$\psi^{(1,2)} = a_2^{(0)}\frac{\sin 2\theta}{R^2}\epsilon^2 + a_1^{(1)}\frac{\sin\theta}{R}\epsilon^2. \tag{3.47}$$

Applying the matching rule $\phi^{(1,2)} \equiv \Phi^{(2,1)},\ \psi^{(1,2)} \equiv \Psi^{(2,1)}$ we get

$$A_1^{(2)} = \frac{\pi\mathrm{i}}{2}a_1^{(1)}, \quad B_1^{(2)} = \frac{\pi\mathrm{i}}{2}Pa_1^{(1)}. \tag{3.48}$$

Again, from the inner expansions of the outer solutions (3.37) and (3.38), we find the next inner terms should be at $\epsilon^2\log\epsilon$ and ϵ^2, therefore we have

$$\phi^{(2)} = \phi_0 + \epsilon\phi_1 + \epsilon^2\log\epsilon\ \phi_{21} + \epsilon^2\phi_2, \tag{3.49}$$

$$\psi^{(2)} = \psi_0 + \epsilon\psi_1 + \epsilon^2\log\epsilon\ \psi_{21} + \epsilon^2\psi_2, \tag{3.50}$$

ϕ_{21} and ψ_{21} are inner eigensolutions and $\epsilon^2\phi_{21}(R/\epsilon)$ and $\epsilon^2\psi_{21}(R/\epsilon)$ can be no larger than $O(\epsilon^2)$, which is the order of the outer potential. There are many eigensolutions having these properties but they will not all match with the outer solutions. The only possibility is to take them be constants

$$\phi_{21} = a_0^{(21)}, \quad \psi_{21} = 0.$$

For ϕ_2 and ψ_2, after substituting (3.49) and (3.50) into the inner field equations (3.25) and (3.26) and collecting like terms in ϵ^2 we find ϕ_2 and ψ_2 satisfy the following Poisson equations

$$\nabla_\rho^2\phi_2 = -\phi_0 = -a_2^{(0)}\frac{\cos 2\theta}{\rho^2}, \tag{3.51}$$

$$\nabla_\rho^2\psi_2 = -P^2\psi_0 = -P^2a_2^0\frac{\sin 2\theta}{\rho^2}, \tag{3.52}$$

and the boundary conditions

$$\left.\begin{aligned}&\frac{\partial\phi_2}{\partial\rho}+\frac{\partial^2\phi_2}{\partial\rho^2}+\frac{\partial^2\phi_2}{\partial\theta^2}+\frac{2}{P^2-2}\left(\frac{\partial^2\phi_2}{\partial\rho^2}+\frac{\partial^2\psi_2}{\partial\rho\partial\theta}-\frac{\partial\psi_2}{\partial\theta}\right)=1+\frac{1}{P^2-2}(1+\cos 2\theta),\\&2\frac{\partial^2\phi_2}{\partial\rho\partial\theta}-2\frac{\partial\phi_2}{\partial\theta}+\frac{\partial^2\psi_2}{\partial\theta^2}-\frac{\partial^2\psi_2}{\partial\rho^2}+\frac{\partial\psi_2}{\partial\rho}=-\sin 2\theta.\end{aligned}\right\} \tag{3.53}$$

The solutions of (3.51), (3.52) and (3.53) needed to effect the matching are

$$\phi_2=\frac{a_2^{(0)}}{4}\cos 2\theta+B_2\frac{\cos 2\theta}{\rho^2}+C_2\log\rho+D_2+B_4\frac{\cos 4\theta}{\rho^4}, \tag{3.54}$$

$$\psi_2=\frac{a_2^{(0)}}{4}\sin 2\theta+E_2\frac{\sin 2\theta}{\rho^2}+E_4\frac{\sin 4\theta}{\rho^4}, \tag{3.55}$$

where the first two terms of involving $1/4$ are particular solutions of (3.51) and (3.52), the second eigensolution terms involving $1/\rho^2$ are introduced to satisfy the boundary conditions (3.53) and $\log\rho$ in ϕ_2 will be used when we do the matching later. The last two terms in 4θ are needed in the higher order matching. Substituting for ϕ_2 and ψ_2 by (3.54) and (3.55) in the boundary conditions (3.53), and because the boundary conditions holds for arbitrary θ, the coefficients of the trigonometric functions and other constants must be zero. Therefore we obtain

$$a_2^{(0)}=\frac{2}{1-P^2},\quad B_2-E_2=-\frac{1}{4},\quad C_2=\frac{1-P^2}{2}. \tag{3.56}$$

Then by the matching result we already obtained (3.41),

$$A_2^{(2)}=\frac{\pi\mathrm{i}}{4}a_2^{(0)}=\frac{\pi\mathrm{i}}{2-2P^2},\quad B_2^{(2)}=\frac{\pi\mathrm{i}}{4}P^2a_2^{(0)}=\frac{P^2\pi\mathrm{i}}{2-2P^2}. \tag{3.57}$$

The matching rules $\phi^{(2,2)}\equiv\Phi^{(2,2)}$ and $\psi^{(2,2)}\equiv\Psi^{(2,2)}$ give

$$\epsilon^2\frac{1-P^2}{2}\log R=\epsilon^2A_0^{(2)}\frac{2\mathrm{i}}{\pi}\log R, \tag{3.58}$$

$$0=\epsilon^2B_0^{(2)}\frac{2\mathrm{i}}{\pi}\log R, \tag{3.59}$$

and thus

$$A_0^{(2)}=\frac{P^2-1}{4}\pi\mathrm{i},\quad B_0^{(2)}=0. \tag{3.60}$$

In a similar way to ϕ_2 and ψ_2, ϕ_3 and ψ_3 satisfy the Poisson equations

$$\nabla_\rho^2 \phi_3 = -\phi_1 = -\left(a_1^{(1)} \frac{\cos\theta}{\rho} + a_3^{(1)} \frac{\cos 3\theta}{\rho^3} \right), \tag{3.61}$$

$$\nabla_\rho^2 \psi_3 = -P^2 \psi_1 = -P^2 \left(a_1^{(1)} \frac{\sin\theta}{\rho} + a_3^{(1)} \frac{\sin 3\theta}{\rho^3} \right), \tag{3.62}$$

and boundary conditions

$$\left.\begin{aligned} &\frac{\partial \phi_3}{\partial \rho} + \frac{\partial^2 \phi_3}{\partial \rho^2} + \frac{\partial^2 \phi_3}{\partial \theta^2} + \frac{2}{P^2-2}\left(\frac{\partial^2 \phi_3}{\partial \rho^2} + \frac{\partial^2 \psi_3}{\partial \rho \partial \theta} - \frac{\partial \psi_3}{\partial \theta} \right) \\ &\qquad = \mathrm{i}\left[\left(1 + \frac{3}{2(P^2-2)} \right) \cos\theta + \frac{1}{2(P^2-2)} \cos 3\theta \right], \\ &2\frac{\partial^2 \phi_3}{\partial \rho \partial \theta} - 2\frac{\partial \phi_3}{\partial \theta} + \frac{\partial^2 \psi_3}{\partial \theta^2} - \frac{\partial^2 \psi_3}{\partial \rho^2} + \frac{\partial \psi_3}{\partial \rho} = -\frac{\mathrm{i}}{2}(\sin\theta + \sin 3\theta). \end{aligned}\right\} \tag{3.63}$$

The solution forms needed to effect the matching are

$$\phi_3 = -\frac{1}{2} a_1^{(1)} \rho \log\rho \cos\theta + a_3^{(1)} \frac{\cos 3\theta}{8\rho} + B_3 \frac{\cos 3\theta}{\rho^3} + B_5 \frac{\cos 5\theta}{\rho^5}, \tag{3.64}$$

$$\psi_3 = -\frac{1}{2} P^2 a_1^{(1)} \rho \log\rho \sin\theta + P^2 a_3^{(1)} \frac{\sin 3\theta}{8\rho} + C_3 \frac{\sin 3\theta}{\rho^3} + E_5 \frac{\sin 5\theta}{\rho^5}, \tag{3.65}$$

where the first two terms involving $1/2$ and $1/\rho$ are particular solutions of (3.61) and (3.62), the terms involving ρ^3 are to make sure the boundary conditions be satisfied and the terms involving ρ^5 will be need in the higher order matching. The boundary conditions (3.63) give

$$a_1^{(1)} = -\frac{\mathrm{i}}{2}, \quad a_3^{(1)} = \frac{\mathrm{i}}{1-P^2}, \quad B_3 - C_3 = -\frac{\mathrm{i}}{12}, \tag{3.66}$$

where the last two relations will not be needed in the matching. By the obtained relations between the coefficients of the inner solutions and outer solutions (3.48),

$$A_1^{(2)} = \frac{\pi \mathrm{i}}{2} a_1^{(1)} = \frac{\pi}{4}, \quad B_1^{(2)} = P \frac{\pi \mathrm{i}}{2} a_1^{(1)} = \frac{\pi}{4} p. \tag{3.67}$$

So far we have got the first three coefficients of dilatational part and shear part

$$\begin{aligned} A_0^{(2)} &= \frac{P^2-1}{4}\pi \mathrm{i}, & B_0^{(2)} &= 0, \\ A_1^{(2)} &= \frac{\pi}{4}, & B_1^{(2)} &= \frac{\pi}{4} P, \\ A_2^{(2)} &= \frac{\pi \mathrm{i}}{2-2P^2}, & B_2^{(2)} &= \frac{\pi \mathrm{i}}{2-2P^2} P^2, \end{aligned}$$

which agree with what we get from the expansions of the exact solutions. Similarly, when we solve the shear wave scattering by cavity cylinder using matched asymptotic expansions, the results agree with those from the expansions of the exact solutions as well.

3.2 Wave propagation through doubly-periodic arrays

In this section, we consider the elastic wave propagation through doubly-periodic arrays of cavity cylinders. We first present the multiple expansion solutions obtained by Zalipaev *et al.* [105] and then give the perturbed dispersion relation diagrams produced by numerical calculations. The method of matched asymptotic expansions is then used to obtain approximations for small scatterers that are perturbations of the quasi-periodic plane wave solutions that exist in the absence of the scatterers. All solutions considered satisfy a Bloch condition that, for a specified value $\boldsymbol{\beta}_0$ of the Bloch wave vector $\boldsymbol{\beta}$, relates the solutions at corresponding points in different cells of the lattice. In the absence of the scatterers, and for the given Bloch wave vector $\boldsymbol{\beta}_0$, plane wave solutions are possible for discrete values $\omega_1, \omega_2, \ldots$ of the frequency ω. For each ω_i, there are $M \geq 1$ plane waves corresponding to a particular pair $(\boldsymbol{\beta}_0, \omega_i)$ – these solutions may be shear or dilatational waves, or a mixture of the two. With the scatterers present, the asymptotic analysis yields an algebraic system to determine ω for the M perturbed modes that exist for each $\boldsymbol{\beta}$ within a neighbourhood of $(\boldsymbol{\beta}_0, \omega_i)$ in the $(\boldsymbol{\beta}, \omega)$-space. Explicit expressions for the frequencies are readily obtained that show how the mode frequencies depend on $\boldsymbol{\beta}$, the geometry, and the Lamé constants for the medium. Results are given to illustrate the appearance of local band gaps, the splitting and crossing of double modes, and switching between dilatational and shear modes.

3.2.1 Solution by multipole expansions

The results in this section are obtained by Poulton *et al.* [77] and Zalipaev *et al.* [105] for square and oblique periodic structures respectively. We present it here to make comparisons with our method and we also correct a mistake about the quasi-static limit (the lowest dispersion in the limit of the wavenumber going to zero) in Zalipaev *et al.* [105].

The lattice Λ contains doubly-periodic cavity cylinders, each of which is infinitely long

and of radius a. Cartesian coordinates are chosen with origin O on the axis of one the cylinders, and with the z axis directed along the axis of that cylinder; polar coordinates in the x-y plane with origin at O are denoted by (r, θ). In the x-y plane, scatterer j is associated with a local origin O_j located at the lattice point

$$\mathbf{R_j} = n_1\mathbf{a}_1 + n_2\mathbf{a}_2, \quad n_1, n_2 \in \mathbb{Z}, \tag{3.68}$$

for given independent vectors $\mathbf{a}_1$ and $\mathbf{a}_2$. For a specified lattice, the reciprocal lattice is defined by

$$\mathbf{K}_m = 2\pi(m_1\mathbf{b}_1 + m_2\mathbf{b}_2), \quad m_1, m_2 \in \mathbb{Z}, \tag{3.69}$$

where

$$\mathbf{a}_i^T\mathbf{b}_j = \delta_{ij}, \quad i, j = 1, 2. \tag{3.70}$$

The reciprocal lattice vectors have the property that, for any lattice vector $\mathbf{R}_j$,

$$\mathbf{K}_m^T\mathbf{R}_j = 2\pi p, \quad p \in \mathbb{Z}. \tag{3.71}$$

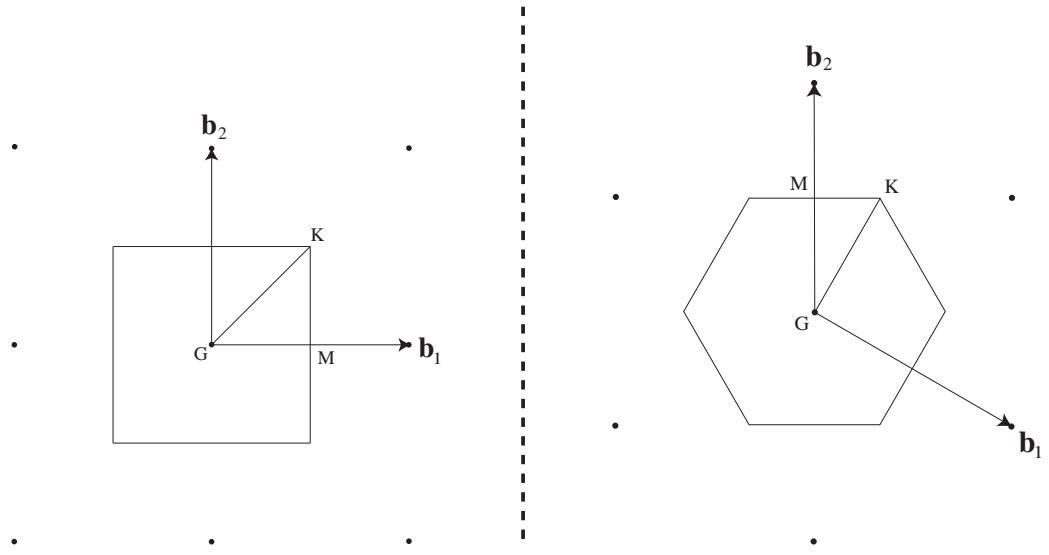

Figure 3.1: The reciprocal lattice for square lattice (left) and Hexagonal lattice (right).

The time-harmonic displacement of the medium outside the cavities is described by Navier's equation (2.2)

$$(\lambda + \mu)\nabla(\nabla \cdot \mathbf{u}) + \mu\nabla^2\mathbf{u} + \rho\omega^2\mathbf{u} = \mathbf{0}, \tag{3.72}$$

where $\mathbf{u}$ is the displacement vector, ω is the angular frequency, λ and μ are Lamé constants, and ρ is the density of the medium. Solutions of equation (3.72) are sought that satisfy the quasi-periodic 'Bloch condition'

$$\mathbf{u}(\mathbf{r}+\mathbf{R_j}) = \mathrm{e}^{\mathrm{i}\boldsymbol{\beta}\cdot\mathbf{R}_j}\mathbf{u}(\mathbf{r}), \tag{3.73}$$

where $\boldsymbol{\beta}$ is a prescribed wave vector, and traction-free boundary conditions (2.30), (2.31) and (2.33) applied on the surface of each scatterer; thus, on $r = a$,

$$\sigma_{rz} = \mu\frac{\partial u_z}{\partial r} = 0, \tag{3.74}$$

$$\sigma_{rr} = \lambda\left(\frac{\partial u_r}{\partial r} + \frac{u_r}{r} + \frac{1}{r}\frac{\partial u_\theta}{\partial \theta}\right) + 2\mu\frac{\partial u_r}{\partial r} = 0, \tag{3.75}$$

$$\sigma_{r\theta} = \mu\left(\frac{\partial u_\theta}{\partial r} - \frac{u_\theta}{r} + \frac{1}{r}\frac{\partial u_r}{\partial \theta}\right) = 0, \tag{3.76}$$

while equation (3.73) guarantees the boundary conditions are applied throughout the lattice.

By the Helmholtz representation,

$$\mathbf{u}(\mathbf{r}) = \nabla\phi + \nabla\times\boldsymbol{\psi}, \tag{3.77}$$

where we take $\boldsymbol{\psi} = \psi\mathbf{e}_z = (0,0,\psi)$, so that

$$u_r = \frac{\partial\phi}{\partial r} + \frac{1}{r}\frac{\partial\psi}{\partial\theta} \quad \text{and} \quad u_\theta = \frac{1}{r}\frac{\partial\phi}{\partial\theta} - \frac{\partial\psi}{\partial r}. \tag{3.78}$$

It follows that ϕ and ψ satisfy the two-dimensional Helmholtz equations

$$(\nabla^2 + k_1^2)\phi = 0 \quad \text{and} \quad (\nabla^2 + k_2^2)\psi = 0, \tag{3.79}$$

while the traction-free boundary conditions (3.75) and (3.76) on $r = a$ become

$$\sigma_{rr} = 2\mu\left(\frac{\partial^2\phi}{\partial r^2} + \frac{1}{a}\frac{\partial^2\psi}{\partial\theta\partial r} - \frac{1}{a^2}\frac{\partial\psi}{\partial\theta}\right) + \lambda\left(\frac{1}{a}\frac{\partial\phi}{\partial r} + \frac{\partial^2\phi}{\partial r^2} + \frac{1}{a^2}\frac{\partial^2\phi}{\partial\theta^2}\right) = 0, \tag{3.80}$$

$$\sigma_{r\theta} = \mu\left(\frac{2}{a}\frac{\partial^2\phi}{\partial\theta\partial r} - \frac{2}{a^2}\frac{\partial\phi}{\partial\theta} + \frac{1}{a}\frac{\partial\psi}{\partial r} + \frac{1}{a^2}\frac{\partial^2\psi}{\partial\theta^2} - \frac{\partial^2\psi}{\partial r^2}\right) = 0. \tag{3.81}$$

By the method of multipole expansion, the dilatational wave ϕ and shear wave ψ are expanded as

$$\phi(\mathbf{r}) = \sum_{l=-\infty}^{+\infty} \left[A_l^{(a)} J_l(k_1 r) + B_l^{(a)} Y_l(k_1 r) \right] \mathrm{e}^{\mathrm{i}l\theta}, \tag{3.82}$$

$$\psi(\mathbf{r}) = \sum_{l=-\infty}^{+\infty} \left[A_l^{(b)} J_l(k_2 r) + B_l^{(b)} Y_l(k_2 r) \right] \mathrm{e}^{\mathrm{i}l\theta}. \tag{3.83}$$

Here the dilatational and shear wavenumbers are denoted by $k_1 = \omega\sqrt{\rho(\lambda + 2\mu)}$ and $k_2 = \omega\sqrt{\rho/\mu}$ respectively. Application of the stress free boundary conditions (3.80) and (3.81) gives

$$\begin{pmatrix} A_l^{(a)} \\ A_l^{(b)} \end{pmatrix} = \begin{pmatrix} M_l^{(aa)} & M_l^{(ab)} \\ M_l^{(ba)} & M_l^{(bb)} \end{pmatrix} \begin{pmatrix} B_l^{(a)} \\ B_l^{(b)} \end{pmatrix}, \tag{3.84}$$

where

$$M_l^{(aa)} = -\frac{E_6 E_3 + E_2 E_7}{E_1 E_6 + E_2 E_5}, \tag{3.85}$$

$$M_l^{(ab)} = \mathrm{i}\frac{E_6 E_4 - E_2 E_8}{E_1 E_6 + E_2 E_5}, \tag{3.86}$$

$$M_l^{(bb)} = -\frac{E_5 E_4 + E_1 E_8}{E_1 E_6 + E_2 E_5}, \tag{3.87}$$

$$M_l^{(ba)} = -M_l^{(ba)}, \tag{3.88}$$

$$E_1 = \frac{2l\mu}{a}\left[k_1 J_l'(k_1 a) - \frac{1}{a}J_l(k_1 a)\right],$$

$$E_2 = \mu\left\{\left[k_2^2 - \frac{2l^2}{a^2}\right]J_l(k_2 a) + \frac{2k_2}{a}J_l'(k_2 a)\right\},$$

$$E_3 = \frac{2l\mu}{a}\left[k_1 Y_l'(k_1 a) - \frac{1}{a}Y_l(k_1 a)\right],$$

$$E_4 = \mu\left\{\left[k_2^2 - \frac{2l^2}{a^2}\right]Y_l(k_2 a) + \frac{2k_2}{a}Y_l'(k_2 a)\right\},$$

$$E_5 = \frac{2\mu}{a}\left[-k_1 J_l'(k_1 a) + \frac{l^2}{a}J_l(k_1 a)\right] - k_1^2(\lambda + 2\mu)J_l(k_1 a),$$

$$E_6 = \frac{2l\mu}{a}\left[k_2 J_l'(k_2 a) - \frac{1}{a}J_l(k_2 a)\right],$$

$$E_7 = \frac{2\mu}{a}\left[-k_1 Y_l'(k_1 a) + \frac{l^2}{a}Y_l(k_1 a)\right] - k_1^2(\lambda + 2\mu)Y_l(k_1 a),$$

$$E_8 = \frac{2l\mu}{a}\left[k_2 Y_l'(k_2 a) - \frac{1}{a}Y_l(k_2 a)\right].$$

Application of the generalised Rayleigh method [77] (apply the Green's theorem to the two-dimensional quasi-periodic Green's function and any function satisfying the Helmholtz equation then use Graf's addition theorem [1, page 363] to get the Rayleigh identities between the coefficients A_l^α and B_l^α, $\alpha = a, b$) leads to the infinite linear system

$$\left.\begin{aligned} M_l^{(aa)}B_l^{(a)} + M_l^{(ab)}B_l^{(b)} - \sum_{m=-\infty}^{\infty}(-1)^{l+m}S_{m-l}^Y(k_1,\boldsymbol{\beta})B_m^{(a)} = 0, \\ M_l^{(ba)}B_l^{(a)} + M_l^{(bb)}B_l^{(b)} - \sum_{m=-\infty}^{\infty}(-1)^{l+m}S_{m-l}^Y(k_2,\boldsymbol{\beta})B_m^{(b)} = 0, \end{aligned}\right\} \tag{3.89}$$

where the lattice sums

$$S_n^J(k,\boldsymbol{\beta}) = {\sum_{\mathbf{R}_j\in\Lambda}}' \mathrm{e}^{\mathrm{i}\boldsymbol{\beta}^T\cdot\mathbf{R}_j}J_n(kR_j)\mathrm{e}^{\mathrm{i}n\alpha_j},\ k = k_1,\ k_2,$$

$$S_n^Y(k,\boldsymbol{\beta}) = {\sum_{\mathbf{R}_j\in\Lambda}}' \mathrm{e}^{\mathrm{i}\boldsymbol{\beta}^T\cdot\mathbf{R}_j}Y_n(kR_j)\mathrm{e}^{\mathrm{i}n\alpha_j}.$$

Define

$$x_l = \sqrt{|M_l^{(aa)}|}\left(B_l^{(a)} + \frac{M_l^{(ab)}}{M_l^{(aa)}}B_l^{(b)}\right), \tag{3.90}$$

$$y_l = \sqrt{|M_l^{(bb)}|}\left(B_l^{(b)} + \frac{M_l^{(ba)}}{M_l^{(bb)}}B_l^{(a)}\right), \tag{3.91}$$

then after normalisation, the system (3.89) is changed into

$$\left.\begin{aligned} x_l + \sum_{m=-\infty}^{\infty}(D_{lm}^{(aa)}x_m + D_{lm}^{(ab)}y_m) = 0, \\ y_l + \sum_{m=-\infty}^{\infty}(D_{lm}^{(ba)}x_m + D_{lm}^{(bb)}y_m) = 0, \end{aligned}\right\} \tag{3.92}$$

where

$$D_{lm}^{(aa)} = -\frac{\mathrm{sgn}(M_l^{(aa)})}{\Delta_m}\left\{\left|\frac{M_m^{(bb)}}{M_l^{(aa)}}\right|^{1/2}\right\}(-1)^{l+m}S_{m-l}^{Y}(k_1,\boldsymbol{\beta}),$$

$$D_{lm}^{(ab)} = \frac{\mathrm{sgn}(M_l^{(aa)})\mathrm{sgn}M_m^{(aa)}M_m^{(ab)}}{\{|M_l^{aa}M_m^{(aa)}|^{1/2}\}\Delta_m}(-1)^{l+m}S_{m-l}^{Y}(k_1,\boldsymbol{\beta}),$$

$$D_{lm}^{(ba)} = \frac{\mathrm{sgn}(M_l^{(bb)})\mathrm{sgn}M_m^{(bb)}M_m^{(ab)}}{\{|M_l^{aa}M_m^{(aa)}|^{1/2}\}\Delta_m}(-1)^{l+m}S_{m-l}^{Y}(k_2,\boldsymbol{\beta}),$$

$$D_{lm}^{(bb)} = -\frac{\mathrm{sgn}(M_l^{(bb)})}{\Delta_m}\left\{\left|\frac{M_m^{(aa)}}{M_l^{(bb)}}\right|^{1/2}\right\}(-1)^{l+m}S_{m-l}^{Y}(k_2,\boldsymbol{\beta}),$$

$$\Delta_m = |M_m^{(aa)}M_m^{(bb)}|^{1/2}\left(1 - \frac{M_m^{(ab)}M_m^{(ba)}}{M_m^{(aa)}M_m^{(bb)}}\right). \tag{3.93}$$

The linear system (3.92) is of the form

$$(\boldsymbol{I} + \boldsymbol{D})\boldsymbol{x} = 0. \tag{3.94}$$

It is shown in Zalipaev *et al.* [105] that all the off-diagonal elements decay exponentially away from the main diagonal. Therefore the above system can be truncated and then the determinant of the truncated matrix can be evaluated to give the dispersion diagrams, which is the values for k_1 and k_2 for a given Bloch vector $\boldsymbol{\beta}$. Example diagrams are given as following. They are the dispersion relation diagrams for square lattice and hexagonal lattice just as those in [77] and [105]; the same physical constants $\lambda/\mu = 2.3$ are adopted,

so that $P^2 = (\lambda + 2\mu)/\mu = 4.3$ and the Poisson ratio $\nu = 0.35$. Dispersion relation diagrams are given when the Bloch vector $\boldsymbol{\beta}$ moves along the boundary of the irreducible region of the first Brillouin zone of the reciprocal lattice (labelled GMK in each part of figure 3.1) for square and hexagonal lattices. In these diagrams, the horizontal axis is the dimensionless modulus of the Bloch vector, while the vertical axis is the dimensionless shear wavenumber. A double precision Fortran code is used to solve the system (3.92) for square and hexagonal lattices. For all calculations we include all multipoles up to fifth order in the calculations so that the dimension for the truncated matrix (3.92) is 22 by 22. The perturbed dispersion diagrams are given for square lattice when the cylinder radius is $a/L = 0.1,\ 0.4$ and for hexagonal lattice when the cylinder radius is $a/L = 0.1,\ 0.333$. The diagrams are shown in figures 3.2 – 3.5, where we can see a whole band gap appears when the cylinder radius is $a/L = 0.4$ for square lattice, but for the hexagonal lattice, there is no whole band gap for the radii size we choose.

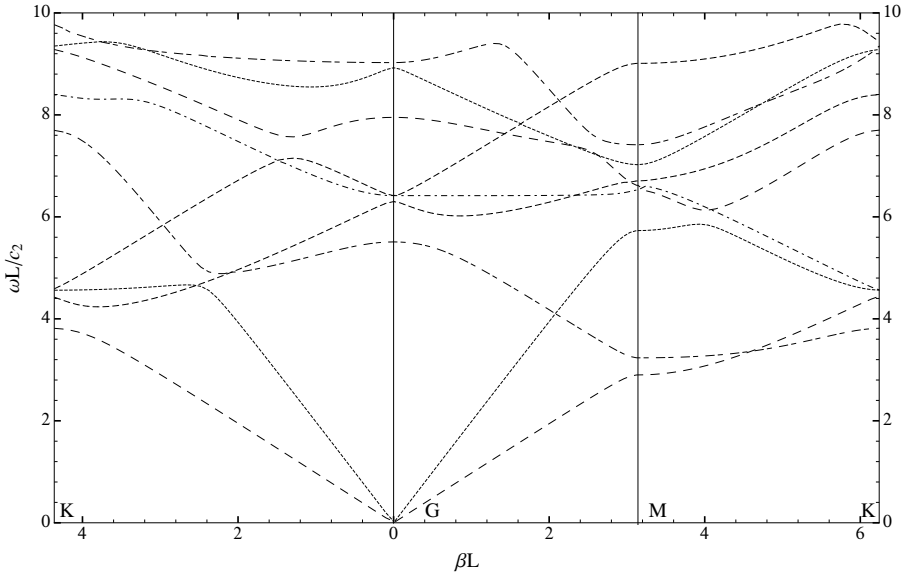

Figure 3.2: Dispersion diagram for square array of cylindrical cavity of radius $a/L = 0.1$.

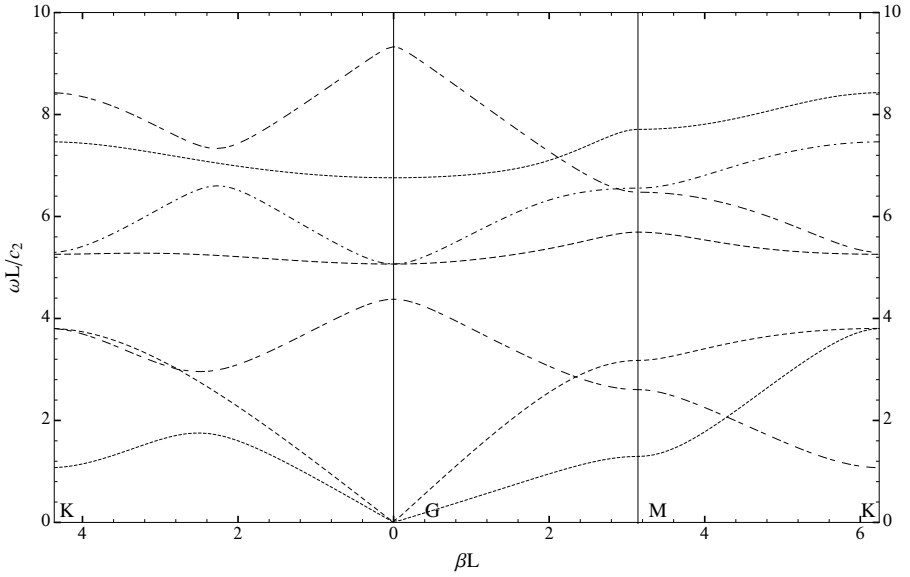

Figure 3.3: Dispersion diagram for square array of cylindrical cavity of radius $a/L = 0.4$.

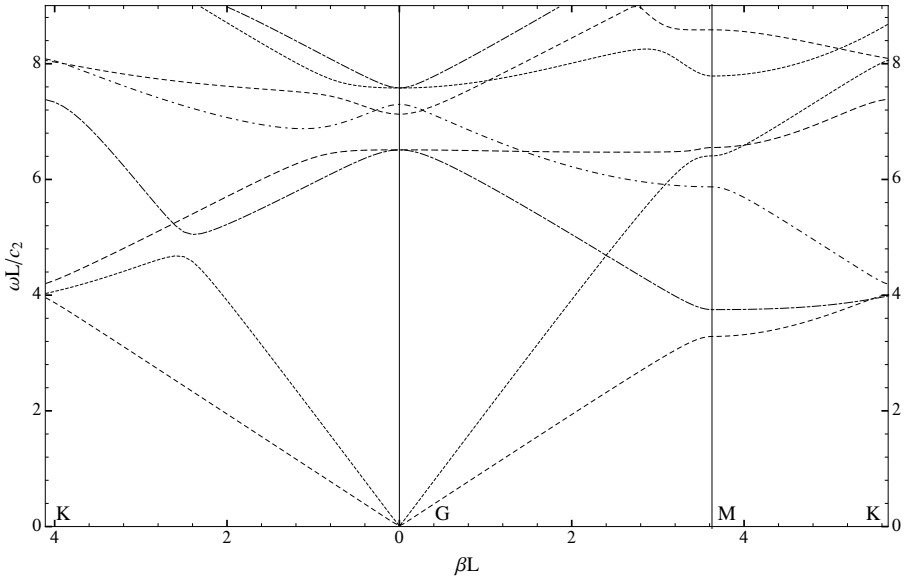

Figure 3.4: Dispersion diagram for hexagonal array of cylindrical cavity of radius $a/L = 0.1$.

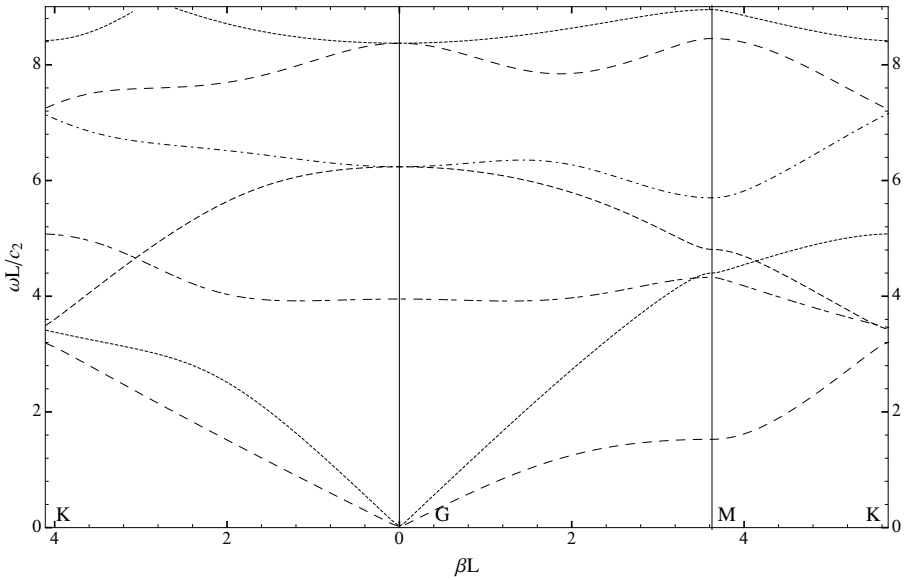

Figure 3.5: Dispersion diagram for hexagonal array of cylindrical cavity of radius $a/L = 0.333$.

From these diagrams, some modes cross each other, for example, the lowest two modes along MK for square array as shown in figure 3.2, and some modes are nearly parallel to each other, for example, the fifth and sixth mode (counted near point M) along MK for hexagonal array when the cavity radius is $a/L = 0.1$ as shown in figure 3.4. There are some more complicated mode interactions, for example, there are three modes in the neighbourhood of $(2, 5)$ along GK in figure 3.2. Why are the dispersion diagrams like this and how they are perturbed by the scatterers? How do the dilatational modes and shear modes interact with each other? In the next part, we use the matched asymptotic expansions to solve the same problem. By this method, the perturbed dispersion relations can be expressed explicitly and we will see how they are perturbed by the presence of the scatterers and how the modes interact with each other.

Zalipaev *et al.* also considered the quasi-static limit for the acoustic band (the lowest mode on the dispersion diagram), and obtained simple approximate formulae for the dispersion relation, which are

$$k_1^2 = \beta_1^2 \left[1 + \frac{\pi a^2}{\mathcal{A}} \frac{\lambda + \mu}{\mu} \right]^{-1}, \tag{3.95}$$

for the dilatational mode and

$$k_2^2 = \beta_1^2 \left[1 + \frac{\pi a^2}{\mathcal{A}} \frac{\lambda + 2\mu}{\lambda + \mu} \right]^{-1}, \tag{3.96}$$

for the shear mode. Here $\mathcal{A}$ is the area of one cell of the lattice. From these expressions, we can see the order of $k_{1,2}^2 - \beta^2$ in the small parameter $\epsilon = k_1 a$ is ϵ^2, but in their approximation procedure, they took $k_{1,2}^2 - \beta^2$ in the lattice sum be strictly order one, which is obviously not consistent with their results (3.95) and (3.96). To get the correct dispersion relation for the lowest mode, we first make an assumption that the order of $k_{1,2}^2 - \beta^2$ is ϵ^2 and then use this order in the lattice sums to obtain dispersion relations that are consistent with the initial assumption.

A quadrupole approximation (because the Rayleigh matrix has elements $D_{lm}^{\alpha\beta}$ that decay exponentially as $l, m \to \infty$, $\alpha,\ \beta = a, b$, [77] and the other terms other than up to quadrupole terms are all in higher order in ϵ) is used by Zalipaev *et al.* [105] to get the quasi-static limit (also for small fractions), that is to say, $-2 \leq l, m \leq 2$, and the Rayleigh matrix

$$\boldsymbol{R} = \begin{pmatrix} \boldsymbol{I} + \boldsymbol{D}^{(aa)} & \boldsymbol{D}^{(ab)} \\ \boldsymbol{D}^{(ba)} & \boldsymbol{I} + \boldsymbol{D}^{(bb)} \end{pmatrix} \tag{3.97}$$

is truncated into

$$\begin{pmatrix} \boldsymbol{A} & \boldsymbol{B} \\ \boldsymbol{C} & \boldsymbol{D} \end{pmatrix}. \tag{3.98}$$

For example the matrix $\boldsymbol{A}$ is

$$\begin{pmatrix}
1 + \frac{S_0^{Y,a}}{\Delta_2} \left| \frac{M_2^{(bb)}}{M_2^{(aa)}} \right|^{1/2} & -\frac{S_1^{Y,a}}{\Delta_1} \left| \frac{M_1^{(bb)}}{M_2^{(aa)}} \right|^{1/2} & \frac{S_2^{Y,a}}{\Delta_0} \left| \frac{M_0^{(bb)}}{M_2^{(aa)}} \right|^{1/2} & -\frac{S_3^{Y,a}}{\Delta_1} \left| \frac{M_1^{(bb)}}{M_2^{(aa)}} \right|^{1/2} & \frac{S_4^{Y,a}}{\Delta_2} \left| \frac{M_2^{(bb)}}{M_2^{(aa)}} \right|^{1/2} \\
-\frac{S_{-1}^{Y,a}}{\Delta_2} \left| \frac{M_2^{(bb)}}{M_1^{(aa)}} \right|^{1/2} & 1 + \frac{S_0^{Y,a}}{\Delta_1} \left| \frac{M_1^{(bb)}}{M_1^{(aa)}} \right|^{1/2} & -\frac{S_1^{Y,a}}{\Delta_0} \left| \frac{M_0^{(bb)}}{M_1^{(aa)}} \right|^{1/2} & \frac{S_2^{Y,a}}{\Delta_1} \left| \frac{M_1^{(bb)}}{M_1^{(aa)}} \right|^{1/2} & -\frac{S_3^{Y,a}}{\Delta_2} \left| \frac{M_2^{(bb)}}{M_1^{(aa)}} \right|^{1/2} \\
\frac{S_{-2}^{Y,a}}{\Delta_2} \left| \frac{M_2^{(bb)}}{M_0^{(aa)}} \right|^{1/2} & -\frac{S_{-1}^{Y,a}}{\Delta_1} \left| \frac{M_1^{(bb)}}{M_0^{(aa)}} \right|^{1/2} & 1 + \frac{S_0^{Y,a}}{\Delta_0} \left| \frac{M_0^{(bb)}}{M_0^{(aa)}} \right|^{1/2} & -\frac{S_1^{Y,a}}{\Delta_1} \left| \frac{M_1^{(bb)}}{M_0^{(aa)}} \right|^{1/2} & \frac{S_2^{Y,a}}{\Delta_2} \left| \frac{M_2^{(bb)}}{M_0^{(aa)}} \right|^{1/2} \\
-\frac{S_{-3}^{Y,a}}{\Delta_2} \left| \frac{M_2^{(bb)}}{M_1^{(aa)}} \right|^{1/2} & \frac{S_{-2}^{Y,a}}{\Delta_1} \left| \frac{M_1^{(bb)}}{M_1^{(aa)}} \right|^{1/2} & -\frac{S_{-1}^{Y,a}}{\Delta_0} \left| \frac{M_0^{(bb)}}{M_1^{(aa)}} \right|^{1/2} & 1 + \frac{S_0^{Y,a}}{\Delta_1} \left| \frac{M_1^{(bb)}}{M_1^{(aa)}} \right|^{1/2} & -\frac{S_1^{Y,a}}{\Delta_2} \left| \frac{M_2^{(bb)}}{M_1^{(aa)}} \right|^{1/2} \\
\frac{S_{-4}^{Y,a}}{\Delta_2} \left| \frac{M_2^{(bb)}}{M_2^{(aa)}} \right|^{1/2} & -\frac{S_{-3}^{Y,a}}{\Delta_1} \left| \frac{M_1^{(bb)}}{M_2^{(aa)}} \right|^{1/2} & \frac{S_{-2}^{Y,a}}{\Delta_0} \left| \frac{M_0^{(bb)}}{M_2^{(aa)}} \right|^{1/2} & -\frac{S_{-1}^{Y,a}}{\Delta_1} \left| \frac{M_1^{(bb)}}{M_2^{(aa)}} \right|^{1/2} & 1 + \frac{S_0^{Y,a}}{\Delta_2} \left| \frac{M_2^{(bb)}}{M_2^{(aa)}} \right|^{1/2}
\end{pmatrix}.$$

By the approximation of $M_m^{(\alpha\beta)}$ and Δ_m, $\alpha\beta = \{aa,\ ab,\ ba,\ bb\}$, in the limit as $\epsilon = k_1 a \to 0$, the orders of the elements in $\boldsymbol{A}$ as indicated by Zalipaev *et al.* [105] are

$$\begin{pmatrix} 1+\epsilon^2 & \epsilon^3 & \epsilon^4 & \epsilon^3 & \epsilon^2 \\ \epsilon & 1+\epsilon^2 & \epsilon^3 & \epsilon^2 & \epsilon \\ 1 & \epsilon & 1+\epsilon^2 & \epsilon & 1 \\ \epsilon & \epsilon^2 & \epsilon^3 & \epsilon^2 & \epsilon \\ \epsilon^2 & \epsilon^3 & \epsilon^4 & \epsilon^3 & 1+\epsilon^2 \end{pmatrix}. \tag{3.99}$$

Note that the lattice sums $S_l^{Y,a}$ are taken as strictly order one. By our assumption, the lattice sums are actually order $1/\epsilon^2$ (this can also be shown in the next part (3.132)), so that the orders of the terms in matrix $\mathbf{A}$ are actually

$$\begin{pmatrix} 1 & \epsilon & \epsilon^2 & \epsilon & 1 \\ 1/\epsilon & 1 & \epsilon & 1 & 1/\epsilon \\ 1/\epsilon^2 & 1/\epsilon & 1 & 1/\epsilon & 1/\epsilon^2 \\ 1/\epsilon & 1 & \epsilon & 1 & 1/\epsilon \\ 1 & \epsilon & \epsilon^2 & \epsilon & 1 \end{pmatrix}. \tag{3.100}$$

When calculating the determinant of the truncated $\boldsymbol{R}$, Zalipaev *et al.* consider the terms of order ϵ^3 and ϵ^4 in the third column of (3.99) as zero. But these terms do contribute to the determinant of $\boldsymbol{R}$ and cannot be omitted. Because they are actually of order ϵ and order ϵ^2 after taking the order of the lattice sums into account, and the products of them and terms of order $1/\epsilon$ and order $1/\epsilon^2$ are as large as the diagonal terms. Here is a simple example to explain why such terms cannot be neglected in a matrix like (3.100).

Given

$$G = \begin{pmatrix} 1+\delta & \delta\epsilon & \delta \\ 2\delta/\epsilon & 1+2\delta & 2\delta/\epsilon \\ \delta & \delta\epsilon & 1+\delta \end{pmatrix},\ \mathbf{x} = \begin{pmatrix} x_1 \\ x_2 \\ x_3 \end{pmatrix}, \tag{3.101}$$

$\epsilon \neq 0$, for what values of δ does $G\mathbf{x} = 0$ have non-trivial solutions for $\mathbf{x}$? For $\epsilon \to 0$, an

argument similar to that used by Zalipaev *et al.* gives

$$G \approx G' = \begin{pmatrix} 1+\delta & 0 & \delta \\ 2\delta/\epsilon & 1+2\delta & 2\delta/\epsilon \\ \delta & 0 & 1+\delta \end{pmatrix}, \tag{3.102}$$

and hence $\det G' = 0$ for $\delta = -1/2$. However, $\det G = 1+4\delta = 0$ for $\delta = -1/4$, irrespective of the value of ϵ. With $\delta = -1/2$, there are no non-trivial solutions. The confusion arises because of the particular form of G in which ϵ does not play a fundamental role. To see this, make the change of variable $\mathbf{x} = (y_1,\ y_2/\epsilon,\ y_3)^T$, then

$$G\mathbf{x} = \begin{pmatrix} (1+\delta)y_1 + \delta y_2 + \delta y_3 \\ 2\delta y_1/\epsilon + (1+2\delta)y_2/\epsilon + 2\delta y_3/\epsilon \\ \delta y_1 + \delta y_2 + (1+\delta)y_3 \end{pmatrix} = \begin{pmatrix} 0 \\ 0 \\ 0 \end{pmatrix}. \tag{3.103}$$

The factor of $1/\epsilon$ may be cancelled from the second equation and hence $G\mathbf{x} = 0$ is equivalent to $U\mathbf{y} = 0$, where

$$U = \begin{pmatrix} 1+\delta & \delta & \delta \\ 2\delta & 1+2\delta & 2\delta \\ \delta & \delta & 1+\delta \end{pmatrix} \tag{3.104}$$

is independent of ϵ.

In order to illuminate the quasi-static limit more clearly, we use new scaled variables. In these variables, in the limit $\epsilon \to 0$ all the diagonal terms except for the top 5 tend to 1 and all the non-diagonal terms except for the top left 5×10 matrix tend to 0, therefore the determinant of the Rayleigh matrix will be reduced to the determinant of a top left 5×5 matrix. Substituting the new variables

$$X_l = M_l^{(aa)} B_l^{(a)} + M_l^{(ab)} B_l^{(b)}, \tag{3.105}$$

$$Y_l = M_l^{(ba)} B_l^{(a)} + M_l^{(bb)} B_l^{(b)}, \tag{3.106}$$

into the linear system (3.89), we can rewrite the Rayleigh system as

$$X_l + \sum_{m=-\infty}^{+\infty} F_{lm}^{(aa)} X_m + F_{lm}^{(ab)} Y_m = 0, \tag{3.107}$$

$$Y_l + \sum_{m=-\infty}^{+\infty} F_{lm}^{(ba)} X_m + F_{lm}^{(bb)} Y_m = 0, \tag{3.108}$$

where

$$F_{lm}^{(aa)} = \frac{M_m^{(bb)}}{M_m^{ab} M_m^{ba} - M_m^{aa} M_m^{bb}} (-1)^{l+m} S_{m-l}^Y(k_1, \boldsymbol{\beta}),$$

$$F_{lm}^{(ab)} = \frac{M_m^{(ab)}}{M_m^{aa} M_m^{bb} - M_m^{ab} M_m^{ba}} (-1)^{l+m} S_{m-l}^Y(k_1, \boldsymbol{\beta}),$$

$$F_{lm}^{(ba)} = \frac{M_m^{(ba)}}{M_m^{aa} M_m^{bb} - M_m^{ab} M_m^{ba}} (-1)^{l+m} S_{m-l}^Y(k_2, \boldsymbol{\beta}),$$

$$F_{lm}^{(bb)} = \frac{M_m^{(aa)}}{M_m^{ab} M_m^{ba} - M_m^{aa} M_m^{bb}} (-1)^{l+m} S_{m-l}^Y(k_2, \boldsymbol{\beta}).$$

Then the Rayleigh matrix $\boldsymbol{R} = \begin{pmatrix} \boldsymbol{I} + \boldsymbol{F}_{lm}^{(aa)} & \boldsymbol{F}_{lm}^{(ab)} \\ \boldsymbol{F}_{lm}^{(ba)} & \boldsymbol{I} + \boldsymbol{F}_{lm}^{(bb)} \end{pmatrix}$, $l,\ m = 0,\ -1,\ 1,\ -2,\ 2 \ldots$.

By the forms of $M_m^{(\alpha\beta)}$, we have

$$\lim_{\epsilon \to 0} F_{lm}^{(\alpha\beta)} = 0, \quad |m| > 2, \tag{3.109}$$

and because the lattice sums for shear waves $S_{m-l}^Y(k_2, \boldsymbol{\beta})$ are not singular in the vicinity of $k_1 = \beta_m$, all the $F_{lm}^{(ba)}$ and $F_{lm}^{(bb)}$ tend to zero as $\epsilon \to 0$. Define $\boldsymbol{A'} = \left(\boldsymbol{I} + \boldsymbol{F}_{lm}^{(aa)} \right)_{\substack{|l| \le 2 \\ |m| \le 2}}$ and $\boldsymbol{B'} = \left(\boldsymbol{F}_{lm}^{(ab)} \right)_{\substack{|l| \le 2 \\ |m| \le 2}}$, then in the limit $\epsilon \to 0$ the structure of the whole Rayleigh matrix is (here we have rearranged the equations so that $\boldsymbol{B'}$ is moved to the next right of $\boldsymbol{A'}$ to make the matrix look neater)

$$\begin{pmatrix} \boldsymbol{A'}_{5\times5} & \boldsymbol{B'}_{5\times5} & \boldsymbol{0}_{10\times\infty} \\ \boldsymbol{0}_{5\times5} & \boldsymbol{I}_{5\times5} & \\ \boldsymbol{0}_{\infty\times10} & & \boldsymbol{I}_{\infty} \end{pmatrix}, \tag{3.110}$$

where

$$\boldsymbol{A}'_{5\times5} =$$

$$\begin{pmatrix}
1+\dfrac{\pi L^2(\lambda+\mu)}{A\delta\mu} & \dfrac{\pi L^2 \mathrm{i}\mathrm{e}^{\mathrm{i}\tau}}{2A\delta} & -\dfrac{\pi L^2 \mathrm{i}\mathrm{e}^{-\mathrm{i}\tau}}{2A\delta} & -\dfrac{\pi L^2 \mathrm{e}^{2\mathrm{i}\tau}\mu}{A\delta(\lambda+\mu)} & -\dfrac{\pi L^2 \mathrm{e}^{-2\mathrm{i}\tau}\mu}{A\delta(\lambda+\mu)} \\
\dfrac{\pi L^2 \mathrm{i}\mathrm{e}^{-\mathrm{i}\tau}(\lambda+\mu)}{A\delta\mu} & 1-\dfrac{\pi L^2}{2A\delta} & \dfrac{\pi L^2 \mathrm{e}^{-2\mathrm{i}\tau}}{2A\delta} & -\dfrac{\pi L^2 \mathrm{i}\mathrm{e}^{\mathrm{i}\tau}\mu}{A\delta(\lambda+\mu)} & -\dfrac{\pi L^2 \mathrm{i}\mathrm{e}^{-3\mathrm{i}\tau}\mu}{A\delta(\lambda+\mu)} \\
-\dfrac{\pi L^2 \mathrm{i}\mathrm{e}^{\mathrm{i}\tau}(\lambda+\mu)}{A\delta\mu} & \dfrac{\pi L^2 \mathrm{e}^{2\mathrm{i}\tau}}{2A\delta} & 1-\dfrac{\pi L^2}{2A\delta} & \dfrac{\pi L^2 \mathrm{i}\mathrm{e}^{3\mathrm{i}\tau}\mu}{A\delta(\lambda+\mu)} & \dfrac{\pi L^2 \mathrm{i}\mathrm{e}^{-\mathrm{i}\tau}\mu}{A\delta(\lambda+\mu)} \\
-\dfrac{\pi L^2 \mathrm{e}^{-2\mathrm{i}\tau}(\lambda+\mu)}{A\delta\mu} & -\dfrac{\pi L^2 \mathrm{i}\mathrm{e}^{-\mathrm{i}\tau}}{2A\delta} & \dfrac{\pi L^2 \mathrm{i}\mathrm{e}^{-3\mathrm{i}\tau}}{2A\delta} & 1+\dfrac{\pi L^2\mu}{A\delta(\lambda+\mu)} & \dfrac{\pi L^2 \mathrm{e}^{-4\mathrm{i}\tau}\mu}{A\delta(\lambda+\mu)} \\
-\dfrac{\pi L^2 \mathrm{e}^{2\mathrm{i}\tau}(\lambda+\mu)}{A\delta\mu} & -\dfrac{\pi L^2 \mathrm{i}\mathrm{e}^{3\mathrm{i}\tau}}{2A\delta} & \dfrac{\pi L^2 \mathrm{i}\mathrm{e}^{\mathrm{i}\tau}}{2A\delta} & \dfrac{\pi L^2 \mathrm{e}^{4\mathrm{i}\tau}\mu}{A\delta(\lambda+\mu)} & 1+\dfrac{\pi L^2\mu}{A\delta(\lambda+\mu)}
\end{pmatrix}.$$

Therefore

$$\lim_{\epsilon\to0}|\boldsymbol{R}| = |\boldsymbol{A}'_{5\times5}| = \frac{\mathcal{A}\delta\mu(\lambda+\mu)+\pi L^2(\lambda^2+\lambda\mu+2\mu^2)}{\mathcal{A}\delta\mu(\lambda+\mu)}, \tag{3.111}$$

and $|\boldsymbol{A}'_{5\times5}| = 0$ gives

$$\delta = -\frac{\pi L^2(\lambda^2+\lambda\mu+2\mu^2)}{\mathcal{A}\mu(\lambda+\mu)}, \tag{3.112}$$

where $\delta = (k_1^2-\beta^2)L^2/\epsilon^2$. Then at last

$$k_1^2 = \beta_1^2\left[1+\frac{\pi a^2}{\mathcal{A}}\left(\frac{\lambda}{\mu}+\frac{2\mu}{\lambda+\mu}\right)\right]^{-1}. \tag{3.113}$$

The perturbation of shear waves (when the lattice sums have poles at $k_2=\beta_1$) gives

$$k_2^2 = \beta_1^2\left[1+\frac{\pi a^2}{\mathcal{A}}\left(\frac{\lambda+3\mu}{\lambda+\mu}\right)\right]^{-1}. \tag{3.114}$$

3.2.2 Solutions by matched asymptotic expansions

The main idea used here is to obtain perturbations of the plane wave solutions that exist in the absence of the scatterers, and this is done using the method of matched asymptotic expansions. The wavenumbers for plane dilatational and shear waves are denoted respectively by k_1 ($\equiv \omega\sqrt{\rho/(\lambda+2\mu)}$) and k_2 ($\equiv \omega\sqrt{\rho/\mu}$) so that $k_2 = Pk_1$, where $P^2 = (\lambda+2\mu)/\mu$. The assumptions made here are that the characteristic size a of a scatterer satisfies both $k_i a \ll 1$, $i=1,2$, and $a/L \ll 1$, where L is the length scale for

the array periodicity, so that the scatterers are small relative to both the wavelengths and the array periodicity. The results given here are distinguished from those obtained through homogenisation in that now each $k_i L$ is allowed to be an order one quantity. This paper is concerned with waves that propagate in a direction normal to the axes of the cylinders, that is in the x-y plane so that $\mathbf{u}$ does not depend on z (the same method is used by McIver, 2007, to obtain results that apply to the simpler case of anti-plane shear waves).

By the Helmholtz representation (3.77), the displacement vector $\mathbf{u}$ of the medium can be decomposed into two parts, the scalar part ϕ and the vector part $\boldsymbol{\psi}$, here we take $\boldsymbol{\psi} = (0, 0, \psi)$. Then in terms of ϕ and ψ, the Bloch conditions are

$$\phi(\mathbf{r} + \mathbf{R_j}) = \mathrm{e}^{\mathrm{i}\boldsymbol{\beta}\cdot\mathbf{R}_j}\phi(\mathbf{r}) \quad \text{and} \quad \psi(\mathbf{r} + \mathbf{R_j}) = \mathrm{e}^{\mathrm{i}\boldsymbol{\beta}\cdot\mathbf{R}_j}\psi(\mathbf{r}). \tag{3.115}$$

In particular, these conditions are satisfied by plane waves of the form

$$\phi_m(\mathbf{r}) = \mathrm{e}^{\mathrm{i}\boldsymbol{\beta}_m^T\mathbf{r}} \quad \text{and} \quad \psi_n(\mathbf{r}) = \mathrm{e}^{\mathrm{i}\boldsymbol{\beta}_n^T\mathbf{r}}, \quad m, n \in \mathbb{Z}, \tag{3.116}$$

where $\boldsymbol{\beta}_m = \boldsymbol{\beta} + \mathbf{K}_m$, $\boldsymbol{\beta} = (q_1, q_2)^T$ is the prescribed Bloch vector and $\mathbf{K}_m$ is the reciprocal lattice defined in (3.69).

In the absence of the scatterers each of ϕ_m and ψ_n provides a solution to the Bloch problem provided k_1, k_2 are chosen to ensure that the field equations (3.79) are satisfied; in other words provided

$$k_1^2 = \beta_m^2, \quad k_2^2 = \beta_n^2, \quad m, n \in \mathbb{Z}, \tag{3.117}$$

where $\beta_m = |\boldsymbol{\beta}_m|$. For example, for a square lattice of side L aligned with the coordinate axes, plane-waves solutions satisfying the Bloch conditions are

$$\phi_m = \exp\left\{\mathrm{i}\left[(q_1 + 2\pi m_1/L)x + (q_2 + 2\pi m_2/L)y\right]\right\}, \quad m_1, m_2 \in \mathbb{Z}, \tag{3.118}$$

$$\psi_n = \exp\left\{\mathrm{i}\left[(q_1 + 2\pi n_1/L)x + (q_2 + 2\pi n_2/L)y\right]\right\}, \quad n_1, n_2 \in \mathbb{Z}, \tag{3.119}$$

and the field equations are satisfied as long as

$$k_1^2 = (q_1 + 2\pi m_1/L)^2 + (q_2 + 2\pi m_2/L)^2, \tag{3.120}$$

$$k_2^2 = (q_1 + 2\pi n_1/L)^2 + (q_2 + 2\pi n_2/L)^2. \tag{3.121}$$

The results given here for the case when scatterers are present arise from the consideration of perturbations to combinations of such plane wave solutions.

The solutions obtained here are in terms of an outer solution, valid everywhere except for a neighbourhood of each scatterer, that matches with inner solutions valid only in the immediate vicinity of each scatterer. However, because of the Bloch conditions (3.115), the matching process used in the construction of solutions need only be carried out in a primary lattice cell chosen to be that containing the origin O of the global coordinates defined in the previous section. The particular scatterer associated with O is denoted by C. In addition to the global coordinates, local polar coordinates (r_j, θ_j) are used that have origin at O_j.

To facilitate the solution, each lattice cell is divided into two overlapping regions. For the primary cell these are an outer region at distances $r \gg a$, and an inner region within distances $r \ll k_i^{-1}$ of the scatterer. A small parameter $\epsilon = k_1 a$ is introduced, and in the inner region a scaled coordinate $\rho = r/a$ is used. With these definitions, $k_1 r = \epsilon\rho$ and $k_2 r = P\epsilon\rho$.

In the outer region, far from each scatterer, the solutions are constructed from solutions of the Helmholtz equations (3.79) that satisfy the Bloch conditions (3.115) and that are singular at the lattice points; such solutions are

$$\overline{G}_n(k_1 r, \theta) = \sum_{\mathbf{R}_j \in \Lambda} \mathrm{e}^{\mathrm{i}\boldsymbol{\beta}^T \cdot \mathbf{R}_j} H_n^{(1)}(k_1 r_j) \mathrm{e}^{\mathrm{i}n\theta_j}, \tag{3.122}$$

and

$$\widehat{G}_n(k_2 r, \theta) = \sum_{\mathbf{R}_j \in \Lambda} \mathrm{e}^{\mathrm{i}\boldsymbol{\beta}^T \cdot \mathbf{R}_j} H_n^{(1)}(k_2 r_j) \mathrm{e}^{\mathrm{i}n\theta_j}, \tag{3.123}$$

where $\overline{G}_n(k_1 r, \theta)$ is associated with dilatational waves, and $\widehat{G}_n(k_2 r, \theta)$ with shear waves. By Graf's addition theorem (Abramowitz & Stegun 1964, equation 9.1.79)

$$\overline{G}_n(k_1 r, \theta) = H_n^{(1)}(k_1 r) \mathrm{e}^{\mathrm{i}n\theta} + \sum_p (-1)^{n-p} J_p(k_1 r) \mathrm{e}^{\mathrm{i}p\theta} \bar{\sigma}_{n-p} \tag{3.124}$$

and

$$\widehat{G}_n(k_2 r, \theta) = H_n^{(1)}(k_2 r) \mathrm{e}^{\mathrm{i}n\theta} + \sum_p (-1)^{n-p} J_p(k_2 r) \mathrm{e}^{\mathrm{i}p\theta} \hat{\sigma}_{n-p}, \tag{3.125}$$

where $\sum_p$ indicates summations over all $p \in \mathbb{Z}$, and the lattice sums are

$$\bar{\sigma}_n = {\sum_{\mathbf{R}_j \in \Lambda}}' \mathrm{e}^{\mathrm{i}\boldsymbol{\beta}^T \cdot \mathbf{R}_j} H_n^{(1)}(k_1 R_j) \mathrm{e}^{\mathrm{i}n\alpha_j} \tag{3.126}$$

and

$$\hat{\sigma}_n = {\sum_{\mathbf{R}_j \in \Lambda}}' \mathrm{e}^{\mathrm{i}\boldsymbol{\beta}^T \cdot \mathbf{R}_j} H_n^{(1)}(k_2 R_j) \mathrm{e}^{\mathrm{i}n\alpha_j}. \tag{3.127}$$

Here α_j is the angle between the x axis and $\mathbf{R}_j$ measured in the anticlockwise direction, and the dashes indicate that $\mathbf{R}_j = 0$ is omitted from the summations. The lattice sums (3.126) and (3.127) have poles wherever, respectively, k_1 and k_2 have a value β_m, $m \in \mathbb{Z}$ – see Linton (2010, equation 3.18), for example – and these poles correspond to the plane wave solutions discussed before. For a given $\boldsymbol{\beta}$ and k_i ($i = 1$ or 2), the number of distinct vectors $\boldsymbol{\beta}_m$ that have the same magnitude β_m is denoted by $M_i \geq 1$.

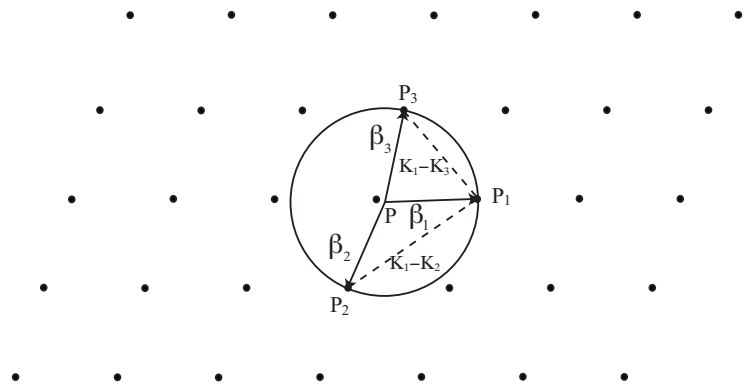

Figure 3.6: Ewald construction, $M = 3$.

The method of Ewald construction [6, page 101] can be used to find these $\boldsymbol{\beta}_m$ with the same magnitude, for a given lattice and Bloch vector. Draw a circle centred at the initial point P of $\boldsymbol{\beta}_1$ with radius β in the reciprocal lattice. Then if another reciprocal lattice point P_2 falls on this circle, the vector $\overrightarrow{PP_2}$ (denoted by $\boldsymbol{\beta}_2$) has the same magnitude as $\boldsymbol{\beta}_1$ and they correspond to same plane wave solutions. For specified lattice and Bloch vector, there may be M vectors falling on that circle. Figure 3.6 gives an example when $M = 3$.

For square and hexagonal lattices, the locations of the poles of the lattice sums (or, equivalently, the plane waves that exist in the absence of the scatterers and satisfy the Bloch conditions) are shown in figures 3.7 and 3.8 for values of the modulus β of the wave vector $\boldsymbol{\beta}$ along the boundaries of the corresponding first irreducible Brillouin zones, as illustrated in figure 3.1. For all of the calculations in this chapter, the Lamé constants

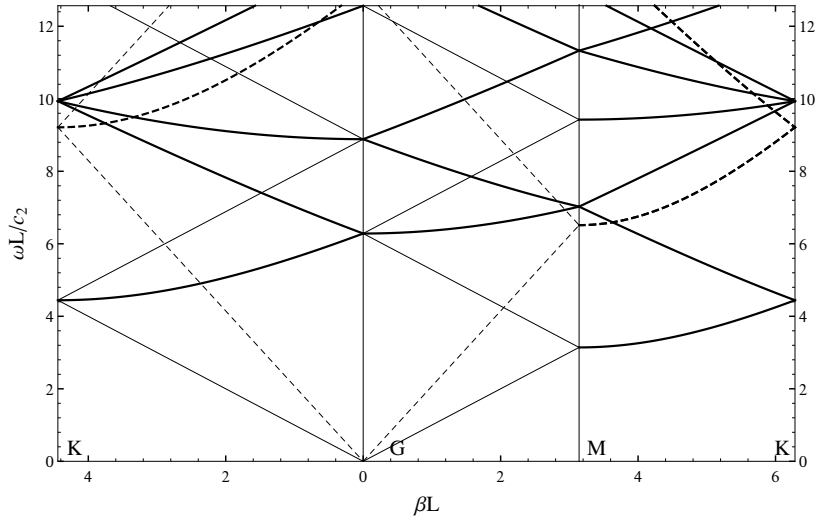

Figure 3.7: Dispersion diagram for square array without scatterers: one-pole shear waves (——); one-pole dilatational waves (- - - -); two-pole shear waves (——); two-pole dilatational waves (- - - -).

are related by $\lambda/\mu = 2.3$, and a non-dimensional frequency parameter

$$\omega L/c_2 \equiv k_2 L \tag{3.128}$$

is used. In these figures it can be seen that, for some combinations of $\boldsymbol{\beta}$ and the frequency ω, there are multiple plane-wave solutions and these can arise in two ways. First of all, as noted above, for one of the lattice sums there may be multiple distinct vectors $\boldsymbol{\beta}_m$ with the same magnitude β_m; this can occur along lines as indicated by the two-pole curves in the figures, and also at isolated points. Secondly, multiple solutions can occur when the two lattice sums have poles corresponding to the same frequency, so that there are crossings of the curves for pure dilatational and pure shear waves. Results are given later for perturbations of all of these types of plane-wave solution, but full details of the derivation are given only for perturbations of purely dilatational waves (that is, in regions of the parameter space not close to the curves in figures 3.7 and 3.8 that correspond to shear waves).

Consider then the perturbation of dilatational plane waves with wavenumber k_1, so that the lattice sums $\bar{\sigma}_n$ have poles at $k_1 = \pm\beta_m$, $m = 1..M_1$, while the lattice sums $\hat{\sigma}_n$ for the shear waves are analytic functions of the frequency within neighbourhoods of these points. For each unique vector $\boldsymbol{\beta}_m$,

$$\bar{\sigma}_n \sim \frac{4i^{n+1}\mathrm{e}^{\mathrm{i}n\tau_m}}{\mathcal{A}(k_1^2 - \beta_m^2)} \quad \text{as} \quad k_1^2 \to \beta_m^2, \tag{3.129}$$

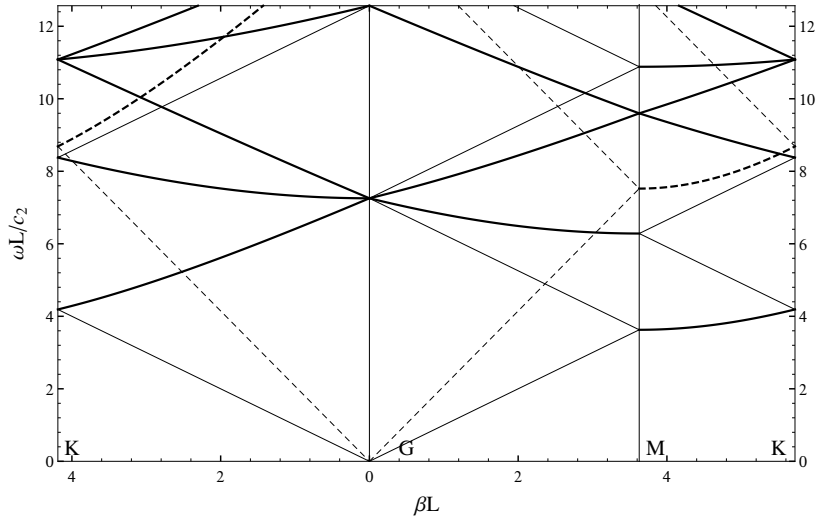

Figure 3.8: Dispersion diagram for hexagonal array without scatterers: one-pole shear waves (——); one-pole dilatational waves (- - - -); two-pole shear waves (——); two-pole dilatational waves (- - - -).

where $\mathcal{A}$ is the area of one cell of the lattice, and the angles τ_m are defined through

$$\boldsymbol{\beta}_m = \beta_m \mathbf{e}_{1m} \quad \text{with} \quad \mathbf{e}_{pm} = \begin{pmatrix} \cos p\tau_m \\ \sin p\tau_m \end{pmatrix} \tag{3.130}$$

– see Linton (2010, equation 3.18). The lattice sums are written

$$\bar{\sigma}_n = \sum_{m=1}^{M_1} \frac{\bar{\sigma}_{nm}^{(1)}}{(k_1^2 - \beta_m^2)L^2} + \bar{\sigma}_n^{(2)}, \quad \text{where} \quad \bar{\sigma}_{nm}^{(1)} = \frac{4i^{n+1}\mathrm{e}^{\mathrm{i}n\tau_m}}{\mathcal{A}/L^2}, \tag{3.131}$$

and each $\bar{\sigma}_n^{(2)}$ is assumed to be an analytic function of k_1 within neighbourhoods of each $k_1 = \pm\beta_m$. Solutions are sought for k_1 in a neighbourhood of β_m and it is assumed here that

$$(k_1^2 - \beta_m^2)L^2 = f(\epsilon)\delta_m, \tag{3.132}$$

where, for $k_1^2 \neq \beta_m^2$, δ_m is strictly of order one in ϵ as $\epsilon \to 0$. This expression will be used within a neighbourhood of the points in $(\boldsymbol{\beta}, k_1)$ space that correspond to plane waves, so that the β_m and hence the δ_m may be distinct. It may be shown that the need to link the first appearance of singular terms in the outer solution of ϕ with the nonsingular leading-order outer solution for ϕ, requires $f(\epsilon) = \epsilon^2$ (the matching would fail if this relation were incorrect) but, for simplicity, this will be adopted from the outset.

In view of (3.132), the matching may be carried out more conveniently if the singular

solutions of the Helmholtz equation defined in (3.122) are modified to be

$$\bar{g}_n(k_1 r,\theta) = \epsilon^2 \overline{G}_n(k_1 r,\theta) = \bar{g}_n^{(1)}(k_1 r,\theta) + \epsilon^2 \bar{g}_n^{(2)}(k_1 r,\theta), \tag{3.133}$$

where the plane-wave part

$$\begin{aligned}\bar{g}_n^{(1)}(k_1 r,\theta) &= \sum_{m=1}^{M_1} \frac{1}{\delta_m} \sum_p (-1)^{n-p} \bar{\sigma}_{n-p,m}^{(1)} J_p(k_1 r) \mathrm{e}^{\mathrm{i}p\theta} \\ &= (-1)^n \sum_{m=1}^{M_1} \frac{\bar{\sigma}_{nm}^{(1)}}{\delta_m} \mathrm{e}^{\mathrm{i}k_1 r\cos(\theta-\tau_m)},\end{aligned} \tag{3.134}$$

and the singular part

$$\bar{g}_n^{(2)}(k_1 r,\theta) = H_n^{(1)}(k_1 r)\mathrm{e}^{\mathrm{i}n\theta} + \sum_p (-1)^{n-p} \bar{\sigma}_{n-p}^{(2)} J_p(k_1 r)\mathrm{e}^{\mathrm{i}p\theta}. \tag{3.135}$$

We will use Φ and $\bar{\phi}$ to denote the outer and inner solutions for ϕ, and Ψ and $\hat{\psi}$ to denote the outer and inner solutions for ψ. As the coupled boundary-value problem is homogeneous, the leading order outer solution may be taken as strictly order zero in ϵ so that

$$\Phi^{(0)} = \sum_n \bar{A}_n \bar{g}_n^{(1)}(k_1 r,\theta), \tag{3.136}$$

where $\Phi^{(m)}$ denotes the outer solution up to terms in ϵ^m. (Because we consider only the perturbation of dilatational waves, shear waves do not appear in the leading-order outer solution.) In the following, $\Phi^{(m,l)}$ denotes the expansion up to ϵ^l of $\Phi^{(m)}$ after it is written in terms of the inner coordinate ρ. The inner solution up to terms in ϵ^l is denoted by $\bar{\phi}^{(l)}$, and $\bar{\phi}^{(l,m)}$ denotes its expansion up to ϵ^m after it is written in terms of the outer coordinate $k_1 r$. Matching is enforced by requiring $\Phi^{(m,l)} = \bar{\phi}^{(l,m)}$ for every m and l when both asymptotic forms are expressed in terms of the same coordinates (Crighton *et al.* 1973). The same principles also apply to the inner and outer expansions for the shear part of the solution.

In terms of the inner variable $\rho = r/a$, the field equations for the inner solutions $\bar{\phi}$ and $\hat{\psi}$ are

$$\frac{1}{\rho}\frac{\partial}{\partial\rho}\left(\rho\frac{\partial\bar{\phi}}{\partial\rho}\right) + \frac{1}{\rho^2}\frac{\partial^2\bar{\phi}}{\partial\theta^2} + \epsilon^2\bar{\phi} = 0 \tag{3.137}$$

and

$$\frac{1}{\rho}\frac{\partial}{\partial\rho}\left(\rho\frac{\partial\hat{\psi}}{\partial\rho}\right) + \frac{1}{\rho^2}\frac{\partial^2\hat{\psi}}{\partial\theta^2} + P^2\epsilon^2\hat{\psi} = 0. \tag{3.138}$$

The inner solutions are constructed with the help of inner eigensolutions that each satisfy the Laplace equation, together with the homogeneous boundary conditions

$$\frac{2\mu}{\lambda}\left(\frac{\partial^2\bar{\phi}}{\partial\rho^2}+\frac{\partial^2\hat{\psi}}{\partial\rho\partial\theta}-\frac{\partial\hat{\psi}}{\partial\theta}\right)=0,\quad \rho=1, \tag{3.139}$$

and

$$2\frac{\partial^2\bar{\phi}}{\partial\rho\partial\theta}-2\frac{\partial\bar{\phi}}{\partial\theta}+\frac{\partial^2\hat{\psi}}{\partial\theta^2}-\frac{\partial^2\hat{\psi}}{\partial\rho^2}+\frac{\partial\hat{\psi}}{\partial\rho}=0,\quad \rho=1. \tag{3.140}$$

It is straightforward to show that the required inner eigensolutions are given by the following pairs (the barred terms refer to the dilatational wave and the hatted terms to the shear wave):

$$\begin{cases}\overline{E}_n(\rho,\theta)=\rho^n\cos n\theta,\\ \widehat{E}_n(\rho,\theta)=-\rho^n\sin n\theta,\end{cases}\quad n\neq 1;\quad \begin{cases}\overline{E}_1(\rho,\theta)=\rho\cos\theta,\\ \widehat{E}_1(\rho,\theta)=0;\end{cases}\quad \begin{cases}\overline{E}_1(\rho,\theta)=\rho\sin\theta,\\ \widehat{E}_1(\rho,\theta)=0;\end{cases}$$

$$\begin{cases}\overline{E}_n(\rho,\theta)=\rho^n\sin n\theta,\\ \widehat{E}_n(\rho,\theta)=\rho^n\cos n\theta,\end{cases}\quad n\neq 1;\quad \begin{cases}\overline{E}_1(\rho,\theta)=0,\\ \widehat{E}_1(\rho,\theta)=\rho\sin\theta;\end{cases}\quad \begin{cases}\overline{E}_1(\rho,\theta)=0,\\ \widehat{E}_1(\rho,\theta)=\rho\cos\theta.\end{cases} \tag{3.141}$$

From equations (3.134) and (3.136), the inner expansion of the leading order outer solution is

$$\Phi^{(0,2)}=\sum_n \bar{A}_n(-1)^n\sum_{m=1}^{M_1}\frac{\bar{\sigma}^{(1)}_{nm}}{\delta_m}\left\{1+\mathrm{i}\epsilon\rho\mathbf{e}^T_{1m}\begin{pmatrix}\cos\theta\\ \sin\theta\end{pmatrix}-\tfrac{1}{4}\epsilon^2\rho^2\left[1+\mathbf{e}^T_{2m}\begin{pmatrix}\cos 2\theta\\ \sin 2\theta\end{pmatrix}\right]\right\}, \tag{3.142}$$

which indicates an initial inner development

$$\bar{\phi}^{(1)}=\bar{\phi}_0+\nu_{11}(\epsilon)\bar{\phi}_{11}+\epsilon\bar{\phi}_1, \tag{3.143}$$

where the term in $\nu_{11}(\epsilon)$ is a possible intermediate term and, because $\overline{\phi}$ and $\hat{\psi}$ are coupled through the boundary conditions, there is a shear component to the inner problem so that

$$\hat{\psi}^{(1)}=\hat{\psi}_0+\nu_{11}(\epsilon)\hat{\psi}_{11}+\epsilon\hat{\psi}_1 \tag{3.144}$$

(higher-order terms in the inner solution are dealt with later). Substituting (3.143) and (3.144) into the field equations (3.137) and (3.138) and equating the coefficients of the

gauge functions in ϵ, we find that $\bar{\phi}_0$, $\bar{\phi}_{11}$, $\bar{\phi}_1$, $\hat{\psi}_0$, $\hat{\psi}_{11}$, $\hat{\psi}_1$ are all harmonic functions that satisfy the homogeneous boundary conditions, and hence are constructed from the inner eigenfunctions detailed in equations (3.141).

The inner expansion (3.142) suggests that $\bar{\phi}_0$ and $\hat{\psi}_0$ might contain only constants. However, the appearance of terms in 2θ at order ϵ^2 in the inner expansion (3.142) is significant. These terms could be matched with the inner solution $\bar{\phi}$ simply by including appropriate eigenfunctions in $\bar{\phi}$ at order ϵ^2, but it then proves impossible to satisfy the boundary conditions. The situation is resolved by including eigenfunctions in 2θ within $\bar{\phi}_0$ and $\hat{\psi}_0$, in order to generate further terms at order ϵ^2 in $\bar{\phi}$ and $\hat{\psi}$ through particular solutions of the field equations (3.137)-(3.138). In general, in order to satisfy the boundary conditions at order ϵ^{n+2}, the inner solution at order ϵ^n must contain singular eigenfunctions up to and including those in $(n+2)\theta$.

With the above in mind, the leading-order inner solutions are written as

$$\bar{\phi}_0 = B_0 + \frac{\mathbf{u}_0^T}{\rho^2}\begin{pmatrix}\cos 2\theta \\ \sin 2\theta\end{pmatrix} \tag{3.145}$$

and

$$\hat{\psi}_0 = \frac{\mathbf{u}_0^T}{\rho^2}\begin{pmatrix}\sin 2\theta \\ -\cos 2\theta\end{pmatrix} = \frac{\mathbf{u}_0^T}{\rho^2}\begin{pmatrix}0 & 1 \\ -1 & 0\end{pmatrix}\begin{pmatrix}\cos 2\theta \\ \sin 2\theta\end{pmatrix}, \tag{3.146}$$

so that, in terms of the outer variables,

$$\bar{\phi}^{(0,2)} = B_0 + \frac{\epsilon^2\mathbf{u}_0^T}{(k_1 r)^2}\begin{pmatrix}\cos 2\theta \\ \sin 2\theta\end{pmatrix} \tag{3.147}$$

and

$$\hat{\psi}^{(0,2)} = \frac{\epsilon^2 P^2\mathbf{u}_0^T}{(k_2 r)^2}\begin{pmatrix}0 & 1 \\ -1 & 0\end{pmatrix}\begin{pmatrix}\cos 2\theta \\ \sin 2\theta\end{pmatrix}, \tag{3.148}$$

where B_0 and $\mathbf{u}_0 = (u_{01}, u_{02})$ are unknowns need to be determined by the matching. The outer expansion $\bar{\phi}^{(0,2)}$ has terms no more singular than a quadrupole, and hence cannot be matched to any higher singularities associated in the leading-order outer solution; thus $\bar{A}_n = 0$ for $|n| > 2$. (It might be argued that more singular terms could be included in the outer solution, and then matched to the inner solution by including inner eigenfunctions at an appropriate order. However, this leads to unresolvable difficulties later.)

With possible intermediate terms included, the dilatational outer solution is continued as

$$\Phi^{(2)} = \sum_{n=-2}^{2} \bar{A}_n \left\{ \bar{g}_n^{(1)}(k_1 r, \theta) + \epsilon^2 \bar{g}_n^{(2)}(k_1 r, \theta) \right\} + \mu_{11}(\epsilon) \sum_n \bar{C}_n \bar{g}_n^{(1)}(k_1 r, \theta)$$

$$+ \ \epsilon \sum_n C_n \bar{g}_n^{(1)}(k_1 r, \theta) + \mu_{21}(\epsilon) \sum_n \bar{D}_n \bar{g}_n^{(1)}(k_1 r, \theta) + \ \epsilon^2 \sum_n D_n \bar{g}_n^{(1)}(k_1 r, \theta), \quad (3.149)$$

so that, in particular,

$$\Phi^{(2,0)} = \sum_{n=-2}^{2} \bar{A}_n (-1)^n \sum_{m=1}^{M_1} \frac{\bar{\sigma}_{nm}^{(1)}}{\delta_m} + \bar{A}_2 \frac{-4\mathrm{i}e^{2\mathrm{i}\theta}}{\pi\rho^2} + \bar{A}_{-2} \frac{-4\mathrm{i}e^{-2\mathrm{i}\theta}}{\pi\rho^2}. \quad (3.150)$$

The matching rule $\Phi^{(2,0)} \equiv \bar{\phi}^{(0,2)}$ then gives

$$B_0 = \sum_{n=-2}^{2} \bar{A}_n (-1)^n \sum_{m=1}^{M_1} \frac{\bar{\sigma}_{nm}^{(1)}}{\delta_m} \quad \text{and} \quad (\bar{A}_2, \bar{A}_{-2}) = \frac{\pi}{8\mathrm{i}} \mathbf{u}_0^T \begin{pmatrix} -1 & -1 \\ \mathrm{i} & -\mathrm{i} \end{pmatrix}. \quad (3.151)$$

Equation (3.148) shows that the leading term in the outer expansion of $\hat{\psi}$ is at ϵ^2, and hence the leading-order outer shear solution is

$$\Psi^{(2)} = \epsilon^2 \sum_{n=-2}^{2} \hat{A}_n \hat{G}_n(k_2 r, \theta). \quad (3.152)$$

(As we have assumed that the shear lattice sums are well behaved, there is no decomposition similar to equation (3.133) for the shear potentials. Also, because the leading inner term is strictly order one, when expressed in terms of the inner coordinates $\Psi^{(2)}$ cannot be larger than order one as $\epsilon \to 0$, and hence $\hat{A}_n = 0$ for $|n| > 2$.) Thus, in particular,

$$\Psi^{(2,0)} = \hat{A}_2 \frac{-4\mathrm{i}e^{2\mathrm{i}\theta}}{\pi P^2 \rho^2} + \hat{A}_{-2} \frac{-4\mathrm{i}e^{-2\mathrm{i}\theta}}{\pi P^2 \rho^2}, \quad (3.153)$$

and the matching rule $\hat{\psi}^{(0,2)} \equiv \Psi^{(0,2)}$ gives

$$(\hat{A}_2, \hat{A}_{-2}) = \frac{\pi P^2}{8\mathrm{i}} \mathbf{u}_0^T \begin{pmatrix} \mathrm{i} & -\mathrm{i} \\ 1 & 1 \end{pmatrix}. \quad (3.154)$$

The inner expansion of the outer solution of ϕ up to order ϵ^2 is

$$\begin{aligned}\Phi^{(2,2)} = &\sum_{n=-2}^{2} \bar{A}_n (-1)^n \sum_{m=1}^{M_1} \frac{\bar{\sigma}_{nm}^{(1)}}{\delta_m} \left\{ 1 + \mathrm{i}\epsilon\rho \boldsymbol{e}_{1m}^T \begin{pmatrix} \cos\theta \\ \sin\theta \end{pmatrix} \right. \\ &\left. - \tfrac{1}{4}\epsilon^2\rho^2 \left[1 + \mathbf{e}_{2m}^T \begin{pmatrix} \cos 2\theta \\ \sin 2\theta \end{pmatrix} \right] \right\} + \epsilon^2 \left\{ \bar{A}_0 \left[1 + \frac{2\mathrm{i}}{\pi}(\log\epsilon\rho + \gamma - \log 2) + \bar{\sigma}_0^{(2)} \right] \right. \\ &+ \bar{A}_1 \left[\frac{-2\mathrm{i}}{\pi\epsilon\rho} \mathrm{e}^{\mathrm{i}\theta} - \bar{\sigma}_1^{(2)} \right] + \bar{A}_{-1} \left[\frac{2\mathrm{i}}{\pi\epsilon\rho} \mathrm{e}^{-\mathrm{i}\theta} - \bar{\sigma}_{-1}^{(2)} \right] \\ &\left. + \bar{A}_2 \left[\left(\frac{-4\mathrm{i}}{\pi\epsilon^2\rho^2} - \frac{\mathrm{i}}{\pi} \right) \mathrm{e}^{2\mathrm{i}\theta} + \bar{\sigma}_2^{(2)} \right] + \bar{A}_{-2} \left[\left(\frac{-4\mathrm{i}}{\pi\epsilon^2\rho^2} - \frac{\mathrm{i}}{\pi} \right) \mathrm{e}^{-2\mathrm{i}\theta} + \bar{\sigma}_{-2}^{(2)} \right] \right\} \\ &+ \sum_n \left[\mu_{11}(\epsilon)\bar{C}_n + \epsilon C_n \right] (-1)^n \sum_{m=1}^{M_1} \frac{\bar{\sigma}_{nm}^{(1)}}{\delta_m} \left[1 + \mathrm{i}\epsilon\rho \begin{pmatrix} \cos\theta \\ \sin\theta \end{pmatrix} \right] \\ &+ \sum_n \left[\mu_{21}(\epsilon)\bar{D}_n + \epsilon^2 D_n \right] (-1)^n \sum_{m=1}^{M_1} \frac{\bar{\sigma}_{nm}^{(1)}}{\delta_m}. \end{aligned} \tag{3.155}$$

Thus, to match with the inner solution, $\mu_{11}(\epsilon) = \nu_{11}(\epsilon)$, and the inner solutions must be continued as

$$\begin{aligned}\bar{\phi}^{(2)} = &B_0 + \frac{\mathbf{u}_0^T}{\rho^2} \begin{pmatrix} \cos 2\theta \\ \sin 2\theta \end{pmatrix} + \nu_{11}(\epsilon)\, B_{11} + \epsilon \left[B_1 + \mathbf{u}_1^T \rho \begin{pmatrix} \cos\theta \\ \sin\theta \end{pmatrix} \right. \\ &\left. + \frac{\mathbf{u}_I^T}{\rho} \begin{pmatrix} \cos\theta \\ \sin\theta \end{pmatrix} + \frac{\mathbf{u}_2^T}{\rho^2} \begin{pmatrix} \cos 2\theta \\ \sin 2\theta \end{pmatrix} + \frac{\mathbf{u}_3^T}{\rho^3} \begin{pmatrix} \cos 3\theta \\ \sin 3\theta \end{pmatrix} \right] \\ &+ \epsilon\, \nu_{11}(\epsilon)\, \mathbf{u}_{11}^T \rho \begin{pmatrix} \cos\theta \\ \sin\theta \end{pmatrix} + \mu_{21}(\epsilon)\, B_{21} + \epsilon^2 \log\epsilon\, B_{22} + \epsilon^2 \bar{\phi}_2, \end{aligned} \tag{3.156}$$

and

$$\begin{aligned}\hat{\psi}^{(2)} = &\frac{\mathbf{u}_0^T}{\rho^2} \begin{pmatrix} 0 & 1 \\ -1 & 0 \end{pmatrix} \begin{pmatrix} \cos 2\theta \\ \sin 2\theta \end{pmatrix} + \epsilon \left[\frac{\mathbf{u}_I^T}{\rho} \begin{pmatrix} 0 & 1 \\ -1 & 0 \end{pmatrix} \begin{pmatrix} \cos\theta \\ \sin\theta \end{pmatrix} \right. \\ &\left. + \frac{\mathbf{u}_2^T}{\rho^2} \begin{pmatrix} 0 & 1 \\ -1 & 0 \end{pmatrix} \begin{pmatrix} \cos 2\theta \\ \sin 2\theta \end{pmatrix} + \frac{\mathbf{u}_3^T}{\rho^3} \begin{pmatrix} 0 & 1 \\ -1 & 0 \end{pmatrix} \begin{pmatrix} \cos 3\theta \\ \sin 3\theta \end{pmatrix} \right] \\ &+ \epsilon^2 \log\epsilon\, \hat{B}_{22} + \epsilon^2 \hat{\psi}_2 \end{aligned} \tag{3.157}$$

(recall that at order n in the inner solution we must include singular eigenfunctions up to those in $(n+2)\theta$). Here the vectors $\mathbf{u}_1, \mathbf{u}_2, \mathbf{u}_3$ and $\mathbf{u}_I$ are unknowns to be determined.

The potentials $\bar{\phi}_2$ and $\hat{\psi}_2$ satisfy the Poisson equations

$$\frac{1}{\rho}\frac{\partial}{\partial\rho}\left(\rho\frac{\partial\bar{\phi}_2}{\partial\rho}\right)+\frac{1}{\rho^2}\frac{\partial^2\bar{\phi}_2}{\partial\theta^2}=-\bar{\phi}_0\equiv-\left[B_0+\frac{\mathbf{u}_0^T}{\rho^2}\begin{pmatrix}\cos 2\theta\\ \sin 2\theta\end{pmatrix}\right] \tag{3.158}$$

and

$$\frac{1}{\rho}\frac{\partial}{\partial\rho}\left(\rho\frac{\partial\hat{\psi}_2}{\partial\rho}\right)+\frac{1}{\rho^2}\frac{\partial^2\hat{\psi}_2}{\partial\theta^2}=-P^2\hat{\psi}_0\equiv-P^2\left[\frac{\mathbf{u}_0^T}{\rho^2}\begin{pmatrix}0 & 1\\ -1 & 0\end{pmatrix}\begin{pmatrix}\cos 2\theta\\ \sin 2\theta\end{pmatrix}\right], \tag{3.159}$$

as well as the boundary conditions (3.139) and (3.140). The solution forms needed to effect the matching are

$$\begin{aligned}\bar{\phi}_2=\tfrac{1}{4}\mathbf{u}_0^T\begin{pmatrix}\cos 2\theta\\ \sin 2\theta\end{pmatrix}-\tfrac{1}{4}B_0\rho^2+\bar{\mathbf{v}}_1^T\rho\begin{pmatrix}\cos\theta\\ \sin\theta\end{pmatrix}+\frac{\bar{\mathbf{v}}_I^T}{\rho}\begin{pmatrix}\cos\theta\\ \sin\theta\end{pmatrix}\\ +\bar{\mathbf{v}}_2^T\rho^2\begin{pmatrix}\cos 2\theta\\ \sin 2\theta\end{pmatrix}+\frac{\bar{\mathbf{v}}_{II}^T}{\rho^2}\begin{pmatrix}\cos 2\theta\\ \sin 2\theta\end{pmatrix}+\ \ldots\ +\bar{v}_0\log\rho+\bar{B}_2\end{aligned} \tag{3.160}$$

and

$$\begin{aligned}\hat{\psi}_2=\frac{P^2\mathbf{u}_0^T}{4}\begin{pmatrix}0 & 1\\ -1 & 0\end{pmatrix}\begin{pmatrix}\cos 2\theta\\ \sin 2\theta\end{pmatrix}+\hat{\mathbf{v}}_1^T\rho\begin{pmatrix}\cos\theta\\ \sin\theta\end{pmatrix}+\frac{\hat{\mathbf{v}}_I^T}{\rho}\begin{pmatrix}\cos\theta\\ \sin\theta\end{pmatrix}\\ +\hat{\mathbf{v}}_2^T\rho^2\begin{pmatrix}\cos 2\theta\\ \sin 2\theta\end{pmatrix}+\frac{\hat{\mathbf{v}}_{II}^T}{\rho^2}\begin{pmatrix}\cos 2\theta\\ \sin 2\theta\end{pmatrix}+\ \ldots\ +\hat{v}_0\log\rho+\hat{B}_2,\end{aligned} \tag{3.161}$$

where the ellipses indicate singular eigenfunctions in 3θ and 4θ and the coefficients of the eigenfunctions are unknowns to be determined. Further, the terms involving $1/4$ are particular solutions of (3.158) and (3.159), $\bar{B}_2$ and $\hat{B}_2$ are eigenfunctions, and the other terms are solutions of the Laplace equation included to satisfy the boundary conditions and to effect the matching. From the boundary conditions

$$u_{01}=\frac{8(\bar{v}_{21}+\hat{v}_{22})}{P^2-1},\qquad u_{02}=\frac{8(\bar{v}_{22}-\hat{v}_{21})}{P^2-1}, \tag{3.162}$$

$$\bar{v}_0=\frac{(1-P^2)B_0}{2},\qquad \hat{v}_0=0, \tag{3.163}$$

where $\mathbf{u}_0^T=(u_{01},u_{02})$, $\bar{\mathbf{v}}_2^T=(\bar{v}_{21},\bar{v}_{22})$ and $\hat{\mathbf{v}}_2^T=(\hat{v}_{21},\hat{v}_{22})$. It follows that the outer

expansions of $\bar{\phi}^{(2)}$ and $\hat{\psi}^{(2)}$ are respectively

$$\bar{\phi}^{(2,2)} = B_0 + \frac{\mathbf{u}_0^T}{\rho^2}\begin{pmatrix}\cos 2\theta\\ \sin 2\theta\end{pmatrix} + B_{11}\nu_{11}(\epsilon) + \epsilon\left\{B_1 + \mathbf{u}_1^T\rho\begin{pmatrix}\cos\theta\\ \sin\theta\end{pmatrix} + \frac{\mathbf{u}_I^T}{\rho}\begin{pmatrix}\cos\theta\\ \sin\theta\end{pmatrix}\right\}$$
$$+ \epsilon\,\nu_{11}(\epsilon)\,\mathbf{u}_{11}^T\rho\begin{pmatrix}\cos\theta\\ \sin\theta\end{pmatrix} + \mu_{21}(\epsilon)\,B_{21} + \epsilon^2\log\epsilon\,B_{22} + \epsilon^2\left\{\tfrac{1}{4}\mathbf{u}_0^T\begin{pmatrix}\cos 2\theta\\ \sin 2\theta\end{pmatrix}\right.$$
$$\left. - \tfrac{1}{4}B_0\rho^2 + \bar{\mathbf{v}}_1^T\rho\begin{pmatrix}\cos\theta\\ \sin\theta\end{pmatrix} + \bar{\mathbf{v}}_2^T\rho^2\begin{pmatrix}\cos 2\theta\\ \sin 2\theta\end{pmatrix} + v_0\log\rho + B_2\right\} \tag{3.164}$$

and

$$\hat{\psi}^{(2,2)} = \mathbf{u}_0^T\frac{1}{\rho^2}\begin{pmatrix}0 & 1\\ -1 & 0\end{pmatrix}\begin{pmatrix}\cos 2\theta\\ \sin 2\theta\end{pmatrix} + \epsilon\mathbf{u}_I^T\frac{1}{\rho}\begin{pmatrix}0 & 1\\ -1 & 0\end{pmatrix}\begin{pmatrix}\cos\theta\\ \sin\theta\end{pmatrix}$$
$$+ \epsilon^2\left\{\frac{T^2}{4}\mathbf{u}_0^T\begin{pmatrix}0 & 1\\ -1 & 0\end{pmatrix}\begin{pmatrix}\cos 2\theta\\ \sin 2\theta\end{pmatrix} + \hat{\mathbf{v}}_1^T\rho\begin{pmatrix}\cos\theta\\ \sin\theta\end{pmatrix} + \hat{\mathbf{v}}_2^T\rho^2\begin{pmatrix}\cos 2\theta\\ \sin 2\theta\end{pmatrix} + \hat{B}_2\right\}. \tag{3.165}$$

The matching rules $\bar{\phi}^{(2,2)} \equiv \Phi^{(2,2)}$ and $\hat{\psi}^{(2,2)} \equiv \Psi^{(2,2)}$ yield the following:

$$\bar{A}_0 = \frac{\pi}{2\mathrm{i}}v_0 = \frac{\pi(1-P^2)}{4\pi}B_0, \quad \hat{A}_0 = 0, \tag{3.166}$$

$$(\bar{A}_1, \bar{A}_{-1}) = \frac{\pi}{4\mathrm{i}}\mathbf{u}_I^T\begin{pmatrix}-1 & 1\\ \mathrm{i} & \mathrm{i}\end{pmatrix}, \quad (\hat{A}_1, \hat{A}_{-1}) = \frac{\pi P}{4\mathrm{i}}\mathbf{u}_I^T\begin{pmatrix}\mathrm{i} & \mathrm{i}\\ 1 & -1\end{pmatrix}, \tag{3.167}$$

$$\bar{\mathbf{v}}_2 = -\frac{1}{4}\sum_{n=-2}^{2}\bar{A}_n(-1)^n\sum_{m=1}^{M_1}\frac{\bar{\sigma}_{nm}^{(1)}}{\delta_m}\mathbf{e}_{2m}, \quad \hat{\mathbf{v}}_2^T = (0,0), \tag{3.168}$$

$$\mathbf{u}_1 = \sum_{n=-2}^{2}\bar{A}_n(-1)^n\sum_{m=1}^{M_1}\frac{\bar{\sigma}_{nm}^{(1)}}{\delta_m}\mathrm{i}\mathbf{e}_{1m}. \tag{3.169}$$

By (3.162) and (3.168), we get

$$\mathbf{u}_0 = \frac{2}{1-P^2}\sum_{n=-2}^{2}\bar{A}_n(-1)^n\sum_{m=1}^{M_1}\frac{\bar{\sigma}_{nm}^{(1)}}{\delta_m}\mathbf{e}_{2m}. \tag{3.170}$$

To obtain a relation between $\mathbf{u}_1$ and $\mathbf{u}_I$, we need the order ϵ^3 inner terms $\bar{\phi}_3$ and $\hat{\psi}_3$ which satisfy the Poisson equations

$$\frac{1}{\rho}\frac{\partial}{\partial\rho}\left(\rho\frac{\partial\bar{\phi}_3}{\partial\rho}\right) + \frac{1}{\rho^2}\frac{\partial^2\bar{\phi}_3}{\partial\theta^2} = -\bar{\phi}_1$$

and

$$\frac{1}{\rho}\frac{\partial}{\partial\rho}\left(\rho\frac{\partial\hat{\psi}_3}{\partial\rho}\right)+\frac{1}{\rho^2}\frac{\partial^2\hat{\psi}_3}{\partial\theta^2}=-P^2\hat{\psi}_1$$

($\bar{\phi}_1$ and $\hat{\psi}_1$ and given by the terms in square brackets in, respectively, equations (3.156) and (3.157)). The required solutions of these Poisson equations are

$$\begin{aligned}\bar{\phi}_3=&-\left[\frac{B_1}{4}\rho^2+\frac{\rho^3}{8}\mathbf{u}_1^T\begin{pmatrix}\cos\theta\\ \sin\theta\end{pmatrix}+\frac{\rho}{2}\log\rho\mathbf{u}_I^T\begin{pmatrix}\cos\theta\\ \sin\theta\end{pmatrix}-\frac{1}{4}\mathbf{u}_2^T\begin{pmatrix}\cos 2\theta\\ \sin 2\theta\end{pmatrix}\right.\\ &\left.-\frac{1}{8\rho}\mathbf{u}_3^T\begin{pmatrix}\cos 3\theta\\ \sin 3\theta\end{pmatrix}\right]+\bar{\mathbf{w}}_1^T\rho\begin{pmatrix}\cos\theta\\ \sin\theta\end{pmatrix}+\bar{\mathbf{w}}_I^T\frac{1}{\rho}\begin{pmatrix}\cos\theta\\ \sin\theta\end{pmatrix}+\bar{\mathbf{w}}_2^T\rho^2\begin{pmatrix}\cos 2\theta\\ \sin 2\theta\end{pmatrix}\\ &+\bar{\mathbf{w}}_{II}^T\frac{1}{\rho^2}\begin{pmatrix}\cos 2\theta\\ \sin 2\theta\end{pmatrix}+\bar{\mathbf{w}}_3^T\rho^3\begin{pmatrix}\cos 3\theta\\ \sin 3\theta\end{pmatrix}+\bar{\mathbf{w}}_{III}^T\frac{1}{\rho^3}\begin{pmatrix}\cos 3\theta\\ \sin 3\theta\end{pmatrix}+\ \ldots\ +\bar{w}_0\log\rho,\end{aligned}\tag{3.171}$$

and

$$\begin{aligned}\bar{\psi}_3=&-P^2\left[\frac{\rho}{2}\log\rho\mathbf{u}_I^T\begin{pmatrix}0&1\\ -1&0\end{pmatrix}\begin{pmatrix}\cos\theta\\ \sin\theta\end{pmatrix}-\frac{1}{4}\mathbf{u}_2^T\begin{pmatrix}0&1\\ -1&0\end{pmatrix}\begin{pmatrix}\cos 2\theta\\ \sin 2\theta\end{pmatrix}\right.\\ &\left.-\frac{1}{8\rho}\mathbf{u}_3^T\begin{pmatrix}0&1\\ -1&0\end{pmatrix}\begin{pmatrix}\cos 3\theta\\ \sin 3\theta\end{pmatrix}\right]+\hat{\mathbf{w}}_1^T\rho\begin{pmatrix}\cos\theta\\ \sin\theta\end{pmatrix}+\hat{\mathbf{w}}_I^T\frac{1}{\rho}\begin{pmatrix}\cos\theta\\ \sin\theta\end{pmatrix}\\ &+\hat{\mathbf{w}}_2^T\rho^2\begin{pmatrix}\cos 2\theta\\ \sin 2\theta\end{pmatrix}+\hat{\mathbf{w}}_{II}^T\frac{1}{\rho^2}\begin{pmatrix}\cos 2\theta\\ \sin 2\theta\end{pmatrix}+\hat{\mathbf{w}}_3^T\rho^3\begin{pmatrix}\cos 3\theta\\ \sin 3\theta\end{pmatrix}\end{aligned}\tag{3.172}$$

$$+\hat{\mathbf{w}}_{III}^T\frac{1}{\rho^3}\begin{pmatrix}\cos 3\theta\\ \sin 3\theta\end{pmatrix}+\ \ldots\ +\hat{w}_0\log\rho,\tag{3.173}$$

where the ellipses indicate singular eigenfunctions in 4θ and 5θ. In these last equations, the terms in square brackets are particular solutions of the Poisson equations, and all other terms are eigenfunctions needed to satisfy the boundary conditions and effect the higher order matching. From the boundary conditions we get, in particular,

$$\mathbf{u}_I=-\tfrac{1}{2}\mathbf{u}_1.\tag{3.174}$$

Using equations (3.166)-(3.167), we now replace $\bar{A}_n$ and $\hat{A}_n$ in B_0 (equation 3.151), $\mathbf{u}_0$ (equation 3.170) and $\mathbf{u}_1$ (equation 3.169) to get

$$B_0=\frac{\pi L^2}{\mathcal{A}}\sum_{m=1}^{M_1}\frac{1}{\delta_m}[(1-P^2)B_0-\mathrm{i}\mathbf{e}_{1m}^T\mathbf{u}_1+\mathbf{e}_{2m}^T\mathbf{u}_0],\tag{3.175}$$

$$\mathbf{u}_0 = \frac{2}{1-P^2}\frac{\pi L^2}{\mathcal{A}}\sum_{m=1}^{M_1}\frac{\mathbf{e}_{2m}}{\delta_m}[(1-P^2)B_0 - \mathrm{i}\mathbf{e}_{1m}^T\mathbf{u}_1 + \mathbf{e}_{2m}^T\mathbf{u}_0] \tag{3.176}$$

and

$$\mathbf{u}_1 = \frac{\mathrm{i}\pi L^2}{\mathcal{A}}\sum_{m=1}^{M_1}\frac{\mathbf{e}_{1m}}{\delta_m}[(1-P^2)B_0 - \mathrm{i}\mathbf{e}_{1m}^T\mathbf{u}_1 + \mathbf{e}_{2m}^T\mathbf{u}_0]. \tag{3.177}$$

A system more amenable to further analysis is obtained by introducing

$$\overline{U}_m = \frac{1}{(1-P^2)\delta_m}\left[(1-P^2)B_0 - \mathrm{i}\mathbf{e}_{1m}^T\mathbf{u}_1 + \mathbf{e}_{2m}^T\mathbf{u_0}\right], \quad m = 1..M_1, \tag{3.178}$$

so that

$$B_0 = \frac{\pi L^2}{\mathcal{A}}\sum_{m=1}^{M_1}(1-P^2)\overline{U}_m, \quad \mathbf{u}_0 = \frac{2\pi L^2}{\mathcal{A}}\sum_{m=1}^{M_1}\mathbf{e}_{2m}\overline{U}_m, \tag{3.179}$$

and

$$\mathbf{u}_1 = \frac{\mathrm{i}\pi L^2}{\mathcal{A}}\sum_{m=1}^{M_1}(1-P^2)\mathbf{e}_{1m}\overline{U}_m, \tag{3.180}$$

and hence by substitution back in to equation (3.178)

$$\delta_p\overline{U}_p = \frac{\pi L^2}{\mathcal{A}}\sum_{m=1}^{M_1}\left[(1-P^2) + \mathbf{e}_{1p}^T\mathbf{e}_{1m} + \frac{2\mathbf{e}_{2p}^T\mathbf{e}_{2m}}{1-P^2}\right]\overline{U}_m, \quad p = 1..M_1. \tag{3.181}$$

For a given $\boldsymbol{\beta}$, equation (3.181) provides an eigenvalue problem for the corresponding wavenumber k_1 (which appears in each δ_p). The geometry of the lattice Λ appears through the reciprocal lattice vectors in the definitions of each δ_p, e_{1p} and e_{2p}.

For the perturbation of shear waves, a similar calculation yields

$$\hat{\delta}_p\widehat{U}_p = \frac{\pi L^2}{\mathcal{A}}\sum_{m=1}^{M_2}\left[\mathbf{e}_{1p}^T\mathbf{e}_{1m} + \frac{2P^2\mathbf{e}_{2p}^T\mathbf{e}_{2m}}{1-P^2}\right]\widehat{U}_m, \tag{3.182}$$

where

$$\hat{\delta}_p = (k_2^2 - \beta_m^2)L^2/k_2^2a^2. \tag{3.183}$$

Equations (3.182) define an eigenvalue problem for the shear wavenumber k_2. Comparing equations (3.181) and (3.182), we see that there is an extra term $1-P^2$ in (3.181). This arises from the form of the boundary condition for σ_{rr} in equation (3.80) which contains a non-derivative term in ϕ; this generates a monopole, and hence the additional term, in the perturbed dilatational wave, but not in the perturbed shear wave.

It is also possible for the frequency of an unperturbed dilatational wave to coincide with the frequency of an unperturbed shear wave. The simultaneous perturbation of dilatational and shear waves will, in general, result in a pair of coupled eigenvalue problems for the wavenumbers k_1 and k_2 and these may be written as

$$\bar{\delta}_{p_1}\overline{U}_{p_1} = \frac{\pi L^2}{\mathcal{A}}\sum_{m_1=1}^{M_1}\left[(1-P^2)+\mathbf{e}_{1m_1}^T\mathbf{e}_{1p_1}+\frac{2}{1-P^2}\mathbf{e}_{2m_1}^T\mathbf{e}_{2p_1}\right]\overline{U}_{m_1}$$
$$+\frac{\pi L^2}{\mathcal{A}}\sum_{m_2=1}^{M_2}\left[P\mathbf{e}_{1m_2}^T\begin{pmatrix}0&-1\\1&0\end{pmatrix}\mathbf{e}_{1p_1}+\frac{2P^2}{1-P^2}\mathbf{e}_{2m_2}^T\begin{pmatrix}0&-1\\1&0\end{pmatrix}\mathbf{e}_{2p_1}\right]\widehat{U}_{m_2}, \quad (3.184)$$

and

$$\hat{\delta}_{p_2}\widehat{U}_{p_2} = \frac{\pi L^2}{\mathcal{A}}\sum_{m_1=1}^{M_1}\left[P\mathbf{e}_{1m_1}^T\begin{pmatrix}0&1\\-1&0\end{pmatrix}\mathbf{e}_{1p_2}+\frac{2P^2}{1-P^2}\mathbf{e}_{2m_1}^T\begin{pmatrix}0&1\\-1&0\end{pmatrix}\mathbf{e}_{2p_2}\right]\overline{U}_{m_1}$$
$$+\frac{\pi L^2}{\mathcal{A}}P^2\sum_{m_2=1}^{M_2}\left[\mathbf{e}_{1m_2}^T\mathbf{e}_{1p_2}+\frac{2P^2}{1-P^2}\mathbf{e}_{2m_2}^T\mathbf{e}_{2p_2}\right]\widehat{U}_{m_2}, \quad (3.185)$$

where $p_1 = 1..M_1$, $p_2 = 1..M_2$. Here the barred terms refer to the perturbed dilatational wave, and the hatted terms to the perturbed shear wave. It is noteworthy that in the case $M_1 = M_2 = 1$, that is the perturbation of one dilatational and one shear wave, the off-diagonal terms in the system matrix are zero and the equations decouple. Equations (3.184) and (3.185) include the cases of the perturbed dilatational waves and shear wave already considered separately; with $\widehat{U}_{m_2} = 0$, equation (3.184) reduces to (3.181), and with $\overline{U}_{m_1} = 0$ equation (3.185) reduces to (3.182).

Results

In this part, we give some examples of explicit approximations to the dispersion relation for perturbed dilatational and shear waves, obtained from the eigenvalue problems in equations (3.181)–(3.185) with the aid of the computer-algebra package Mathematica. Then, some of these approximations are compared with numerical results, therefore the physics constants $\lambda/\mu = 2.3$ is also adopted here. The areas of the primitive cells for square and hexagonal lattices are respectively $\mathcal{A} = L^2$ and $\mathcal{A} = \sqrt{3}L^2/2$.

A. Perturbations of a single plane wave

In the case $M = 1$, equation (3.181) for the perturbation of a dilatational wave reduces to

$$k_1^2 = \beta_1^2 \left[1 + \frac{\pi a^2}{\mathcal{A}} \left(\frac{\lambda}{\mu} + \frac{2\mu}{\lambda + \mu} \right) \right]^{-1}, \tag{3.186}$$

while equation (3.182) for the perturbation of a shear wave gives

$$k_2^2 = \beta_1^2 \left[1 + \frac{\pi a^2}{\mathcal{A}} \left(\frac{\lambda + 3\mu}{\lambda + \mu} \right) \right]^{-1}. \tag{3.187}$$

We can see these results agree with those corrected results obtained by the quasi-static limit (3.113) and (3.114). Actually, these expressions give perturbations of any of the one-pole solutions illustrated in the dispersion diagrams in figures 3.7 and 3.8, regardless of their frequency (i.e. not just for the quasi-static limit), because the only restriction of our method is that the cylinder size is much smaller than the wavelengh. We can see the information about the lattice is not included in equations (3.186) and (3.187), so they actually provide perturbed dispersion relations for an uniform elastic material. As noted at the end of the previous section, this includes any points in the diagrams where one-pole dilatational- and shear-wave modes cross. For the lowest dilatational mode and two-lowest shear modes, and along the line GM of the irreducible Brillouin zone, the present approximations are compared in figure 3.9 with numerical calculations made using the multipole method described by Zalipaev *et al.* (2002), and generally good agreement is observed. The divergence of the curves near the ends of GM is because of the presence of higher-order poles – see figures 3.7 and 3.8.

B. Perturbations of two plane waves

Approximations at appropriate isolated points in the dispersion diagram lead to estimates of local band gaps, and this is illustrated here by consideration of a two-pole solution corresponding to the perturbation of shear waves at the point M in the reciprocal lattice. For the square lattice, the unperturbed values considered are $(q_1 L, q_2 L, k_2 L) = (\pi, 0, 3\pi)$, and within some neighbourhood of this point the appropriate forms for the $\boldsymbol{\beta}_m$ are

$$\boldsymbol{\beta}_1 L = (q_1 L + 2\pi, q_2 L)^T, \ \boldsymbol{\beta}_2 L = (q_1 L - 4\pi, q_2 L)^T \tag{3.188}$$

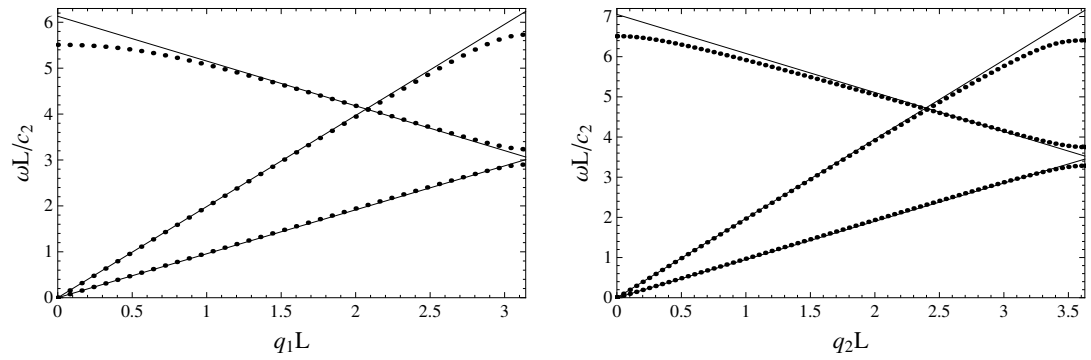

Figure 3.9: Comparison of the present approximations (——) with numerical calculations ($\cdots$) for circles of radius $a = 0.1L$ along GM in a square lattice (left), and a hexagonal lattice (right). With the curves ordered according to their behaviour near $q_1L, q_2L = \pi$, the lowest two curves are perturbations of a shear wave, and the remaining curve is a perturbed dilatational wave.

(this is because when $(q_1L, q_2L) = (\pi, 0)$, $\beta_1L = \beta_2L = 3\pi \equiv k_2L$). For $q_2 = 0$ and in the limit $q_1L \to \pi$, the positive roots of equation (3.182) are

$$k_2L = \frac{3\pi}{\sqrt{1 - 2\pi a^2/L^2}}, \quad \frac{3\pi}{\sqrt{1 + 4\pi P^2 a^2/(P^2-1)L^2}}. \tag{3.189}$$

Similarly, for the hexagonal lattice, with $(q_1L, q_2L, k_2L) = (0, 2\pi/\sqrt{3}, 6\pi/\sqrt{3})$ there are again two poles and the appropriate forms for the $\boldsymbol{\beta}_m$ are

$$\boldsymbol{\beta}_1L = (q_1L, q_2L + 4\pi/\sqrt{3})^T, \ \boldsymbol{\beta}_1L = (q_1L, q_2L - 8\pi/\sqrt{3})^T. \tag{3.190}$$

For $q_1L = 0$ and in the limit $q_2L \to 2\pi/\sqrt{3}$, the positive roots of equation (3.182) are

$$k_2L = \frac{2\sqrt{3}\pi}{\sqrt{1 - 4\pi a^2/\sqrt{3}L^2}}, \quad \frac{2\sqrt{3}\pi}{\sqrt{1 + 8\pi P^2 a^2/\sqrt{3}(P^2-1)L^2}}. \tag{3.191}$$

Equations (3.189) and (3.191) illustrate explicitly the appearance of local band gaps as the radius of the cylinder is increased from zero. In each case, the upper point of the local band gap is independent of the Lamé constants and is determined by the geometry alone. The solution surfaces are shown in figure 3.10, in which we can clearly see the appearance of the local band gaps.

Two-pole lines in the unperturbed dispersion diagrams in figures 3.7 and 3.8 will, in general, split into two modes when the scatterers are present. This is shown firstly for the lowest dilatational two-pole mode on MK with the hexagonal lattice, for which $q_2L = 2\pi/\sqrt{3}$ and $q_1L \in (0, 2\pi/3)$, and the appropriate forms for $\boldsymbol{\beta}_m$ are

$$\boldsymbol{\beta}_1L = (q_1L, q_2L)^T, \ \boldsymbol{\beta}_2L = (q_1L, q_2L - 4\pi/\sqrt{3})^T. \tag{3.192}$$

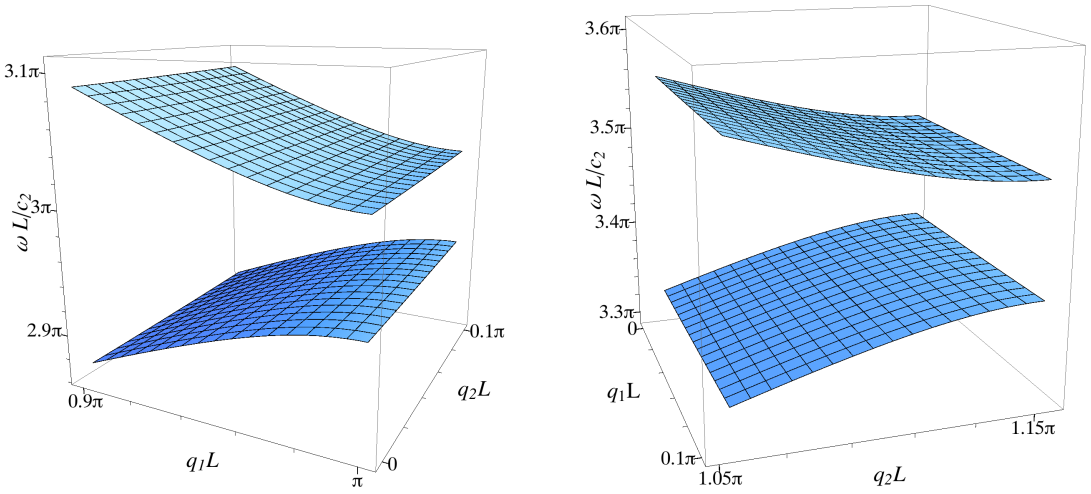

Figure 3.10: Left: solution surfaces in the vicinity of $(q_1L, q_2L, kL) = (\pi, 0, 3\pi)$ for square lattice. Right: solution surfaces in the vicinity of $(q_1L, q_2L, kL) = (0, 2\pi/\sqrt{3}, 6\pi/\sqrt{3})$ for hexagonal lattice. Circle radius $a = L/20$.

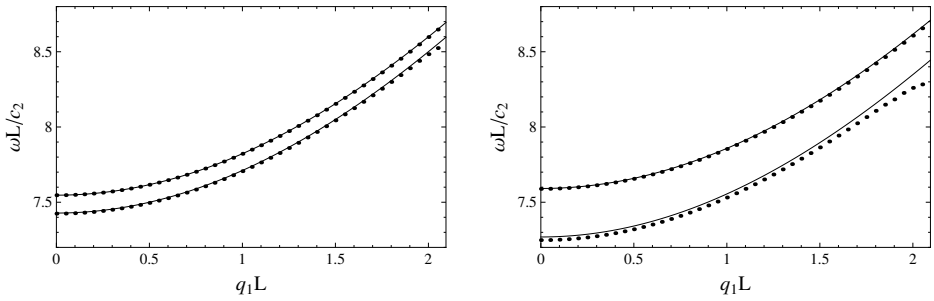

Figure 3.11: Splitting of the lowest two pole dilatational mode along MK for a hexagonal lattice; comparison of the present approximations (——) with numerical calculations ($\cdots$). Left: radius $a = 0.03L$. Right: radius $a = 0.05L$.

The corresponding positive roots of (3.181) are

$$k_2L = \frac{P(4\pi^2 + 3(q_1L)^2)^{3/2}}{\sqrt{27(q_1L)^4 + 24\pi^2(q_1L)^2\left(3 - 2\sqrt{3}\frac{\pi a^2}{L^2}\frac{P^2-9}{P^2-1}\right) + 16\pi^4(3 - 4\sqrt{3}\frac{\pi a^2}{L^2})}}, \tag{3.193}$$

and

$$k_2L = \frac{P(4\pi^2 + 3(q_1L)^2)^{3/2}}{\sqrt{9c_4(q_1L)^4 + 24\pi^2c_2(q_1L)^2 + 16\pi^4c_0}}, \tag{3.194}$$

where

$$c_0 = 3 + 4\sqrt{3}\frac{\pi a^2}{L^2}\frac{P^4 - 2P^2 + 3}{P^2 - 1},\ c_2 = 3 + 2\sqrt{3}\frac{\pi a^2}{L^2}\frac{2P^4 - 5P^2 - 1}{P^2 - 1}, \tag{3.195}$$

$$c_4 = 3 + 4\sqrt{3}\frac{\pi a^2}{L^2}\frac{P^4 - 3P^2 + 4}{P^2 - 1}. \tag{3.196}$$

These solutions are graphed in figure 3.11 which shows how the gap increases with the radius of the cylinder. In figure 3.8, it may be seen that a two-pole shear mode crosses near K but, for simplicity, this is not taken into account here.

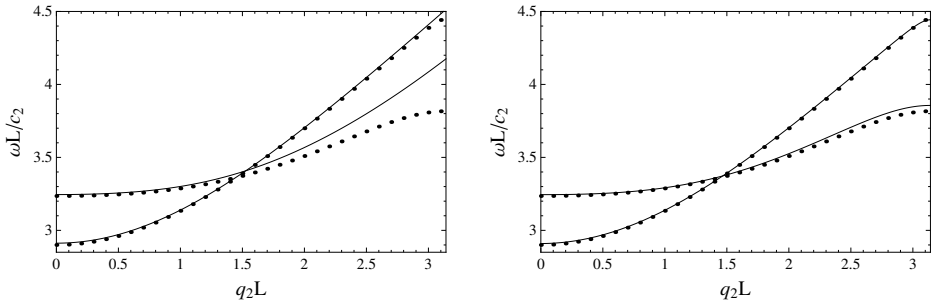

Figure 3.12: Perturbation of the lowest two-pole mode along MK for a square lattice; comparison of the present approximations (——) with numerical calculations ($\cdots$) for a circle of radius $a = 0.1L$. Left: two-pole approximation. Right: four-pole approximation.

Split modes may also cross and this is illustrated using the lowest (shear) two-pole line on MK in figure 3.7 for the square lattice, for which $q_1 L = \pi$ and $q_2 L \in (0, \pi)$, and the appropriate forms for $\boldsymbol{\beta}_m$ are

$$\boldsymbol{\beta}_1 L = (q_1 L, q_2 L)^T,\ \boldsymbol{\beta}_2 L = (q_1 L - 2\pi, q_2 L)^T. \tag{3.197}$$

For these values, the positive roots of equation (3.182) are

$$k_2 L = (k_2 L)_1 \equiv \frac{\left[(q_2 L)^2 + \pi^2\right]^{3/2}}{\sqrt{(q_2 L)^4 + 2\pi^2 (q_2 L)^2 \left[1 + \frac{\pi a^2}{L^2}\frac{7P^2+1}{P^2-1}\right] + \pi^4 \left[1 - \frac{2\pi a^2}{L^2}\right]}}, \tag{3.198}$$

and

$$k_2 L = (k_2 L)_2 \equiv \frac{\left[(q_2 L)^2 + \pi^2\right]^{3/2}}{\sqrt{c_4 (q_2 L)^4 + 2\pi^2 c_2 (q_2 L)^2 + \pi^4 c_0}}, \tag{3.199}$$

where

$$c_0 = 1 + \frac{4\pi a^2}{L^2}\frac{P^2}{P^2 - 1},\ c_2 = 1 - \frac{\pi a^2}{L^2}\frac{5P^2 - 1}{P^2 - 1},\ c_4 = 1 + \frac{2\pi a^2}{L^2}\frac{P^2 + 1}{P^2 - 1}.$$

The gap between the two curves depends on the radius of the scatterer and is

$$(k_2L)_1 - (k_2L)_2 = \pi \frac{(q_2L)^4(P^2+1) - 12\pi^2P^2(q_2L)^2 + \pi^4(3P^2-1)}{(P^2-1)(\pi^2+(q_2L)^2)^{3/2}} \left(\frac{a}{L}\right)^2 + O\left(\frac{a^4}{L^4}\right) \quad (3.200)$$

so that, to a first approximation, the two lines cross at

$$q_1L = \pi\sqrt{\frac{6P^2 - \sqrt{1-2P^2+33P^4}}{P^2+1}}; \quad (3.201)$$

to the left of this point $(k_2L)_1$ is the upper mode, and $(k_2L)_2$ is the lower mode. The above approximations are compared with numerical solutions in the left-hand graph of figure 3.12. The approximations are worst near the right-hand end of the range of q_2L due to the proximity of the four-pole point at K. One feature of the present method is that solutions valid in the neighbourhood of higher-order poles blend smoothly in to lower-order solutions, and hence the former may be used outside their apparent range of validity. This may be shown explicitly in simple cases, and is illustrated graphically in the right-hand graph of figure 3.12 which uses the four-pole approximation (not given explicitly here) from the point K across the whole of MK.

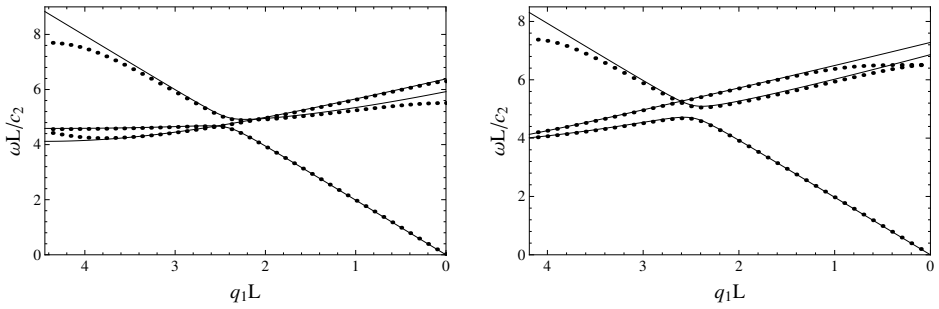

Figure 3.13: The comparison between the present approximation (——) with numerical calculations (· · ·) of the lowest cross point of one dilatational wave and two shear waves on KG for a circle of radius a=0.1L. Left: square lattice. Right: hexagonal lattice.

As well as mode splitting, there can be mode switching where, in the unperturbed dispersion diagram, shear and dilatational modes cross. This is illustrated in figure 3.13 for the intersection of the lowest two-pole shear modes in KG with a dilatational mode. The local solution at the three-pole intersection point correctly shows the switching between the dilatational mode and one of the shear modes. The approximation degrades towards the ends of the range because of the proximity of higher-order poles.

C. Perturbations of three plane waves

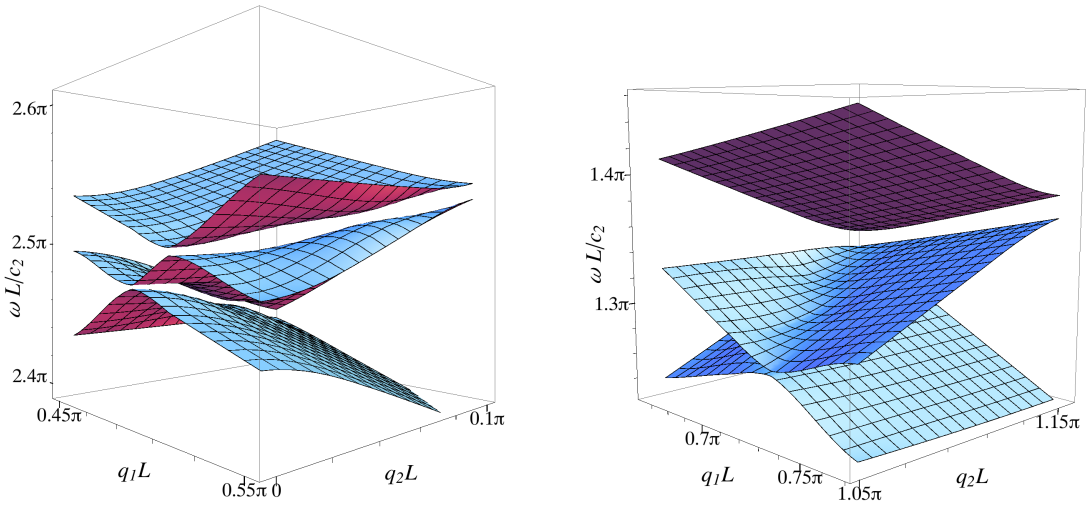

Figure 3.14: Left: solution surfaces in the vicinity of $(q_1L, q_2L, kL) = (\pi/2, 0, 5\pi/2)$ for square lattice. Right: solution surfaces in the vicinity of $(q_1L, q_2L, kL) = (2\pi/3, 2\pi/\sqrt{3}, 4\pi/3)$ for hexagonal lattice. Circle radius $a = L/20$.

For square lattice, at $(q_1L, q_2L, k_2L) = (\pi/2, 0, 5\pi/2)$, there are three poles of the lattice sums that correspond to three unperturbed plane waves, and within some neighbourhood of this point the appropriate forms for the β_m are

$$\boldsymbol{\beta}_1 L = (q_1L + 2\pi, q_2L)^T,\ \boldsymbol{\beta}_2 L = (q_1L - 2\pi, q_2L + 2\pi)^T,\ \boldsymbol{\beta}_3 L = (q_1L - 2\pi, q_2L - 2\pi)^T. \tag{3.202}$$

For hexagonal lattice, at $(q_1L, q_2L, k_2L) = (2\pi/3, 2\pi/\sqrt{3}, 4\pi/3)$ there are three poles and for calculations within a neighbourhood of this point the forms

$$\boldsymbol{\beta}_1 L = (q_1L, q_2L)^T,\ \boldsymbol{\beta}_2 L = \left(q_1L, q_2L - \frac{4\pi}{\sqrt{3}}\right)^T,\ \boldsymbol{\beta}_3 L = \left(q_1L - 2\pi, q_2L - \frac{2\pi}{\sqrt{3}}\right)^T. \tag{3.203}$$

The solutions are shown in figure 3.14.

D. Perturbations of four plane waves

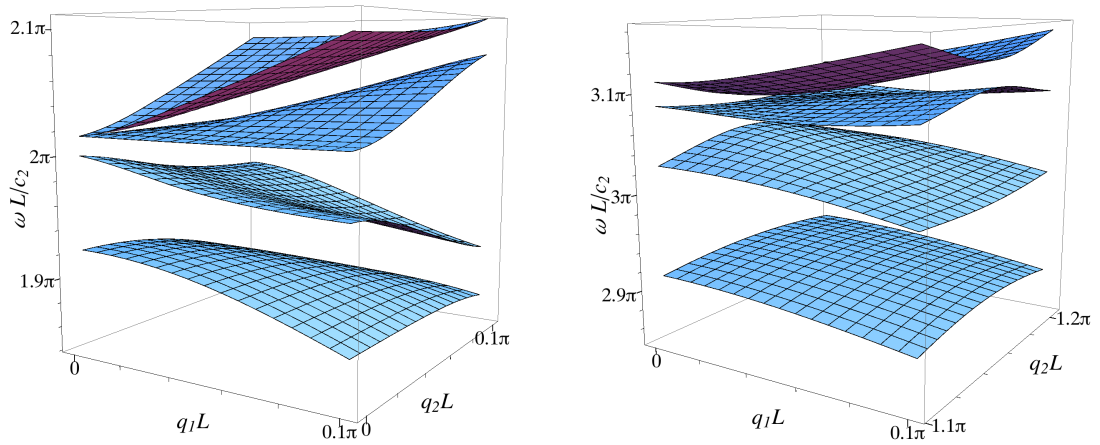

Figure 3.15: Left: solution surfaces in the vicinity of $(q_1L, q_2L, kL) = (0, 0, 2\pi)$ for square lattice. Right: solution surfaces in the vicinity of $(q_1L, q_2L, kL) = (0, 2\pi/\sqrt{3}, 2\sqrt{21}\pi/3)$ for hexagonal lattice. Circle radius $a = L/20$.

For square lattice, at $(q_1L, q_2L, k_2L) = (0, 0, 2\pi)$, there are three poles of the lattice sums that correspond to three unperturbed plane waves, and within some neighbourhood of this point the appropriate forms for the β_m are

$$\boldsymbol{\beta}_{1,2}L = (q_1L \pm 2\pi, q_2L)^T,\ \boldsymbol{\beta}_{3,4}L = (q_1L, q_2L \pm 2\pi)^T. \tag{3.204}$$

For hexagonal lattice, at $(q_1L, q_2L, k_2L) = (2\pi, 0, 2\sqrt{21}\pi/3)$ there are three poles and for calculations within a neighbourhood of this point the forms

$$\boldsymbol{\beta}_{1,2}L = \left(q_1L, q_2L \pm \frac{4\pi}{\sqrt{3}}\right)^T,\ \boldsymbol{\beta}_{3,4}L = \left(q_1L - 4\pi, q_2L \pm \frac{4\pi}{\sqrt{3}}\right)^T. \tag{3.205}$$

The solutions are shown in figure 3.15.

Comparison

The accuracy of the approximations by matched asymptotic expansions is indicated in figure 3.16 and 3.17 through three comparisons with numerical calculations for circular cylinders made with Poulton *et al.* [77] and Zalipaev *et al.* [105]. It is shown that the current approximations are more accurate for smaller cylinder radius as we expected. As seen from the diagrams, our method provides very good approximations for cylinders of radius up to $a/L = 0.05$ for both square and hexagonal lattices. For the two-pole mode

in square lattice and three-pole mode in hexagonal lattice we choose, the approximations are still good for cylinders of radius up to $a/L = 0.1$.

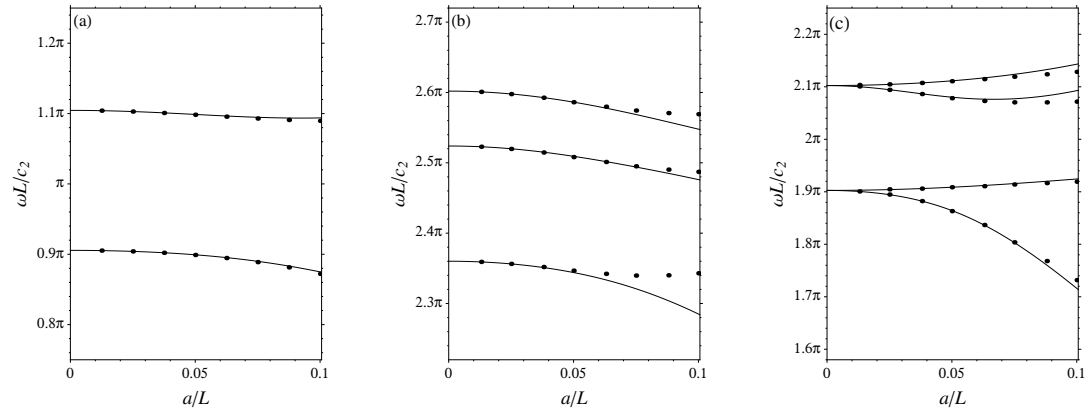

Figure 3.16: Square array: comparison of the present approximations (——) with numerical calculations $(\cdots)$ for a circle of diameter 2a. (a) $(q_1L, q_2L) = (\frac{9}{10}\pi, \frac{1}{10}\pi)$, (b) $(q_1L, q_2L) = (\frac{3}{5}\pi, \frac{1}{10}\pi)$, (c) $(q_1L, q_2L) = (\frac{1}{10}\pi, \frac{1}{10}\pi)$

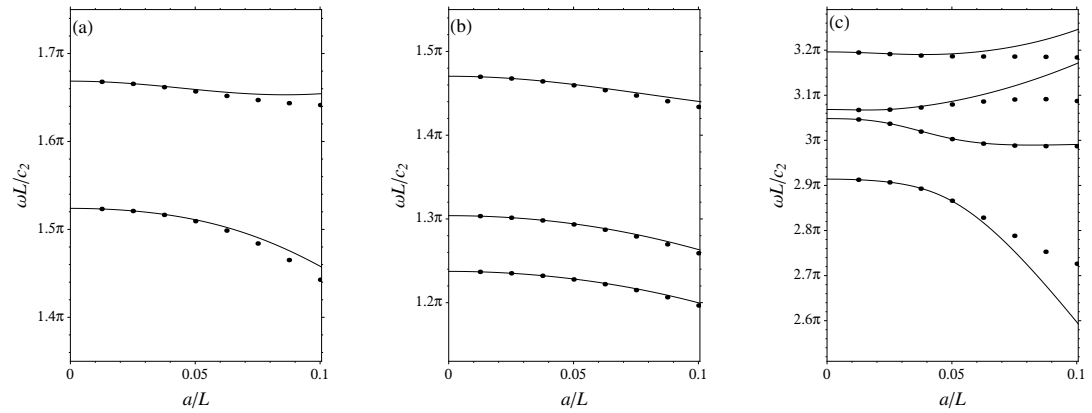

Figure 3.17: Hexagonal array: comparison of the present approximations (——) with numerical calculations $(\cdots)$ for a circle of diameter 2a. (a) $(q_1L, q_2L) = (\frac{9}{10}\pi, \frac{1}{10}\pi)$, (b) $(q_1L, q_2L) = (\frac{37}{10}\pi, \frac{1}{10}\pi)$, (c) $(q_1L, q_2L) = (\frac{21}{10}\pi, \frac{1}{10}\pi)$

Chapter 4

Multiple resonant scattering by two-dimensional arrays

The multiple resonant scattering by two-dimensional arrays for both acoustic and elastic waves are considered in this chapter. Envelope equations (equations about the wave amplitudes with space and time variations) are obtained with the help of results from matched asymptotic expansions in chapter 3 and the method of multiple scales. These equations are then applied to a finite width (only finite in one direction) strip of two-dimensional arrays of cylinders to investigate how waves propagate in the array. The multiple scattering theory for infinite gratings can be traced back to the work by Twersky [91], which followed his earlier work on finite gratings [88, 89, 90]. Integral equation method is used to obtain a formalism for scattering of waves by infinite gratings. The same method is then used on more complicated scatterer geometries, for example Ivanov [31] considered the plane wave diffraction by N-layer gratings and some other cross-section scatterers are considered as well in [33, 34, 37]. Miles [62] combined results of Rayleigh [80] for a single scatter with those of Burke and Twersky [11] to compute explicit expressions for the reflection and transmission coefficients when a plane wave is normally incident on a grating of inclined flat screens. Then Porter and Evans [76] considered the oblique incidence with an infinite array of in-line periodic screens or breakwaters in finite water depth using linear water-wave theory. Using Wiener-Hopf technique, Erbaş and Abrahams [20] considered the scattering of sound waves by infinite grating of rigid plates.

In the multiple scattering theory, the research on the wave interaction with arrays of offshore structure can have variable applications, such as to design floating bridges, construct offshore wave-power station or airport etc. A review paper about the water wave interaction with arrays of structures is available given by McIver [59] in 2002. Because the array contains multiple scatterers, the cumulative effects of the wave motion may be significant. This is first demonstrated by Heathershaw [27], who investigated the water wave resonant interactions between surface water waves and finite numbers of bars installed on the bottom of a long wave tank. Mei [56] then gave a theory of resonant reflection by periodic sandbars using the WKB method (for example, see [15, section 7.3]). Li and Mei [49] considered the multiple resonant scattering of surface water waves by a periodic two-dimensional array of vertical cylinders standing across the depth of an open sea. This can provide theoretical support for offshore airports consisting of a platform supported above water by vertical piles. For material economy, it is assumed that the scatterer size a is smaller than both the array periodicity and the wavelength $1/\beta$, therefore a small parameter $\epsilon_1 = \beta a$ is involved. Although the scattered wave from one small cylinder is of the order ϵ_1^2 [79] compared to the incident wave, it is shown that the accumulated effects of many cylinders over a large region of length scale $1/\epsilon_1^2$ become significant when Bragg condition is nearly met. Therefore the asymptotic method of multiple scales is applicable to use combined with the Bloch theorem because of the periodicity of the cylinder array. This paper followed their earlier work [48] which considered the Bragg scattering by one-dimensional cylinder array in a waveguide. In another paper by Tabaei and Mei [86], they assessed the effects of viscous effects in the boundary layers around the cylinders on the Bragg resonance of surface water waves by a two-dimensional array. The theories for offshore structures have also been studied by others [36, 38, 58].

As Li and Mei [49] assumed the water depth is constant and the array is composed of vertical cylinders, this problem is actually equivalent to a two dimensional acoustic problem with an array of rigid cylinders. Therefore in the first section of this chapter, we first reproduce their results for the corresponding acoustic case by the method of matched asymptotic expansions and multiple scales and then generalise this theory to arbitrary cross section cylinder arrays. The comparison among four different types of cylinders are given for the transmission wave intensity.

In the second part, we consider a semi-infinite array of cylinders, where the number of the boundary conditions are not enough to obtain a unique solution to the envelope equations and an additional condition that waves can not propagate from infinity must be imposed. The wave interactions with semi-infinite structures can be applied to help study the scattering by a large finite array. The wave scattering by semi-infinite arrays were firstly studied by Millar [61] in 1964 using the analysis of a nonlinear integral equation. Some other results were obtained for widely spaced small circular cylinders [29] and for strip gratings [68, 69]. Hills and Karp [28] and Linton and Martin [51] considered the interaction of plane acoustic waves with a linear, semi-infinite array of isotropic point scatterers. Linton *et al.* [52] also considered the acoustic scattering by a semi-infinite array and the excitation of surface waves by using the solutions of the corresponding infinite array. In [96], Tymis and Thompson considered the low-frequency scattering by a two-dimensional semi-infinite lattice of cylinders using the Wiener-Hopf technique (see, for example, [53, page 130]).

In the last section of this chapter, we apply this theory to the elastic resonant scattering, where the cavity cylinder array is embedded in an elastic medium bounded by the same acoustic media on both sides. In this case, the boundary conditions involve the continuity of the stress besides the continuity of the velocity. Numerical results are given for a copper layer with cavity cylinders bounded by air on both sides. Many practical situations involve composite layers of a finite width, for example, the heat exchanger in industry which usually contains a finite array of tube bundles. Another application is the design of sound filter or noise control system. Some methods have been used to consider how the wave propagates in these structures. For example, Lakhtakia and Varadan considered the scattering by an elastic slab containing a one-dimensional periodic array of elastic cylinders for incident SH wave (horizontally polarised shear wave) [44], P wave (or seismic wave, is a kind of dilatational wave) and SV wave (vertically polarised shear wave) [45] to assess the reflection characteristics using the methods of Fourier-Bessel expansions and T-matrix. The T-matrix method [100] is also used to describe the reflection and transmission characteristics. For the finite width two-dimensional arrays, Scarpetta and Sumbatyan [82] investigated the plane wave propagation through a finite doubly periodic array of cracks to give explicit representations for the reflection and transmis-

sion coefficients. Platts *et al.* [75] evaluated the reflection and transmission matrices for a stack of layers which contains a finite array of circular cylindrical cavities using the multipole expansions. The layer multiple scattering method is also used for the similar problems of both one-dimensional gratings [12] and two-dimensional finite width gratings [81].

4.1 Acoustic resonant scattering by a finite array

In this section, we consider the acoustic resonant scattering by a finite width strip of array of rigid cylinders, see figure 4.1. The cylinders are surrounded by an infinite acoustic medium in and out of the array. Given the Cartesian coordinates (x, y, z), the strip is assumed to be finite in x- direction and infinite in y- and z- direction. An incident wave propagates in the positive direction of the x- axis and resonance can happen in the strip for some particular wavenumbers. As we know, the scattered wave from one cylinder is in higher order of the small parameter compared with the incident wave [79] and the scattered wave would not be weak any more over the scattering by a large number of cylinders. Therefore the strip width must be large enough to make the resonance occur. This makes it possible to consider this problem in an infinite array first and then apply the results to approximate those in finite arrays. The size of the cylinder is still assumed to be smaller than both the wavelength and the array periodicity. Both matched asymptotic expansions and multiple scales are used to obtained the envelope equations. So here we first obtain the envelope equations for an infinite array and then they are applied to a strip of cylinder array to give numerical calculations.

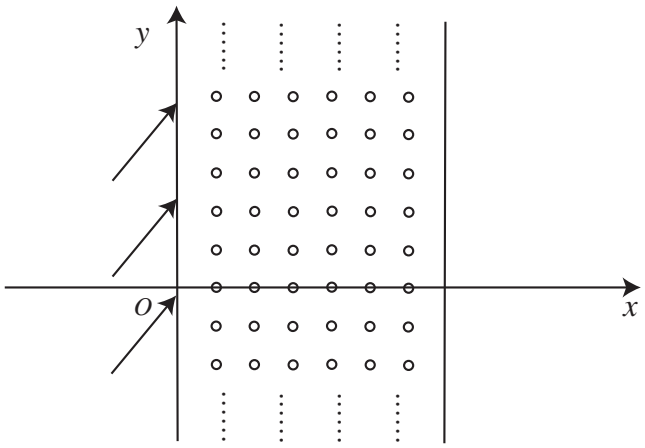

Figure 4.1: Strip

4.1.1 Circular cylinder scatterers

We consider the diffraction of plane acoustic waves by a two-dimensional array of vertical cylinders. The coordinates we use in this chapter are exactly the same as those in chapter 3. Origin O of the Cartesian coordinates (x, y, z) is on the axis of one of the cylinders. The cylinders are infinitely long with axes in the direction of z direction. Polar coordinates with origin O in the x-y plane are denoted by (r, θ). Scatterer j is associated with a local origin O_j located at the lattice point

$$\mathbf{R_j} = n_1\mathbf{a}_1 + n_2\mathbf{a}_2, \quad n_1, n_2 \in \mathbb{Z}, \tag{4.1}$$

for given independent vectors $\mathbf{a}_1$ and $\mathbf{a}_2$. Local polar coordinates (r_j, θ_j) are used with origin at O_j, then the position of any point in space is

$$\mathbf{r} = \mathbf{R}_j + \mathbf{r}_j. \tag{4.2}$$

If the periodic array is infinite in extent, Bloch's theorem requires that a linear wave solution obeys the condition

$$\Phi(\mathbf{r} + \mathbf{R}_j) = \mathrm{e}^{\mathrm{i}\boldsymbol{\beta}_1^T\mathbf{R}_j}\Phi(\mathbf{r}), \tag{4.3}$$

where $\mathbf{r} = (x, y)^T$, $\boldsymbol{\beta}_1$ is the Bloch wave vector.

Another wave in the direction of $\boldsymbol{\beta}_m$ is said to be resonantly scattered if $\boldsymbol{\beta}_m$ and $\boldsymbol{\beta}_1$ are related to a reciprocal lattice vector $\mathbf{K}_m$ (defined in (3.69)) by the Bragg condition

$$\boldsymbol{\beta}_m = \boldsymbol{\beta}_1 + \mathbf{K}_m, \tag{4.4}$$

where $\beta_m = |\boldsymbol{\beta}_m|$ is the same for any m and thus we define $\beta = |\boldsymbol{\beta}_m|$. If more than one wave is resonantly scattered, any two resonated wave vectors are related by

$$\boldsymbol{\beta}_n = \boldsymbol{\beta}_m + \mathbf{K}_n - \mathbf{K}_m. \tag{4.5}$$

The method of Ewald construction described in chapter 3, see figure 3.6, can be used to find the resonantly scattered waves. Draw a circle centred at the initial point P of $\boldsymbol{\beta}_1$ with radius β. Then if another reciprocal lattice points P_2 falls on this circle, the vector $\overrightarrow{PP_2}$ is the resonantly scattered wave vector $\boldsymbol{\beta}_2$, i.e. they satisfy the Bragg resonance condition (4.4). For specified lattice and Bloch vector, there may be M vectors falling on that circle. Figure 3.6 gives an example when $M = 3$.

Now we are going to derive the envelope equations for the incident wave and $M-1$ resonantly scattered waves. The velocity potential Φ must satisfy the wave equation

$$\frac{\partial^2 \Phi}{\partial t^2} - c^2 \nabla^2 \Phi = 0, \tag{4.6}$$

everywhere in the medium, where c is the acoustic wave speed and ∇ is the gradient operator in the x-y plane. On the boundary of the cylinders, the normal flux must vanish

$$\frac{\partial \Phi}{\partial r_j} = 0, \ r_j = |\mathbf{r} - \mathbf{R}_j| = a, \ \text{for all } j. \tag{4.7}$$

We have assumed that the cylinder radius a is much smaller than the typical wavelength $2\pi/\beta$ so that

$$\epsilon_1 = \beta a \ll 1, \tag{4.8}$$

is a small parameter (we use ϵ_1 rather than ϵ because here the small parameter is the product of the Bloch wavenumber and radius of the cylinder. This is different from the one used in chapter 3, where it is the product of the dilatational wavenumber and the radius of the cylinder). When the spacing L between successive scatterers and the wavelength and the incident angle θ satisfy the relation,

$$\beta L = \frac{n_B \pi}{\sin\theta},$$

where n_B is a positive integer, constructive interference gives rise to strong reflection. Since the reflection coefficient from a single cylinder is of order ϵ_1^2 compared to the incident wave, then the accumulated effects over N cylinders becomes of strictly order

one when N is order $1/\epsilon_1^2$. It follows that strong reflection evolves over the dimensionless length scale $\beta(x,y) = O(1/\epsilon_1^2)$. This suggests the asymptotic method of multiple scales is applicable. Therefore we now introduce fast and slow variables

$$x,\ y,\ t;\ X = \epsilon_1^2 x,\ Y = \epsilon_1^2 y,\ T = \epsilon_1^2 t, \tag{4.9}$$

so that $x,\ y,\ t$ describe the fast motion while $X,\ Y,\ T$ describe the slow variation of the envelope. With these fast and slow variables, the differential operators become

$$\frac{\partial}{\partial x} = \frac{\partial}{\partial x} + \epsilon_1^2 \frac{\partial}{\partial X}, \quad \frac{\partial}{\partial y} = \frac{\partial}{\partial y} + \epsilon_1^2 \frac{\partial}{\partial Y}, \quad \frac{\partial}{\partial t} = \frac{\partial}{\partial t} + \epsilon_1^2 \frac{\partial}{\partial T}.$$

The method of matched asymptotic expansions is also used here. Each cell is divided into two regions: the inner region around the scatterer $r_j \ll \beta^{-1}$ and the outer region far from the scatterer $r_j \gg a$, on which inner solutions and outer solutions will be developed respectively.

As the boundary-value problem is homogeneous, the leading order outer solution may be taken as strictly order one in ϵ_1, then we expand the outer solution as follows

$$\Phi = Re\{[\Phi_0 + \epsilon_1^2 \Phi_2 + O(\epsilon_1^4)]\mathrm{e}^{-\mathrm{i}\omega t}\}, \tag{4.10}$$

where Φ_0 and Φ_2 are functions of $(x,\ y,\ X,\ Y,\ T)$ and ω is the frequency associated with β (i.e. $\omega = \beta c$). Substituting (4.10) into the governing equations (4.6), we obtain the perturbation equations for the outer potentials Φ_0 and Φ_2.

The first order outer velocity potential Φ_0 satisfies the wave equation

$$\nabla^2 \Phi_0 = -\frac{\omega^2}{c^2} \Phi_0, \tag{4.11}$$

and also the Bloch's theorem (4.3). The solution form for Φ_0 is the sum of plane waves combined with the envelopes A_m

$$\Phi_0 = \sum_{m=1}^{M} A_m(X,Y,T)\psi_m(x,y), \tag{4.12}$$

where

$$\psi_m(x,y) = \mathrm{e}^{\mathrm{i}\boldsymbol{\beta}_m^T \mathbf{r}}, \tag{4.13}$$

with all $\boldsymbol{\beta}_m = \beta \mathbf{e}_{1m}$ determined by the Bragg condition (4.4). Here

$$\mathbf{e}_{pm} = \begin{pmatrix} \cos p\tau_m \\ \sin p\tau_m \end{pmatrix}. \tag{4.14}$$

Now substituting the outer expansion (4.10) into the governing equation (4.6) and the Bloch condition (4.3) and collecting terms of ϵ_1^2, we obtain the problem for the second order outer potential Φ_2:

$$\nabla^2\Phi_2 + \frac{\omega^2}{c^2}\Phi_2 = -2\overline{\nabla}\cdot\nabla\Phi_0 - \frac{2\mathrm{i}\omega}{c^2}\frac{\partial\Phi_0}{\partial T}, \tag{4.15}$$

$$\Phi_2(\mathbf{r}+\mathbf{R}_j) = \mathrm{e}^{\mathrm{i}\boldsymbol{\beta}_m^T\mathbf{R}_j}\Phi_2(\mathbf{r}),\ m = 1,\ 2,\ \ldots, M, \tag{4.16}$$

where $\overline{\nabla}$ denotes the gradient operator with respect to the slow variables X and Y.

In the far field defined by $r_j \gg a$, the outer potentials Φ_0 and Φ_2 satisfy (4.11) and (4.15) separately and the Bloch conditions as well. In the near field $r_j \ll \beta^{-1}$, the low order terms of the inner solution ϕ satisfy the Laplace equation. Therefore, the inner solution is constructed from the inner eigenfunctions (solutions of the Laplace equation that satisfy the homogeneous boundary conditions) and satisfy the no normal flux boundary condition.

From (4.12) and (4.13), the inner expansion of the leading-order outer solution is

$$\begin{aligned}\Phi_0^{(0,1)} &= \sum_{h=1}^{M} A_h(X,Y,T)\mathrm{e}^{\mathrm{i}\boldsymbol{\beta}_h^T\mathbf{R}_j}\left[1+\mathrm{i}\epsilon_1\rho\cos(\theta-\tau_h)+O(\epsilon_1^2)\right]\\ &= \sum_{h=1}^{M} A_h(X,Y,T)\mathrm{e}^{\mathrm{i}\boldsymbol{\beta}_h^T\mathbf{R}_j}\left[1+\mathrm{i}\epsilon_1\rho\ (\cos\tau_h,\ \sin\tau_h)\begin{pmatrix}\cos\theta\\ \sin\theta\end{pmatrix}+O(\epsilon_1^2)\right]?\end{aligned} \tag{4.17}$$

where the information about the lattice is reflected by the phase change factor $e^{\mathrm{i}\boldsymbol{\beta}_h^T\mathbf{R}_j}$. In contrast to the outer solution in infinite array [60, eq. 34], the information of the lattice is included in the lattice sums. Therefore, to match with the outer solution Φ_0, the inner solution ϕ up to order ϵ_1 takes the form

$$\phi^{(1)} = B_0 + \epsilon_1\left[B_1 + \left(\rho+\frac{1}{\rho}\right)\mathbf{u}_1^T\begin{pmatrix}\cos\theta\\ \sin\theta\end{pmatrix}\right], \tag{4.18}$$

where $\rho = r_j/a$ is the inner coordinate and any constants, terms involving ρ and θ are all inner eigenfunctions and $\mathbf{u}_1$ is an unknown vector that needs to be determined.

To obtain the envelope equations, we now apply Green's identity to ψ_m^* and the composite solution in a cell C (the cylinder in this cell is marked as S), where ψ_m^* denotes the complex conjugate of ψ_m. As we know, the inner solution is only valid in the inner region and the outer solution is only valid in the outer region. To find a solution

that is valid everywhere in the whole region, we need to do some work to the inner and outer solutions. One of the methods may be called additive composition. Since the inner expansion and the outer expansion have a common region of validity, the composite expansion can be constructed by subtracting the part they have in common, so that it is not counted twice [102, page 94]. We denote the composite expansion by ξ and take

$$\xi = \Phi^{(2)} + \phi^{(1)} - \phi^{(1,2)}. \tag{4.19}$$

Then the Green's identity is

$$\int\int_{C_s} \left(\xi \nabla^2 \psi_m^* - \psi_m^* \nabla^2 \xi\right) ds = \int_{\partial C_s} \left(\xi \frac{\partial \psi_m^*}{\partial n} - \psi_m^* \frac{\partial \xi}{\partial n}\right) dl, \tag{4.20}$$

where C_s is the cell C excluding the cylinder S, ds means the integration is taken over the cross-section of the cylinder S and dl means the integration is along the boundary of the cross-section of S. Then noting that we have $\phi^{(1)} - \phi^{(1,2)} = 0$ by (4.18), the left hand side of the Green's identity becomes

$$LHS(4.20) = \int\int_{C_s} \left(\Phi^{(2)} \nabla^2 \psi_m^* - \psi_m^* \nabla^2 \Phi^{(2)}\right) ds.$$

Using equation (4.11) and (4.15) and dropping terms of order higher than ϵ_1^2

$$\begin{aligned}
LHS(4.20) &= \int\int_{C_s} \left(\Phi_0 \nabla^2 \psi_m^* - \psi_m^* \nabla^2 \Phi_0\right) ds + \epsilon_1^2 \int\int_{C_s} \left(\Phi_2 \nabla^2 \psi_m^* - \psi_m^* \nabla^2 \Phi_2\right) ds \\
&= \int\int_{C_s} \left[\Phi_0(-\beta^2 \psi_m^*) - \psi_m^* \left(-\frac{\omega^2}{c^2}\Phi_0\right)\right] ds \\
&\quad + \epsilon_1^2 \int\int_{C_s} \left[-\Phi_2 \beta^2 \psi_m^* - \psi_m^*(-2\overline{\nabla} \cdot \nabla \Phi_0 - \frac{\omega^2}{c^2}\Phi_2 - \frac{2\mathrm{i}\omega}{c^2}\frac{\partial \Phi_0}{\partial T})\right] ds \\
&= \epsilon_1^2 \int\int_{C_s} \left(2\psi_m^* \overline{\nabla} \cdot \nabla \Phi_0 + \frac{2\mathrm{i}\omega}{c^2}\psi_m^* \frac{\partial \Phi_0}{\partial T}\right) ds \\
&= \epsilon_1^2 \left(2\mathrm{i} \sum_{h=1}^{M} \overline{\nabla} A_h \cdot \boldsymbol{\beta}_h + \frac{2\mathrm{i}\omega}{c^2} \sum_{h=1}^{M} \frac{\partial A_h}{\partial T}\right) \int\int_{C_s} \mathrm{e}^{\mathrm{i}(\boldsymbol{\beta}_h - \boldsymbol{\beta}_m)^T \mathbf{r}} ds \\
&= \epsilon_1^2 \sum_{h=1}^{M} \left(\frac{2\mathrm{i}\omega}{c^2}\frac{\partial A_h}{\partial T} + 2\mathrm{i}\overline{\nabla} A_h \cdot \boldsymbol{\beta}_h\right) \int\int_{C_s} \mathrm{e}^{\mathrm{i}(\boldsymbol{\beta}_h - \boldsymbol{\beta}_m)^T \mathbf{r}} ds.
\end{aligned} \tag{4.21}$$

Since the cylinder radius is much smaller than the periodicity of the lattice, the cross-sectional area of a cylinder $\mathcal{A}_s$ is much smaller than that of the cell $\mathcal{A}_c$, therefore the area

of the cell excluding the cylinder is: $\mathcal{A}_{cs} = \mathcal{A}_c - \pi a^2 = \mathcal{A}_c[1 + O(\epsilon_1^2)] \approx \mathcal{A}_c$. Therefore the integral in (4.21) can be approximated by

$$\int\int_{C_s} \mathrm{e}^{\mathrm{i}(\boldsymbol{\beta}_h - \boldsymbol{\beta}_m)^T \mathbf{r}} ds \approx \int\int_{C} \mathrm{e}^{\mathrm{i}(\boldsymbol{\beta}_h - \boldsymbol{\beta}_m)^T \mathbf{r}} ds = \delta_{hm} \mathcal{A}_c \tag{4.22}$$

Substituting (4.22) into (4.21) and dropping terms of higher order, we get

$$LHS(4.20) = \epsilon_1^2 \frac{2\mathrm{i}\omega}{c^2} \mathcal{A}_c \left(\frac{\partial A_m}{\partial T} + \frac{c^2}{\omega} \overline{\nabla} A_m \cdot \boldsymbol{\beta}_m \right). \tag{4.23}$$

On the cylinder $r_j = a$, we have

$$\begin{aligned} \psi_m^*|_{r_j=a} &= \mathrm{e}^{-\mathrm{i}\boldsymbol{\beta}_m^T(\mathbf{r}_j + \mathbf{R}_j)}|_{r_j=a} \\ &= \mathrm{e}^{-\mathrm{i}\boldsymbol{\beta}_m^T \mathbf{R}_j}[1 - \mathrm{i}\beta a \cos(\theta - \tau_m) + O(\epsilon_1^2)], \end{aligned} \tag{4.24}$$

and

$$\begin{aligned} \left.\frac{\partial \psi_m^*}{\partial r_j}\right|_{r_j=a} &= \mathrm{i}\beta \cos(\theta - \tau_m) \mathrm{e}^{\mathrm{i}\boldsymbol{\beta}_m^T(\mathbf{r}_j + \mathbf{R}_j)}\Big|_{r_j=a} \\ &= \mathrm{e}^{\mathrm{i}\boldsymbol{\beta}_m^T \mathbf{R}_j}[\mathrm{i}\beta \cos(\theta - \tau_m)][1 + \mathrm{i}\beta a \cos(\theta - \tau_m) + O(\epsilon_1^2)]. \end{aligned} \tag{4.25}$$

Therefore, noting that the normal flux on the cylinder vanishes and the contribution from the outer boundaries of the primary cell vanishes by the Bloch condition, the right hand side of Green's identity (4.20) becomes

$$\begin{aligned} RHS(4.20) &= \int_{\partial S} \left(\phi^{(1)} \frac{\partial \psi_m^*}{\partial n} - \psi_m^* \frac{\partial \phi^{(1)}}{\partial n} \right) dl \\ &= -\int_{\partial S} \phi^{(1)} \frac{\partial \psi_m^*}{\partial r_j} dl \\ &= -\int_0^{2\pi} \left\{ B_0 + \epsilon_1 \left[B_1 + \left(\rho + \frac{1}{\rho} \right) \mathbf{u}_1^T \begin{pmatrix} \cos\theta \\ \sin\theta \end{pmatrix} \right] \right\} \\ &\qquad \mathrm{e}^{-\mathrm{i}\boldsymbol{\beta}_m^T \mathbf{R}_j}[-\mathrm{i}\beta \cos(\theta - \tau_m)][1 - \mathrm{i}\beta a \cos(\theta - \tau_m) + O(\epsilon_1^2)] a d\theta \\ &= \mathrm{e}^{-\mathrm{i}\boldsymbol{\beta}_m^T \mathbf{R}_j} \int_0^{2\pi} \left\{ B_0 + \epsilon_1 \left[B_1 + \left(\rho + \frac{1}{\rho} \right) \mathbf{u}_1^T \begin{pmatrix} \cos\theta \\ \sin\theta \end{pmatrix} \right] \right\} \\ &\qquad \mathrm{i}\epsilon_1 \cos(\theta - \tau_m)[1 - \mathrm{i}\epsilon_1 \cos(\theta - \tau_m) + O(\epsilon_1^2)] d\theta \\ &= \pi \epsilon_1^2 \mathrm{e}^{-\mathrm{i}\boldsymbol{\beta}_m^T \mathbf{R}_j} \left[B_0 + 2\mathrm{i}\mathbf{u}_1^T \begin{pmatrix} \cos\tau_m \\ \sin\tau_m \end{pmatrix} \right] + O(\epsilon_1^3). \end{aligned}$$

To eliminate the unknowns B_0 and $\mathbf{u}_1$, we need to do the matching between the inner solution $\phi^{(1)}$ and the outer solution $\Phi^{(0)}$. Therefore by (4.17) and (4.18) and the matching rule $\Phi^{(0,1)} \equiv \phi^{(1,0)}$, we have

$$B_0 = \sum_{h=1}^{M} A_h \mathrm{e}^{\mathrm{i}\boldsymbol{\beta}_h^T \mathbf{R}_j}, \tag{4.26}$$

$$\mathbf{u}_1^T = \mathrm{i} \sum_{h=1}^{M} A_h \mathrm{e}^{\mathrm{i}\boldsymbol{\beta}_h^T \mathbf{R}_j} (\cos\tau_h, \sin\tau_h). \tag{4.27}$$

Therefore, dropping the higher order terms

$$\begin{aligned} RHS(4.20) &= \pi\epsilon_1^2 \mathrm{e}^{-\mathrm{i}\boldsymbol{\beta}_m^T \mathbf{R}_j} \left[B_0 + 2\mathrm{i}\mathbf{u}_1^T \begin{pmatrix} \cos\tau_m \\ \sin\tau_m \end{pmatrix} \right] \\ &= \pi\epsilon_1^2 \mathrm{e}^{-\mathrm{i}\boldsymbol{\beta}_m^T \mathbf{R}_j} \sum_{h=1}^{M} A_h \mathrm{e}^{\mathrm{i}\boldsymbol{\beta}_h^T \mathbf{R}_j} \left[1 - 2(\cos\tau_h, \sin\tau_h) \begin{pmatrix} \cos\tau_m \\ \sin\tau_m \end{pmatrix} \right] \\ &= \epsilon_1^2 \pi \sum_{h=1}^{M} A_h [1 - 2\cos(\tau_m - \tau_h)], \ m = 1, \ldots, M. \end{aligned} \tag{4.28}$$

Then, by (4.23) and (4.28), we obtain the envelope equations

$$\frac{\partial A_m}{\partial T} + \mathbf{C}_g^{(m)} \cdot \overline{\nabla} A_m = -\frac{1}{2}\mathrm{i}\Omega_0 \sum_{h=1}^{M} A_h [1 - 2\cos(\tau_m - \tau_h)], \ m = 1, \ldots, M, \tag{4.29}$$

where

$$\mathbf{C}_g^{(m)} = \frac{c^2 \boldsymbol{\beta}_m}{\omega} = \frac{c\boldsymbol{\beta}_m}{\beta} = c \begin{pmatrix} \cos\tau_m \\ \sin\tau_m \end{pmatrix}, \quad \Omega_0 = \frac{\pi c^2}{\omega \mathcal{A}_c} = \frac{\pi c}{\beta \mathcal{A}_c}. \tag{4.30}$$

These envelope equations agree with those in Li and Mei [49]. Outside the strip, the envelope equations reduce to

$$\frac{\partial A_m}{\partial T} + \mathbf{C}_g^{(m)} \cdot \overline{\nabla} A_m = 0, \ m = 1, \ldots, M. \tag{4.31}$$

4.1.2 Arbitrary shape scatterers

Formulation

When the scatterers are of arbitrary shape, it is more difficult to perform the integration over the scatterer when using Green's identity to obtain the envelope equations. To overcome this, we need to use Green's identity again in the inner region. In contrast to the circular cylinder case, here we need the inner solution up to order ϵ_1^2, because it includes

the information about the shape of the scatterer and contributes to the integration on the scatterer. In this case the Neumann boundary condition is

$$\frac{\partial \Phi}{\partial n} = 0, \tag{4.32}$$

where n is a coordinate measured normal to each scatterer. The form of the inner solution up to order ϵ_1^2 is [60, eq 40]

$$\phi^{(2)} = B_0 + \epsilon_1 \left\{ B_1 + \mathbf{u}_1^T \left[\rho \begin{pmatrix} \cos\theta \\ \sin\theta \end{pmatrix} + \chi_1(\rho,\theta) \right] \right\} + \epsilon_1^2 \left\{ B_0 \left[-\frac{1}{4}\rho^2 + \Gamma(\rho,\theta) \right] + \right.$$
$$\left. B_2 + \mathbf{u}_2^T \left[\rho \begin{pmatrix} \cos\theta \\ \sin\theta \end{pmatrix} + \chi_1(\rho,\theta) \right] + \mathbf{v}_2^T \left[\rho^2 \begin{pmatrix} \cos 2\theta \\ \sin 2\theta \end{pmatrix} + \chi_2(\rho,\theta) \right] + \cdots \right\}, \tag{4.33}$$

where Γ is a harmonic function introduced to compensate for the flux across the scatterer S that is induced by the term in ρ^2 and from the Neumann condition (4.32)

$$\frac{\partial \chi_1}{\partial n} = -\frac{\partial}{\partial n} \left[\begin{pmatrix} \cos\theta \\ \sin\theta \end{pmatrix} \right] \text{ on } S, \tag{4.34}$$

$$\chi_1 - \frac{\mathbf{M}}{\rho} \begin{pmatrix} \cos\theta \\ \sin\theta \end{pmatrix} = o(\rho^{-1}) \text{ as } \rho \to \infty \tag{4.35}$$

and

$$\mathbf{M} = \begin{pmatrix} m_{11} & m_{12} \\ m_{21} & m_{22} \end{pmatrix} \tag{4.36}$$

is the matrix of dipole coefficients determined by the shape of the scatterer [8, page 127] and $\chi_2(\rho,\theta) = o(1)$ as $\rho \to \infty$. The ellipsis in (4.33) denote those eigenfunctions in slow variations that will be needed to match with the extra terms in outer solution Φ_2 arise from the right hand side of (4.15). These eigenfunctions satisfy the Laplace equation and the homogeneous boundary condition. Now we are going to find the form of Γ. By the Neumann boundary condition (4.7), we have

$$\frac{\partial \Gamma}{\partial n} = -\frac{\partial}{\partial n} \left(-\frac{1}{4}\rho^2 \right) = \frac{1}{4} \frac{\partial \rho^2}{\partial n}. \tag{4.37}$$

The flux across the scatterer S induced by the term in ρ^2 must be compensated by the flux induced by Γ across the outer 'boundary' of the inner region C_ρ as $\rho \to \infty$, where we denote the outer boundary by a circle ∂S^* centred within the scatterer S. Therefore

$$\int_{\partial S^*} \frac{\partial \Gamma}{\partial n} dl = -\frac{1}{4} \int_{\partial S} \frac{\partial \rho^2}{\partial n} dl, \tag{4.38}$$

Because Γ must be a solution of the Laplace equation that correspond to a non-zero flux and of the inner region, we know that

$$\Gamma(\rho,\theta) \sim A\log\rho, \text{ as } \rho\to\infty. \tag{4.39}$$

The left hand side of (4.38) is

$$\int_{\partial S^*}\frac{\partial\Gamma}{\partial n}dl = -\int_0^{2\pi} A\frac{1}{\rho}\rho d\theta = -2\pi A,$$

where the minus sign is because the surface normal on the scatterer is directed into the scatterer. Applying the divergence theorem to the right hand side of (4.38) gives

$$-\frac{1}{4}\int_{\partial S}\frac{\partial\rho^2}{\partial n}dl = -\frac{1}{4}\iint_S \nabla^2(\rho^2)ds = -\frac{\mathcal{A}_s}{a^2},$$

where $\mathcal{A}_s$ is the area contained within S and a^2 is to make the area dimensionless. Thus, we get

$$A = \frac{\mathcal{A}_s}{2\pi a^2}, \tag{4.40}$$

and then

$$\Gamma(\rho,\theta) - \frac{\mathcal{A}_s}{2\pi a^2}\log\rho \to 0, \text{ as } \rho\to\infty. \tag{4.41}$$

Similar to the circular cylinders, Green's identity is going to be used in the cell C excluding the scatterer S, C_s, to obtain the envelope equations. The composite solution containing the inner and outer expansions up to order ϵ^2 is

$$\xi = \Phi^{(2)} + \phi^{(2)} - \phi^{(2,2)}. \tag{4.42}$$

Then the conjugate of the plane waves ψ_m^* and the composite solution ξ valid in the entire cell are used in Green's identity to give

$$\iint_{C_s}(\xi\nabla^2\psi_m^* - \psi_m^*\nabla^2\xi)ds = \int_{\partial C_s}\left(\xi\frac{\partial\psi_m^*}{\partial n} - \psi_m^*\frac{\partial\xi}{\partial n}\right)dl, \tag{4.43}$$

where the integration on the right hand side includes the integration over the scatterer and the integration over the outer boundaries of the cell C which vanish by the Bloch condition; thus Green's identity becomes

$$\iint_{C_s}(\xi\nabla^2\psi_m^* - \psi_m^*\nabla^2\xi)ds = \int_{\partial S}\left(\phi^{(2)}\frac{\partial\psi_m^*}{\partial n} - \psi_m^*\frac{\partial\phi^{(2)}}{\partial n}\right)dl. \tag{4.44}$$

We know $\phi^{(2)} - \phi^{(2,2)} = o(\epsilon_1^2)$, then the left hand side of the Green's identity becomes

$$\begin{aligned} LHS(4.44) &= \int\int_{C_s} \left[\left(\Phi^{(2)} + \phi^{(2)} - \phi^{(2,2)} \right) \nabla^2 \psi_m^* - \psi_m^* \nabla^2 \left(\Phi^{(2)} + \phi^{(2)} - \phi^{(2,2)} \right) \right] ds \\ &= \int\int_{C_s} \left(\Phi^{(2)} \nabla^2 \psi_m^* - \psi_m^* \nabla^2 \Phi^{(2)} \right) ds \\ &+ \int\int_{C_s} \left[\left(\phi^{(2)} - \phi^{(2,2)} \right) \nabla^2 \psi_m^* - \psi_m^* \nabla^2 \left(\phi^{(2)} - \phi^{(2,2)} \right) \right] ds \\ &= \int\int_{C_s} \left(\Phi^{(2)} \nabla^2 \psi_m^* - \psi_m^* \nabla^2 \Phi^{(2)} \right) ds + o(\epsilon_1^2). \end{aligned} \tag{4.45}$$

Using equations (4.11) and (4.15) that the first and second order outer solutions satisfy and dropping terms of order higher than ϵ_1^2

$$\begin{aligned} LHS(4.44) &= \int\int_{C_s} \left(\Phi_0 \nabla^2 \psi_m^* - \psi_m^* \nabla^2 \Phi_0 \right) ds + \epsilon_1^2 \int\int_{C_s} \left(\Phi_2 \nabla^2 \psi_m^* - \psi_m^* \nabla^2 \Phi_2 \right) ds \\ &= \int\int_{C_s} \left[\Phi_0 (-\beta^2 \psi_m^*) - \psi_m^* \left(-\frac{\omega^2}{c^2} \Phi_0 \right) \right] ds \\ &\quad + \epsilon_1^2 \int\int_{C_s} \left[-\Phi_2 \beta^2 \psi_m^* - \psi_m^* \left(-2\overline{\nabla} \cdot \nabla \Phi_0 - \frac{\omega^2}{c^2} \Phi_2 - \frac{2\mathrm{i}\omega}{c^2} \frac{\partial \Phi_0}{\partial T} \right) \right] ds \\ &= \epsilon_1^2 \int\int_{C_s} \left(2\psi_m^* \overline{\nabla} \cdot \nabla \Phi_0 + \frac{2\mathrm{i}\omega}{c^2} \psi_m^* \frac{\partial \Phi_0}{\partial T} \right) ds \\ &= \epsilon_1^2 \left(2\mathrm{i} \sum_{h=1}^{M} \overline{\nabla} A_h \cdot \boldsymbol{\beta}_h + \frac{2\mathrm{i}\omega}{c^2} \sum_{h=1}^{M} \frac{\partial A_h}{\partial T} \right) \int\int_{C_s} \mathrm{e}^{\mathrm{i}(\boldsymbol{\beta}_h - \boldsymbol{\beta}_m)^T \mathbf{r}} ds \\ &= \epsilon_1^2 \sum_{h=1}^{M} \left(\frac{2\mathrm{i}\omega}{c^2} \frac{\partial A_h}{\partial T} + 2\mathrm{i} \overline{\nabla} A_h \cdot \boldsymbol{\beta}_h \right) \int\int_{C_s} \mathrm{e}^{\mathrm{i}(\boldsymbol{\beta}_h - \boldsymbol{\beta}_m)^T \mathbf{r}} ds \\ &= \epsilon_1^2 \frac{2\mathrm{i}\omega}{c^2} \mathcal{A}_c \left(\frac{\partial A_m}{\partial T} + \frac{c^2}{\omega} \overline{\nabla} A_m \cdot \boldsymbol{\beta}_m \right) + o(\epsilon_1^2). \end{aligned} \tag{4.46}$$

We have denoted the outer 'boundary' of the inner region by a circle ∂S^* as $\rho \to \infty$. To get the integration over the scatterer, next we are going to apply Green's identity in the inner region C_ρ bounded by the surface of the scatterer, ∂S, and the circle, ∂S^*, to ψ_m^* and the inner solution $\phi^{(2)}$. Before doing this, we first expand ψ_m^*,

$$\begin{aligned} \psi_m^* &= \mathrm{e}^{-\mathrm{i}\boldsymbol{\beta}_m^T \mathbf{r}} = \mathrm{e}^{-\mathrm{i}\boldsymbol{\beta}_m^T \mathbf{R}_j} \left\{ 1 - \mathrm{i}\epsilon_1 \rho \cos(\theta - \tau_m) - \frac{1}{4} \epsilon_1^2 \rho^2 [1 + \cos 2(\theta - \tau_m)] + O(\epsilon_1^3) \right\} \\ &:= \hat{\psi}_m^* + O(\epsilon_1^3). \end{aligned} \tag{4.47}$$

That's because the expansion of ψ_m^* is only valid when $\rho = O(1)$, i.e. near the scatterer, this expansion makes the omitted terms be in higher order. Then we have

$$\begin{aligned}\nabla^2\hat{\psi}_m^* &= \nabla^2\left\{\mathrm{e}^{-\mathrm{i}\boldsymbol{\beta}_m^T\mathbf{R}_j}\left[1-\mathrm{i}\epsilon_1\rho\cos(\theta-\tau_m)-\frac{1}{4}\epsilon_1^2\rho^2[1+\cos 2(\theta-\tau_m)]\right]\right\}\\ &= -\epsilon_1^2\mathrm{e}^{-\mathrm{i}\boldsymbol{\beta}_m^T\mathbf{R}_j}. \end{aligned} \tag{4.48}$$

Now we apply Green's identity to $\hat{\psi}_m^*$ and the inner solution up to order ϵ_1^2, $\phi^{(2)}$, over the inner region C_ρ

$$\iint_{C_\rho}(\phi^{(2)}\nabla^2\hat{\psi}_m^* - \hat{\psi}_m^*\nabla^2\phi^{(2)})ds = \int_{\partial C_\rho}\left(\phi^{(2)}\frac{\partial\hat{\psi}_m^*}{\partial n} - \hat{\psi}_m^*\frac{\partial\phi^{(2)}}{\partial n}\right)dl, \tag{4.49}$$

where $\partial C_\rho = \partial S + \partial S^*$.

In the inner coordinates,

$$\nabla_\rho^2\phi + \epsilon_1^2\phi = 0, \tag{4.50}$$

$$\phi = \phi_0 + \epsilon_1\phi_1 + \epsilon_1^2\phi_2 + O(\epsilon_1^3), \tag{4.51}$$

then substituting for (4.51) in (4.50) and collecting the like power terms we obtain

$$\nabla_\rho^2\phi_0 = 0, \quad \nabla_\rho^2\phi_1 = 0, \quad \nabla_\rho^2\phi_2 = -\phi_0. \tag{4.52}$$

Therefore

$$\begin{aligned} LHS(4.49) &= \iint_{C_\rho}\left\{[\phi_0+\epsilon_1\phi_1+\epsilon_1^2\phi_2+O(\epsilon_1^3)](-\epsilon_1^2\hat{\psi}_m^*) - \hat{\psi}_m^*(-\epsilon_1^2\phi_0)\right\}ds\\ &= O(\epsilon_1^3), \end{aligned} \tag{4.53}$$

which gives

$$\int_{\partial S}\phi^{(2)}\frac{\hat{\psi}_m^*}{\partial n} - \hat{\psi}_m^*\frac{\partial\phi^{(2)}}{\partial n}dl = -\int_{\partial S^*}\phi^{(2)}\frac{\hat{\psi}_m^*}{\partial n} - \hat{\psi}_m^*\frac{\partial\phi^{(2)}}{\partial n}dl + O(\epsilon_1^3) \tag{4.54}$$

By the inner solution (4.33) and the expansion of ψ_m^* (4.47)

$$
\begin{aligned}
RHS(4.54) =& -\int_0^{2\pi}\left(\phi^{(2)}\frac{\hat{\psi}_m^*}{\partial\rho}-\hat{\psi}_m^*\frac{\partial\phi^{(2)}}{\partial\rho}\right)\rho d\theta+O(\epsilon_1^3)\\
=& -\int_0^{2\pi}\mathrm{e}^{-\mathrm{i}\boldsymbol{\beta}_m^T\cdot\mathbf{R}_j}\Bigg\{\left[B_0+\epsilon_1\left(B_1+\mathbf{u}_1^T\left[\rho\begin{pmatrix}\cos\theta\\ \sin\theta\end{pmatrix}+\frac{\mathbf{M}}{\rho}\begin{pmatrix}\cos\theta\\ \sin\theta\end{pmatrix}\right]\right)\right]\\
&\left[-\mathrm{i}\epsilon_1\cos(\theta-\tau_m)-\frac{1}{2}\epsilon_1^2\rho\left[1+\cos 2(\theta-\tau_m)\right]\right]-\\
&\left[1-\mathrm{i}\epsilon_1\rho\cos(\theta-\tau_m)-\frac{1}{4}\epsilon_1^2\rho^2\left[1+\cos 2(\theta-\tau_m)\right]\right]\\
&\left(\epsilon_1\left[\mathbf{u}_1^T\begin{pmatrix}\cos\theta\\ \sin\theta\end{pmatrix}-\frac{\mathbf{M}}{\rho^2}\begin{pmatrix}\cos\theta\\ \sin\theta\end{pmatrix}\right]+\epsilon_1^2\Bigg[B_0\left(-\frac{1}{2}+\frac{\mathcal{A}_s}{2\pi a^2}\frac{1}{\rho}\right)+\right.\\
&\left.\left.\mathbf{u}_2^T\left[\begin{pmatrix}\cos\theta\\ \sin\theta\end{pmatrix}-\frac{\mathbf{M}}{\rho^2}\begin{pmatrix}\cos\theta\\ \sin\theta\end{pmatrix}\right]+\mathbf{v}_2^T\left[\rho\begin{pmatrix}\cos 2\theta\\ \sin 2\theta\end{pmatrix}-\frac{\mathbf{M}}{\rho^2}\begin{pmatrix}\cos 2\theta\\ \sin 2\theta\end{pmatrix}\right]\right]\right)\Bigg\}\rho d\theta\\
&+O(\epsilon_1^3)\\
=&\mathrm{e}^{-\mathrm{i}\boldsymbol{\beta}_m^T\cdot\mathbf{R}_j}\pi\epsilon_1^2\left[B_0\frac{\mathcal{A}_s}{\pi a^2}+2\mathrm{i}\mathbf{u}_1^T\mathbf{M}\begin{pmatrix}\cos\theta\\ \sin\theta\end{pmatrix}\right]+O(\epsilon_1^3).
\end{aligned}
\tag{4.55}
$$

Therefore, by (4.44), (4.54) and (4.55)

$$
\iint_{C_s}(\xi\nabla^2\psi_m^*-\psi_m^*\nabla^2\xi)ds=\mathrm{e}^{-\mathrm{i}\boldsymbol{\beta}_m^T\cdot\mathbf{R}_j}\pi\epsilon_1^2\left[B_0\frac{\mathcal{A}_s}{\pi a^2}+2\mathrm{i}\mathbf{u}_1^T\mathbf{M}\begin{pmatrix}\cos\theta\\ \sin\theta\end{pmatrix}\right]+O(\epsilon_1^3). \tag{4.56}
$$

By the results of the left hand side of Green's identity (4.46), we have

$$
\epsilon_1^2\frac{2\mathrm{i}\omega}{c^2}\mathcal{A}_c\left(\frac{\partial A_m}{\partial T}+\frac{c^2}{\omega}\overline{\nabla}A_m\cdot\boldsymbol{\beta}_m\right)=\mathrm{e}^{-\mathrm{i}\boldsymbol{\beta}_m^T\cdot\mathbf{R}_j}\pi\epsilon_1^2\left[B_0\frac{\mathcal{A}_s}{\pi a^2}+2\mathrm{i}\mathbf{u}_1^T\mathbf{M}\begin{pmatrix}\cos\theta\\ \sin\theta\end{pmatrix}\right]+o(\epsilon_1^2), \tag{4.57}
$$

which is

$$
\frac{\partial A_m}{\partial T}+\frac{c^2}{\omega}\overline{\nabla}A_m\cdot\boldsymbol{\beta}_m=\frac{\pi c^2}{2\mathrm{i}\omega\mathcal{A}_c}\mathrm{e}^{-\mathrm{i}\boldsymbol{\beta}_m^T\cdot\mathbf{R}_j}\pi\epsilon_1^2\left[B_0\frac{\mathcal{A}_s}{\pi a^2}+2\mathrm{i}\mathbf{u}_1^T\mathbf{M}\begin{pmatrix}\cos\theta\\ \sin\theta\end{pmatrix}\right]+o(\epsilon_1^2). \tag{4.58}
$$

To eliminate the unknowns B_0 and $\mathbf{u}_1$, doing the matching between the outer solutions (4.17) and the inner solutions (4.33) we obtain

$$
B_0=\sum_{h=1}^{M}A_h\mathrm{e}^{-\mathrm{i}\boldsymbol{\beta}_m^T\cdot\mathbf{R}_j}, \tag{4.59}
$$

$$\mathbf{u}_1^T = \mathrm{i}\sum_{h=1}^{M} A_h \mathrm{e}^{-\mathrm{i}\boldsymbol{\beta}_m^T\cdot\mathbf{R}_j}(\cos\tau_m, \sin\tau_m). \tag{4.60}$$

Now substituting for the last two equations in (4.58) we obtain the envelope equations

$$\frac{\partial A_m}{\partial T} + \mathbf{C}_g^{(m)}\cdot\overline{\nabla}A_m = -\frac{1}{2}\mathrm{i}\Omega_0\sum_{h=1}^{M} A_h\left[\frac{\mathcal{A}_s}{\pi a^2} - 2(\cos\tau_h, \sin\tau_h)\mathbf{M}\begin{pmatrix}\cos\tau_m\\ \sin\tau_m\end{pmatrix}\right], \tag{4.61}$$

for all $m = 1, 2, \ldots, M$, where $\mathbf{C}_g^{(m)} = c\boldsymbol{\beta}_m/\beta$ and $\Omega_0 = \pi c/(\beta\mathcal{A}_c)$. When the scatterers are circular, the cross-sectional area of the cylinder $\mathcal{A}_s = \pi a^2$, and the matrix of dipole coefficients $\mathbf{M}$ is a two-dimensional identity matrix, therefore the envelope equations reduce to

$$\frac{\partial A_m}{\partial T} + \mathbf{C}_g^{(m)}\cdot\overline{\nabla}A_m = -\frac{1}{2}\mathrm{i}\Omega_0\sum_{h=1}^{M} A_h\left[1 - 2\cos(\tau_m - \tau_h)\right], \tag{4.62}$$

which is in agreement with the results of circular cylinder array (4.29).

If we multiply both sides of equation (4.61) by A_m^* (the conjugate of A_m) and add the resulting equation with its complex conjugate, after summation over m, we obtain

$$\begin{aligned}
&\sum_{m=1}^{M}\left(\frac{\partial|A_m|^2}{\partial T} + \mathbf{C}_g^{(m)}\cdot\overline{\nabla}|A_m|^2\right)\\
&= -\frac{\Omega_0}{2}\sum_{m=1}^{M}\sum_{h=1}^{M}\left[\frac{\mathcal{A}_s}{\pi a^2} - 2(\cos\tau_h, \sin\tau_h)\mathbf{M}\begin{pmatrix}\cos\tau_m\\ \sin\tau_m\end{pmatrix}\right](\mathrm{i}A_hA_m^* - \mathrm{i}A_h^*A_m)\\
&= 0.
\end{aligned} \tag{4.63}$$

Thus the total energy is conserved in the array, for example, when the primary wave (the continuation of the incident wave in the array) is weak for some particular detuning or strip width, the resonant scattered waves are strong. Therefore it is possible to use this theory to design structures to transfer the incident energy into scattered energy.

If the array is infinite, the amplitude doesn't depend on the space variation, thus only the time variation is involved. If we search for solutions in the form of $A_m(T) = a_m\mathrm{e}^{-\mathrm{i}\Omega T}$, the envelope equations (4.61) become

$$\Omega a_m = \frac{\pi c^2}{2\omega\mathcal{A}_c}\sum_{h=1}^{M} a_h\left[\frac{\mathcal{A}_s}{\pi a^2} - 2(\cos\tau_h, \sin\tau_h)\mathbf{M}\begin{pmatrix}\cos\tau_m\\ \sin\tau_m\end{pmatrix}\right], \tag{4.64}$$

where $\Omega = \mathcal{K}c$. $\mathcal{K}$ is the detuning of the wavenumber and the detuned wavenumber $k = \beta + \epsilon_1^2\mathcal{K}$, and the detuned frequency $\omega' = kc = \omega + \epsilon_1^2\Omega$. McIver [60] considered the

same case for infinite two-dimensional array of arbitrary shape scatterers and obtained [60, eq 47, 48]

$$U_m\delta_m = \frac{\pi L^2}{\mathcal{A}_c}\sum_{h=1}^{M}\left[\frac{\mathcal{A}_s}{\pi a^2} - 2(\cos\tau_h, \sin\tau_h)\mathbf{M}\begin{pmatrix}\cos\tau_m\\ \sin\tau_m\end{pmatrix}\right]U_h, \tag{4.65}$$

where $\delta_m = (k^2 - \beta_m^2)L^2/\epsilon^2$, $\beta_m = |\boldsymbol{\beta}_m| = \beta$ and $\epsilon = ka$. Equations (4.64) and (4.65) define same eigenvalue problems, therefore

$$\delta_m = \frac{2\omega L^2}{c^2}\Omega = \frac{2\beta(k-\beta)L^2}{\epsilon_1^2}, \tag{4.66}$$

which is consistent with the definition of δ_m [60, eq 21]

$$\delta_m = \frac{(k^2-\beta^2)L^2}{\epsilon^2} = \frac{(k+\beta)(k-\beta)L^2}{\epsilon^2} \approx \frac{2\beta(k-\beta)L^2}{\epsilon_1^2}, \tag{4.67}$$

on a first approximation in the limit $k \to \beta$.

Numerical results

We now apply the envelope equations to a long strip of cylinder occupying $0 \leq x \leq d$, see figure 4.2. A train of plane incident acoustic waves arrives from the south-west at an angle τ_1 with respect to the x-axis. Without loss of generality we limit the direction of the incident wave to be $0 < \tau_1 < \pi/2$. Let the width d of the strip be of order $1/\epsilon_1^2$ in the x direction (this is to make sure the array width is big enough for the resonance to occur) and the length be infinite in $\pm y$ directions. As the Bloch's theorem is only used in the integration on one cell and the strip width must be of order $1/\epsilon_1^2$, then as $\epsilon_1 \to 0$ the finite array goes to an infinite one from the view point of that cell. Thus we can use the envelope equations obtained for infinite arrays to approximate those in finite arrays.

Write the leading order outer wave potentials in the three zones (left side, right side and in the strip) in the form

$$\Phi_0 = \sum_{m=1}^{M} A_m(X,Y,T)\mathrm{e}^{\mathrm{i}\boldsymbol{\beta}_m^T\mathbf{r}}, \tag{4.68}$$

where

$$A_m = \begin{cases} A_m^-, & X < 0, \\ A_m, & 0 \leqslant X \leqslant D, \\ A_m^+, & X > D, \end{cases} \tag{4.69}$$

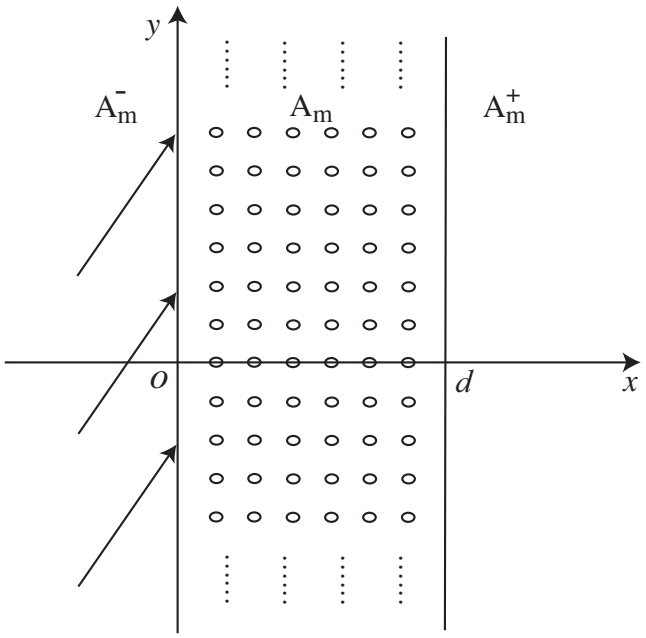

Figure 4.2: Strip

with $D = \epsilon_1^2 d$. Note that, with $\boldsymbol{\beta}_m = \beta \begin{pmatrix} \cos\tau_m \\ \sin\tau_m \end{pmatrix}$,

$$\mathrm{e}^{\mathrm{i}\boldsymbol{\beta}_m^T \mathbf{r}} = \mathrm{e}^{\mathrm{i}\beta(x\cos\tau_m + y\sin\tau_m)}. \tag{4.70}$$

We choose $\boldsymbol{\beta}_1$ as the incident wavenumber and allow a small perturbation (the detuning) of the wavenumber and frequency, thus the incident wave is

$$A_1^-(X,Y,T)\mathrm{e}^{\mathrm{i}\boldsymbol{\beta}_1^T \mathbf{r}} = A_0 \mathrm{e}^{\mathrm{i}(\mathcal{K}\cos\tau_1 X + \mathcal{K}\sin\tau_1 Y - \Omega T)} \mathrm{e}^{\mathrm{i}\boldsymbol{\beta}_1^T \mathbf{r}}, \tag{4.71}$$

where $\epsilon_1^2\mathcal{K}$ is the detuning of the wavenumber and $\epsilon_1^2\Omega$ is the detuning of the frequency, related by $\mathcal{K} = \Omega/c$. We include the detuning in the incident wave means that we change the frequency of the incident wave slightly to assess what will happen in and on the right side of the array. By the continuity conditions at $X = 0, D$, the y dependence must be the same in every component of the solution. Thus, look for solutions in the form

$$\begin{pmatrix} A_m^-(X,Y,T) \\ A_m(X,Y,T) \\ A_m^+(X,Y,T) \end{pmatrix} = A_0 \begin{pmatrix} B_m^-(X) \\ B_m(X) \\ B_m^+(X) \end{pmatrix} \mathrm{e}^{\mathrm{i}(\mathcal{K}\sin\tau_1 Y - \Omega T)}, \ m = 1, 2, \ldots, M. \tag{4.72}$$

Along the edges of the strip $X = 0, D$, the acoustic pressure and the normal velocity must be continuous

$$\sum_{m=1}^{M} A_m^-(0,Y,T)\mathrm{e}^{\mathrm{i}\boldsymbol{\beta}_m^T\mathbf{r}} = \sum_{m=1}^{M} A_m(0,Y,T)\mathrm{e}^{\mathrm{i}\boldsymbol{\beta}_m^T\mathbf{r}}, \tag{4.73}$$

$$\sum_{m=1}^{M} A_m(D,Y,T)\mathrm{e}^{\mathrm{i}\boldsymbol{\beta}_m^T\mathbf{r}} = \sum_{m=1}^{M} A_m^+(D,Y,T)\mathrm{e}^{\mathrm{i}\boldsymbol{\beta}_m^T\mathbf{r}}, \tag{4.74}$$

$$\frac{\partial}{\partial x}\sum_{m=1}^{M} A_m^-(X,Y,T)\mathrm{e}^{\mathrm{i}\boldsymbol{\beta}_m^T\mathbf{r}}\bigg|_{X=0} = \frac{\partial}{\partial x}\sum_{m=1}^{M} A_m(X,Y,T)\mathrm{e}^{\mathrm{i}\boldsymbol{\beta}_m^T\mathbf{r}}\bigg|_{X=0}, \tag{4.75}$$

$$\frac{\partial}{\partial x}\sum_{m=1}^{M} A_m(X,Y,T)\mathrm{e}^{\mathrm{i}\boldsymbol{\beta}_m^T\mathbf{r}}\bigg|_{X=D} = \frac{\partial}{\partial x}\sum_{m=1}^{M} A_m^+(X,Y,T)\mathrm{e}^{\mathrm{i}\boldsymbol{\beta}_m^T\mathbf{r}}\bigg|_{X=D}, \tag{4.76}$$

which lead to

$$\sum_{m=1}^{M}(B_m^-(0) - B_m(0))\mathrm{e}^{\mathrm{i}\beta y\sin\tau_m} = 0, \tag{4.77}$$

$$\sum_{m=1}^{M}(B_m^-(D) - B_m(D))\mathrm{e}^{\mathrm{i}\frac{\beta D}{\epsilon_1^2}\cos\tau_m}\mathrm{e}^{\mathrm{i}\beta y\sin\tau_m} = 0, \tag{4.78}$$

and

$$\sum_{m=1}^{M}(B_m^-(0) - B_m(0))\mathrm{i}\beta\cos\tau_m\mathrm{e}^{\mathrm{i}\beta y\sin\tau_m} = O(\epsilon_1^2), \tag{4.79}$$

$$\sum_{m=1}^{M}(B_m^-(D) - B_m(D))\mathrm{i}\beta\cos\tau_m\mathrm{e}^{\mathrm{i}\frac{\beta D}{\epsilon_1^2}\cos\tau_m}\mathrm{e}^{\mathrm{i}\beta y\sin\tau_m} = O(\epsilon_1^2). \tag{4.80}$$

Then using the orthogonality of the trigonometric functions, we obtain

$$\begin{aligned} B_m^-(0) &= B_m(0), \\ B_m(D) &= B_m^+(D), \end{aligned} \tag{4.81}$$

for $m = 1, 2, \ldots, M$. Arrange the components so that

$$\cos\tau_m > 0 \quad \text{for} \quad m \in \{1, 2, \ldots, M^+\} \equiv Z_1,$$

and

$$\cos\tau_m < 0 \quad \text{for} \quad m \in \{M^+ + 1, M^+ + 2, \ldots, M\} \equiv Z_2.$$

In the field without cylinders $X < 0$, the only forward propagating wave is the incident wave so that

$$B_m^-(X) = 0, \quad m \in Z_1 \setminus \{1\}. \tag{4.82}$$

On the right side of the strip $X > D$, there are no backward propagating waves so that

$$B_m^+(X) = 0, \quad m \in Z_2. \tag{4.83}$$

The governing equations in the strip and outside the strip are given by (4.61) and (4.31) respectively. Outside the cylinder strip, from (4.72) and (4.31), we have

$$\frac{dB_m^\pm}{dX} = \mathrm{i}\mathcal{K}\frac{1 - \sin\tau_1 \sin\tau_m}{\cos\tau_m}, \quad m = 1, 2, \ldots, M. \tag{4.84}$$

Thus

$$B_m^\pm(X) = b_m^\pm \mathrm{e}^{\mathrm{i}\mathcal{K}_m X}, \tag{4.85}$$

where

$$\mathcal{K}_m = \frac{(1 - \sin\tau_1 \sin\tau_m)\mathcal{K}}{\cos\tau_m}, \quad m = 1, 2, \ldots, M.$$

Inside the cylinder array, from (4.72) and (4.61), the envelope equations become

$$\frac{dB_m}{dX} = \frac{\mathrm{i}\Omega_0}{C_g \cos\tau_m}\left\{\frac{\Omega}{\Omega_0}(1 - \sin\tau_1 \sin\tau_m)B_m + \frac{1}{2}\sum_{p=1}^{M} B_p\left[2\mathbf{e}_{1p}^T \mathbf{M}\mathbf{e}_{1m} - \frac{\mathcal{A}_s}{\pi a^2}\right]\right\}, \tag{4.86}$$

which is

$$\frac{d}{dX}\begin{pmatrix} B_1 \\ B_2 \\ \vdots \\ B_M \end{pmatrix} = \frac{\mathrm{i}\Omega_0}{C_g}\mathbf{F}\begin{pmatrix} B_1 \\ B_2 \\ \vdots \\ B_M \end{pmatrix}, \tag{4.87}$$

where $C_g = |\mathbf{C}_g^{(m)}| = c$ and the elements of the matrix $\mathbf{F}$ are

$$F_{ii} = \frac{1}{\cos\tau_i}\left[\frac{\Omega}{\Omega_0}(1 - \sin\tau_1 \sin\tau_i) + \mathbf{e}_{1i}^T \mathbf{M}\mathbf{e}_{1j} - \frac{\mathcal{A}_s}{2\pi a^2}\right], \tag{4.88}$$

$$F_{ij} = \frac{1}{\cos\tau_i}\left[\mathbf{e}_{1j}^T \mathbf{M}\mathbf{e}_{1i} - \frac{\mathcal{A}_s}{2\pi a^2}\right], \ i, \ j = 1, 2, \ldots, M, \ i \neq j. \tag{4.89}$$

Here we only consider the case that none of the eigenvalues are equal to each other. In this case, the general solution of the linear system (4.87) is of the form

$$\begin{aligned}\mathbf{B} &= (B_1, B_2, \ldots, B_M)^T \\ &= C_1\mathbf{V}^{(1)}\mathrm{e}^{\mathrm{i}\lambda_1\Omega_0 X/C_g} + C_2\mathbf{V}^{(2)}\mathrm{e}^{\mathrm{i}\lambda_2\Omega_0 X/C_g} + \ldots + C_M\mathbf{V}^{(M)}\mathrm{e}^{\mathrm{i}\lambda_M\Omega_0 X/C_g},\end{aligned} \tag{4.90}$$

where $\mathbf{V}^{(j)}$ is the eigenvector corresponding to the eigenvalue λ_j, $j = 1, 2, \ldots, M$. The unknown coefficients $C_1, C_2, \ldots, C_M$ will be determined by the boundary conditions (4.82) and (4.83). The properties of this solution form depend on whether the eigenvalues of the matrix $\mathbf{F}$ are real or complex, and the form of the eigenvalues depends on the sign of the discriminant of the characteristic equation, which is, for example,

$$\lambda^2 - (F_{11} + F_{22})\lambda + (F_{11}F_{22} - F_{12}F_{21}) = 0, \text{ for } M = 2, \tag{4.91}$$

and

$$\lambda^3 + \alpha_2\lambda^2 + \alpha_1\lambda + \alpha_0 = 0, \text{ for } M = 3, \tag{4.92}$$

where

$$\alpha_2 = -(F_{11} + F_{22} + F_{33}), \tag{4.93}$$

$$\alpha_1 = \det\begin{pmatrix} F_{11} & F_{12} \\ F_{21} & F_{22} \end{pmatrix} + \det\begin{pmatrix} F_{11} & F_{13} \\ F_{31} & F_{33} \end{pmatrix} + \det\begin{pmatrix} F_{22} & F_{23} \\ F_{32} & F_{33} \end{pmatrix}, \tag{4.94}$$

$$\alpha_0 = -\det(\mathbf{F}). \tag{4.95}$$

The discriminants are

$$\Delta_2 = (F_{11} + F_{22})^2 - 4(F_{11}F_{22} - F_{12}F_{21}), \text{ for } M = 2, \tag{4.96}$$

$$\Delta_3 = 4\alpha_1^3 - \alpha_1^2\alpha_2^2 + 4\alpha_0\alpha_2^3 - 18\alpha_0\alpha_1\alpha_2 + 27\alpha_0^2, \text{ for } M = 3. \tag{4.97}$$

The discriminant Δ is a function of the detuning of the frequency Ω/Ω_0, which is contained in F_{ij}. For example, when $\Delta_3 < 0$, one of the eigenvalues is real and the other two are complex. Therefore one of the eigensolutions (4.90) is oscillatory in X with constant amplitude. The remaining two are oscillatory with exponentially decaying or growing amplitude. When $\Delta_3 > 0$, all the eigenvalues are real and all the waves in the array will oscillate in X with constant amplitudes.

Next, we consider and compare the transmission wave intensity $|B_1(X)|^2$ for four types of scatterers. We always take the length of the axis of the scatterer in y direction as b and the length of the axis in x direction as a. Given a length H, we take the typical size of the four types of scatterers are as follows

1. Circular cylinder: $b = a = H$.

2. Elliptical cylinder (i): $b = a/2 = H$.

3. Line grating: $a = 0,\ b = 2H$.

4. Elliptical cylinder (ii): $b = 2a = 2H$.

For every type of scatterer, the matrix of the dipole coefficients is

$$\begin{pmatrix} \dfrac{b(a+b)}{8H^2} & 0 \\ 0 & \dfrac{a(a+b)}{8H^2} \end{pmatrix} \tag{4.98}$$

[65, page 145] and $S = \pi ab$. To compare the diagrams for these four types of scatterers, here we use $2H$ as the dimensionless parameter, and the small parameter $\epsilon_1 = 2kH$.

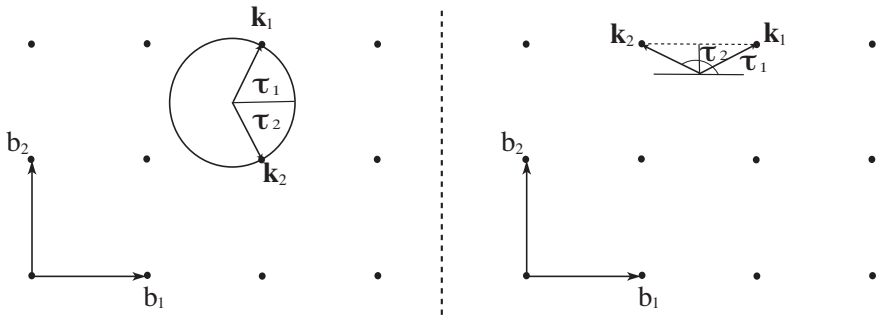

Figure 4.3: $M = 2$, forward (left) and backward (right) scattering by a square lattice.

Next, we will do the numerical calculations for $M = 2$ and $M = 3$. We have limited the incident angle to be in interval $(0, \pi/2)$. If we define the positive x-axis direction as the forward and the negative x-axis direction as the backward, then the incident wave always propagates forward. There are two different cases for the scattered wave, forward scattering (angle of the scattered wave is in the range of $[-\pi/2, \pi/2]$) and backward scattering (angle of the scattered wave is in the range of $[\pi/2, 3\pi/2]$). In figure 4.3 we give the example angles employed to do the calculations

$$\text{Forward scattering: } \tau_1 = \pi/3,\ \tau_2 = -\pi/3,$$

$$\text{Backward scattering: } \tau_1 = \pi/6,\ \tau_2 = 5\pi/6,$$

where τ_1 is the incident angle and τ_2 is the resonant angle.

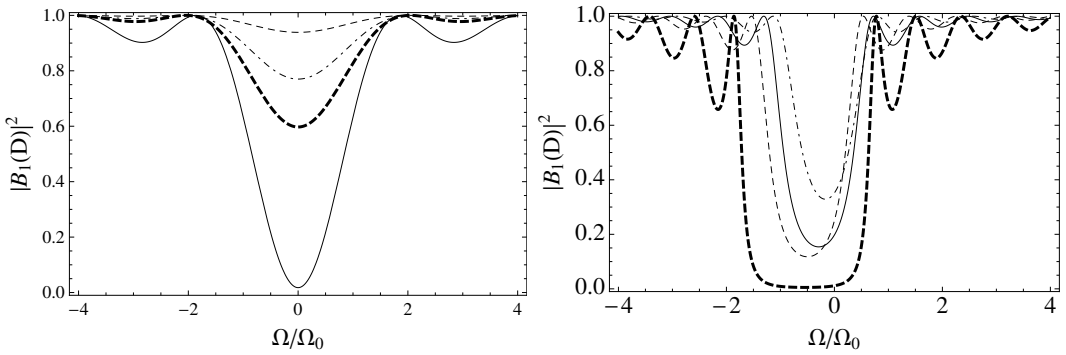

Figure 4.4: M=2. Comparison of the transmission wave intensity $|B_1(D)|^2$ over the detuning Ω/Ω_0. Left: forward scattering, $\Omega_0 D/C_g = 1$. Right: backward scattering, $\Omega_0 D/C_g = 4$. Dot-dashed line: $b = a$, solid line: $b = a/2$, dashed line: $a = 0$, thick dashed line: $b = 2a$.

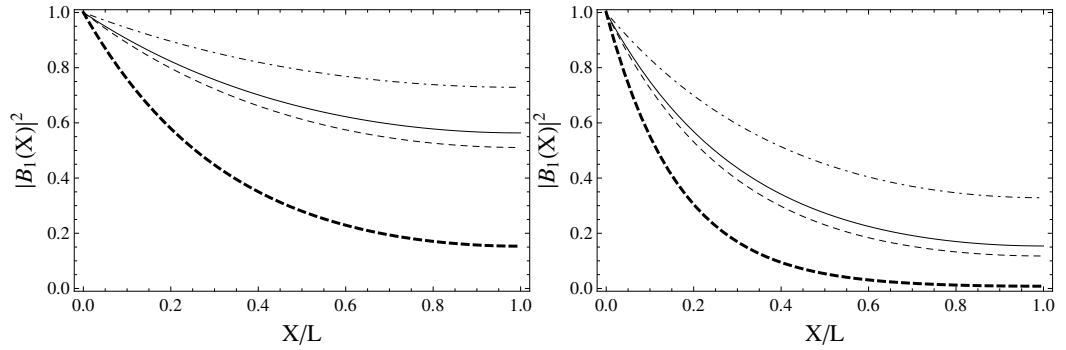

Figure 4.5: M=2, backward scattering. Comparison of the primary wave intensity $|B_1(X)|^2$ across the strip. Left: $\Omega_0 D/C_g = 2$, right: $\Omega_0 D/C_g = 4$. Dot-dashed line: $b = a$, solid line: $b = a/2$, dashed line: $a = 0$, thick dashed line: $b = 2a$.

In figure 4.4 we plot the transmission wave intensity $|B_1(D)|^2$ against the detuning Ω/Ω_0 for strip width $\Omega_0 D/C_g = 1$ for forward scattering and $\Omega_0 D/C_g = 4$ for backward scattering. For forward scattering, from the left hand diagram of figure 4.4, the elliptical cylinder (i) is most efficient in blocking the primary wave (the continuation of the incident wave in the array) while the line grating is the least efficient one. For backward scattering, as is seen from the right hand diagram of figure 4.4, the elliptical cylinder (ii) is the most efficient in blocking the primary wave while the circular cylinder is the least efficient one. The existence of the difference between forward scattering and backward scattering is because of the different incident angles. For forward scattering, the incident angle is $\pi/3$, which is bigger than $\pi/4$. Therefore the incident wave is easier to be blocked by scatterers whose axis length in direction of x-axis is longer, which is the elliptical cylinder (i). Similarly, for backward scattering, the primary angle is $\pi/6$, which is smaller than

$\pi/4$. Therefore the primary wave is easier to be blocked by scatterer whose axis length in direction of y-axis is longer, which is the elliptical cylinder (ii). The line grating has the same axis length in y-axis direction with elliptical cylinder (ii) but its area is zero, which makes it less efficient than elliptical cylinder (ii) in blocking the incident wave.

In the case of backward scattering, there is a region of detuning that gives eigenvalues that are complex conjugates. In this region, the solutions $B_1(X)$ and $B_2(X)$ are oscillatory with exponential decaying or growing amplitude. We define this region as the stop band. In figure 4.5 we compare the primary wave intensity $|B_1(X)|^2$ across the strip for scattering configuration in figure 4.3 when the detuning lies in the centre of their stop band. From figure 4.5, when the strip width $\Omega_0 D/C_g = 2$, the primary wave intensity decays most slowly for circular cylinder and decays fastest for elliptical cylinder (ii). When the strip width increases to 4, the transmission wave intensity decays to nearly zero for elliptical cylinder (ii) at the right edge of the strip and it decays more slowly for all the other scatterers. When the strip width is large enough, the transmission wave intensities of all four types of scatterers will decay to nearly zero at the exit edge of the strip.

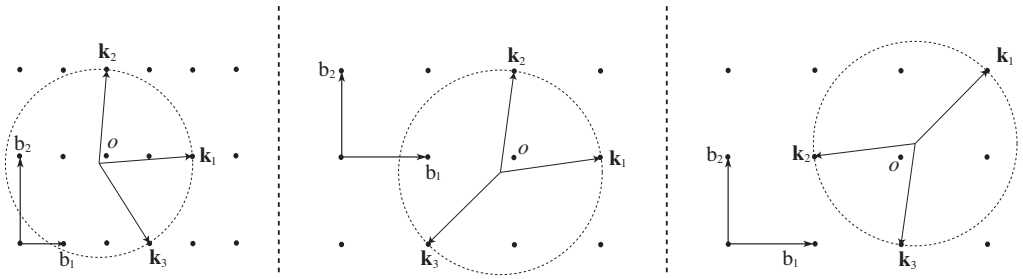

Figure 4.6: $M = 3$, forward-forward scattering (left), forward-backward scattering (middle), backward-backward scattering (right)

Next we consider the case of $M = 3$, i.e. one incident wave and two resonantly scattered waves. Three types of scattering are possible.

1. Type I (forward-forward): both resonated waves propagate forward as shown in the left hand diagram of figure 4.6. We consider a rectangular lattice of x spacing L and y spacing $2L$. $\tau_1 = \tan^{-1}(1/13) \approx 4.4°$, $\tau_2 = \tan^{-1} 13 \approx 85.6°$, $\tau_3 = -\tan^{-1}(11/7) \approx -57.53°$.

2. Type II (forward-backward): one resonated wave is reflected and the other one propagates forward as shown in the middle diagram of figure 4.6. A square lattice of

spacing L will be considered. $\tau_1 = \tan^{-1}(1/7) \approx 8.13°$, $\tau_2 = -3\pi/4 = -135°$, $\tau_3 = \tan^{-1} 7 \approx 81.87°$.

3. Type III (backward-backward): Both resonated waves are reflected, therefore propagate backward as shown in the right hand diagram of figure 4.6. A square lattice of spacing L will be considered. $\tau_1 = \pi/4 = 45°$, $\tau_2 = -\pi + \tan^{-1}(1/7) \approx -171.87°$, $\tau_3 = -\pi/2 - \tan^{-1}(1/7) \approx -98.13°$.

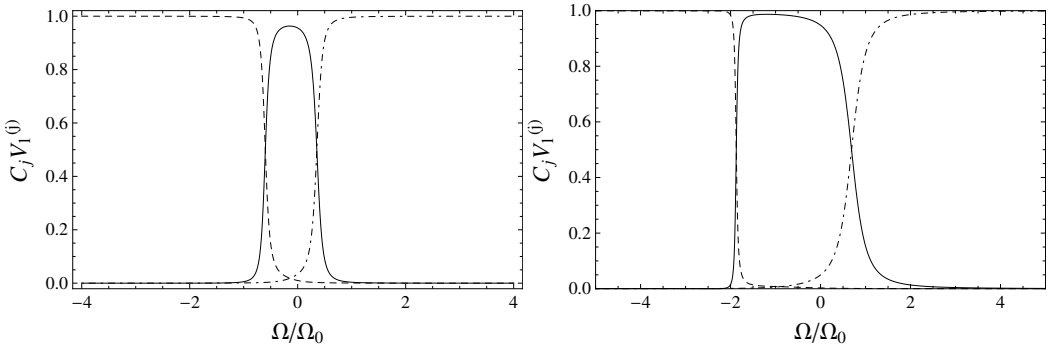

Figure 4.7: Three coefficients of the primary wave $B_1(X)$ in type I scattering. Left: circular cylinder ($b = a$), right: elliptical cylinder ($b = a/2$). Dashed line: $C_1 V_1^{(1)}$, solid line: $C_2 V_1^{(2)}$, dot-dashed line: $C_3 V_1^{(3)}$.

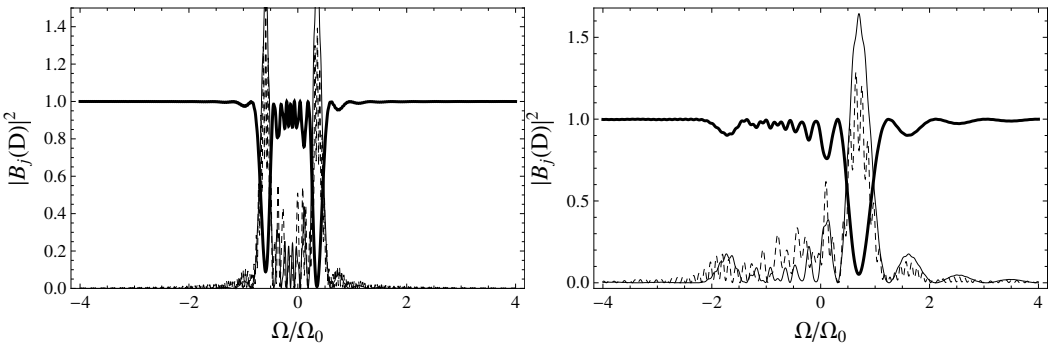

Figure 4.8: Dependence of wave intensities for type I scattering on the detuning frequency Ω/Ω_0. Left: $b = a$, $\Omega_0 D/C_g = 15$; right: $b = a/2$, $\Omega_0 D/C_g = 6$. Thick solid curve: $|B_1(D)|^2$, dashed curve: $|B_2(D)|^2$, thin solid curve: $|B_3(D)|^2$.

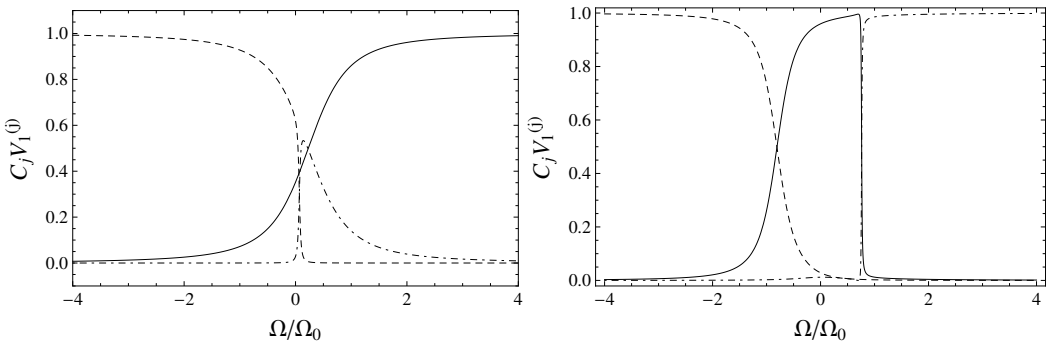

Figure 4.9: Three coefficients of the primary wave $B_1(X)$ in type I scattering. Left: line grating ($a = 0$), right: elliptical cylinder ($b = 2a$). Dashed line: $C_1V_1^{(1)}$, solid line: $C_2V_1^{(2)}$, dot-dashed line: $C_3V_1^{(3)}$.

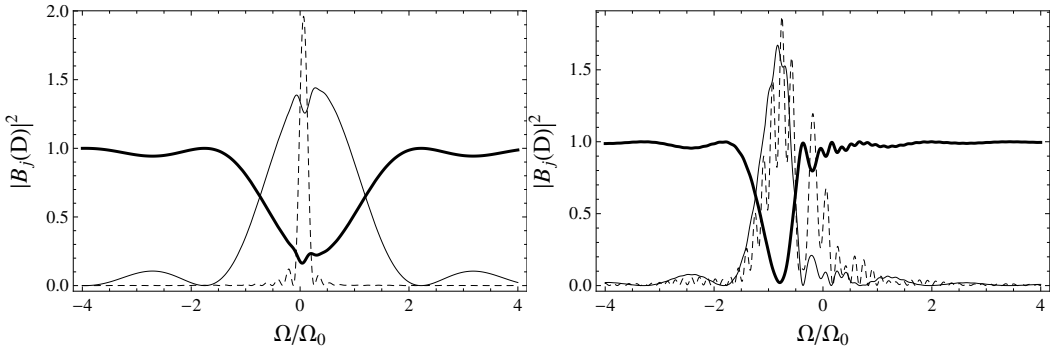

Figure 4.10: Dependence of wave intensities for type I scattering on the detuning frequency Ω/Ω_0. Left: $a = 0$, $\Omega_0 D/C_g = 3$; right: $b = 2a$, $\Omega_0 D/C_g = 4$. Thick solid curve: $|B_1(D)|^2$, dashed curve: $|B_2(D)|^2$, thin solid curve: $|B_3(D)|^2$.

In figure 4.7 and 4.9 we give the three coefficients of the transmitted wave $B_1(X)$ in type I scattering shown in the left hand diagram of figure 4.6. In figure 4.8 and 4.10 we give the dependence of wave intensities $|B_j(X)|^2$ on the right edge of the strip $X = D$ for type I scattering over the detuning frequency Ω/Ω_0. If we compare figure 4.7 with 4.8 and figure 4.9 with 4.10 respectively, we find there are valleys where two of the three transmitted wave coefficients are nearly equal. For example, in the right hand diagram of figure 4.7, at $\Omega/\Omega_0 \approx 0.69$, the coefficients $C_2V_1^{(2)}$ and $C_3V_1^{(3)}$ cross each other and nearly equal to 0.5. On the other hand, the other coefficient $C_1V_1^{(1)}$ is nearly zero. Therefore, the transmitted wave $B_1(X)$ is dominated by the last two eigenvectors; its intensity can

be approximated by

$$\begin{aligned} |B_1(X)|^2 &\approx \left| C_2 V_1^{(2)} \mathrm{e}^{\mathrm{i}\lambda_2 \Omega_0 X/C_g} + C_3 V_1^{(3)} \mathrm{e}^{\mathrm{i}\lambda_3 \Omega_0 X/C_g} \right|^2 \\ &\approx \frac{1}{4} \left| 1 + \mathrm{e}^{\mathrm{i}(\lambda_2-\lambda_3)\Omega_0 X/C_g} \right|^2 \\ &= \cos^2 \frac{(\lambda_2-\lambda_3)\Omega_0 X}{C_g}. \end{aligned} \tag{4.99}$$

Therefore the minimum transmission wave intensity occurs around

$$\begin{aligned} \frac{\Omega_0 X}{C_g} &= \frac{(2n+1)\pi}{|\lambda_2-\lambda_3|},\ n = 1, 2, \ldots \\ &\approx 5.26, 15.68, 26.13, \ldots. \end{aligned} \tag{4.100}$$

In the right hand diagram of 4.8, the strip width we use is $\Omega_0 D/C_g = 6$, which is near the minimum transmission wave intensity occurring at $\Omega_0 D/C_g = 5.26$. We can see the minimum transmission wave intensity for this strip width is quite close to zero. For the line grating $a = 0$, as we can see from the left hand diagram of figure 4.9, there is only one region (outside this region, one of the three coefficients $C_j V_j^{(1)},\ j = 1, 2, 3$, is nearly 1 and the other two are nearly zero, therefore $|B_1(X)|^2$ is nearly one) in which none of the coefficients $C_j V_j^{(1)}$ is absolutely dominant, therefore only one valley appears in the transmitted wave intensity as shown in the left hand diagram of 4.10. For elliptical cylinders (both of $b = a/2$ and $b = 2a$), from diagrams 4.7 and 4.9 we can see two regions of the detuning where two of the three transmitted coefficients are nearly equal (the eigenvalues are close correspondingly) and the other one nearly zero. But only one valley appears in the diagrams of the transmitted wave intensity. That is because in one of those two regions of the detuning, the two eigenvalues are quite close which makes the strip width be very big to let the second valley appears by (4.100). In figure 4.11 we give the second valley for the elliptical scatterers when the strip width is quite big (we only give the local diagrams, the whole diagram looks quite untidy when the strip width is so big).

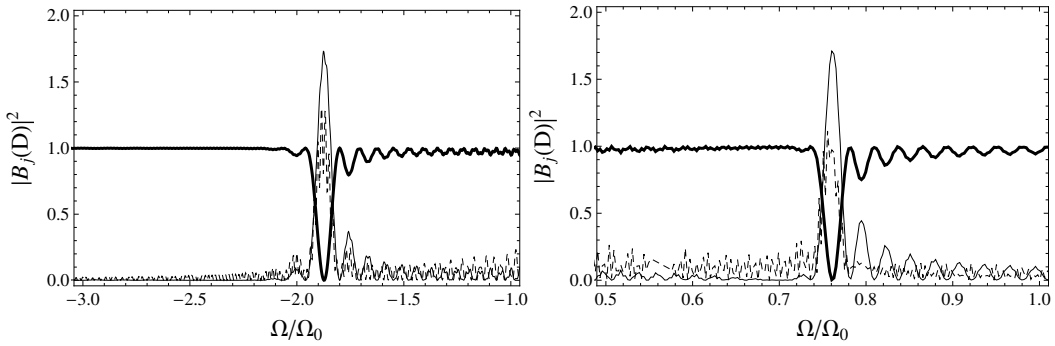

Figure 4.11: The local diagrams of the second valley for type I scattering. Left: $b = a/2$, $\Omega_0 D/C_g = 38$; right: $b = 2a$, $\Omega_0 D/C_g = 145$.

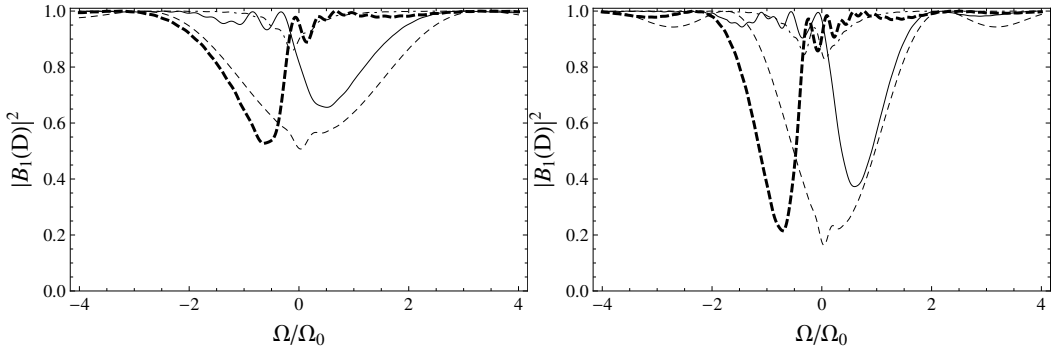

Figure 4.12: M=3. Comparison of the transmitted wave intensity for type I on the exit edge of the strip $|B_1(D)|^2$ over the detuning. Left: $\Omega_0 D/C_g = 2$. Right: $\Omega_0 D/C_g = 3$. Dot-dashed line: $b = a$, solid line: $b = a/2$, dashed line: $a = 0$, thick dashed line: $b = 2a$.

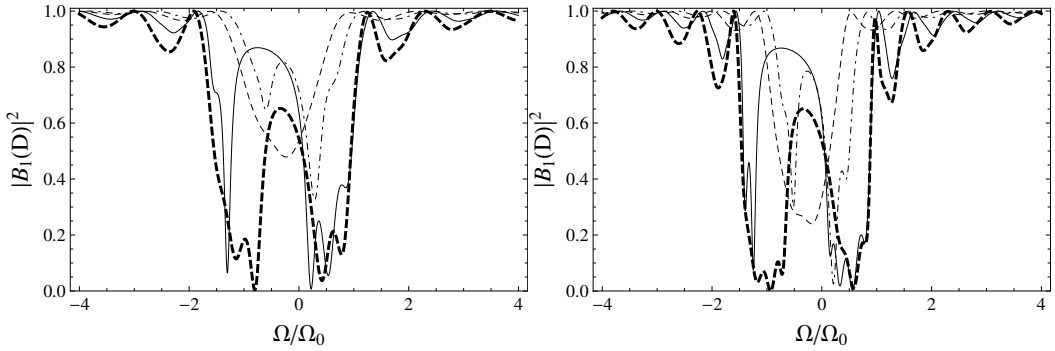

Figure 4.13: M=3. Comparison of the transmitted wave intensity for type II on the exit edge of the strip $|B_1(D)|^2$ over the detuning. Left: $\Omega_0 D/C_g = 2$. Right: $\Omega_0 D/C_g = 3$. Dot-dashed line: $b = a$, solid line: $b = a/2$, dashed line: $a = 0$, thick dashed line: $b = 2a$.

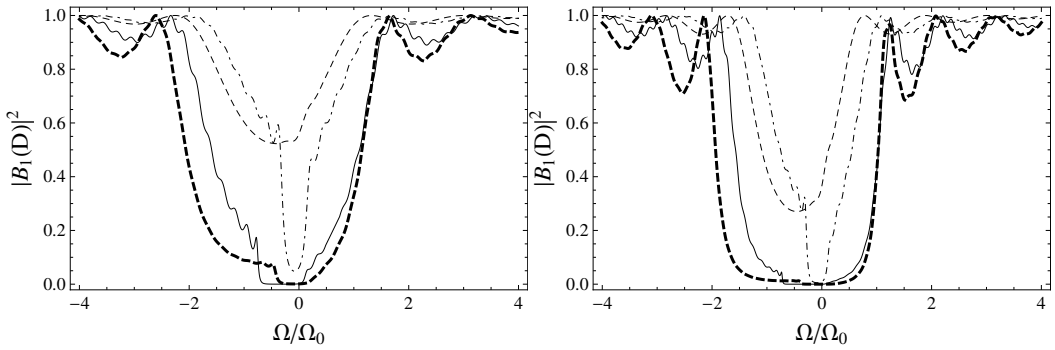

Figure 4.14: M=3. Comparison of the transmitted wave intensity for type III on the exit edge of the strip $|B_1(D)|^2$ over the detuning. Left: $\Omega_0 D/C_g = 2$. Right: $\Omega_0 D/C_g = 3$. Dot-dashed line: $b = a$, solid line: $b = a/2$, dashed line: $a = 0$, thick dashed line: $b = 2a$.

In figure 4.12, we compare the transmitted wave intensity for type I scattering on the exit edge of the strip against the detuning. We can see that the valley for line grating is the widest and one of the two valleys for elliptical cylinders is wider than circular cylinder. Therefore the line grating is most efficient to block the incident wave (Because the total energy is conserved in the array by (4.63), part of the incident energy is transferred into scattered energy by the array).

For type II forward-backward scattering and type III backward-backward scattering, two of the three eigenvalues will be complex conjugates for some region of detuning (the stop band). The stop band is always widest for elliptical cylinder (ii) and narrowest for circular cylinder. In figure 4.13 and 4.14, we compare the transmission wave intensity on the right edge of the strip $|B_1(D)|^2$ against the detuning Ω/Ω_0 and we can see the valleys are always widest for elliptical cylinder (ii). Thus the elliptical cylinder (ii) is the most efficient scatterer in blocking the incident wave and most energy is transferred into scattered energy when the detuning lies in the stop band.

4.2 Resonant scattering of acoustic waves by semi-infinite array

Here we consider the Bragg scattering of acoustic waves by a semi-infinite array of periodic arbitrary shape scatterers occupied $0 < X < \infty$ using the envelope equations (4.61) obtained in last section. Note that there will not enough boundary conditions to determine the unknowns because one edge of the strip goes to infinity. The additional condition

that no waves propagate from infinity must be applied to determine the unknowns in the envelopes uniquely.

We take the wave potentials in the left and right side of the y axis be

$$\Phi_0 = \sum_{m=1}^{M} A_m(X,Y,T)\mathrm{e}^{\mathrm{i}\boldsymbol{\beta}_m^T\mathbf{r}}, \tag{4.101}$$

where

$$A_m = \begin{cases} A_m^-, & X < 0, \\ \\ A_m, & X \geqslant 0. \end{cases} \tag{4.102}$$

As in (4.71), we allow a small detuning in the incident wave

$$A_1^-(X,Y,T)\mathrm{e}^{\mathrm{i}\boldsymbol{\beta}_1\mathbf{r}} = A_0\mathrm{e}^{\mathrm{i}(\mathcal{K}\cos\tau_1 X + \mathcal{K}\sin\tau_1 Y - \Omega T)}\mathrm{e}^{\mathrm{i}\boldsymbol{\beta}_1\mathbf{r}}, \tag{4.103}$$

and look for solutions in the form

$$\begin{pmatrix} A_m^-(X,Y,T) \\ A_m(X,Y,T) \end{pmatrix} = A_0 \begin{pmatrix} B_m^-(X) \\ B_m(X) \end{pmatrix} \mathrm{e}^{\mathrm{i}(\mathcal{K}\sin\tau_1 Y - \Omega T)},\ m = 1,2,\ldots,M, \tag{4.104}$$

Where the y variations are required to be same in every component of the solution by the continuity conditions on the left edge of the array $X = 0$. The boundary conditions are different from the finite strip width case because, for the semi-infinite array, there is only one boundary $X = 0$. On this boundary, the pressure and normal velocity are continuous and the continuity conditions are given by (4.73) and (4.75). These two continuity conditions give

$$\begin{aligned} &B_1^-(0) = B_1(0), \\ \\ &B_m^-(0) = B_m(0), \quad \text{if} \quad \cos\tau_m < 0, \\ \\ &B_m(0) = 0, \quad \text{if} \quad \cos\tau_m > 0, \end{aligned} \tag{4.105}$$

where τ_m are angles of the waves, and we always assume the incident wave is directed to north-east, i.e. $0 < \tau_1 < \pi/2$.

If all scattered waves propagate forward (wave vectors lie in first quadrant), the solutions are exactly same as the scattering by a finite width lattice. But when some of the scattered waves propagate backward, because the array only has one boundary, there

are not enough boundary conditions to get the solutions and some other conditions are needed. The conditions that need to be applied are that the group velocities for every term in the lattice must be directed into the lattice. The direction of the group velocity determines the direction of energy transport, and it must be ensured that there is no energy coming from infinity within the lattice. Now, we consider the case of only one wave in the lattice and propagating backward to illustrate how to get enough conditions to solve the problem.

From (4.88) and (4.89), when $M = 2$, the elements of matrix $\mathbf{F}$ are

$$F_{11} = \frac{\Omega}{\Omega_0}\cos\tau_1 + \frac{1}{\cos\tau_1}\left(\mathbf{e}_{11}^T\mathbf{M}\mathbf{e}_{11} - \frac{\mathcal{A}_s}{2\pi a^2}\right),$$

$$F_{12} = \frac{1}{\cos\tau_1}\left(\mathbf{e}_{12}^T\mathbf{M}\mathbf{e}_{11} - \frac{\mathcal{A}_s}{2\pi a^2}\right),$$

$$F_{21} = \frac{1}{\cos\tau_2}\left(\mathbf{e}_{11}^T\mathbf{M}\mathbf{e}_{12} - \frac{\mathcal{A}_s}{2\pi a^2}\right),$$

$$F_{22} = \frac{\Omega}{\Omega_0}\frac{1-\sin\tau_1\sin\tau_2}{\cos\tau_2} + \frac{1}{\cos\tau_2}\left(\mathbf{e}_{12}^T\mathbf{M}\mathbf{e}_{12} - \frac{\mathcal{A}_s}{2\pi a^2}\right),$$

where a is a typical dimension of the scatterers. The matrix $\mathbf{F}$ hence has the following characteristic equation

$$\lambda^2 - (F_{11}+F_{22})\lambda + F_{11}F_{22} - F_{12}F_{21} = 0, \tag{4.106}$$

whose eigenvalues are

$$\lambda_{1,2} = \frac{F_{11}+F_{22} \pm \Delta^{1/2}}{2}, \tag{4.107}$$

where Δ is the discriminant

$$\begin{aligned}
\Delta &= (F_{11}+F_{22})^2 - 4(F_{11}F_{22} - F_{12}M_{21}) \\
&= (F_{11}-F_{22})^2 + 4F_{12}F_{21} \\
&= \left[\frac{\Omega}{\Omega_0}\frac{\cos(\tau_1-\tau_2)-1}{\cos\tau_2} + \frac{1}{\cos\tau_1}\left(\mathbf{e}_{11}^T\mathbf{M}\mathbf{e}_{11} - \frac{\mathcal{A}_s}{2\pi a^2}\right) - \frac{1}{\cos\tau_2}\left(\mathbf{e}_{12}^T\mathbf{M}\mathbf{e}_{12} - \frac{\mathcal{A}_s}{2\pi a^2}\right)\right]^2 \\
&\quad + \frac{4}{\cos\tau_1\cos\tau_2}\left(\mathbf{e}_{12}^T\mathbf{M}\mathbf{e}_{11} - \frac{\mathcal{A}_s}{2\pi a^2}\right)^2.
\end{aligned} \tag{4.108}$$

When the scattered wave propagates backward, i.e. $\cos\tau_2 < 0$, which makes the sign of the discriminant Δ depend on the detuning Ω/Ω_0 when τ_2 is specified. It can be seen that $\Delta < 0$ within the stop band defined by

$$\frac{\Omega_c^-}{\Omega_0} < \frac{\Omega}{\Omega_0} < \frac{\Omega_c^+}{\Omega_0}, \tag{4.109}$$

where

$$\frac{\Omega_c^{\mp}}{\Omega_0} = \frac{\cos\tau_2}{\cos(\tau_1-\tau_2)-1} \times$$
$$\left[\mp\frac{2|\mathbf{e}_{12}^T\mathbf{M}\mathbf{e}_{11} - \frac{\mathcal{A}_s}{2\pi a^2}|}{\sqrt{-\cos\tau_1\cos\tau_2}} - \frac{1}{\cos\tau_1}\left(\mathbf{e}_{11}^T\mathbf{M}\mathbf{e}_{11} - \frac{\mathcal{A}_s}{2\pi a^2}\right) + \frac{1}{\cos\tau_2}\left(\mathbf{e}_{12}^T\mathbf{M}\mathbf{e}_{12} - \frac{\mathcal{A}_s}{2\pi a^2}\right)\right]. \tag{4.110}$$

As an example, we choose the square lattice of spacing L and a reciprocal vector $\mathbf{K}_{-1,0} = -\mathbf{b}_1 = -2\pi\mathrm{i}/L$, as shown in the right hand diagram of figure 4.3. We choose $\tau_1 = \pi/6$ so $\tau_2 = 5\pi/6$ and the incident wavenumber is $\beta = 2\pi/\sqrt{3}L$. If we consider the circular cylinder with radius of a, $\mathcal{A}_s = \pi a^2$ and $\mathbf{M}$ is a two-dimensional identity matrix. Then it follows from equation (4.110) that the band gap boundaries are

$$\frac{\Omega_c^-}{\Omega_0} = -2, \ \frac{\Omega_c^+}{\Omega_0} = \frac{2}{3}. \tag{4.111}$$

Outside and inside the lattice, $B_m^-(X)$ and $B_m(X)$ satisfy (4.84) and (4.87) respectively. When $M = 2$, outside the lattice we get

$$B_1^-(X) = \mathrm{e}^{\mathrm{i}\mathcal{K}\cos\tau_1 X}, \quad B_2^-(X) = R\mathrm{e}^{\mathrm{i}\mathcal{K}_2 X}, \tag{4.112}$$

where R is the reflection coefficient needs to be determined, $\mathcal{K}_2 = \mathcal{K}(1-\sin\tau_1\sin\tau_2)/\cos\tau_2$. In the case of finite strip width, R is determined by the continuity condition on the right edge of the strip. Inside the lattice we have

$$\frac{dB_1(X)}{dX} = \frac{\mathrm{i}\Omega_0}{C_g}\Big[F_{11}B_1(X) + F_{12}B_2(X)\Big], \tag{4.113}$$

$$\frac{dB_2(X)}{dX} = \frac{\mathrm{i}\Omega_0}{C_g}\Big[F_{21}B_1(X) + F_{22}B_2(X)\Big]. \tag{4.114}$$

If we denote the eigenvalues of the matrix $\mathbf{F}$ by λ_1 and λ_2 then

$$B_1(X) = b_{11}\mathrm{e}^{\mathrm{i}\frac{\lambda_1\Omega_0}{C_g}X} + b_{12}\mathrm{e}^{\mathrm{i}\frac{\lambda_2\Omega_0}{C_g}X}, \tag{4.115}$$

$$B_2(X) = b_{21}\mathrm{e}^{\mathrm{i}\frac{\lambda_1\Omega_0}{C_g}X} + b_{22}\mathrm{e}^{\mathrm{i}\frac{\lambda_2\Omega_0}{C_g}X}, \tag{4.116}$$

where $b_{ij},\ i,j=1,2$ are unknowns that need to be determined. By the boundary conditions (4.105),

$$B_1(0) = b_{11} + b_{12} = B_1^-(0) = 1, \tag{4.117}$$

$$B_2(0) = b_{21} + b_{22} = B_2^-(0) = R. \tag{4.118}$$

Thus by (4.113), (4.114), (4.117) and (4.118), we have

$$B_1(X) = \frac{F_{11} - \lambda_2 + RF_{12}}{\lambda_1 - \lambda_2} \mathrm{e}^{\mathrm{i}\frac{\lambda_1 \Omega_0}{C_g} X} - \frac{F_{11} - \lambda_1 + RF_{12}}{\lambda_1 - \lambda_2} \mathrm{e}^{\mathrm{i}\frac{\lambda_2 \Omega_0}{C_g} X}, \tag{4.119}$$

$$B_2(X) = -\frac{(F_{11} - \lambda_1)(F_{11} - \lambda_2 + RF_{12})}{F_{12}(\lambda_1 - \lambda_2)} \mathrm{e}^{\mathrm{i}\frac{\lambda_1 \Omega_0}{C_g} X} + \frac{(F_{11} - \lambda_2)(F_{11} - \lambda_1 + RF_{12})}{F_{12}(\lambda_1 - \lambda_2)} \mathrm{e}^{\mathrm{i}\frac{\lambda_2 \Omega_0}{C_g} X}. \tag{4.120}$$

Within the stop band $-2 < \Omega/\Omega_0 < 2/3$, $\Delta < 0$, the eigenvalues $\lambda_{1,2}$ are complex conjugates which makes one of the coefficients of $B_1(X)$ and $B_2(X)$ zero under the constraint that $B_1(X)$ and $B_2(X)$ cannot be infinity when $X \to \infty$. If we set $\mathrm{Im}(\lambda_1) > 0$, then b_{12} and b_{22} must be zero and hence

$$R = \frac{\lambda_1 - F_{11}}{F_{12}}, \tag{4.121}$$

so that the solutions are

$$B_1(X) = \mathrm{e}^{\mathrm{i}\frac{\lambda_1 \Omega_0}{C_g} X}, \tag{4.122}$$

$$B_2(X) = \frac{F_{11} - \lambda_1}{F_{12}} \mathrm{e}^{\mathrm{i}\frac{\lambda_1 \Omega_0}{C_g} X}. \tag{4.123}$$

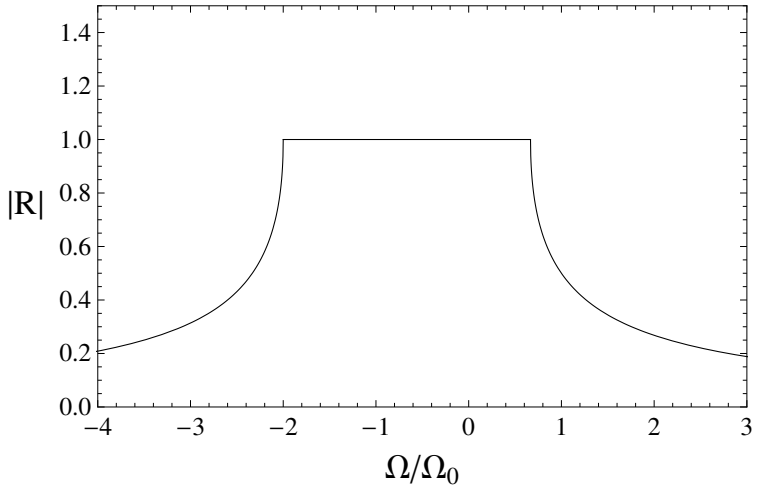

Figure 4.15: The reflection coefficient R over the detuning Ω/Ω_0.

Outside the stop band, if $\Omega/\Omega_0 > 2/3$, and we assume $\lambda_1 = \sqrt{\Delta} > 0$, $\lambda_2 = -\sqrt{\Delta} < 0$, the group velocity associated with λ_1 is

$$C_g^1 = \frac{\Delta\omega}{\Delta k} = \frac{\Omega}{\lambda_1 \Omega_0 / C_g} > 0, \tag{4.124}$$

then the energy propagates to the right. The group velocity associated with λ_2 is

$$C_g^2 = \frac{\Delta\omega}{\Delta k} = \frac{\Omega}{\lambda_2 \Omega_0 / C_g} < 0, \tag{4.125}$$

then the energy propagates to the left. But because the lattice is semi-infinite, there should not be energy coming from the infinity, therefore the coefficient of terms associated λ_2 should be zero, which means that

$$R = \frac{\lambda_1 - F_{11}}{F_{12}}, \tag{4.126}$$

and the solutions are the same as (4.122) and (4.123). Finally when $\Omega/\Omega_0 < -2$, because $\Omega < 0$ and $\lambda_1 > 0$, the group velocity associated with λ_1 will be negative which leads to

$$R = \frac{\lambda_2 - F_{11}}{F_{12}}, \tag{4.127}$$

and the solutions are

$$B_1(X) = \mathrm{e}^{\mathrm{i}\frac{\lambda_2 \Omega_0}{C_g} X}, \tag{4.128}$$

$$B_2(X) = \frac{F_{11} - \lambda_2}{F_{12}} \mathrm{e}^{\mathrm{i}\frac{\lambda_2 \Omega_0}{C_g} X}. \tag{4.129}$$

In figure 4.15 we give the diagram of the reflection coefficient $|R|$ against the detuning Ω. In the stop band $(-2, 2/3)$, $|R| = 1$, and out of the band gap, $|R|$ decays to zero when the detuning is big enough, which means most energy propagates into the array.

4.3 Elastic resonant scattering by doubly-periodic arrays

In this section we generalise Li and Mei's method in [49] to the multiple resonant scattering of elastic waves by a doubly-periodic array of identical cavity cylinders. We first derive the envelope equations in an infinite array of cavity cylinders in an elastic medium and then apply them to a finite width (finite in one direction and infinite in the other directions) elastic strip of cavity cylinder array bounded by the same acoustic media on both sides.

4.3.1 Formulation

As in the previous two sections, we assume that the cylinders are infinitely long and then the problem is inherently two dimensional. The coordinate systems, lattice vectors, reciprocal vectors and Bloch vector are exactly the same as those used in section 4.1.

In the acoustic case, only dilatational waves are present, but in an elastic medium there will be dilatational and shear waves coupled together through the boundary conditions. The dilatational potentials ϕ and shear ψ satisfy the two-dimensional wave equations

$$\frac{\partial^2 \phi}{\partial t^2} - c_1^2 \nabla^2 \phi = 0, \tag{4.130}$$

$$\frac{\partial^2 \psi}{\partial t^2} - c_2^2 \nabla^2 \psi = 0. \tag{4.131}$$

The periodicity of the problem implies that the potentials ϕ and ψ also satisfy the Bloch conditions (4.3). The boundary conditions in the array for the problem come from the stress free condition on the surface of each cavity and are

$$\begin{cases} \mu \left(-\dfrac{2}{a^2}\dfrac{\partial \phi}{\partial \theta} + \dfrac{2}{a}\dfrac{\partial^2 \phi}{\partial \theta \partial r} + \beta_2^2 \psi + \dfrac{2}{a}\dfrac{\partial \psi}{\partial r} + \dfrac{2}{a^2}\dfrac{\partial^2 \psi}{\partial \theta^2} \right) = 0, \quad r_j = a, \\ 2\mu \left(\dfrac{1}{a}\dfrac{\partial^2 \psi}{\partial \theta \partial r} - \dfrac{1}{a^2}\dfrac{\partial \psi}{\partial \theta} - \dfrac{1}{a}\dfrac{\partial \phi}{\partial r} - \dfrac{1}{a^2}\dfrac{\partial^2 \phi}{\partial \theta^2} \right) - \beta_1^2 (\lambda + 2\mu)\phi = 0, \quad r_j = a, \end{cases} \tag{4.132}$$

where β_1 and β_2 are wavenumbers of dilatational and shear wave without the detuning. We denote the detuning of the wavenumbers by $\mathcal{K}_1$ and $\mathcal{K}_2$ for dilatational and shear wave respectively (the detuning of the frequency is written to be $\Omega = \mathcal{K}c = \mathcal{K}_1 c_1 = \mathcal{K}_2 c_2$), then the detuned wavenumbers $k_1 = \beta_1 + \epsilon_1^2 \mathcal{K}_1$ and $k_2 = \beta_2 + \epsilon_1^2 \mathcal{K}_2$, where $\epsilon_1 = \beta_1 a \ll 1$ is the small parameter we are going to use. The detuned frequencies $\omega' = \omega + \epsilon_1^2 \Omega$, where $\omega = \beta_1 c_1 = \beta_2 c_2$. The method of matched asymptotic expansions and multiple scales will be used. Each cell is separated into two regions, the inner region around the cylinder and the outer region far away from the cylinder. The fast and slow variables are introduced in (4.9).

Here, we consider the perturbation of the dilatational wave. From section 3.2 we know that if the leading order outer potential of the dilatational wave is $O(1)$, then the leading order outer potential for the shear wave is $O(\epsilon_1^2)$. Then, if we denote the outer potentials by Φ and Ψ for dilatational and shear wave respectively, they can be expanded as follows

$$\Phi = Re\{[\Phi_0 + \epsilon_1^2 \Phi_2 + O(\epsilon_1^4)]\mathrm{e}^{-\mathrm{i}\omega t}\}, \tag{4.133}$$

$$\Psi = Re\{[\epsilon_1^2 \Psi_2 + O(\epsilon_1^4)]\mathrm{e}^{-\mathrm{i}\omega t}\}, \tag{4.134}$$

where $\Phi_0,\ \Phi_2$ and Ψ_2 are all functions of fast and slow variables $(x,\ y,\ X,\ Y,\ T)$, where the slow variables $X = \epsilon_1^2 x,\ Y = \epsilon_1^2 y$ and $T = \epsilon_1^2 t$. Substituting (4.133) and (4.134) into the governing equations (4.130) and (4.131), we obtain the governing equations for the outer potentials $\Phi_0,\ \Phi_2$ and Ψ_2.

At the first order, the outer dilatational potential Φ_0 is governed by

$$\nabla^2 \Phi_0 + \frac{\omega^2}{c_1^2} \Phi_0 = 0. \tag{4.135}$$

At the second order, the dilatational potential Φ_2 is governed by

$$\nabla^2 \Phi_2 + \frac{\omega^2}{c_1^2} \Phi_2 = -2\overline{\nabla} \cdot \nabla \Phi_0 - \frac{2\mathrm{i}\omega}{c_1^2} \frac{\partial \Phi_0}{\partial T}, \tag{4.136}$$

and the shear potential Ψ_2 is governed by

$$\nabla^2 \Psi_2 + \frac{\omega^2}{c_2^2} \Psi_2 = 0. \tag{4.137}$$

In addition, Φ_0, Φ_2 and Ψ_2 satisfy Bloch theorem (4.3). The leading order solution is the dilatational wave, which is formally the sum of all mutually resonant progressive waves

$$\Phi_0 = \sum_{m=1}^{M} A_m(X, Y, T) \psi_m(x, y), \tag{4.138}$$

where

$$\psi_m(x,y) = \mathrm{e}^{\mathrm{i}\boldsymbol{\beta}_m^T\mathbf{r}}, \tag{4.139}$$

with all $\boldsymbol{\beta}_m = \beta(\cos\tau_m\mathbf{i} + \sin\tau_m\mathbf{j})$ determined by the Bragg condition (4.4). Then

$$\Phi_0 = \sum_{m=1}^{M} A_m(X,Y,T)\mathrm{e}^{\mathrm{i}\boldsymbol{\beta}_m^T\mathbf{r}} = \sum_{m=1}^{M} A_m(X,Y,T)\mathrm{e}^{\mathrm{i}\boldsymbol{\beta}_m^T\mathbf{R}_j}\mathrm{e}^{\mathrm{i}\beta r_j\cos(\theta-\tau_m)} \tag{4.140}$$

From (4.140), the inner expansion of the leading order outer solution up to order ϵ_1^2 for the dilatational wave is

$$\begin{aligned}
\Phi^{(0,2)} &= \sum_{m=1}^{M} A_m\mathrm{e}^{\mathrm{i}\boldsymbol{\beta}_m^T\mathbf{R}_j}\left[1 + i\epsilon_1\rho\cos(\theta-\tau_m) + \frac{1}{2}i^2\epsilon_1^2\rho^2\cos^2(\theta-\tau_m)\right] \\
&= \sum_{m=1}^{M} A_m\mathrm{e}^{\mathrm{i}\boldsymbol{\beta}_m^T\mathbf{R}_j}\left\{1 + i\epsilon_1\rho\ (\cos\tau_m,\ \sin\tau_m)\begin{pmatrix}\cos\theta\\ \sin\theta\end{pmatrix}\right. \\
&\qquad \left. -\frac{1}{4}\epsilon_1^2\rho^2\left[1 + (\cos 2\tau_m,\ \sin 2\tau_m)\begin{pmatrix}\cos 2\theta\\ \sin 2\theta\end{pmatrix}\right]\right\}.
\end{aligned} \tag{4.141}$$

From equation (3.156) in section 3.2, the inner solution for the dilatational wave $\bar{\phi}$ is

$$\begin{aligned}
\bar{\phi} =& B_0 + \mathbf{u}_0^T\frac{1}{\rho^2}\begin{pmatrix}\cos 2\theta\\ \sin 2\theta\end{pmatrix} + B_{11}\nu_{11}(\epsilon_1) + \epsilon_1\left[B_1 + \mathbf{u}_1^T\rho\begin{pmatrix}\cos\theta\\ \sin\theta\end{pmatrix} + \mathbf{u}_I^T\frac{1}{\rho}\begin{pmatrix}\cos\theta\\ \sin\theta\end{pmatrix} + \ldots\right] \\
&+ \epsilon_1\nu_{11}(\epsilon_1)\mathbf{u}_{11}^T\rho\begin{pmatrix}\cos\theta\\ \sin\theta\end{pmatrix} + \mu_{21}(\epsilon_1)B_{21} + \epsilon_1^2\log\epsilon_1 B_{22} \\
&+ \epsilon_1^2\left[\bar{B}_2 + \bar{v}_0\log\rho - \frac{1}{4}B_0\rho^2 + \frac{1}{4}\mathbf{u}_0^T\begin{pmatrix}\cos 2\theta\\ \sin 2\theta\end{pmatrix} + \bar{\mathbf{v}}_1^T\rho\begin{pmatrix}\cos\theta\\ \sin\theta\end{pmatrix} + \bar{\mathbf{v}}_2^T\rho^2\begin{pmatrix}\cos 2\theta\\ \sin 2\theta\end{pmatrix} + \ldots\right] \\
&+ O(\epsilon_1^3),
\end{aligned} \tag{4.142}$$

where the ellipses indicate eigenfunctions that are not needed in the current part.

As in the acoustic case, to obtain the envelope equations, we apply Green's identity to ψ_m^* and the composite solution in a cell C (the cylinder in this cell is marked as S), where ψ_m^* denotes the complex conjugate of ψ_m. We use ξ as the composite expansion and take

$$\xi = \Phi^{(2)} + \phi^{(2)} - \phi^{(2,2)}. \tag{4.143}$$

Here we include the inner solution up to order ϵ_1^2 which is different with the acoustic case. This is because the order ϵ_1^2 term in the inner solution will contribute to the integration in Green's identity. The Green's identity is

$$\int\int_{C_s}\left(\xi\nabla^2\psi_m^* - \psi_m^*\nabla^2\xi\right)ds = \int_{\partial C_s}\left(\xi\frac{\partial\psi_m^*}{\partial n} - \psi_m^*\frac{\partial\xi}{\partial n}\right)dl, \tag{4.144}$$

where C_s is the cell C excluding the cylinder S. Then noting that $\phi^{(2)} - \phi^{(2,2)}$ contains only singular terms of order ϵ_1^2 and hence when written in terms of outer coordinates $\phi^{(2)} - \phi^{(2,2)} = o(\epsilon_1^2)$ by section (3.2). Then the left hand side of Green's identity becomes

$$\begin{aligned} LHS(4.144) &= \int\int_{\mathcal{C}_s} \left[(\Phi^{(2)} + \phi^{(2)} - \phi^{(2,2)}) \nabla^2 \psi_m^* - \psi_m^* \nabla^2 (\Phi^{(2)} + \phi^{(2)} - \phi^{(2,2)}) \right] ds \\ &= \int\int_{\mathcal{C}_s} \left(\Phi^{(2)} \nabla^2 \psi_m^* - \psi_m^* \nabla^2 \Phi^{(2)} \right) ds \\ &+ \int\int_{\mathcal{C}_s} \left[(\phi^{(2)} - \phi^{(2,2)}) \nabla^2 \psi_m^* - \psi_m^* \nabla^2 (\phi^{(2)} - \phi^{(2,2)}) \right] ds \\ &= \int\int_{C_s} \left(\Phi^{(2)} \nabla^2 \psi_m^* - \psi_m^* \nabla^2 \Phi^{(2)} \right) ds + o(\epsilon_1^2). \end{aligned} \tag{4.145}$$

Using equation (4.135) and (4.136) and dropping terms of order higher than ϵ_1^2

$$\begin{aligned} LHS(4.144) &= \int\int_{C_s} \left(\Phi_0 \nabla^2 \psi_m^* - \psi_m^* \nabla^2 \Phi_0 \right) ds + \epsilon_1^2 \int\int_{C_s} \left(\Phi_2 \nabla^2 \psi_m^* - \psi_m^* \nabla^2 \Phi_2 \right) ds \\ &= \int\int_{C_s} \left[\Phi_0 (-\beta^2 \psi_m^*) - \psi_m^* \left(-\frac{\omega^2}{c^2} \Phi_0 \right) \right] ds \\ &\quad + \epsilon_1^2 \int\int_{C_s} \left[-\Phi_2 \beta^2 \psi_m^* - \psi_m^* (-2\overline{\nabla} \cdot \nabla \Phi_0 - \frac{\omega^2}{c^2} \Phi_2 - \frac{2\mathrm{i}\omega}{c^2} \frac{\partial \Phi_0}{\partial T}) \right] ds \\ &= \epsilon_1^2 \int\int_{C_s} \left(2\psi_m^* \overline{\nabla} \cdot \nabla \Phi_0 + \frac{2\mathrm{i}\omega}{c^2} \psi_m^* \frac{\partial \Phi_0}{\partial T} \right) ds \\ &= \epsilon_1^2 \left(2\mathrm{i} \sum_{h=1}^{M} \overline{\nabla} A_h \cdot \boldsymbol{\beta}_h + \frac{2\mathrm{i}\omega}{c^2} \sum_{h=1}^{M} \frac{\partial A_h}{\partial T} \right) \int\int_{C_s} \mathrm{e}^{\mathrm{i}(\boldsymbol{\beta}_h - \boldsymbol{\beta}_m)^T \mathbf{r}} ds \\ &= \epsilon_1^2 \sum_{h=1}^{M} \left(\frac{2\mathrm{i}\omega}{c^2} \frac{\partial A_h}{\partial T} + 2\mathrm{i} \overline{\nabla} A_h \cdot \boldsymbol{\beta}_h \right) \int\int_{C_s} \mathrm{e}^{\mathrm{i}(\boldsymbol{\beta}_h - \boldsymbol{\beta}_m)^T \mathbf{r}} ds. \end{aligned} \tag{4.146}$$

Since the cylinder radius is much smaller than the periodicity of the lattice, the cross-sectional area of a cylinder $\mathcal{A}_s$ is much smaller than that of the cell $\mathcal{A}_c$, therefore the area of the cell excluding the cylinder is: $\mathcal{A}_{cs} = \mathcal{A}_c - \pi a^2 = \mathcal{A}_c[1 + O(\epsilon_1^2)] \approx \mathcal{A}_c$. Therefore the integral in (4.146) can be approximated by

$$\begin{aligned} \int\int_{C_s} \mathrm{e}^{\mathrm{i}(\boldsymbol{\beta}_h - \boldsymbol{\beta}_m)^T \mathbf{r}} ds &= \int\int_{C} \mathrm{e}^{\mathrm{i}(\boldsymbol{\beta}_h - \boldsymbol{\beta}_m)^T \mathbf{r}} ds + O(\epsilon_1^2) \mathcal{A}_c \\ &= [\delta_{hm} + O(\epsilon_1^2)] \mathcal{A}_c. \end{aligned} \tag{4.147}$$

Substituting (4.147) into (4.146) and dropping terms of higher order, we get

$$LHS(4.144) = \epsilon_1^2 \frac{2\mathrm{i}\omega}{c^2} \mathcal{A}_c \left(\frac{\partial A_m}{\partial T} + \frac{c^2}{\omega} \overline{\nabla} A_m \cdot \boldsymbol{\beta}_m \right). \tag{4.148}$$

The right hand side of Green's identity is

$$
\begin{aligned}
&RHS(4.144)\\
&= -\int_0^{2\pi}\left(\bar{\phi}\frac{\partial\psi_m^*}{\partial\rho}-\psi_m^*\frac{\partial\bar{\phi}}{\partial\rho}\right)a d\theta\\
&= -\int_0^{2\pi}\left\{B_0+\mathbf{u}_0^T\begin{pmatrix}\cos 2\theta\\ \sin 2\theta\end{pmatrix}+\epsilon_1\left[B_1+\mathbf{u}_1^T\begin{pmatrix}\cos\theta\\ \sin\theta\end{pmatrix}+\mathbf{u}_I^T\begin{pmatrix}\cos\theta\\ \sin\theta\end{pmatrix}+\ldots\right]\right.\\
&\quad+\epsilon_1\nu_{11}(\epsilon_1)\mathbf{u}_{11}^T\begin{pmatrix}\cos\theta\\ \sin\theta\end{pmatrix}+\mu_{21}(\epsilon_1)B_{21}+\epsilon_1^2\log\epsilon_1 B_{22}\\
&\quad\left.+\epsilon_1^2\left[\bar{B}_2-\frac{1}{4}B_0+\frac{1}{4}\mathbf{u}_0^T\begin{pmatrix}\cos 2\theta\\ \sin 2\theta\end{pmatrix}+\bar{\mathbf{v}}_1^T\begin{pmatrix}\cos\theta\\ \sin\theta\end{pmatrix}+\bar{\mathbf{v}}_2^T\begin{pmatrix}\cos 2\theta\\ \sin 2\theta\end{pmatrix}+\ldots\right]\right\}\times\\
&\left\{-\mathrm{i}\epsilon_1\cos(\theta-\tau_m)\left[1-\mathrm{i}\epsilon_1\cos(\theta-\tau_m)\ -\frac{1}{4}\epsilon_1^2[1+\cos 2(\theta-\tau_m)]+O(\epsilon_1^3)\right]\right\}\mathrm{e}^{-\mathrm{i}\boldsymbol{\beta}_m^T\mathbf{R}_j}d\theta\\
&+\int_0^{2\pi}\left\{1-\mathrm{i}\epsilon_1\cos(\theta-\tau_m)-\frac{1}{4}\epsilon_1^2[1+\cos 2(\theta-\tau_m)]+O(\epsilon_1^3)\right\}\times\\
&\left\{-2\mathbf{u}_0^T\begin{pmatrix}\cos 2\theta\\ \sin 2\theta\end{pmatrix}+\epsilon_1\left[\mathbf{u}_1^T\begin{pmatrix}\cos\theta\\ \sin\theta\end{pmatrix}-\mathbf{u}_I^T\begin{pmatrix}\cos\theta\\ \sin\theta\end{pmatrix}\right]\right.\\
&\quad\left.+\epsilon_1^2\left[\bar{v}_0-\frac{1}{2}B_0+\bar{\mathbf{v}}_1^T\begin{pmatrix}\cos\theta\\ \sin\theta\end{pmatrix}+2\bar{\mathbf{v}}_2^T\begin{pmatrix}\cos\theta\\ \sin\theta\end{pmatrix}+\ldots\right]\right\}\mathrm{e}^{-\mathrm{i}\boldsymbol{\beta}_m^T\mathbf{R}_j}d\theta\\
&=\epsilon_1^2\pi\left[2\bar{v}_0+\mathbf{u}_0^T\begin{pmatrix}\cos 2\theta\\ \sin 2\theta\end{pmatrix}+2\mathrm{i}\mathbf{u}_I^T\begin{pmatrix}\cos 2\theta\\ \sin 2\theta\end{pmatrix}\right]\mathrm{e}^{-\mathrm{i}\boldsymbol{\beta}_m^T\mathbf{R}_j}+O(\epsilon_1^3). \qquad (4.149)
\end{aligned}
$$

Next we need to eliminate the unknowns $\bar{v}_0$, $\mathbf{u}_0$ and $\mathbf{u}_I$. To achieve this, we need to do the matching between the outer solutions and the inner solutions. The inner expansion of the outer solution for dilatational wave is given by (4.141). The inner solution for dilatational wave is given by (4.142), in which the order ϵ_1^2 term is

$$
\bar{\phi}_2=\bar{B}_2+\bar{v}_0\log\rho-\tfrac{1}{4}B_0\rho^2+\tfrac{1}{4}\mathbf{u}_0^T\begin{pmatrix}\cos 2\theta\\ \sin 2\theta\end{pmatrix}+\bar{\mathbf{v}}_1^T\rho\begin{pmatrix}\cos\theta\\ \sin\theta\end{pmatrix}+\bar{\mathbf{v}}_2^T\rho^2\begin{pmatrix}\cos 2\theta\\ \sin 2\theta\end{pmatrix}+\ldots, \qquad (4.150)
$$

The order ϵ_1^2 term for shear wave is given by (3.161)

$$
\hat{\psi}_2=\hat{B}_2+\hat{v}_0\log\rho+\frac{P^2\mathbf{u}_0^T}{4}\begin{pmatrix}0 & 1\\ -1 & 0\end{pmatrix}\begin{pmatrix}\cos 2\theta\\ \sin 2\theta\end{pmatrix}+\hat{\mathbf{v}}_1^T\rho\begin{pmatrix}\cos\theta\\ \sin\theta\end{pmatrix}+\hat{\mathbf{v}}_2^T\rho^2\begin{pmatrix}\cos 2\theta\\ \sin 2\theta\end{pmatrix}+\ldots. \qquad (4.151)
$$

Substituting for $\bar{\phi}_2$ and $\hat{\psi}_2$ by (4.150) and (4.151) in the stress free boundary conditions in inner coordinates (3.139) and (3.140), the orthogonality of the trigonometric functions requires their coefficients must be zero, which gives

$$\bar{v}_0 = \frac{1}{2}(1-P^2)B_0, \tag{4.152}$$

$$u_{01} = \frac{8(\bar{v}_{21}+\hat{v}_{22})}{P^2-1}, \qquad u_{02} = \frac{8(\bar{v}_{22}-\hat{v}_{21})}{P^2-1}, \tag{4.153}$$

where $\mathbf{u}_0^T = (u_{01}, u_{02})$, $\bar{\mathbf{v}}_2 = (\bar{v}_{21}, \bar{v}_{22})$ and $\hat{\mathbf{v}}_2 = (\hat{v}_{21}, \hat{v}_{22})$. By the matching rule $\Phi^{(0,2)} \equiv \bar{\phi}^{(2,0)}$ we obtain

$$B_0 = \sum_{m=1}^{M} A_m \mathrm{e}^{\mathrm{i}\boldsymbol{\beta}_m^T \mathbf{R}_j}, \tag{4.154}$$

$$\mathbf{u}_1^T = \mathrm{i}\sum_{m=1}^{M} A_m \mathrm{e}^{\mathrm{i}\boldsymbol{\beta}_m^T \mathbf{R}_j}(\cos\tau_m, \sin\tau_m), \tag{4.155}$$

$$\bar{\mathbf{v}}_0^T = -\frac{1}{4}\sum_{m=1}^{M} A_m \mathrm{e}^{\mathrm{i}\boldsymbol{\beta}_m^T \mathbf{R}_j}(\cos 2\tau_m, \sin 2\tau_m). \tag{4.156}$$

Because the leading order is from the dilatational wave, the outer solution for shear wave Ψ starts from order ϵ_1^2, so $\Psi^{(0,2)} = 0$. Therefore the matching rule $\Psi^{(0,2)} \equiv \hat{\psi}^{(2,0)}$ gives

$$\hat{\mathbf{v}}_2 = 0, \tag{4.157}$$

then, by (4.153), (4.156) and (4.157), we have

$$\mathbf{u}_0^T = \frac{2}{1-P^2}\sum_{m=1}^{M} A_m \mathrm{e}^{\mathrm{i}\boldsymbol{\beta}_m^T \mathbf{R}_j}(\cos 2\tau_m, \sin 2\tau_m). \tag{4.158}$$

By (4.152) and (4.154) we have

$$\bar{v}_0 = \frac{1}{2}(1-P^2)\sum_{m=1}^{M} A_m \mathrm{e}^{\mathrm{i}\boldsymbol{\beta}_m^T \mathbf{R}_j}. \tag{4.159}$$

In (4.149), there are three unknowns, $\bar{v}_0$, $\mathbf{u}_0$ and $\mathbf{u}_I$. We have obtained the expressions for $\bar{v}_0$ and $\mathbf{u}_0$ in the last two equations. $\mathbf{u}_I$ is related to $\mathbf{u}_1$ and the relation can be found by substituting for the order ϵ_1^3 inner solutions $\bar{\phi}_3$ and $\hat{\psi}_3$ in the stress free boundary conditions (3.139) and (3.140) and making the coefficients of the trigonometric functions

be zero. This procedure has already been done in section 3.2. The relation between $\mathbf{u}_I$ and $\mathbf{u}_1$ is given by equation (3.174)

$$\mathbf{u}_I = -\frac{1}{2}\mathbf{u}_1. \tag{4.160}$$

Now by (4.155) and the relation between $\mathbf{u}_1$ and $\mathbf{u}_I$ we have

$$\mathbf{u}_I = -\frac{1}{2}\mathrm{i}\sum_{m=1}^{M} A_m \mathrm{e}^{\mathrm{i}\boldsymbol{\beta}_m^T \mathbf{R}_j}(\cos\tau_m, \sin\tau_m), \tag{4.161}$$

Therefore, by (4.149), (4.158), (4.159) and (4.161) the right hand side of Green's identity becomes

$$RHS(4.144) = \epsilon_1^2 \pi \sum_{h=1}^{M}\left[1 - P^2 + \frac{2}{1-P^2}\cos 2(\tau_h - \tau_m) + \cos(\tau_h - \tau_m)\right]\mathrm{e}^{\mathrm{i}(\boldsymbol{\beta}_h - \boldsymbol{\beta}_m)^T \mathbf{R}_j}. \tag{4.162}$$

Then by the integration result of the both sides of Green's identity (4.148) and (4.162), we obtain the envelope equations

$$\frac{\partial A_m}{\partial T} + \mathbf{C}_g^{(m)} \cdot \overline{\nabla} A_m = -\frac{1}{2}\mathrm{i}\Omega_0 \sum_{h=1}^{M} A_h \left[1 - P^2 + \frac{2}{1-P^2}\cos 2(\tau_h - \tau_m) + \cos(\tau_h - \tau_m)\right], \tag{4.163}$$

where $\mathbf{C}_g^{(m)} = \dfrac{c_1^2}{\omega}\boldsymbol{\beta}_m$, $m = 1, 2, \ldots, M$ and $\Omega_0 = \dfrac{\pi c_1}{\beta_1 \mathcal{A}_c}$. Outside the cylinder strip, there are no cylinders, therefore the envelope equations become

$$\frac{\partial A_m}{\partial T} + \mathbf{C}_g^{(m)} \cdot \overline{\nabla} A_m = 0, \ m = 1, 2, \ldots, M. \tag{4.164}$$

Same as the acoustic case, if we multiply both sides of equation (4.163) by A_m^* (the conjugate of A_m) and add the resulting equation with its complex conjugate, after summation over m, we obtain the energy conservation equations

$$\sum_{m=1}^{M}\left(\frac{\partial |A_m|^2}{\partial T} + \mathbf{C}_g^{(m)} \cdot \overline{\nabla}|A_m|^2\right) = 0. \tag{4.165}$$

Thus the total energy is conserved in the array.

If the array is infinite, the amplitude does not depend on the space variation, thus only the time variation is involved. If we search for solutions in the form of $A_m(T) = a_m \mathrm{e}^{-\mathrm{i}\Omega T}$, the envelope equations (4.163) become

$$\Omega a_m = \frac{\pi c_1^2}{2\omega \mathcal{A}_c}\sum_{h=1}^{M} a_h \left[1 - P^2 + \frac{2}{1-P^2}\cos 2(\tau_h - \tau_m) + \cos(\tau_h - \tau_m)\right], \tag{4.166}$$

where $\Omega = \mathcal{K}_1 c_1$. $\mathcal{K}_1$ is the detuning of the wavenumber β_1 and the detuned wavenumber $k_1 = \beta_1 + \epsilon_1^2 \mathcal{K}_1$, and the detuned frequency $\omega' = k_1 c_1 = \omega + \epsilon_1^2 \Omega$. In chapter 3, we considered the same case for infinite two-dimensional array of cavity cylinders and obtained (3.181)

$$\overline{U}_m \delta_m = \frac{\pi L^2}{\mathcal{A}_c} \sum_{h=1}^{M} \left[1 - P^2 + \frac{2}{1 - P^2} \cos 2(\tau_h - \tau_m) + \cos(\tau_h - \tau_m) \right] \overline{U}_h, \tag{4.167}$$

where $\delta_m = (k_1^2 - \beta_m^2) L^2 / \epsilon^2$, $\beta_m = |\boldsymbol{\beta}_m| = \beta$ and $\epsilon = k_1 a$. Equations (4.166) and (4.167) define same eigenvalue problems, therefore

$$\delta_m = \frac{2\omega L^2}{c_1^2} \Omega = \frac{2\beta(k_1 - \beta) L^2}{\epsilon_1^2}, \tag{4.168}$$

which is consistent with the definition of δ_m (3.132)

$$\delta_m = \frac{(k_1^2 - \beta^2) L^2}{\epsilon^2} = \frac{(k_1 + \beta)(k_1 - \beta) L^2}{\epsilon^2} \approx \frac{2\beta(k_1 - \beta) L^2}{\epsilon_1^2}, \tag{4.169}$$

on a first approximation in the limit $k_1 \to \beta$.

Similarly, when we consider the perturbation of shear waves the envelope equations are

$$\frac{\partial \widehat{A}_m}{\partial T} + \widehat{\mathbf{C}}_g^{(m)} \cdot \overline{\nabla} \widehat{A}_m = -\frac{1}{2} \mathrm{i} \widehat{\Omega}_0 \sum_{h=1}^{M} \widehat{A}_h \left[\frac{2P^4}{1 - P^2} \cos 2(\tau_h - \tau_m) + P^2 \cos(\tau_h - \tau_m) \right], \tag{4.170}$$

where $m = 1, 2, \ldots, M$, $\widehat{\mathbf{C}}_g^{(m)} = \dfrac{c_2^2}{\omega} \boldsymbol{\beta}_m$ and $\widehat{\Omega}_0 = \dfrac{\pi c_2}{\beta_2 \mathcal{A}_c}$. Outside the cylinder strip, the envelope equations become

$$\frac{\partial \widehat{A}_m}{\partial T} + \widehat{\mathbf{C}}_g^{(m)} \cdot \overline{\nabla} \widehat{A}_m = 0, \ m = 1, 2, \ldots, M. \tag{4.171}$$

The corresponding equations for energy conservation are

$$\sum_{m=1}^{M} \left(\frac{\partial |\widehat{A}_m|^2}{\partial T} + \mathbf{C}_g^{(m)} \cdot \overline{\nabla} |\widehat{A}_m|^2 \right) = 0. \tag{4.172}$$

Same as the perturbation of dilatational waves, when the array is infinite and we search for solutions in the form of $\widehat{A}_m(T) = \hat{a}_m \mathrm{e}^{-\mathrm{i}\Omega T}$, then the envelope equations (4.170) become

$$\Omega \hat{a}_m = \frac{\pi c_2^2}{2\omega \mathcal{A}_c} \sum_{h=1}^{M} a_h \left[\frac{2P^4}{1 - P^2} \cos 2(\tau_h - \tau_m) + P^2 \cos(\tau_h - \tau_m) \right]. \tag{4.173}$$

In chapter 3, the corresponding eigenvalue problem for perturbation of shear waves when the array is infinite is

$$\widehat{U}_m\hat{\delta}_m = \frac{\pi L^2}{\mathcal{A}_c}\sum_{h=1}^{M}\left[\frac{2P^4}{1-P^2}\cos 2(\tau_h-\tau_m)+P^2\cos(\tau_h-\tau_m)\right]\widehat{U}_h, \tag{4.174}$$

Equations (4.173) and (4.174) define same eigenvalue problems, therefore

$$\hat{\delta}_m = \frac{2\omega L^2}{c_2^2}\Omega = \frac{2\beta(k_2-\beta)L^2}{\epsilon_1^2}, \tag{4.175}$$

which is consistent with the definition of δ_m (3.132)

$$\hat{\delta}_m = \frac{(k_2^2-\beta^2)L^2}{k_2^2a^2} = \frac{(k_2+\beta)(k_2-\beta)L^2}{k_2^2a^2} \approx \frac{2\beta(k_2-\beta)L^2}{\epsilon_1^2}, \tag{4.176}$$

on a first approximation in the limit $k_2 \to \beta$.

4.3.2 Elastic strip with cylinder scatterers bounded by acoustic medium

In this part, we consider how the wave propagates in an elastic medium containing infinitely long cavity cylinders whose axes are along z axis and are arranged doubly periodically along x and y axes, see figure 4.16. The strip width in the direction of the x axis is finite, but the strip is unbounded in the direction of y axis. The elastic strip is bounded by the same acoustic medium on both sides. We denote by λ the Lamé constant for the acoustic medium, and λ_1 and μ_1 are the Lamé constants for the elastic medium. A train of plane acoustic waves is incident on the elastic strip from its left boundary. When the incident waves impinge on the elastic medium, both dilatational and shear waves will be generated and they all propagate through the elastic lattice until they arrive at the right boundary of the strip. Because the acoustic medium does not support shear waves only dilatational waves propagate into the acoustic medium on the right side of the strip. In the cylinder strip, the governing equations for the Bragg resonated envelopes are equations (4.163) and (4.170) for dilatational and shear wave respectively. Here we consider the case that only dilatational waves are resonated in the array.

Same as the acoustic layer problem in section 4.1, the elastic strip width d is required to be order $1/\epsilon_1^2$ to make sure the cylinder array is big enough to make the resonance happen. Plane acoustic waves arrive from the left side of the strip at an angle α_1 with respect to the x-axis. We write the waves in the three zones (left side acoustic medium,

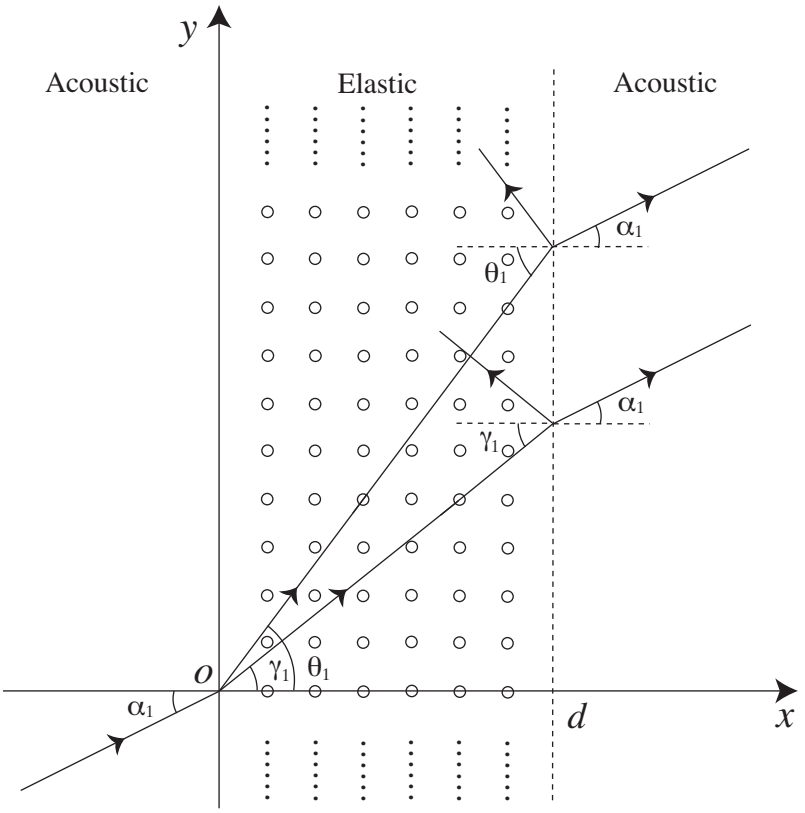

Figure 4.16: Elastic strip bounded by acoustic media. $M = 1$.

elastic strip, right side acoustic medium) in the form

$$\phi^- = \sum_{m=1}^{M} \left[A_m^-(X,Y,T) \mathrm{e}^{\mathrm{i}\beta(x\cos\alpha_m + y\sin\alpha_m)} \right] + A_1^{-r}(X,Y,T)\mathrm{e}^{\mathrm{i}\beta(-x\cos\alpha_1 + y\sin\alpha_1)}, \ X < 0, \tag{4.177}$$

$$\phi = \sum_{m=1}^{M} \left[A_m(X,Y,T)\mathrm{e}^{\mathrm{i}\beta_1(x\cos\theta_m + y\sin\theta_m)} + A_m^r(X,Y,T)\mathrm{e}^{\mathrm{i}\beta_1(-x\cos\theta_m + y\sin\theta_m)} \right], \quad 0 \le X \le D, \tag{4.178}$$

$$\psi = \sum_{m=1}^{M} \left[\widehat{A}_m(X,Y,T)\mathrm{e}^{\mathrm{i}\beta_2(x\cos\gamma_m + y\sin\gamma_m)} + \widehat{A}_m^r(X,Y,T)\mathrm{e}^{\mathrm{i}\beta_2(-x\cos\gamma_m + y\sin\gamma_m)} \right], \quad 0 \le X \le D, \tag{4.179}$$

$$\phi^+ = \sum_{m=1}^{M} A_m^+(X,Y,T)\mathrm{e}^{\mathrm{i}\beta[(x-d)\cos\alpha_m + y\sin\alpha_m]}, \ X > D, \tag{4.180}$$

where $D = \epsilon_1^2 d$, ϕ^- is the dilatational wave potential (with unperturbed wavenumber β) in the left side acoustic medium, ϕ and ψ are the dilatational (with unperturbed

wavenumber β_1) and shear (with unperturbed wavenumber β_2) wave potentials respectively in the elastic medium and ϕ^+ is the dilatational wave potential in the right side acoustic medium. In the wave potentials, A_1^{-r} is the envelope of the reflected wave of the incident wave in the left side acoustic medium, A_m^r and $\widehat{A}_m^r$ are envelopes of the reflected dilatational and shear waves in elastic medium respectively, α_m are angles for dilatational waves in the acoustic medium and θ_m and γ_m are angels for dilatational and shear waves respectively in elastic medium. By Snell's law, we have

$$\beta \sin \alpha_m = \beta_1 \sin \theta_m = \beta_2 \sin \gamma_m, \ m = 1, 2, \ldots, M. \tag{4.181}$$

Now it is the time to impose the boundary conditions, which include the continuity of the velocity and stress. At first, it is the continuity of the normal component of the displacement u_x,

$$u_x^- = u_x, \text{ on } x = 0, \tag{4.182}$$

$$u_x^+ = u_x, \text{ on } x = d, \tag{4.183}$$

where

$$u_x = \frac{\partial \phi}{\partial x} + \frac{\partial \psi}{\partial y}.$$

In acoustic medium, there is no shear wave existing so $\psi = 0$. Secondly, we consider the continuity of the stress on the boundaries. The components of the stress tensor have expressions

$$\sigma_{xy} = \mu_1 \left(\frac{\partial^2 \psi}{\partial y^2} - \frac{\partial^2 \psi}{\partial x^2} + 2 \frac{\partial^2 \phi}{\partial x \partial y} \right), \tag{4.184}$$

$$\sigma_{xx} = \lambda_1 \nabla^2 \phi + 2\mu_1 \left(\frac{\partial^2 \phi}{\partial x^2} + \frac{\partial^2 \psi}{\partial x \partial y} \right), \tag{4.185}$$

for the elastic medium. For the acoustic medium, the stress can be obtained by replacing λ_1 by λ and setting $\mu_1 = 0$. The normal components of the stress σ_{xx} must be continuous. The tangential components σ_{xy} of the stress must also be continuous, but since the tangential stresses in the acoustic medium vanish, this condition reduces simply to the requirement that the tangential components of the elastic stress be zero at the boundary

of the elastic strip. Therefore we obtain the following four continuity conditions

$$\sigma_{xy} = 0, \text{ on } x = 0, \tag{4.186}$$

$$\sigma_{xy} = 0, \text{ on } x = d, \tag{4.187}$$

$$\sigma_{xx}^{-} = \sigma_{xx}, \text{ on } x = 0, \tag{4.188}$$

$$\sigma_{xx}^{+} = \sigma_{xx}, \text{ on } x = d, \tag{4.189}$$

where σ_{xx}^{-} and σ_{xx}^{+} are the normal components of the stress in the left side and right side acoustic medium of the strip. Substituting for ϕ^{-}, ϕ, ψ and ϕ^{+} in the boundary conditions (4.182), (4.183), (4.186)-(4.189), we obtain

$$\frac{\partial \phi^{-}}{\partial x} = \frac{\partial \phi}{\partial x} + \frac{\partial \psi}{\partial y}, \text{ on } X = 0, \tag{4.190}$$

$$\frac{\partial \phi^{+}}{\partial x} = \frac{\partial \phi}{\partial x} + \frac{\partial \psi}{\partial y}, \text{ on } X = D, \tag{4.191}$$

$$\mu_1 \left(\frac{\partial^2 \psi}{\partial y^2} - \frac{\partial^2 \psi}{\partial x^2} + 2\frac{\partial^2 \phi}{\partial x \partial y} \right) = 0, \text{ on } X = 0, \tag{4.192}$$

$$\mu_1 \left(\frac{\partial^2 \psi}{\partial y^2} - \frac{\partial^2 \psi}{\partial x^2} + 2\frac{\partial^2 \phi}{\partial x \partial y} \right) = 0, \text{ on } X = D, \tag{4.193}$$

$$\lambda \nabla^2 \phi^{-} = \lambda_1 \nabla^2 \phi + 2\mu_1 \left(\frac{\partial^2 \phi}{\partial x^2} + \frac{\partial^2 \psi}{\partial x \partial y} \right), \text{ on } X = 0, \tag{4.194}$$

$$\lambda \nabla^2 \phi^{+} = \lambda_1 \nabla^2 \phi + 2\mu_1 \left(\frac{\partial^2 \phi}{\partial x^2} + \frac{\partial^2 \psi}{\partial x \partial y} \right), \text{ on } X = D. \tag{4.195}$$

If we combine the solutions forms in (4.177)-(4.180), these boundary conditions become

$$\beta_1 \cos\theta_m \big[A_m(0,Y,T) - A_m^r(0,Y,T)\big] + \beta_1 \sin\gamma_m \big[\widehat{A}_m(0,Y,T) + \widehat{A}_m^r(0,Y,T)\big]$$
$$= \beta \cos\alpha_m \big[A_m^-(0,Y,T) - \delta_{m1} A_1^{-r}(0,Y,T)\big], \tag{4.196}$$

$$\beta_1 \cos\theta_m \big[A_m(D,Y,T)\mathrm{e}^{\mathrm{i}\beta_1 d\cos\theta_m} - A_m^r(D,Y,T)\mathrm{e}^{-\mathrm{i}\beta_1 d\cos\theta_m}\big] +$$
$$\beta_1 \sin\gamma_m \big[\widehat{A}_m(D,Y,T)\mathrm{e}^{\mathrm{i}\beta_2 d\cos\gamma_m} + \widehat{A}_m^r(D,Y,T)\mathrm{e}^{-\mathrm{i}\beta_2 d\cos\gamma_m}\big]$$
$$= \beta \cos\alpha_m A_m^+(D,Y,T)\mathrm{e}^{\mathrm{i}\beta d\cos\alpha_m}, \tag{4.197}$$

$$\beta_2^2 \cos 2\gamma_m \big[\widehat{A}_m(0,Y,T) + \widehat{A}_m^r(0,Y,T)\big] - \beta_1^2 \sin 2\theta_m \big[A_m(0,Y,T) - A_m^r(0,Y,T)\big] = 0, \tag{4.198}$$

$$\beta_2^2 \cos 2\gamma_m \big[\widehat{A}_m(D,Y,T)\mathrm{e}^{\mathrm{i}\beta_2 d\cos\gamma_m} + \widehat{A}_m^r(D,Y,T)\mathrm{e}^{-\mathrm{i}\beta_2 d\cos\gamma_m}\big]$$
$$= \beta_1^2 \sin 2\theta_m \big[A_m(D,Y,T)\mathrm{e}^{\mathrm{i}\beta_1 d\cos\theta_m} - A_m^r(D,Y,T)\mathrm{e}^{-\mathrm{i}\beta_1 d\cos\theta_m}\big], \tag{4.199}$$

$$\lambda_1\beta_1^2 \big[A_m(0,Y,T) + A_m^r(0,Y,T)\big] + 2\mu_1 \Big\{ \beta_1^2 \cos^2\theta_m \big[A_m(0,Y,T) + A_m^r(0,Y,T)\big]$$
$$+ \beta_2^2 \cos\gamma_m \sin\gamma_m \big[\widehat{A}_m(0,Y,T) - \widehat{A}_m^r(0,Y,T)\big] \Big\} = \lambda\beta^2 \big[A_m^-(0,Y,T) + \delta_{m1} A_1^{-r}(0,Y,T)\big], \tag{4.200}$$

$$\lambda_1\beta_1^2 \big[A_m(D,Y,T)\mathrm{e}^{\mathrm{i}\beta_1 d\cos\theta_m} + A_m^r(D,Y,T)\mathrm{e}^{-\mathrm{i}\beta_1 d\cos\theta_m}\big]$$
$$+ 2\mu_1 \Big\{ \beta_1^2 \cos^2\theta_m \big[A_m(D,Y,T)\mathrm{e}^{\mathrm{i}\beta_1 d\cos\theta_m} + A_m^r(D,Y,T)\mathrm{e}^{-\mathrm{i}\beta_1 d\cos\theta_m}\big]$$
$$+ \beta_2^2 \cos\gamma_m \sin\gamma_m \big[\widehat{A}_m(D,Y,T)\mathrm{e}^{\mathrm{i}\beta_2 d\cos\gamma_m} - \widehat{A}_m^r(D,Y,T)\mathrm{e}^{-\mathrm{i}\beta_2 d\cos\gamma_m}\big] \Big\}$$
$$= \lambda\beta^2 A_m^+(D,Y,T)\mathrm{e}^{\mathrm{i}\beta d\cos\alpha_m}, \tag{4.201}$$

where $m = 1, 2, \ldots, M$. In the above $6M$ equations, there are $6M$ unknowns A_m^- ($m = 2, \ldots, M$), A_1^{-r}, A_m, A_m^r, $\widehat{A}_m$, $\widehat{A}_m^r$ and A_m^+, so the system is solvable.

Next we are going to do some numerical calculations using the above systems. At first, we consider the case of $M = 1$, i.e. there is one dilatational and one shear wave

in the cylinder array and only one dilatational wave outside the array (reflected waves should also be included). We allow a small detuning in the incident wave

$$A_1^-(X,Y,T)\mathrm{e}^{\mathrm{i}\boldsymbol{\beta}_1\mathbf{r}} = A_0\mathrm{e}^{\mathrm{i}(\mathcal{K}\cos\alpha_1 X+\mathcal{K}\sin\alpha_1 Y-\Omega T)}\mathrm{e}^{\mathrm{i}\boldsymbol{\beta}_1\mathbf{r}},\ X<0, \tag{4.202}$$

where $\mathcal{K}$ is the detuning of the wavenumber β and Ω is the detuning of the frequency, related by $\mathcal{K}=\Omega/c$, and $c=\sqrt{\lambda/\rho}$ is the wave speed in acoustic medium. By the continuity conditions at $X=0,D$, the y dependence must be same in every component of the solution. Thus, the envelopes in the strip and the acoustic medium on the right side of the strip have the form

$$A_1(X,Y,T) = B_1(X)\mathrm{e}^{\mathrm{i}(\mathcal{K}_1\sin\theta_1 Y-\Omega T)}, \tag{4.203}$$

$$\widehat{A}_1(X,Y,T) = \widehat{B}_1(X)\mathrm{e}^{\mathrm{i}(\mathcal{K}_2\sin\gamma_1 Y-\Omega T)}, \tag{4.204}$$

$$A_1^+(X,Y,T) = A_2\mathrm{e}^{\mathrm{i}[\mathcal{K}\cos\alpha_1(X-D)+\mathcal{K}\sin\alpha_1 Y-\Omega T]}, \tag{4.205}$$

where by the Snell's law $\mathcal{K}\sin\alpha_1=\mathcal{K}_1\sin\theta_1=\mathcal{K}_2\sin\gamma_1$ (i.e. $\mathcal{K}c=\mathcal{K}_1c_1=\mathcal{K}_2c_2$).

Within the strip, the slow variations of the dilatational and shear wave satisfy the envelope equations (4.163) and (4.170), that is

$$\frac{\partial A_1}{\partial T}+c_1(\cos\theta_1,\sin\theta_1)\cdot\left(\frac{\partial A_1}{\partial X},\frac{\partial A_1}{\partial Y}\right)=\frac{1}{2}\mathrm{i}\Omega_0 P_1 A_1, \tag{4.206}$$

$$\frac{\partial \widehat{A}_1}{\partial T}+c_2(\cos\gamma_1,\sin\gamma_1)\cdot\left(\frac{\partial \widehat{A}_1}{\partial X},\frac{\partial \widehat{A}_1}{\partial Y}\right)=\frac{1}{2}\mathrm{i}\widehat{\Omega}_0 P_2 \widehat{A}_1, \tag{4.207}$$

where $P_1=P^2-2+2/(P^2-1)$, $P_2=P^2(P^2+1)/(P^2-1)$. From (4.203), (4.204) and (4.206), (4.207), we obtain

$$B_1(X) = A_1\mathrm{e}^{\mathrm{i}\nu_1 X}, \tag{4.208}$$

$$\widehat{B}_1(X) = C_1\mathrm{e}^{\mathrm{i}\nu_2 X}, \tag{4.209}$$

where

$$\nu_1=\mathcal{K}_1\cos\theta_1+\frac{\Omega_0 P_1}{2c_1\cos\theta_1},\ \nu_2=\mathcal{K}_2\cos\gamma_1+\frac{\widehat{\Omega}_0 P_2}{2c_2\cos\gamma_1}, \tag{4.210}$$

$$\Omega_0=\frac{\pi c_1}{\beta_1\mathcal{A}_c},\ \widehat{\Omega}_0=\frac{\pi c_2}{\beta_2\mathcal{A}_c}. \tag{4.211}$$

Therefore, we have

$$A_1^-(X,Y,T) = A_0 \mathrm{e}^{\mathrm{i}(\mathcal{K}\cos\alpha_1 X + \mathcal{K}\sin\alpha_1 Y - \Omega T)},\ X < 0, \tag{4.212}$$

$$A_1^{-r}(X,Y,T) = B_0 \mathrm{e}^{\mathrm{i}(-\mathcal{K}\cos\alpha_1 X + \mathcal{K}\sin\alpha_1 Y - \Omega T)},\ X < 0, \tag{4.213}$$

$$A_1(X,Y,T) = A_1 \mathrm{e}^{\mathrm{i}\nu_1 X} \mathrm{e}^{\mathrm{i}(\mathcal{K}_1\sin\theta_1 Y - \Omega T)},\ 0 \le X \le D, \tag{4.214}$$

$$A_1^r(X,Y,T) = B_1 \mathrm{e}^{-\mathrm{i}\nu_1 X} \mathrm{e}^{\mathrm{i}(\mathcal{K}_1\sin\theta_1 Y - \Omega T)},\ 0 \le X \le D, \tag{4.215}$$

$$\widehat{A}_1(X,Y,T) = C_1 \mathrm{e}^{\mathrm{i}\nu_2 X} \mathrm{e}^{\mathrm{i}(\mathcal{K}_2\sin\gamma_1 Y - \Omega T)},\ 0 \le X \le D, \tag{4.216}$$

$$\widehat{A}_1^r(X,Y,T) = D_1 \mathrm{e}^{-\mathrm{i}\nu_2 X} \mathrm{e}^{\mathrm{i}(\mathcal{K}_2\sin\gamma_1 Y - \Omega T)},\ 0 \le X \le D, \tag{4.217}$$

$$A_1^+(X,Y,T) = A_2 \mathrm{e}^{\mathrm{i}[\mathcal{K}\cos\alpha_1 (X-D) + \mathcal{K}\sin\alpha_1 Y - \Omega T]},\ X > D. \tag{4.218}$$

Substituting for the forms of these envelopes in the continuity conditions (4.196) -(4.201) we obtain the following system

$$\mathbf{M}\cdot\mathbf{a} = \mathbf{b}, \tag{4.219}$$

where $\mathbf{M} =$

$$\begin{pmatrix}
k\cos\alpha_1 & f_1 & -f_1 & k_y & k_y & 0 \\
0 & f_1\mathrm{e}^{\mathrm{i}df_1} & -f_1\mathrm{e}^{-\mathrm{i}df_1} & k_y\mathrm{e}^{\mathrm{i}df_2} & k_y\mathrm{e}^{-\mathrm{i}df_2} & -k\cos\alpha_1 \\
0 & -2k_y f_1 & 2k_y f_1 & f_2^2 - k_y^2 & f_2^2 - k_y^2 & 0 \\
0 & -2k_y f_1\mathrm{e}^{\mathrm{i}df_1} & 2k_y f_1\mathrm{e}^{-\mathrm{i}df_1} & (f_2^2 - k_y^2)\mathrm{e}^{\mathrm{i}df_2} & (f_2^2 - k_y^2)\mathrm{e}^{-\mathrm{i}df_2} & 0 \\
-\lambda k^2 & \lambda_1(f_1^2 + k_y^2) + 2\mu_1 f_1^2 & \lambda_1(f_1^2 + k_y^2) + 2\mu_1 f_1^2 & 2\mu_1 k_y f_2 & -2\mu_1 k_y f_2 & 0 \\
0 & [\lambda_1(f_1^2 + k_y^2) + 2\mu_1 f_1^2]\mathrm{e}^{\mathrm{i}df_1} & [\lambda_1(f_1^2 + k_y^2) + 2\mu_1 f_1^2]\mathrm{e}^{-\mathrm{i}df_1} & 2\mu_1 k_y f_2\mathrm{e}^{\mathrm{i}df_2} & -2\mu_1 k_y f_2\mathrm{e}^{-\mathrm{i}df_2} & -\lambda k^2
\end{pmatrix},$$

$$k_y = k\sin\alpha_1,$$

$$\mathbf{a} = \big(B_0,\ A_1,\ B_1,\ C_1,\ D_1,\ A_2\big),$$

$$\mathbf{b} = \big(\beta\cos\alpha_1 A_0,\ 0,\ 0,\ 0,\ \lambda\beta^2 A_0,\ 0\big),$$

and

$$f_1 = (\beta_1 + \epsilon_1^2 P_1 Q_1)\cos\theta_1,\ f_2 = (\beta_2 + \epsilon_1^2 P_2 Q_2)\cos\gamma_1,$$

$$Q_1 = \Omega_0/(2c_1\cos^2\theta_1),\ Q_2 = \widehat{\Omega}_0/(2c_2\cos^2\gamma_1),$$

$$\theta_1 = \sin^{-1}\left(\frac{\beta\sin\alpha_1}{\beta_1}\right), \gamma_1 = \sin^{-1}\left(\frac{\beta\sin\alpha_1}{\beta_2}\right).$$

From the system (4.219), we can express the unknowns $B_0,\ A_1,\ B_1,\ C_1,\ D_1,\ A_2$ in terms of the incident wave coefficient A_0 and then assess how the waves propagate through the strip. For example, we consider the transmitted wave ϕ_1^+.

For an acoustic layer without cylinder array bounded by another acoustic medium on both sides, the modulus of the transmission coefficient is [10, page 67]

$$\begin{aligned}|Tr| =& 2cc_1\rho\rho_1\sec\alpha_1 \Big/ \sqrt{\Big\{4c^2c_1^2\rho^2\rho_1^2\cos^2(k_1 d\cos\theta_1)\sec^2\alpha_1 + [c_1^4\rho_1^4\sec^2\theta_1} \\ &+ 2c^2c_1^2\rho^2\rho_1^2\sec^2\alpha_1 + c^4\rho^4\sec^4\alpha_1\cos^2\theta_1]\sin^2(k_1 d\cos\theta_1)\Big\}. \end{aligned} \tag{4.220}$$

From (4.220) we can see the transmission coefficient is periodic in $k_1 d\cos\theta_1$ (see figure 4.17), and the minimum and maximum of the transmission coefficient are

$$|Tr|_{max} = 1,\ \text{at } k_1 d\cos\theta_1 = n\pi, \tag{4.221}$$

$$|Tr|_{min} = \frac{2cc_1\rho\rho_1\sec\alpha_1}{\sqrt{c_1^4\rho_1^4\sec^2\theta_1 + 2c^2c_1^2\rho^2\rho_1^2\sec^2\alpha_1 + c^4\rho^4\sec^4\alpha_1\cos^2\theta_1}},$$

$$\text{at } k_1 d\cos\theta_1 = (n - 1/2)\pi, \tag{4.222}$$

where $n \in Z$. When the layer is elastic and with no scatterers, the transmission coefficient is a function of both of $k_1 d\cos\theta_1$ and $k_2 d\cos\gamma_1$, see [10, page 67]. When the scatterers are present in the strip, the transmission coefficient is a function of not only the wavenumbers $k_{1,2}$, strip width d and angles θ_1, γ_1, but also the size of the scatterer.

In figures 4.17-4.19 we plot the transmission coefficients (the ratio of the acoustic pressures in the transmitted and the incident waves) over the parameter containing the strip width and incident angle, $k_1 d\cos\theta_1/\pi$ or $\beta_1 d\cos\theta_1/\pi$, for three kinds of strip when the incident wave is a plane sound wave. The first strip is a water layer without scatterers bounded by air on both sides (note that this is only an illustration as there is no such structure in reality), in which there are no shear waves. The second one is a copper layer

without scatterers bounded by air on both sides (with shear waves), and the last one is also a copper layer bounded by air but with doubly-periodic array of cavity circular cylinders in the layer (also with shear waves).

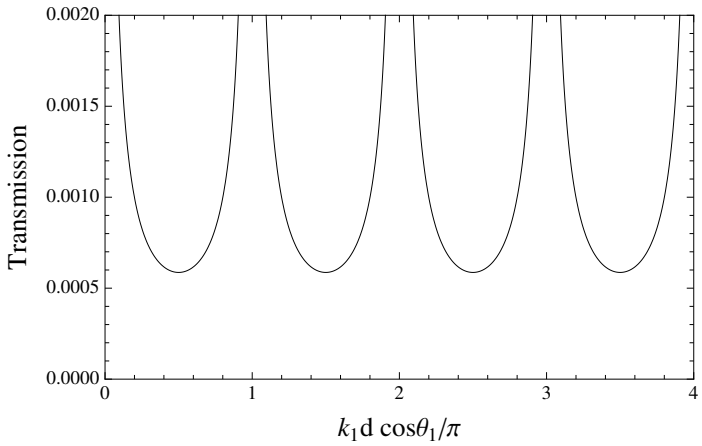

Figure 4.17: Transmission coefficients for water layer bounded by air.

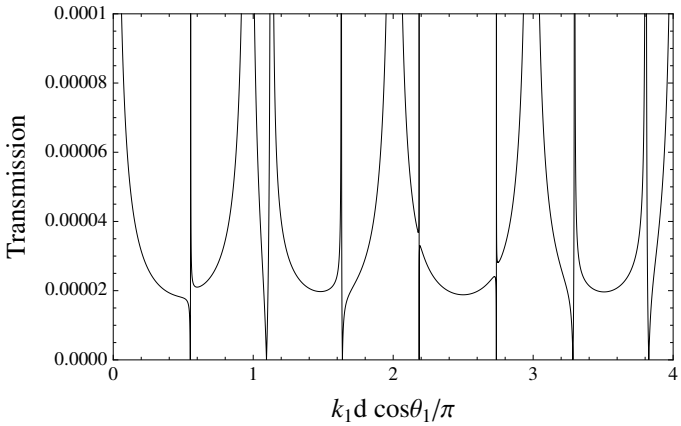

Figure 4.18: Transmission coefficients for steel layer without scatterers bounded by air.

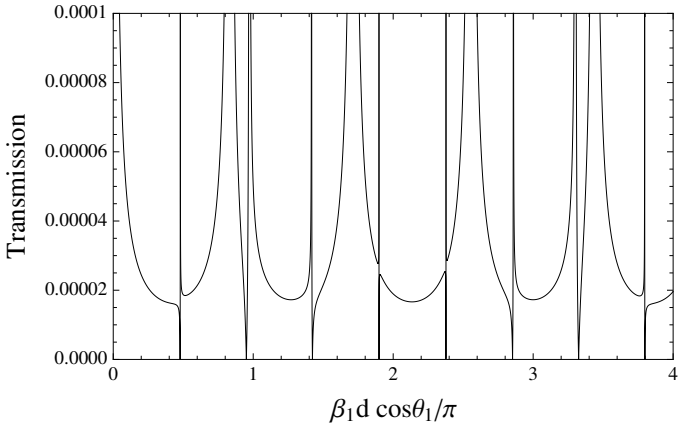

Figure 4.19: Transmission coefficients for steel layer with scatterers bounded by air. The scatterer size is $a/L = 0.2$.

The parameters we use to plot figures 4.17-4.19 are

Material/Parameter	Density (kg/m^3)	Lamé constants (Pa)
Air	1.25	$\lambda = 144500$
Water	998	$\lambda_1 = 2.1 \times 10^9$
Steel	8000	$\lambda_1 = 9.94 \times 10^{10}$, $\mu_1 = 7.81 \times 10^{10}$

Table 4.1: Parameters.

When the layer is an acoustic medium, only dilatational wave exists in the layer for both of normal and oblique incidence. But when the layer is elastic, the elastic medium in the vicinity of the boundary thus suffer both dilatational and shear stresses when the incidence is oblique. In the majority of practical cases, the velocity of sound in acoustic medium is less than the velocity of dilatational waves in elastic medium. It may also be less than the velocity of shear waves in elastic medium. The velocities and directions of the different waves are given, in accordance with Snell's law, by the expression:

$$\frac{c}{\sin\alpha_1} = \frac{c_1}{\sin\theta_1} = \frac{c_2}{\sin\gamma_1}. \tag{4.223}$$

Because the shear wave velocity is less than the dilatational wave velocity, θ_1 is always greater than γ_1. Let the incidence be increased to its first critical value for which the refracted dilatational wave is directed along the boundary, i.e. $\theta_1 = \pi/2$. For angles of incidence greater than this, the dilatational wave is totally reflected and only shear

wave is transmitted through the layer. When the incident angle is increased to its second critical value, the refracted shear wave is then directed along the boundary and becomes a surface wave.

Now we consider the case that one dilatational wave is resonated in the strip array (steel layer bounded by air), i.e. $M = 2$. For simplicity, here we consider the normal incidence, i.e. the incident angle $\alpha_1 = 0$, and then the angle of the primary wave in the strip is $\theta_1 = 0$. We assume the resonated dilatational wave is in the angel $\theta_2 = \pi$, therefore no shear waves exist in the strip. We look for solutions in the form

$$\begin{pmatrix} A_m^-(X,Y,T) \\ A_m(X,Y,T) \\ A_m^+(X,Y,T) \end{pmatrix} = A_0 \begin{pmatrix} B_m^-(X) \\ B_m(X) \\ B_m^+(X) \end{pmatrix} \mathrm{e}^{\mathrm{i}(\mathcal{K}\sin\alpha_1 Y - \Omega T)}, \ m = 1, 2. \tag{4.224}$$

Then, inside the the cylinder strip, from (4.163) the envelope equations become

$$\frac{d}{dX}\begin{pmatrix} B_1(X) \\ B_2(X) \end{pmatrix} = \frac{\mathrm{i}\Omega_0}{C_g}\mathbf{F}\begin{pmatrix} B_1(X) \\ B_2(X) \end{pmatrix}, \tag{4.225}$$

where the matrix $\mathbf{F}$ has elements

$$F_{11} = \frac{1}{\cos\theta_1}\left(\frac{\Omega}{\Omega_0}\cos^2\theta_1 + \frac{1}{2}P_1\right), \tag{4.226}$$

$$F_{12} = \frac{1}{2\cos\theta_1}\left[P^2 - 1 + \frac{2}{P^2-1}\cos(2\theta_2 - 2\theta_1) - \cos(\theta_2 - \theta_1)\right], \tag{4.227}$$

$$F_{21} = \frac{1}{2\cos\theta_2}\left[P^2 - 1 + \frac{2}{P^2-1}\cos(2\theta_2 - 2\theta_1) - \cos(\theta_2 - \theta_1)\right], \tag{4.228}$$

$$F_{22} = \frac{1}{\cos\theta_2}\left[\frac{\Omega}{\Omega_0}(1 - \sin\theta_1\sin\theta_2) + \frac{1}{2}P_1\right]. \tag{4.229}$$

Here $P_1 = P^2 - 2 + 2/(P^2-1)$ and $\Omega_0 = \pi c_1/(\beta_1 \mathcal{A}_c)$. The eigenvalues of this matrix are

$$\lambda_{1,2} = \frac{F_{11} + F_{22} \pm \sqrt{\Delta}}{2}, \tag{4.230}$$

where Δ is the discriminant

$$\begin{aligned}
\Delta &= (F_{11} + F_{22})^2 - 4(F_{11}F_{22} - F_{12}F_{21}) \\
&= (F_{11} - F_{22})^2 + 4F_{12}F_{21} \\
&= \left[\frac{\Omega}{\Omega_0}\frac{\cos(\theta_2 - \theta_1) - 1}{\cos\theta_2} + \frac{1}{2}P_1\left(\frac{1}{\cos\theta_1} - \frac{1}{\cos\theta_2}\right)\right]^2 \\
&\quad + \frac{1}{\cos\theta_1\cos\theta_2}\left[P^2 - 1 + \frac{2}{P^2-1}\cos(2\theta_2 - 2\theta_1) - \cos(\theta_2 - \theta_1)\right]^2.
\end{aligned} \tag{4.231}$$

When the scattered wave propagates backward, i.e. $\cos\theta_2 < 0$, which makes the sign of the discriminant Δ depend on the detuning Ω/Ω_0. It can be seen that $\Delta < 0$ within the stop band defined by

$$\frac{\Omega_c^-}{\Omega_0} < \frac{\Omega}{\Omega_0} < \frac{\Omega_c^+}{\Omega_0}, \tag{4.232}$$

where

$$\frac{\Omega_c^\pm}{\Omega_0} = \frac{\cos\theta_2}{\cos(\theta_1-\theta_2)-1}\left[\pm\frac{\left|P^2-1+\frac{2}{P^2-1}\cos(2\theta_2-2\theta_1)-\cos(\theta_2-\theta_1)\right|}{\sqrt{-\cos\theta_1\cos\theta_2}}\right.$$
$$\left.-\frac{1}{2}P_1\left(\frac{1}{\cos\theta_1}-\frac{1}{\cos\theta_2}\right)\right]. \tag{4.233}$$

In the case we consider, $\theta_1 = 0$ and $\theta_2 = \pi$, thus the boundary of the stop band is

$$\frac{\Omega_c^-}{\Omega_0} = -3.05, \quad \frac{\Omega_c^+}{\Omega_0} = 1. \tag{4.234}$$

In figure 4.20 and 4.21, we compare the transmission coefficient for a steel layer bounded by air on both sides when there are no cylinder array in the steel layer and there are cavity cylinder array in the steel layer. We can see the transmission coefficient is nearly zero when the detuning of the frequency Ω/Ω_0 lies in the stop band. The size and the location of the stop band depend on the incident and resonated angles and the Lamé constants of the material. Therefore by using this theory, we can design soundproof materials to block sound waves with particular frequencies by choosing different materials of the strip.

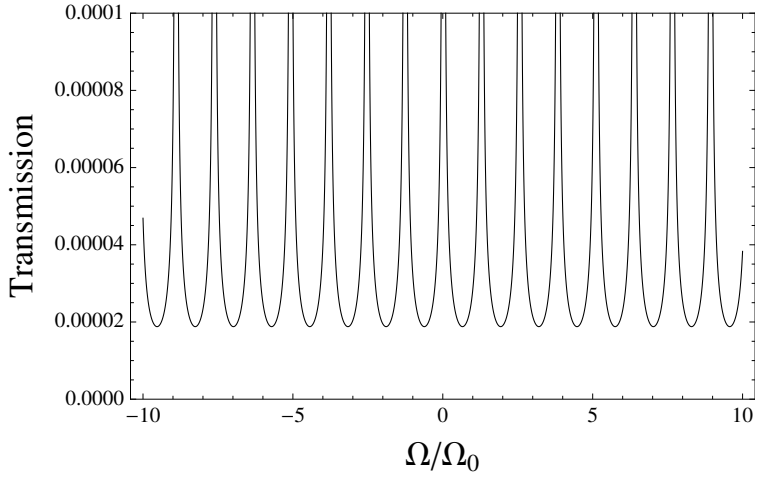

Figure 4.20: Transmission coefficients for steel layer without scatterers bounded by air.

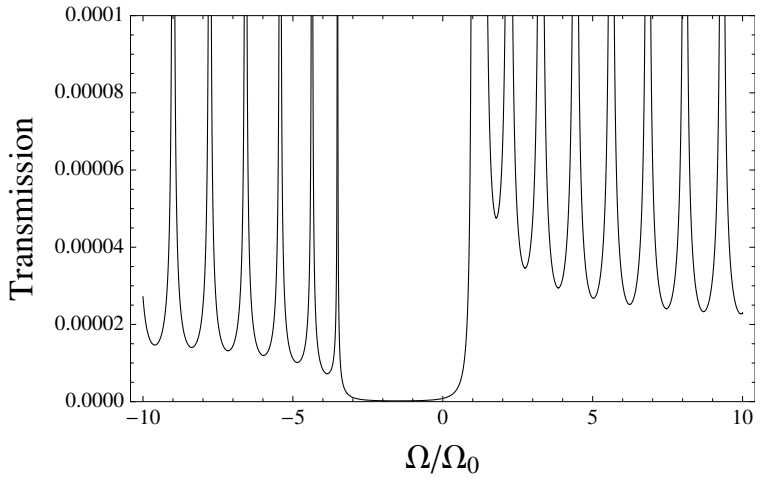

Figure 4.21: Transmission coefficients for steel layer with scatterers bounded by air. The cylinder size is $a/L = 0.05$.

Chapter 5

Three-dimensional acoustic wave scattering by arrays

We have considered the elastic wave propagation through two-dimensional periodic arrays of cavity cylinders in chapter 3. Now we move to the case of three-dimensional arrays using the same method as chapter 3. In this chapter, we consider the acoustic wave propagation through triply-periodic arrays of arbitrary shape scatterers using the method of matched asymptotic expansions. In the first section, we consider the scattering of a plane incident wave by one fixed rigid sphere of radius using the method of matched asymptotic expansions. This problem has already been done using the same method in [15, page 184], we present it here as an introduction to the three-dimensional scattering and to motivate the leading order term in the outer expansion in scattering by a triply-periodic array. The acoustic scattering of a plane wave by a rigid sphere was first considered by Rayleigh [80], where the sphere is assumed to be small compared the incident wavelength. Then Anderson [4] considered the case when the sphere size is comparable to the wavelength, where the scatterer is a fluid sphere. The elastic scattering by solid spheres was considered by Faran [22] taking account of the shear waves presented in the solid medium. The dilatational wave scattering by a spherical obstacle embedded in solid medium is also considered by Ying and Truell [104]. Later, Pao and Mow [70] reconsider Ying and Truell's work [104] and show the scattering by a rigid sphere, a cavity or even a fluid sphere can all be derived from the general solution of scattering due to an elastic inclusion; in Ying and Truell's work, these cases are treated separately.

The wave propagation through three-dimensional infinite periodic arrays of spherical obstacles are considered widely for acoustic [83, 40, 42, 41, 35], elastic [78, 43, 97, 98] and electromagnetic waves [66, 7]. For the acoustic case, Kushwaha *et al.* [40, 41, 42] obtain eigenvalue equations for various spherical inclusions and give band gap diagrams by numerical calculations. The plane wave expansion method is used to search for the band gaps for acoustic [83], elastic [43] and electromagnetic [97, 98] cases. But this method is proved not able to describe liquid-solid composites, therefore Kafesaki and Economou [35] develop a variational multiple scattering approach based on the Korringa-Kohn-Rostoker (KKR) theory [6, page 202] (KKR method is a classical technique for the solution of the Schrödinger equation in periodic media, which is to find the Green's function of those media). Based on the KKR theory, Nicorovici and McPhedran [66] make a generalization to this method while considering the electromagnetic waves in periodic lattices of spheres. They discuss the long-wavelength limit and obtain the effective dielectric constant for lattices of perfectly conducting spheres. The multiple scattering method is also used by Psarobas and Siglas [78] to obtain the elastic band gaps in a face-centred cubic lattice of mercury spheres in aluminium. In all these works, the band gaps are searched numerically and the scatterer is a sphere. In the second section of this chapter, we are going to consider the acoustic wave propagation through three-dimensional periodic arrays using the method of matched asymptotic expansions. The scatterers must be identical and can be of arbitrary shape as long as the characteristic size a of the scatterer is small compared than both the wavelength k^{-1} and the length scale of the array periodicity L. Bao *et al.* [7] discuss the propagation of electromagnetic waves in a triply periodic lattice of dielectric spheres and evaluate the effective dielectric constant of a homogenised crystal in the long wavelength limit. Compared to the homogenisation method, which is not able to describe phenomena associated with the periodicity of the array such as band gaps, the method we use can give explicit approximations for the perturbed dispersion relation and explicit expressions for the size of the local band gap everywhere in the dispersion diagram.

5.1 Scattering by a sphere

A rigid sphere is placed in an infinite isotropic acoustic medium. Cartesian coordinates (x, y, z) are chosen with origin O at the centre of the sphere. Spherical coordinates are given by (see figure 5.1)

$$x = r\sin\theta\cos\varphi, \quad y = r\sin\theta\sin\varphi, \quad z = r\cos\theta, \tag{5.1}$$

with origin at O and $0 \leq \varphi < 2\pi$, $0 \leq \theta \leq \pi$.

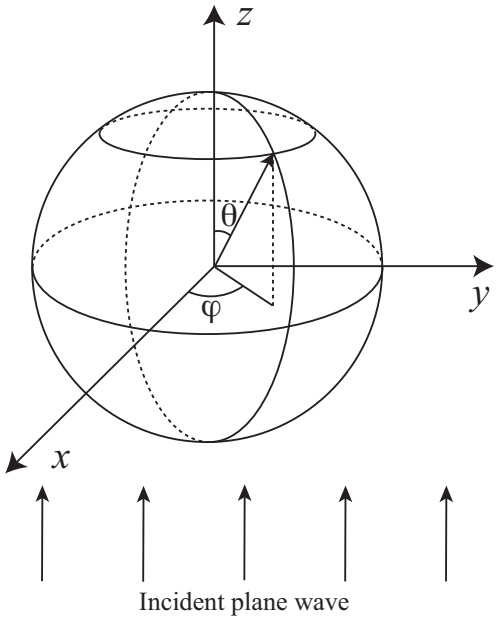

Figure 5.1: Spherical coordinates and incident wave.

An incident wave with potential $\phi^i = \mathrm{e}^{\mathrm{i}kz} = \mathrm{e}^{\mathrm{i}kr\cos\theta}$ propagates in the positive direction of z-axis, and so the potential has no dependence on φ. The scattered wave potential ϕ^s satisfies the three-dimensional Helmholtz equation

$$(\nabla^2 + k^2)\phi^s = 0, \tag{5.2}$$

and Neumann boundary condition

$$\frac{\partial\phi^s}{\partial r} = -\frac{\partial\phi^i}{\partial r} = -\mathrm{i}k\cos\theta\mathrm{e}^{\mathrm{i}kr\cos\theta}. \tag{5.3}$$

We separate the whole region into two: the inner region near the sphere $r \ll k^{-1}$ and outer region far away from the sphere $r \gg a$. The outer problem is in terms of the outer

coordinate $R = kr$ and satisfies

$$(\nabla_R^2 + 1)\Psi = 0, \tag{5.4}$$

$$\Psi \sim \frac{1}{\sqrt{R}} \mathrm{e}^{\mathrm{i}R} f(\theta), \quad \text{as} \quad R \to \infty, \tag{5.5}$$

where (5.5) is the radiation condition to make sure the scattered wave is outgoing. In the outer region, the outer solution is constructed from the outgoing spherical wavefunctions

$$\Psi^s = \sum_0^\infty a_n h_n^{(1)}(kr) P_n(\cos\theta), \tag{5.6}$$

where $h_n^{(1)}$ is a spherical Hankel function of the first kind and P_n is a Legendre polynomial. The spherical Hankel function is defined through the Hankel function

$$h_n^{(1)}(z) = \sqrt{\frac{\pi}{2z}} H_{n+\frac{1}{2}}^{(1)}(z), \quad n \in Z, \tag{5.7}$$

where the leading order of $h_n^{(1)}$ is always singular at the origin.

The inner problem is in terms of the inner coordinate $\rho = r/a$ and satisfies

$$(\nabla_\rho^2 + \epsilon^2)\psi = 0, \tag{5.8}$$

$$\frac{\partial \psi}{\partial \rho} = -\mathrm{i}\epsilon \cos\theta \mathrm{e}^{\mathrm{i}\epsilon\cos\theta}, \quad \text{on} \quad \rho = 1, \tag{5.9}$$

where the small parameter $\epsilon = ka$. The low order inner solutions are constructed from the inner eigensolutions, which satisfy the Laplace equation

$$\nabla_\rho^2 E_n(\rho, \theta) = 0, \tag{5.10}$$

and the homogeneous boundary condition

$$\frac{\partial E_n(\rho,\theta)}{\partial \rho} = 0, \quad \text{on} \quad \rho = 1. \tag{5.11}$$

Here the Laplace operator in terms of the spherical coordinates is

$$\nabla^2 = \frac{2}{r}\frac{\partial}{\partial r} + \frac{\partial^2}{\partial r^2} + \frac{\cot\theta}{r^2} + \frac{1}{r^2}\frac{\partial^2}{\partial \theta^2} + \frac{1}{r^2\sin\theta}\frac{\partial^2}{\partial \varphi^2}. \tag{5.12}$$

Therefore the inner eigensolutions are

$$E_0(\rho, \theta) = 1, \tag{5.13}$$

$$E_n(\rho,\theta) = \left(\frac{n+1}{n}\rho^n + \frac{1}{\rho^{n+1}}\right) P_n(\cos\theta), \quad \mathrm{n} > 0. \tag{5.14}$$

The inner problem (5.8) and the boundary condition (5.9) suggests the inner expansion starts from order ϵ term so that

$$\psi = \epsilon\psi_1 + \dots. \tag{5.15}$$

Substituting for ψ in (5.8) with (5.15) and equating like powers of ϵ, we obtain

$$\nabla_\rho^2 \psi_1 = 0, \tag{5.16}$$

$$\frac{\partial \psi_1}{\partial \rho} = \mathrm{i}\cos\theta, \quad \text{on} \quad \rho = 1. \tag{5.17}$$

These two equations suggest that ψ_1 has the form

$$\psi_1 = \frac{\mathrm{i}}{2\rho^2}\cos\theta + \sum_{n=0}^{\infty} A_n^{(1)} E_n(\rho), \tag{5.18}$$

where the first term is a solution of Laplace equation to satisfy the boundary condition (5.17) and the second term is a combination of the inner eigensolutions. Because the leading terms in the inner expansion of (5.6) are all inverse power of r, we have

$$A_n^{(1)} = 0, \quad \text{for all} \quad n, \tag{5.19}$$

otherwise the ρ^n terms in the inner eigensolutions could not be matched by the outer solution. Therefore the first term in outer expansion of the inner solution is

$$\psi^{(1,3)} = \epsilon^3 \frac{\mathrm{i}}{2R^2}\cos\theta, \tag{5.20}$$

which suggests that the leading order term in the outer expansion must be $O(\epsilon^3)$. In the next part, we are going to consider the wave scattering by a triply-periodic lattice, where the outer solution is started from $O(\epsilon^3)$ as well. The leading order term in the outer solution in the wave scattering by arrays can be seen as a consequence of the leading order term in the outer solution here. We start the outer expansion with

$$\Psi = \epsilon^3 \Psi_3 + \dots, \tag{5.21}$$

where Ψ_3 is in terms of the outer eigensolutions (5.6). The inner expansion of the outer solution $\epsilon^3\Psi_3(\epsilon\rho)$ is required to be not larger than the leading inner term, which is order ϵ, so we have

$$\Psi_3 = a_0 h_0^{(1)}(kr) + a_1 h_1^{(1)}(kr) P_n(\cos\theta) = -a_0 \frac{\mathrm{i}}{\epsilon\rho} - a_1 \frac{\mathrm{i}}{\epsilon^2\rho^2}\cos\theta. \tag{5.22}$$

The inner expansion of the outer solution is

$$\Psi^{(3,2)} = -a_0\epsilon^2\frac{\mathrm{i}}{\rho} - a_1\epsilon\frac{\mathrm{i}}{\rho^2}\cos\theta, \tag{5.23}$$

where the second term on the right hand side is $\Psi^{(3,1)}$. By the matching rule $\psi^{(1,3)} \equiv \Psi^{(3,1)}$, (5.20) and (5.23) give

$$a_1 = -\frac{1}{2}. \tag{5.24}$$

Suggested by the inner expansion of the outer solution (5.23), the inner expansion should be continued as

$$\psi = \epsilon\psi_1 + \epsilon^2\psi_2 + \ldots. \tag{5.25}$$

Substituting for this inner expansion (5.25) in the inner problem (5.8) and (5.9) and collecting the like powers of ϵ we obtain

$$\nabla_\rho^2\psi_2 = 0, \tag{5.26}$$

$$\frac{\partial\psi_2}{\partial\rho} = \cos^2\theta, \quad \text{on} \quad \rho = 1. \tag{5.27}$$

Thus ψ_2 has the form

$$\psi_2 = -\frac{1}{3\rho} - \frac{1}{18\rho^3}(3\cos 2\theta + 1) + \sum_{n=0}^{\infty} A_n^{(2)} E_n(\rho), \tag{5.28}$$

where the first two terms constitute the particular solution satisfying (5.26) and (5.27). To match with the outer solution we must set

$$A_n^{(2)} = 0, \quad \text{for all} \quad n. \tag{5.29}$$

The outer expansion of the inner solution is then

$$\psi^{(2,3)} = \epsilon\frac{\mathrm{i}}{2\rho^2}\cos\theta - \epsilon^2\frac{1}{3\rho}. \tag{5.30}$$

Using the matching rule $\psi^{(2,3)} \equiv \Psi^{(3,2)}$, (5.23) and (5.30) give

$$a_0 = -\frac{\mathrm{i}}{3}. \tag{5.31}$$

So far, we have obtained the coefficients of the leading order outer solutions

$$a_0 = -\frac{\mathrm{i}}{3}, \quad a_1 = -\frac{1}{2}. \tag{5.32}$$

This is consistent with the approximation expansions of the exact solutions [64, page 354] which can be easily obtained and therefore not presented here.

5.2 Acoustic wave propagation through a triply-periodic lattice of arbitrary shape scatterers

5.2.1 Fomulation

Consider the acoustic wave propagation through a three-dimensional lattice Λ of arbitrarily shaped rigid scatterers. We choose the origin O of the Cartesian coordinates (x, y, z) to be at the centre of one of the scatterers in the lattice. The wave potential $\phi(x, y, z)$ satisfies the three dimensional Helmholtz equation

$$\frac{\partial^2\phi}{\partial x^2} + \frac{\partial^2\phi}{\partial y^2} + \frac{\partial^2\phi}{\partial z^2} + k^2\phi = 0 \tag{5.33}$$

and the Neumann boundary condition

$$\frac{\partial\phi}{\partial n} = 0 \tag{5.34}$$

on each of the identical scatterers C_j uniformly distributed in the infinite lattice Λ, where k is the acoustic wavenumber and n is a coordinate measured normal to C_j. Scatterer j is associated with a local origin O_j located at the lattice point

$$\mathbf{R}_j = n_1\mathbf{a}_1 + n_2\mathbf{a}_2 + n_3\mathbf{a}_3, \qquad n_1, n_2, n_3 \in \mathbb{Z}, \tag{5.35}$$

for given independent vectors $\mathbf{a}_1$, $\mathbf{a}_2$ and $\mathbf{a}_3$. In particular, solutions are sought that, for all lattice vectors $\mathbf{R}_j$, satisfy the Bloch condition

$$\phi(\mathbf{r} + \mathbf{R_j}) = \phi(\mathbf{r})\mathrm{e}^{\mathrm{i}\boldsymbol{\beta}\cdot\mathbf{R}_j}, \tag{5.36}$$

for a given Bloch vector $\boldsymbol{\beta}$. This may be satisfied by plane waves of the form

$$\phi_m(\mathbf{r}) = \mathrm{e}^{\mathrm{i}\boldsymbol{\beta}_m^T\mathbf{r}}, \qquad m \in \mathbb{Z}, \tag{5.37}$$

where $\mathbf{r} = (x, y, z)^T$, $\boldsymbol{\beta}_m = \boldsymbol{\beta} + \mathbf{K}_m$, $\boldsymbol{\beta} = (q_1, q_2, q_3)^T$ is the prescribed Bloch vector and each

$$\mathbf{K}_m = 2\pi(m_1\mathbf{b}_1 + m_2\mathbf{b}_2 + m_3\mathbf{b}_3), \qquad m_1, m_2, m_3 \in \mathbb{Z}, \tag{5.38}$$

is a reciprocal lattice vector with

$$\mathbf{a}_i^T\mathbf{b}_j = \delta_{ij}, \qquad i, j = 1, 2, 3. \tag{5.39}$$

The reciprocal lattice vectors have the property that, for any lattice vector $\mathbf{R}_j$,

$$\mathbf{K}_m^T \mathbf{R}_j = 2\pi p, \qquad p \in \mathbb{Z}. \tag{5.40}$$

In the absence of the scatterers each ϕ_m provides a solution to the Bloch problems provided k is chosen to ensure that the field equation (5.33) is satisfied, in other words provided

$$k^2 = \beta_m^2, \qquad m \in \mathbb{Z}, \tag{5.41}$$

where $\beta_m = |\boldsymbol{\beta}_m|$. For example, for a simple cubic lattice of side L aligned with the coordinate axes, plane-wave solutions satisfying the Bloch condition are

$$\phi_m = \mathrm{e}^{\mathrm{i}\left[(q_1+\frac{2\pi m_1}{L})x+(q_2+\frac{2\pi m_2}{L})y+(q_3+\frac{2\pi m_3}{L})z\right]}, \qquad m_1, m_2, m_3 \in \mathbb{Z}, \tag{5.42}$$

and the field equations are satisfied as long as

$$k^2 = \left(q_1 + \frac{2\pi m_1}{L}\right)^2 + \left(q_2 + \frac{2\pi m_2}{L}\right)^2 + \left(q_3 + \frac{2\pi m_3}{L}\right)^2. \tag{5.43}$$

The results given here for the case when scatterers are present arise from consideration of perturbations to combinations of the plane wave solutions (5.37).

In addition to the global coordinates, local spherical coordinates $(r_j, \theta_j, \varphi_j)$ are used with origin at O_j. The Bloch condition (5.36) allows the solutions to be obtained through consideration of a primary lattice cell chosen to be that containing the origin O of the global coordinates. The spherical coordinates with origin at O are denoted by (r, θ, φ) and illustrated in figure 5.1, and the scatterer associated with O is denoted by S.

To facilitate the solution, each lattice cell is divided into two overlapping regions. For the primary cell these are an outer region at distances $r \gg a$, and an inner region within distances $r \ll k^{-1}$ of the scatterer. A small parameter $\epsilon = ka$ is introduced, and in the inner region a scaled coordinate $\rho = r/a$ is used. With these definitions, $kr = \epsilon\rho$.

In the outer region, far from each scatterer $r \gg a$, the solutions are constructed from solution of the three-dimensional Helmholtz equation (5.33) that satisfy the Bloch condition (5.36) and that are singular at the lattice points. Such solutions are

$$G_n^m(kr, \theta, \varphi) = \sum_{\mathbf{R}_j \in \Lambda} \mathrm{e}^{\mathrm{i}\boldsymbol{\beta}^T \mathbf{R}_j} \mathcal{H}_n^m(kr_j, \theta_j, \varphi_j), \tag{5.44}$$

where $\mathcal{H}_n^m$ is the outgoing spherical wavefunctions defined by

$$\mathcal{H}_n^m(kr_j, \theta_j, \varphi_j) = h_n^{(1)}(kr_j) Y_n^m(\hat{\mathbf{r}}_j). \tag{5.45}$$

Here $\hat{\mathbf{r}}_j$ is the unit vector in the direction of $\mathbf{r}_j$ and [55, page 64]

$$Y_n^m(\hat{\mathbf{r}}_j) = b_n^m P_n^m(\cos\theta_j) \mathrm{e}^{\mathrm{i}m\varphi_j}. \tag{5.46}$$

are normalised spherical harmonics. Here the normalisation factor

$$b_n^m = (-1)^m \sqrt{\frac{(2n+1)(n-m)!}{4\pi(n+m)!}}. \tag{5.47}$$

P_n^m is the associated Legendre function and $h_n^{(1)}(kr_j)$ is the spherical Hankel function of the first kind.

By the three dimensional addition theorem [55, page 90]

$$\begin{aligned} G_n^m(kr, \theta, \varphi) =& h_n(kr) Y_n^m(\hat{\mathbf{r}}) + \\ & \sum_{\nu=0}^{\infty} \sum_{\mu=-\nu}^{\nu} \sum_{q=0}^{\infty} 4\pi i^{\nu+q-n} (-1)^{\nu-\mu-n} \sigma_q^{m-\mu}(\boldsymbol{\beta}) \mathcal{G}(n, m; \nu, -\mu; q) j_\nu^{(1)}(kr) Y_\nu^\mu(\hat{\mathbf{r}}), \end{aligned} \tag{5.48}$$

where $j_\nu^{(1)}(kr)$ is the spherical Bessel function of the first kind, $\mathcal{G}$ is a Gaunt coefficient defined by [55, page 83]

$$\mathcal{G}(n, m; \nu, \mu; q) = (-1)^{m+\mu} \int_\Omega Y_n^m(\hat{\mathbf{r}}) Y_\nu^\mu(\hat{\mathbf{r}}) Y_q^{-m-\mu}(\hat{\mathbf{r}}) d\Omega, \tag{5.49}$$

and $\Omega = \{(\theta, \varphi) : 0 \leq \theta \leq \pi, 0 \leq \varphi < 2\pi\}$ is the surface of a unit ball. The lattice sum

$$\sigma_n^m(\boldsymbol{\beta}) = {\sum_{\mathbf{R}_j \in \Lambda}}' \mathrm{e}^{\mathrm{i}\boldsymbol{\beta}^T \mathbf{R}_j} \mathcal{H}_n^m(\mathbf{R}_j), \tag{5.50}$$

where the dash indicates that $\mathbf{R}_j = 0$ is omitted from the summation. The lattice sums have poles at $k = \pm\beta_m$ – see [50], for example – and these poles correspond to the plane wave solutions defined in (5.37).

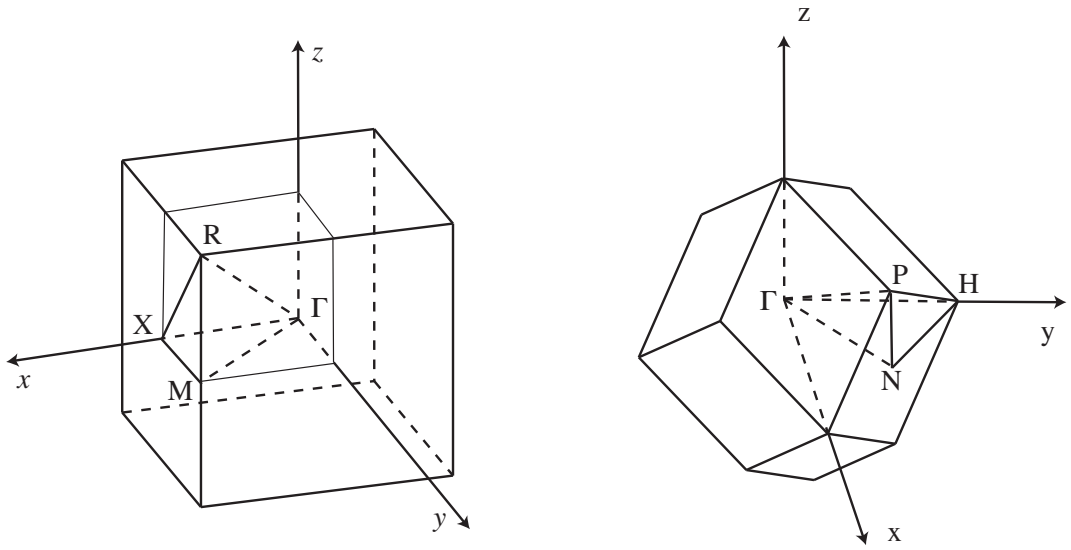

Figure 5.2: The first irreducible Brillouin zone for simple cubic lattice (left) and body-centred cubic lattice (right).

For simple cubic and body-centred cubic lattices, figure 5.2 gives their first Brillouin zones and the irreducible regions. To produce the dispersion diagrams, for convenience, we only consider when the Bloch vector is along the edges of the irreducible region of the first Brillouin zone . The locations of the poles of the lattice sums (or, equivalently, the plane waves that exist in the absence of the scatterers) are shown in figures 5.3 and 5.4 for values of the modulus β of the wave vector $\boldsymbol{\beta}$. In these figures it can be seen that, for some combinations of $\boldsymbol{\beta}$ and the frequency ω, there are multiple plane-wave solutions. There may be multiple distinct vectors $\boldsymbol{\beta}_j$ with the same magnitude β_j; this can occur along lines as indicated by the two or more-pole curves in the figures, and also at isolated points where two or more curves intersect. Comparisons between simple cubic and body-centred lattices are given later for perturbations of two, three and four-pole curves.

The lattice sums have poles at $k = \pm\beta_j$, $j = 1, ..M$. For each unique vector $\boldsymbol{\beta}_j$ [50]

$$\sigma_n^m \sim \frac{4\pi i^{n+1} Y_n^m(\hat{\boldsymbol{\beta}}_j)}{kV_c(k^2 - \beta_j^2)}, \quad \text{as} \quad k^2 \to \beta_j^2, \tag{5.51}$$

where V_c is the volume of one cell of the lattice and $\hat{\boldsymbol{\beta}}_j = (\sin\tau_j \cos\gamma_j, \sin\tau_j \sin\gamma_j, \cos\tau_j)$ is the unit vector in the direction of $\boldsymbol{\beta}_j$. The poles of the lattice sums correspond to the plane wave solutions (5.37). For these plane waves there may be $M \geq 1$ distinct vectors

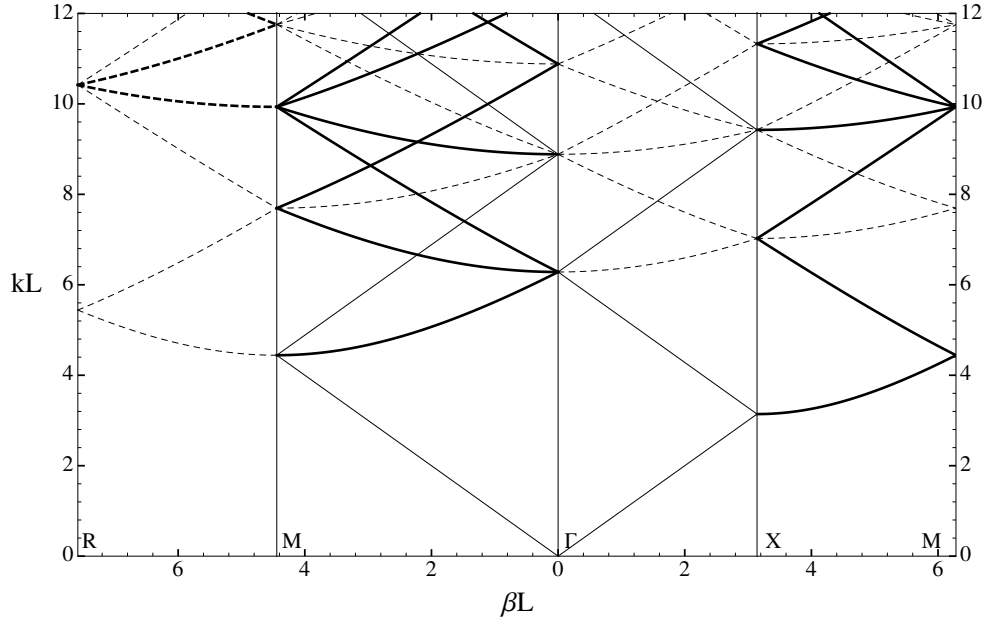

Figure 5.3: The unperturbed dispersion relation for simple cubic lattice. Solid line: one-pole, dashed line: two-pole, thick solid line: four-pole, thick dashed line: eight-pole.

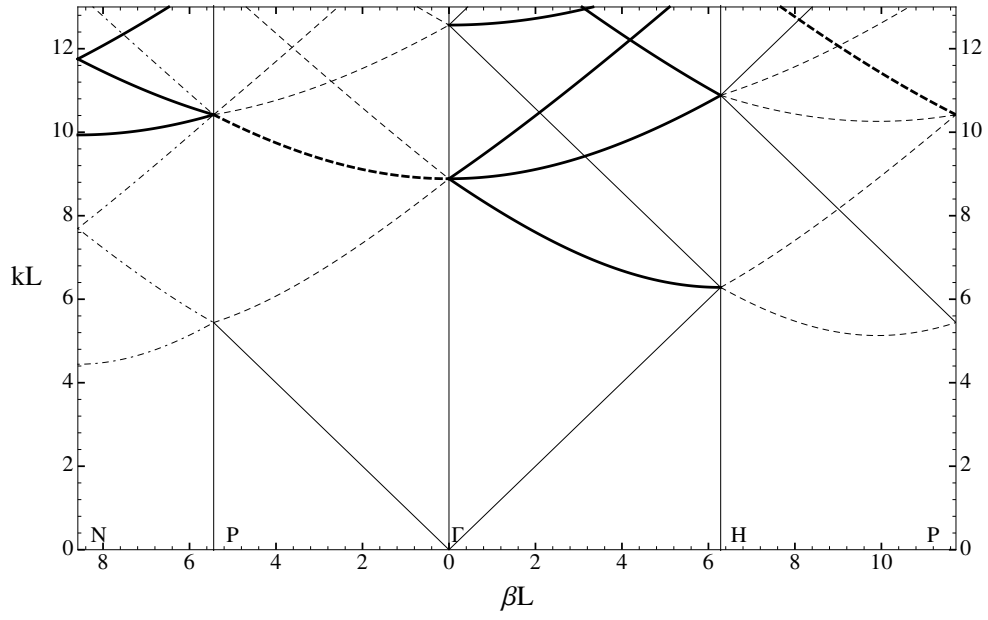

Figure 5.4: The unperturbed dispersion relation for body-centred cubic lattice. Solid line: one-pole, dot-dashed line: two-pole, dashed line: three-pole, thick solid line: four-pole, thick dashed line: six-pole.

$\boldsymbol{\beta}_j$ with the same magnitude β_j and, with this in mind, the lattice sum is written

$$\sigma_n^m = \sum_{j=1}^{M} \frac{\sigma_{nj}^{m,(1)}}{(k^2-\beta_j^2)L^2} + \sigma_n^{m,(2)} \tag{5.52}$$

where

$$\sigma_{nj}^{m,(1)} = \frac{4\pi i^{n+1} Y_n^m(\hat{\boldsymbol{\beta}}_j)}{kV_c/L^2} \tag{5.53}$$

and each $\sigma_n^{m,(2)}$ is an analytic function of k within neighbourhoods of $k = \pm\beta_j$. Solutions are sought for k in a neighbourhood of β_j and here we take

$$(k^2-\beta_j^2)L^2 = \epsilon^3\delta_j \tag{5.54}$$

where δ_j is strictly of order one in ϵ for $k^2 \neq \beta_j^2$ as $\epsilon \to 0$. This expression will be used within a neighbourhood of the points in $(\boldsymbol{\beta}, k)$ space that correspond to plane waves, so that the β_j and hence the δ_j may be distinct. The choice of ϵ^3 is because of the need to couple the first appearance of singular terms in the outer solution with the nonsingular leading-order outer solution, and the matching would fail if this relation (5.54) were incorrect. Actually, this order is also suggested by equation (5.21) in section 5.1, where the order of the scattered wave is ϵ^3 compared to the incident wave.

In view of (5.54), the matching may be carried out more conveniently if the singular solutions of the Helmholtz equation defined in (5.44) are modified to be

$$g_n^m(kr,\theta,\varphi) = \epsilon^3 G_n^m(kr,\theta,\varphi) = g_n^{m,(1)}(kr,\theta,\varphi) + \epsilon^3 g_n^{m,(2)}(kr,\theta,\varphi), \tag{5.55}$$

where

$$\begin{aligned}
&g_n^{m,(1)}(kr,\theta,\varphi) \\
&= \sum_{\nu=0}^{\infty}\sum_{\mu=-\nu}^{\nu}\sum_{q=0}^{\infty} 4\pi i^{\nu+q-n}(-1)^{\nu-\mu-n}\frac{\sigma_q^{m-\mu,(1)}}{(k^2-\beta_j^2)L^2}(\boldsymbol{\beta})\mathcal{G}(n,m;\nu,-\mu;q)j_\nu^{(1)}(kr)Y_\nu^\mu(\hat{\mathbf{r}}) \\
&= \sum_{\nu=0}^{\infty}\sum_{\mu=-\nu}^{\nu} 4\pi i^{\nu+1-n}(-1)^{\nu-\mu-n}\frac{1}{k\delta_j\mathcal{V}/L^2}j_\nu^{(1)}(kr)Y_\nu^\mu(\hat{\mathbf{r}})Y_n^m(-\hat{\boldsymbol{\beta}}_j)Y_\nu^{-\mu}(-\hat{\boldsymbol{\beta}}_j) \\
&= (-1)^n\sum_{j=1}^{M}\frac{\sigma_{nj}^{m,(1)}}{\delta_j}4\pi\sum_{\nu=0}^{\infty} i^\nu j_\nu(kr)\sum_{\mu=-\nu}^{\nu} Y_\nu^\mu(\hat{\mathbf{r}})\overline{Y_\nu^\mu(\hat{\boldsymbol{\beta}}_j)} \\
&= (-1)^n\sum_{j=1}^{M}\frac{\sigma_{nj}^{m,(1)}}{\delta_j}\mathrm{e}^{\mathrm{i}k\mathbf{r}\cdot\hat{\boldsymbol{\beta}}_j},
\end{aligned} \tag{5.56}$$

and

$$g_n^{m,(2)}(kr,\theta,\varphi) = h_n(kr)Y_n^m(\hat{\mathbf{r}}) + \sum_{\nu=0}^{\infty}\sum_{\mu=-\nu}^{\nu}\sum_{q=0}^{\infty} 4\pi i^{\nu+q-n}(-1)^{\nu-\mu-n}\sigma_q^{m-\mu,(2)}(\boldsymbol{\beta})\mathcal{G}(n,m;\nu,-\mu;q)j_\nu^{(1)}(kr)Y_\nu^\mu(\hat{\mathbf{r}}). \tag{5.57}$$

In (5.56), the linearisation formula for Y_n^m [55, page 83]

$$\sum_{q=0}^{\infty}\mathcal{G}(n,m;\nu,\mu;q)Y_q^{m+\mu}(\hat{\boldsymbol{\beta}}_j) = Y_n^m(\hat{\boldsymbol{\beta}}_j)Y_\nu^\mu(\hat{\boldsymbol{\beta}}_j) \tag{5.58}$$

has been used.

As the boundary-value problem is homogeneous, the leading-order outer solution may be taken as strictly order one in ϵ and written

$$\begin{aligned}\Psi^{(0)} &= \sum_{n=0}^{\infty}\sum_{m=-n}^{n} A_n^m g_n^{m,(1)}(kr,\theta,\varphi)\\ &= \sum_{n=0}^{\infty}\sum_{m=-n}^{n} A_n^m(-1)^n\sum_{j=1}^{M}\frac{\sigma_{nj}^{m,(1)}}{\delta_j}4\pi\Big\{j_0(kr)Y_0^0(\hat{\mathbf{r}})Y_0^0(\hat{\boldsymbol{\beta}}_j)^* + \\ &\qquad \mathrm{i}j_1(kr)\sum_{\mu=-1}^{1}Y_1^\mu(\hat{\mathbf{r}})Y_1^\mu(\hat{\boldsymbol{\beta}}_j)^* - j_2(kr)\sum_{\mu=-2}^{2}Y_2^\mu(\hat{\mathbf{r}})Y_2^\mu(\hat{\boldsymbol{\beta}}_j)^* + \ldots\Big\},\end{aligned} \tag{5.59}$$

where $*$ denote the conjugate complex. Then the inner expansion of the leading-order outer solution is

$$\Psi^{(0,1)} = \sum_{n=0}^{\infty}\sum_{m=-n}^{n} A_n^m(-1)^n\sum_{j=1}^{M}\frac{\sigma_{nj}^{m,(1)}}{\delta_j}\Big\{1 + \frac{4\pi}{3}i\epsilon\rho\sum_{\mu=-1}^{1}Y_1^\mu(\hat{\mathbf{r}})Y_1^\mu(\hat{\boldsymbol{\beta}}_j)^*\Big\}. \tag{5.60}$$

In terms of the inner variables the field equation for the inner solution ψ is

$$\frac{1}{\rho^2}\frac{\partial}{\partial\rho}\left(\rho^2\frac{\partial\psi}{\partial\rho}\right) + \frac{1}{\rho^2\sin\theta}\frac{\partial}{\partial\theta}\left(\sin\theta\frac{\partial\psi}{\partial\theta}\right) + \frac{1}{\rho^2\sin\theta}\frac{\partial\psi}{\partial\varphi} + \epsilon^2\psi = 0. \tag{5.61}$$

The inner solutions are constructed with the help of inner eigensolutions that each satisfies the Laplace equation, together with the homogeneous Neumann conditions

$$\frac{\partial\psi}{\partial n} = 0. \tag{5.62}$$

The solutions of the three-dimensional Laplace equation take the form

$$r^n P_n^m(\cos\theta)\mathrm{e}^{\pm \mathrm{i}m\varphi}, \quad r^{-n-1} P_n^m(\cos\theta)\mathrm{e}^{\pm \mathrm{i}m\varphi}. \tag{5.63}$$

For spherical scatterers, the normalised eigensolutions (to make it easier to match with the outer solutions) are

$$1, \quad \left(\frac{n+1}{n} r^n + \frac{1}{r^{n+1}}\right) Y_n^m(\hat{\mathbf{r}}), \quad n = 1, 2, \ldots, \ m = 0, 1, \ldots, n. \tag{5.64}$$

The form of $\Psi^{(0,1)}$ indicates an inner development

$$\psi^{(1)} = \psi_0 + \nu_{11}(\epsilon)\psi_{11} + \epsilon\psi_1. \tag{5.65}$$

where the term in $\nu_{11}(\epsilon)$ is a possible intermediate term. Substituting (5.65) into the field equations (5.61) and (5.62) and equating the coefficients of the gauge functions in ϵ, we find that ψ_0, ψ_{11}, ψ_1 are all harmonic functions that satisfy the homogeneous boundary conditions, and hence are constructed from the inner eigenfunctions. Therefore, to effect the matching it is necessary to take

$$\psi^{(1)} = B_0 + \nu_{11} B_{11} + \epsilon \left\{ B_1 + (u_1^{-1}, u_1^0, u_1^1) \left[\rho \begin{pmatrix} Y_1^{-1}(\hat{\mathbf{r}}) \\ Y_1^0(\hat{\mathbf{r}}) \\ Y_1^1(\hat{\mathbf{r}}) \end{pmatrix} + \chi_1(\hat{\mathbf{r}}) \right] \right\}, \tag{5.66}$$

where from the Neumann boundary condition (5.34),

$$\frac{\partial \chi_1}{\partial n} = -\frac{\partial}{\partial n} \left[\rho \begin{pmatrix} Y_1^{-1}(\hat{\mathbf{r}}) \\ Y_1^0(\hat{\mathbf{r}}) \\ Y_1^1(\hat{\mathbf{r}}) \end{pmatrix} \right] \quad \text{on } C, \tag{5.67}$$

$$\chi_1 - \frac{\mathbf{M}}{\rho^2} \begin{pmatrix} Y_1^{-1}(\hat{\mathbf{r}}) \\ Y_1^0(\hat{\mathbf{r}}) \\ Y_1^1(\hat{\mathbf{r}}) \end{pmatrix} = o(\rho^{-2}) \ \text{ as } \ \rho \to \infty, \tag{5.68}$$

and

$$\mathbf{M} = \begin{pmatrix} m_{11} & m_{12} & m_{13} \\ m_{21} & m_{22} & m_{23} \\ m_{31} & m_{32} & m_{33} \end{pmatrix} \tag{5.69}$$

is the matrix of dipole coefficients determined by the shape of the scatterer [8, page 121]. At order ϵ^3 the outer expansion of the inner solution $\psi^{(1)}$, when written in terms of the

outer variable kr, has terms no more singular than a dipole and hence cannot be matched to any higher singularities associated with the leading-order outer solution; thus

$$A_n^m = 0,\ n \geq 2, m = -n,\ \ldots, n, \tag{5.70}$$

and so

$$\Psi^{(0,1)} = \sum_{n=0}^{1}\sum_{m=-n}^{n} A_n^m (-1)^n \sum_{j=1}^{M} \frac{\sigma_{nj}^{m,(1)}}{\delta_j} \left\{ 1 + \frac{4\pi}{3} i\epsilon\rho \sum_{\mu=-1}^{1} Y_1^\mu(\hat{\mathbf{r}}) Y_1^\mu(\hat{\boldsymbol{\beta}}_j)^* \right\}. \tag{5.71}$$

From the inner solution (5.66)

$$\psi^{(1,0)} = B_0 + \epsilon\rho(u_1^{-1}, u_1^0, u_1^1) \begin{pmatrix} Y_1^{-1}(\hat{\mathbf{r}}) \\ Y_1^0(\hat{\mathbf{r}}) \\ Y_1^1(\hat{\mathbf{r}}) \end{pmatrix}, \tag{5.72}$$

and the matching of $\Psi^{(0,1)}$ with $\psi^{(1,0)}$ yields

$$B_0 = \sum_{n=0}^{1}\sum_{m=-n}^{n} A_n^m (-1)^n \sum_{j=1}^{M} \frac{\sigma_{nj}^{m,(1)}}{\delta_j}, \tag{5.73}$$

$$u_1^\mu = i\frac{4\pi}{3} \sum_{n=0}^{1}\sum_{m=-n}^{n} A_n^m (-1)^n \sum_{j=1}^{M} \frac{\sigma_{nj}^{m,(1)}}{\delta_j} Y_1^\mu(\hat{\boldsymbol{\beta}}_j)^*, \quad \mu = -1, 0, 1. \tag{5.74}$$

With possible intermediate terms included, the outer solution is continued as

$$\begin{aligned}
\Psi^{(3)} = &\sum_{n=0}^{1}\sum_{m=-n}^{n} A_n^m [g_n^{m,(1)}(kr,\theta,\varphi) + \epsilon^3 g_n^{m,(2)}(kr,\theta,\varphi)] \\
&+ \mu_{11}(\epsilon) \sum_{n=0}^{\infty}\sum_{m=-n}^{n} \widehat{C}_n^m g_n^{m,(1)}(kr,\theta,\varphi) + \epsilon \sum_{n=0}^{\infty}\sum_{m=-n}^{n} C_n^m g_n^{m,(1)}(kr,\theta,\varphi) \\
&+ \mu_{21}(\epsilon) \sum_{n=0}^{\infty}\sum_{m=-n}^{n} \widehat{D}_n^m g_n^{m,(1)}(kr,\theta,\varphi) + \epsilon^2 \sum_{n=0}^{\infty}\sum_{m=-n}^{n} D_n^m g_n^{m,(1)}(kr,\theta,\varphi) \\
&+ \mu_{31}(\epsilon) \sum_{n=0}^{\infty}\sum_{m=-n}^{n} \widehat{E}_n^m g_n^{m,(1)}(kr,\theta,\varphi) + \epsilon^3 \sum_{n=0}^{\infty}\sum_{m=-n}^{n} E_n^m g_n^{m,(1)}(kr,\theta,\varphi),
\end{aligned} \tag{5.75}$$

which has an inner expansion

$$\Psi^{(3,2)} = \sum_{n=0}^{1}\sum_{m=-n}^{n} A_n^m(-1)^n \sum_{j=1}^{M} \frac{\sigma_{nj}^{m,(1)}}{\delta_j} \left\{ 1 - \frac{\epsilon^2\rho^2}{6} + \frac{4\pi}{3} i\epsilon\rho \sum_{\mu=-1}^{1} Y_1^\mu(\hat{\mathbf{r}}) Y_1^\mu(\hat{\boldsymbol{\beta}}_j)^* \right.$$

$$\left. - \frac{4\pi}{15}\epsilon^2\rho^2 \sum_{\mu=-2}^{2} Y_2^\mu(\hat{\mathbf{r}}) Y_2^\mu(\hat{\boldsymbol{\beta}}_j)^* \right\} + \epsilon^3 \sum_{n=0}^{1}\sum_{m=-n}^{n} A_n^m h_n(kr) Y_n^m(\widehat{\mathbf{r}})$$

$$+ \sum_{n=0}^{\infty}\sum_{m=-n}^{n} \left[\mu_{11}(\epsilon)\widehat{C}_n^m + \epsilon C_n^m\right](-1)^n \sum_{j=1}^{M} \frac{\sigma_{nj}^{m,(1)}}{\delta_j} \left\{ 1 + \frac{4\pi}{3} i\epsilon\rho \sum_{\mu=-1}^{1} Y_1^\mu(\hat{\mathbf{r}}) Y_1^\mu(\hat{\boldsymbol{\beta}}_j)^* \right\}$$

$$+ \sum_{n=0}^{\infty}\sum_{m=-n}^{n} \left[\mu_{21}(\epsilon)\widehat{D}_n^m + \epsilon^2 D_n^m\right](-1)^n \sum_{j=1}^{M} \frac{\sigma_{nj}^{m,(1)}}{\delta_j}. \tag{5.76}$$

Thus to match with the inner solution, $\mu_{11}(\epsilon) = \nu_{11}(\epsilon)$ and the inner solution must be continued as

$$\psi^{(2)} = B_0 + \nu_{11}(\epsilon)B_{11} + \epsilon \left\{ B_1 + (u_1^{-1}, u_1^0, u_1^1) \left[\rho \begin{pmatrix} Y_1^{-1}(\hat{\mathbf{r}}) \\ Y_1^0(\hat{\mathbf{r}}) \\ Y_1^1(\hat{\mathbf{r}}) \end{pmatrix} + \chi_1(\hat{\mathbf{r}}) \right] \right\}$$

$$+ \epsilon \left\{ \nu_{11}(\epsilon)(u_{11}^{-1}, u_{11}^0, u_{11}^1) \left[\rho \begin{pmatrix} Y_1^{-1}(\hat{\mathbf{r}}) \\ Y_1^0(\hat{\mathbf{r}}) \\ Y_1^1(\hat{\mathbf{r}}) \end{pmatrix} + \chi_1(\hat{\mathbf{r}}) \right] \right\} + \mu_{21}(\epsilon)B_{21} + \epsilon^2\psi_2, \tag{5.77}$$

where, from (5.61), ψ_2 satisfies the poisson equation

$$\frac{1}{\rho^2}\frac{\partial}{\partial\rho}\left(\rho^2\frac{\partial\psi}{\partial\rho}\right) + \frac{1}{\rho^2\sin\theta}\frac{\partial}{\partial\theta}\left(\sin\theta\frac{\partial\psi}{\partial\theta}\right) + \frac{1}{\rho^2\sin\theta}\frac{\partial\psi}{\partial\varphi} = -B_0 \tag{5.78}$$

and also the homogeneous boundary condition

$$\frac{\partial\psi_2}{\partial n} = 0 \quad \text{on} \quad C. \tag{5.79}$$

The form required to effect the matching with $\Psi^{(3,2)}$ is

$$\psi_2 = B_0\left[-\frac{1}{6}\rho^2+\Gamma(\rho,\theta,\varphi)\right]+B_2+(u_2^{-1},u_2^0,u_2^1)\left[\rho\begin{pmatrix}Y_1^{-1}(\hat{\mathbf{r}})\\ Y_1^0(\hat{\mathbf{r}})\\ Y_1^1(\hat{\mathbf{r}})\end{pmatrix}+\chi_1(\hat{\mathbf{r}})\right]$$

$$+(v_2^{-2},v_2^{-1},v_2^0,v_2^1,v_2^2)\left[\rho^2\begin{pmatrix}Y_2^{-2}(\hat{\mathbf{r}})\\ Y_2^{-1}(\hat{\mathbf{r}})\\ Y_2^0(\hat{\mathbf{r}})\\ Y_2^1(\hat{\mathbf{r}})\\ Y_2^2(\hat{\mathbf{r}})\end{pmatrix}+\chi_2(\hat{\mathbf{r}})\right], \tag{5.80}$$

where the term involving $-1/6$ is a particular solution of (5.78) and Γ is a harmonic function introduced to compensate for the flux across the scatterer S that is induced by the term in $-1/6$. By the Neumann boundary condition (5.79), we have

$$\frac{\partial\Gamma}{\partial n}=-\frac{\partial}{\partial n}\left(-\frac{1}{6}\rho^2\right)=\frac{1}{6}\frac{\partial\rho^2}{\partial n}. \tag{5.81}$$

The flux across the scatterer S induced by the term in ρ^2 must be compensated by the flux induced by Γ across the outer 'boundary' of the inner region as $\rho\to\infty$, the sphere S^*. Therefore, we obtain

$$\iint_{\partial S^*}\frac{\partial\Gamma}{\partial n}ds=-\frac{1}{6}\iint_{\partial S}\frac{\partial\rho^2}{\partial n}ds, \tag{5.82}$$

Because Γ is a solution of the Laplace equation, we take its form as

$$\Gamma(\rho,\theta)\sim\frac{B}{\rho}, \tag{5.83}$$

where B is a unknown constant and this form is chosen to effect the matching. The left hand side of (5.82) is

$$\iint_{\partial S^*}\frac{\partial\Gamma}{\partial n}ds=-\int_0^{\pi}\int_0^{2\pi}\frac{\partial\Gamma}{\partial\rho}\rho^2\sin\theta d\varphi d\theta=4\pi B,$$

where the minus sign is because the surface normal on the scatterer is directed into the scatterer. Applying the divergence theorem to the right hand side of (5.82) gives

$$-\frac{1}{6}\iint_{\partial S}\frac{\partial\rho^2}{\partial n}ds=-\frac{1}{6}\iiint_S\nabla^2(\rho^2)dv=-\frac{V_s}{a^3},$$

where V_s is the volume contained within the scatterer S and a^3 is to make the area dimensionless. Thus, we get

$$B = -\frac{V_s}{4\pi a^3}, \tag{5.84}$$

and then

$$\Gamma(\rho,\theta,\varphi) + \frac{V_s}{4\pi a^3}\frac{1}{\rho} \to 0, \text{ as } \rho \to \infty. \tag{5.85}$$

It follows immediately that

$$\begin{aligned}\psi^{(2,3)} = B_0 + \nu_{11}(\epsilon)B_{11} + \epsilon\left\{B_1 + \left(u_1^{-1},u_1^0,u_1^1\right)\left[\rho\begin{pmatrix}Y_1^{-1}(\hat{\mathbf{r}})\\ Y_1^0(\hat{\mathbf{r}})\\ Y_1^1(\hat{\mathbf{r}})\end{pmatrix} + \frac{\mathbf{M}}{\rho^2}\begin{pmatrix}cY_1^{-1}(\hat{\mathbf{r}})\\ Y_1^0(\hat{\mathbf{r}})\\ Y_1^1(\hat{\mathbf{r}})\end{pmatrix}\right]\right\}\\ + \epsilon\left\{\nu_{11}(\epsilon)\left(u_{11}^{-1},u_{11}^0,u_{11}^1\right)\left[\rho\begin{pmatrix}Y_1^{-1}(\hat{\mathbf{r}})\\ Y_1^0(\hat{\mathbf{r}})\\ Y_1^1(\hat{\mathbf{r}})\end{pmatrix} + \chi_1(\hat{\mathbf{r}})\right]\right\} + \mu_{21}(\epsilon)B_{21}\\ + \epsilon^2\left\{B_0\left[-\frac{1}{6}\rho^2 - \frac{V_s}{4\pi a^3}\frac{1}{\rho}\right] + B_2 + \rho\sum_{\mu=-1}^{1}u_2^\mu Y_1^\mu(\hat{\mathbf{r}}) + \rho^2\sum_{\mu=-2}^{1}v_2^\mu Y_1^\mu(\hat{\mathbf{r}})\right\}\end{aligned} \tag{5.86}$$

and matching with $\Phi^{(3,2)}$ gives, in particular,

$$A_0^0 = -\frac{i\sqrt{4\pi}V_s}{4\pi a^3}B_0, \quad (A_1^{-1},A_1^0,A_1^1) = i(u_1^{-1},u_1^0,u_1^1)\mathbf{M}. \tag{5.87}$$

With the values of A_n^m given by (5.87), equation (5.73) becomes

$$B_0 = \frac{4\pi L^2}{kV_c}\sum_{j=1}^{M}\frac{1}{\delta_j}\left\{\frac{V_s}{4\pi a^3}B_0 + i\left(u_1^{-1},u_1^0,u_1^1\right)\mathbf{M}\begin{pmatrix}Y_1^{-1}(\hat{\boldsymbol{\beta}}_j)\\ Y_1^0(\hat{\boldsymbol{\beta}}_j)\\ Y_1^1(\hat{\boldsymbol{\beta}}_j)\end{pmatrix}\right\} \tag{5.88}$$

and equation (5.74) becomes

$$u_1^\mu = \frac{4\pi i}{3}\frac{4\pi L^2}{kV_c}\sum_{j=1}^{M}\frac{Y_1^\mu(\hat{\boldsymbol{\beta}}_j)^*}{\delta_j}\left\{\frac{V_s}{4\pi a^3}B_0 + i\left(u_1^{-1},u_1^0,u_1^1\right)\mathbf{M}\begin{pmatrix}Y_1^{-1}(\hat{\boldsymbol{\beta}}_j)\\ Y_1^0(\hat{\boldsymbol{\beta}}_j)\\ Y_1^1(\hat{\boldsymbol{\beta}}_j)\end{pmatrix}\right\}, \quad \mu = -1,0,1. \tag{5.89}$$

Equations (5.88) and (5.89) define an eigenvalue problem for the wavenumber k. If we

introduce

$$U_j = \frac{1}{\delta_j}\left\{ \frac{V_s}{4\pi a^3} B_0 + i\big(u_1^{-1}, u_1^0, u_1^1\big)\mathbf{M} \begin{pmatrix} Y_1^{-1}(\hat{\boldsymbol{\beta}}_j) \\ Y_1^0(\hat{\boldsymbol{\beta}}_j) \\ Y_1^1(\hat{\boldsymbol{\beta}}_j) \end{pmatrix} \right\}, \tag{5.90}$$

and substitute (5.88) and (5.89) back into (5.90) this yields

$$\delta_p U_p = \frac{4\pi L^2}{kV_c} \sum_{j=1}^{M} \left\{ \frac{V_s}{4\pi a^3} - \frac{4\pi}{3} \Big(Y_1^{-1}(\hat{\boldsymbol{\beta}}_j)^*, Y_1^0(\hat{\boldsymbol{\beta}}_j)^*, Y_1^1(\hat{\boldsymbol{\beta}}_j)^* \Big) \mathbf{M} \begin{pmatrix} Y_1^{-1}(\hat{\boldsymbol{\beta}}_j) \\ Y_1^0(\hat{\boldsymbol{\beta}}_j) \\ Y_1^1(\hat{\boldsymbol{\beta}}_j) \end{pmatrix} \right\} U_j, \tag{5.91}$$

where $p = 1, 2, \ldots, M$. For a given $\boldsymbol{\beta}$, equation (5.91) provides an eigenvalue problem for the corresponding wavenumber k (which appears in every δ_p). The geometry of the lattice Λ appears through the reciprocal lattice vectors in the definitions of each δ_p and $\boldsymbol{\beta}_j$.

5.2.2 Results

In this section we give some examples of explicit approximations to the dispersion relation, obtained from the eigenvalue problems in equation (5.91) with the aid of the computer-algebra package Mathematica. Results are given on the edges of the irreducible region of the first Brillouin zone (labelled ΓXMR for simple cubic lattice and ΓHPN for body-centred cubic lattice) for simple cubic and body-centred cubic lattices, shown in figure 5.2. The areas of the corresponding primitive cells are $V_c = L^3$.

We consider two different shapes of scatterers, sphere and prolate spheroid. The sphere has radius a and the prolate spheroid has semi-axes of length a_1, b_1 and c_1 ($b_1 = c_1$) parallel to the x, y and z axes respectively. For each prolate spheroid the matrix of dipole coefficients we use is defined in (5.68), where the dipole is written in normalised spherical harmonics. This is different from the classic definition [65, page 142] where the dipole takes the form

$$-\frac{\mathbf{D}}{r^2} \begin{pmatrix} \sin\theta\cos\varphi \\ \sin\theta\sin\varphi \\ \cos\theta \end{pmatrix} = -\frac{\mathbf{D}}{r^3} \begin{pmatrix} x \\ y \\ z \end{pmatrix} \tag{5.92}$$

Here $\mathbf{D}$ is the dipole coefficient matrix. Now we are going to find what's the relation between our definition $\mathbf{M}$ and the classic definition $\mathbf{D}$. The eigensolution including the

dipole we use is in the form

$$r\begin{pmatrix} Y_1^{-1}(\hat{\mathbf{r}}) \\ Y_1^{0}(\hat{\mathbf{r}}) \\ Y_1^{1}(\hat{\mathbf{r}}) \end{pmatrix} + \frac{\mathbf{M}}{r^2}\begin{pmatrix} Y_1^{-1}(\hat{\mathbf{r}}) \\ Y_1^{0}(\hat{\mathbf{r}}) \\ Y_1^{1}(\hat{\mathbf{r}}) \end{pmatrix} = \mathbf{R}^{-1}\left[\begin{pmatrix} x \\ y \\ z \end{pmatrix} + \frac{\mathbf{RMR}^{-1}}{r^3}\begin{pmatrix} x \\ y \\ z \end{pmatrix}\right]. \tag{5.93}$$

Compare (5.92) and (5.93), we find

$$\mathbf{M} = -\mathbf{R}^{-1}\mathbf{DR}, \tag{5.94}$$

where

$$\mathbf{R}\begin{pmatrix} Y_1^{-1}(\hat{\mathbf{r}}) \\ Y_1^{0}(\hat{\mathbf{r}}) \\ Y_1^{1}(\hat{\mathbf{r}}) \end{pmatrix} = \begin{pmatrix} \sin\theta\cos\varphi \\ \sin\theta\sin\varphi \\ \cos\theta \end{pmatrix}. \tag{5.95}$$

Then it is easy to get

$$\mathbf{R} = \sqrt{\frac{8\pi}{3}}\begin{pmatrix} -\frac{1}{2} & 0 & \frac{1}{2} \\ -\frac{\mathrm{i}}{2} & 0 & -\frac{\mathrm{i}}{2} \\ 0 & \frac{\sqrt{2}}{2} & 0 \end{pmatrix}. \tag{5.96}$$

When the scatterer is symmetric about the axes, all the non-diagonal elements are equal to zero, i.e. $D_{ij} = 0,\ i \neq j$, therefore

$$\mathbf{M} = \begin{pmatrix} -\frac{1}{2}(D_{11}+D_{22}) & 0 & \frac{1}{2}(D_{11}-D_{22}) \\ 0 & D_{33} & 0 \\ \frac{1}{2}(D_{11}-D_{22}) & 0 & -\frac{1}{2}(D_{11}+D_{22}) \end{pmatrix}. \tag{5.97}$$

The dipole matrix coefficients D_{ii} are related to the added mass coefficients a_{ii} [65, page 143]

$$D_{ii} = -\frac{1}{4\pi a^3}\left(a_{ii}/\rho + V_s\right). \tag{5.98}$$

For a sphere, the added mass coefficients are [65, page 144]

$$a_{11} = a_{22} = a_{33} = \rho V_s/2, \tag{5.99}$$

For a prolate spheroid, the added mass coefficients are [32, page 153]

$$a_{11} = \frac{\alpha_0}{2-\alpha_0}\frac{4}{3}\pi\rho a_1 b_1^2, \tag{5.100}$$

$$a_{22} = a_{33} = \frac{\beta_0}{2-\beta_0}\frac{4}{3}\pi\rho a_1 b_1^2, \tag{5.101}$$

where

$$\alpha_0 = \frac{2(1-\mathrm{e}^2)}{\mathrm{e}^3}\left(\frac{1}{2}\log\frac{1+e}{1-e} - e\right), \tag{5.102}$$

$$\beta_0 = \frac{1}{\mathrm{e}^2} - \frac{1-\mathrm{e}^2}{2\mathrm{e}^3}\log\frac{1+e}{1-e}, \tag{5.103}$$

$$\mathrm{e}^2 = 1 - \frac{b_1^2}{a_1^2}. \tag{5.104}$$

In the diagrams below we compare the perturbations between a sphere with radius $a = 0.15$ and a prolate spheroid with semi-axes $a_1 = 0.3$ and $b_1 = c_1 = 0.15$.

A. Perturbation of one plane wave

In the case $M = 1$, equation (5.91) reduces to

$$k^2 = \beta_1^2\left\{1 - \frac{4\pi a^3}{V_c}\left[\frac{V_s}{4\pi a^3} - \frac{4\pi}{3}\left(Y_1^{-1}(\hat{\boldsymbol{\beta}}_j)^*, Y_1^0(\hat{\boldsymbol{\beta}}_j)^*, Y_1^1(\hat{\boldsymbol{\beta}}_j)^*\right)\mathbf{M}\begin{pmatrix} Y_1^{-1}(\hat{\boldsymbol{\beta}}_j) \\ Y_1^0(\hat{\boldsymbol{\beta}}_j) \\ Y_1^1(\hat{\boldsymbol{\beta}}_j)\end{pmatrix}\right]\right\}^{-1}. \tag{5.105}$$

This expression gives perturbations of any of the one-pole solutions illustrated in the dispersion diagrams in figure 5.3 and 5.4, regardless their frequency. For a given $\boldsymbol{\beta}$, this expression shows how the wavenumber k depends on the geometry of the scatterer through the volume V_s contained with the scatterer S and the dipole matrix $\mathbf{M}$ defined through (5.68).

By the relation between our dipole matrix and the classic dipole matrix (5.97), the dispersion relation (5.105) becomes

$$k^2 = \beta_1^2\left\{1 - \frac{4\pi a^3}{V_c}\left[\frac{V_s}{4\pi a^3} + D_{11}\sin^2\tau_1\cos^2\gamma_1 + D_{22}\sin^2\tau_1\sin^2\gamma_1 + D_{33}\cos^2\tau_1\right]\right\}. \tag{5.106}$$

In terms of the added mass equation (5.106) becomes

$$k^2 = \beta_1^2\left\{1 + \frac{V_s}{V_c}\left[\frac{a_{11}}{\rho V_s}\sin^2\tau_1\cos^2\gamma_1 + \frac{a_{22}}{\rho V_s}\sin^2\tau_1\sin^2\gamma_1 + \frac{a_{33}}{\rho V_s}\cos^2\tau_1\right]\right\}^{-1}. \tag{5.107}$$

In the case of S is a sphere of radius a

$$k^2 = \beta_1^2\left[1 + \frac{2\pi a^3}{3V_c}\right]^{-1}, \tag{5.108}$$

where the second term in the square bracket is half of the sphere volume divided by the volume of one lattice cell. This is different from two dimensional case, where the corresponding dispersion relation is [60, eq. 60]

$$k^2 = \beta_1^2 \left[1 + \frac{\pi a^2}{\mathcal{A}}\right]^{-1}, \tag{5.109}$$

where $\mathcal{A}$ is the area of one cell of the two-dimensional lattice. Here the second term in the square bracket is the area (not half) of the cross section of the cylinder divided by the volume of one lattice cell. This difference is caused by the different forms of the dipole coefficients for two and three dimensions.

These results may be compared with results obtained by method of homogenisation for the the lowest mode, that is when

$$\boldsymbol{\beta}_1 = \beta_1 \begin{pmatrix} \sin\tau_1 \cos\gamma_1 \\ \sin\tau_1 \sin\gamma_1 \\ \cos\tau_1 \end{pmatrix}. \tag{5.110}$$

Using the same method as [21], which is a two-dimensional problem, we get the three-dimensional field equation

$$\left[1 + \frac{V_s}{V_c}\frac{a_{11}}{\rho V}\right]^{-1} \frac{\partial^2\phi}{\partial x^2} + \left[1 + \frac{V_s}{V_c}\frac{a_{22}}{\rho V}\right]^{-1} \frac{\partial^2\phi}{\partial y^2} + \left[1 + \frac{V_s}{V_c}\frac{a_{33}}{\rho V}\right]^{-1} \frac{\partial^2\phi}{\partial z^2} + k^2\phi = 0, \tag{5.111}$$

and seeking solutions in the form

$$\phi = \mathrm{e}^{\mathrm{i}\beta_1(x\sin\tau_1\cos\gamma_1 + y\sin\tau_1\sin\gamma_1 + z\cos\tau_1)} \tag{5.112}$$

yields

$$\begin{aligned} k^2 = \beta_1^2 \Bigg\{ & \left[1 + \frac{V_s}{V_c}\frac{a_{11}}{\rho V}\right]^{-1} \sin^2\tau_1 \cos^2\gamma_1 + \\ & \left[1 + \frac{V_s}{V_c}\frac{a_{22}}{\rho V}\right]^{-1} \sin^2\tau_1 \sin^2\gamma_1 + \left[1 + \frac{V_s}{V_c}\frac{a_{33}}{\rho V}\right]^{-1} \cos^2\tau_1 \Bigg\} \end{aligned} \tag{5.113}$$

However, by assumption the scatterer size is much smaller than the periodicity of the lattice, so $V/V_c \ll 1$ and expansion of (5.113) in powers of V/V_c yields

$$k^2 = \beta_1^2 \left\{1 - \frac{V_s}{V_c}\left[\frac{a_{11}}{\rho V_s}\sin^2\tau_1\cos^2\gamma_1 + \frac{a_{22}}{\rho V_s}\sin^2\tau_1\sin^2\gamma_1 + \frac{a_{33}}{\rho V_s}\cos^2\tau_1\right]\right\} \tag{5.114}$$

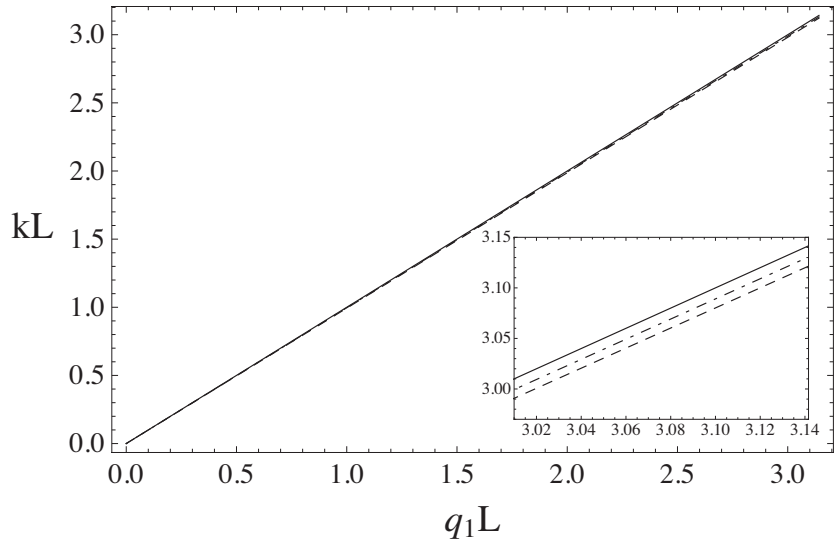

Figure 5.5: The perturbation of the first one-pole line along ΓX for simple cubic lattice. Dot-dashed curve: sphere, dashed curve: spheroid, solid curve: no scatterers.

Expansion of (5.107) in powers of V/V_c yields (5.114) as well, so the results from two different methods are consistent.

The comparisons of the lowest one-pole solution of simple cubic lattice and body-centred cubic lattice along the edges of the irreducible region of the first irreducible Brillouin zone are shown in figure 5.5 and 5.6. As we can see, the perturbed modes are quite close to the unperturbed curves for both of two lattices. In these two diagrams, we give the local magnification of the right top corner of the whole diagrams and we see both perturbed curves are below the unperturbed ones and as the volume of the prolate spheroid is bigger than that of the sphere, the modes perturbed by spheroids are further away from the unperturbed modes than by the spheres.

B. Perturbations of two plane waves

When $M = 2$, there are two plane wave solutions along one curve in the dispersion diagrams without scatterers. The two-pole curves are generally perturbed into two separate curves with the scatterers present. First, we consider the lowest two-pole mode along XM for the simple cubic lattice, where $q_1 L = \pi$, $q_3 L = 0$ and $q_2 L \in (0, \pi)$. The appropriate forms for β_m are

$$\beta_1 L = (q_1 L, q_2 L, q_3 L)^T, \quad \beta_2 L = (q_1 L - 2\pi, q_2 L, q_3 L)^T. \tag{5.115}$$

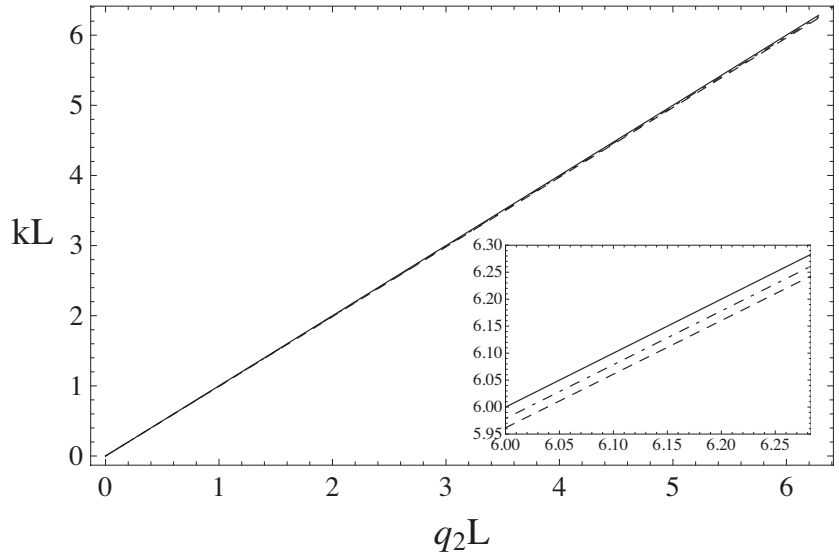

Figure 5.6: The perturbation of the first one-pole line along ΓH for body-centred cubic lattice. Dot-dashed curve: sphere, dashed curve: spheroid, solid curve: no scatterers.

Then the corresponding positive roots of (5.91) are

$$kL = \frac{q_2L^2+\pi^2}{\sqrt{q_2L^2+\pi^2(1+4\pi a^3)}}, \quad \frac{q_2L^2+\pi^2}{\sqrt{q_2L^2\left(1+\frac{4}{3}\pi a^3\right)+\pi^2\left(1-\frac{8}{3}\pi a^3\right)}}, \tag{5.116}$$

for an array of sphere. If we consider the left end of this two-pole curve, which is $(q_1L, q_2L, q_3L, kL) = (\pi, 0, 0, \pi)$, the dispersion relation (5.116) reduces to

$$kL = \frac{\pi}{\sqrt{1+4\pi a^3}}, \quad \frac{\pi}{\sqrt{1-8\pi a^3/3}}. \tag{5.117}$$

For the spheroid array, from (5.97) we can take the dipole coefficients matrix to be

$$\begin{pmatrix} m_{11} & 0 & 0 \\ 0 & m_{22} & 0 \\ 0 & 0 & m_{11} \end{pmatrix}. \tag{5.118}$$

Then the positive roots of (5.91) are

$$\begin{aligned} kL =& \frac{q_2L^2+\pi^2}{\sqrt{q_2L^2+\pi^2(1+8\pi m_{11}b_1^3)}}, \\ & \frac{q_2L^2+\pi^2}{\sqrt{q_2L^2\left[1-\frac{8}{3}\pi b_1^2(a_1-3m_{11}b_1)\right]+\pi^2\left(1-\frac{8}{3}\pi a_1 b_1^2\right)}}. \end{aligned} \tag{5.119}$$

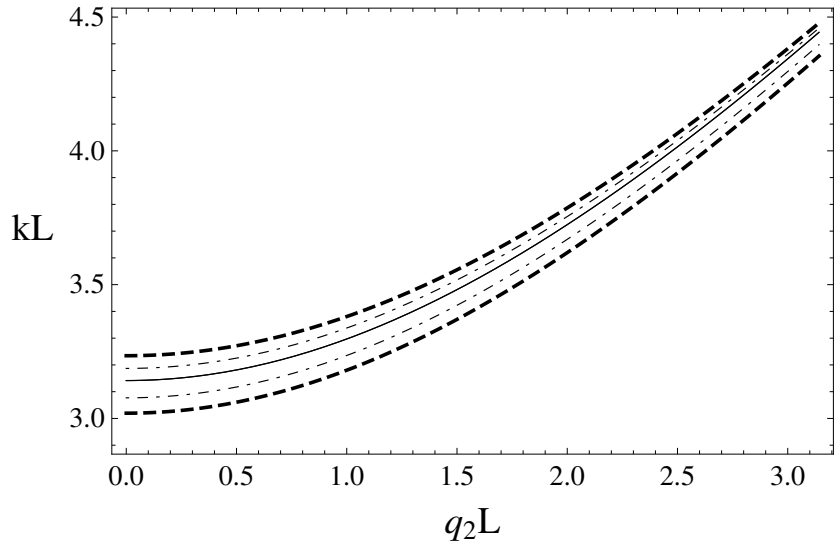

Figure 5.7: The comparison of the lowest two-pole mode along XM. Solid curve: no scatterers, dot-dashed curves: sphere, thick dashed curves: prolate spheroid.

When $a_1 = b_1 = a$, by the relations between the dipole matrix and added mass (5.97), (5.98) and (5.99), we obtain $m_{11} = m_{22} = 1/2$, then (5.119) reduces to (5.116). As with (5.117), at the left end of this two-pole curve (5.119) reduces to

$$kL = \frac{\pi}{\sqrt{1 + 8m_{11}\pi b_1^3}}, \quad \frac{\pi}{\sqrt{1 - 8\pi a_1 b_1^2/3}}. \tag{5.120}$$

Both of (5.117) and (5.120) show that a local band gap will appear as the scatterer size is increased from zero.

The comparison of the perturbation of the lowest two-pole mode along XM by sphere and prolate spheroid is shown in figure 5.7. The curves perturbed by the spheroid array are further apart than those perturbed by the sphere array, because the volume of the spheroid is larger than the sphere. The same phenomenon happens for some other two-pole mode perturbations, for example, the lowest two-pole mode on ΓM in simple cubic lattice and the lowest two-pole mode on PN in body-centred cubic lattice are considered next. For the lowest two-pole mode along ΓM in simple cubic lattice, where $q_3 L = 0$ and $q_1 L = q_2 L \in (0, \pi)$. The appropriate forms for β_m are

$$\beta_1 L = (q_1 L - 2\pi, q_2 L, q_3 L)^T, \quad \beta_2 L = (q_1 L, q_2 L - 2\pi, q_3 L)^T. \tag{5.121}$$

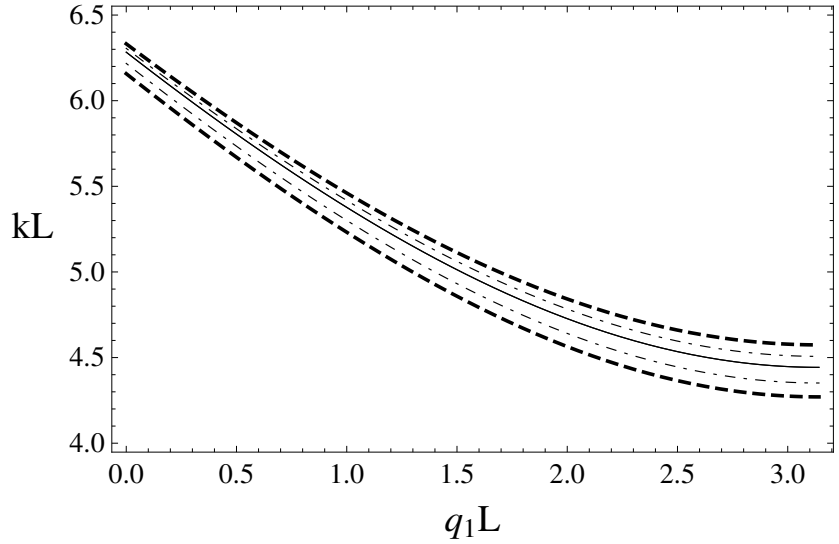

Figure 5.8: The comparison of the lowest two-pole mode along ΓM. Solid curve: no scatterers, dot-dashed curves: sphere, thick dashed curves: prolate spheroid.

The corresponding positive roots of (5.91) are

$$kL = \frac{\sqrt{2}(q_1L^2 - 2\pi q_1 L + 2\pi^2)}{\sqrt{q_1L^2 - 2\pi q_1 L + 2\pi^2(1 + 2\pi a^3)}},$$
$$\frac{\sqrt{2}(q_1L^2 - 2\pi q_1 L + 2\pi^2)}{\sqrt{\left(1 + \frac{4}{3}\pi a^3\right)(q_1L^2 - 2\pi q_1 L) + 2\pi^2\left(1 - \frac{2}{3}\pi a^3\right)}}, \tag{5.122}$$

for sphere array. For the prolate spheroid array, with the dipole coefficients matrix (5.118) we obtain the two positive roots of (5.91)

$$kL = \frac{\sqrt{2}(q_1L^2 - 2\pi q_1 L + 2\pi^2)}{\sqrt{q_1L^2 - 2\pi q_1 L + 2\pi^2(1 + 4m_{11}\pi b_1^3)}},$$
$$\frac{\sqrt{2}(q_1L^2 - 2\pi q_1 L + 2\pi^2)}{\sqrt{\left(1 - \frac{8}{3}\pi a_1 b_1^2 + 8m_{11}\pi b_1^3\right)(q_1L^2 - 2\pi q_1 L) + 2\pi^2\left[1 - \frac{4}{3}\pi b_1^2(2a_1 - 3m_{11}b_1)\right]}}. \tag{5.123}$$

When $a_1 = b_1 = a$, (5.123) reduces to (5.122). The comparison between the sphere array and the prolate spheroid array is shown in figure 5.8.

Lastly, for the body-centred cubic lattice, we consider the lowest two-pole mode on PN, where $q_1L = q_2L = \pi$ and q_3L is from 0 to π. The appropriate forms of β_m are

$$\beta_1 L = (q_1L, q_2L, q_3L)^T, \quad \beta_2 L = (q_1L - 2\pi, q_2L - 2\pi, q_3L)^T. \tag{5.124}$$

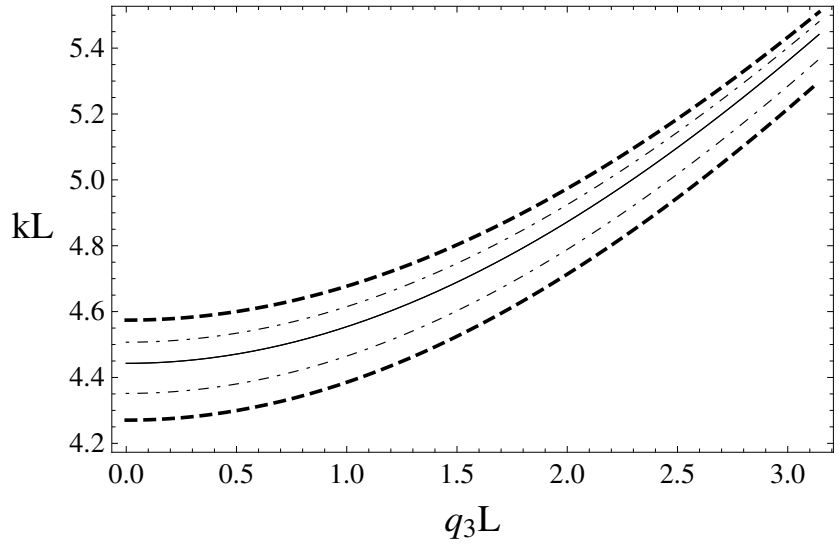

Figure 5.9: The comparison of the first two-pole mode along PN of the body-centred cubic lattice. Solid curve: no scatterers, dot-dashed curves: sphere, thick dashed curves: prolate spheroid.

The corresponding positive roots of (5.91) are

$$kL = \frac{q_3L^2 + 2\pi^2}{\sqrt{q_3L^2 + 2\pi^2(1 + 4\pi a^3)}}, \quad \frac{q_3L^2 + 2\pi^2}{\sqrt{q_3L^2\left(1 + \frac{4}{3}\pi a^3\right) + 2\pi^2\left(1 - \frac{8}{3}\pi a^3\right)}} \tag{5.125}$$

for the sphere array and

$$\begin{aligned} kL =& \frac{q_3L^2 + 2\pi^2}{\sqrt{q_3L^2 + 2\pi^2(1 + 8\pi m_{11}b_1^3)}}, \\ & \frac{q_3L^2 + 2\pi^2}{\sqrt{q_3L^2\left[1 - \frac{8}{3}\pi b_1^2(a_1 - 3m_{22}b_1)\right] + 2\pi^2\left(1 - \frac{8}{3}\pi a_1 b_1^2\right)}}, \end{aligned} \tag{5.126}$$

for the spheroid array. The comparison between the sphere array and the prolate spheroid array is shown in figure 5.9. From figure 5.8 and 5.9, the perturbed curves by spheroid array are further apart than those perturbed by the sphere array as the spheroid has bigger volume. In addition, in the perturbed mode expressions by spheroid (5.119), (5.123) and (5.126), the first perturbed modes are all independent of the spheroid equatorial axis a_1.

C. Perturbation of three plane waves

The three-pole modes curves only appear in the body-centred cubic lattice (in simple cubic lattice, there are isolated three-pole points crossed by a one-pole curve and a two-

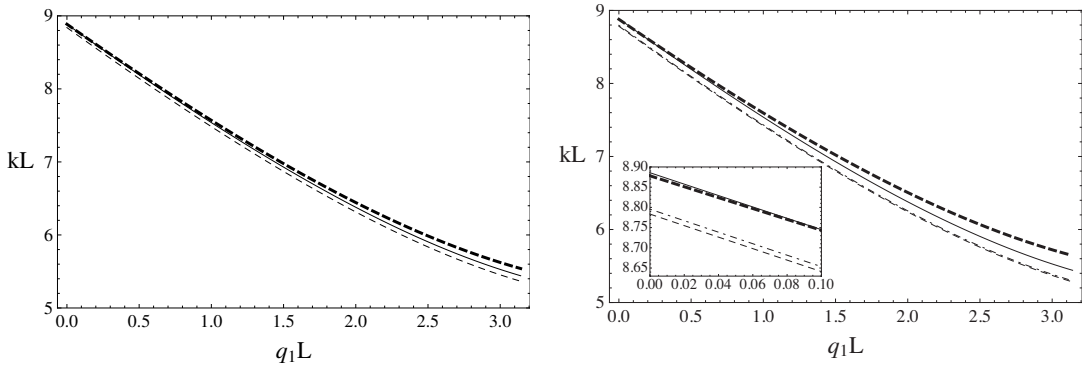

Figure 5.10: The perturbation of the first three-pole mode along ΓP of the body-centred cubic lattice. Dashed curve in left hand diagram: two equal perturbed modes. Solid curves: unperturbed mode. Left: sphere, right: prolate spheroid.

pole curve). It seems a three-pole mode should be perturbed into three different curves with the presence of the scatterer, but it is not always the case. For example, we consider the lowest three-pole mode on ΓP, where $q_1L = q_2L = q_3L \in (0, \pi)$. The appropriate forms for β_m are

$$\beta_1 L = (q_1 L - 2\pi, q_2 L - 2\pi, q_3 L)^T,$$
$$\beta_2 L = (q_1 L - 2\pi, q_2 L, q_3 L - 2\pi)^T,$$
$$\beta_3 L = (q_1 L, q_2 L - 2\pi, q_3 L - 2\pi)^T.$$

Because of the complexity of the structure of the body-centred cubic lattice, the explicit expressions for the perturbed modes are quite complicated, therefore we do not give them here. The results are shown in figure 5.10. For the sphere array, two of the three perturbed curves below the unperturbed curve are completely coincident and the third one is above the unperturbed curve. For the spheroid array, two of the three perturbed curves are quite close below the unperturbed curve which can be seen from the local diagram on the left corner, and the third perturbed mode is above the unperturbed curve.

D. Perturbations of four plane waves

Perturbations of a four-pole mode leads to similar results to three-pole modes described above; that is to say, some of the perturbed modes are exactly the same. But the difference is that coincident modes happen for both the sphere array and the spheroid array. For example, we consider the first four-pole mode on MR in the simple cubic lattice, where

$q_1L = q_2L = \pi$ and q_3L is from 0 to π. The appropriate forms for β_m are

$$\beta_1 L = (q_1L, q_2L, q_3L)^T, \quad \beta_2 L = (q_1L - 2\pi, q_2L, q_3L)^T,$$

$$\beta_3 L = (q_1L, q_2L - 2\pi, q_3L)^T, \quad \beta_4 L = (q_1L - 2\pi, q_2L - 2\pi, q_3L)^T.$$

Then the corresponding positive roots of (5.91) are

$$\begin{aligned} kL =& \sqrt{q_3L^2 + 2\pi^2}, \qquad \frac{q_3L + 2\pi^2}{\sqrt{q_3L^2 + 2\pi^2(1 + 4\pi a^3)}} \\ & \frac{q_3L + 2\pi^2}{\sqrt{q_3L^2 + 2\pi^2(1 + 4\pi a^3)}}, \quad \frac{q_3L + 2\pi^2}{\sqrt{q_3L^2\left(1 + \frac{8}{3}\pi a^3\right) + 2\pi^2\left(1 - \frac{16}{3}\pi a^3\right)}}, \end{aligned} \tag{5.127}$$

for sphere array. For spheroid array, the positive roots are

$$\begin{aligned} kL =& \sqrt{q_3L^2 + 2\pi^2}, \ \frac{q_3L + 2\pi^2}{\sqrt{q_3L^2 + 2\pi^2(1 + 8m_{11}\pi b_1^3)}}, \ \frac{q_3L + 2\pi^2}{\sqrt{q_3L^2 + 2\pi^2(1 + 8m_{11}\pi b_1^3)}} \\ & \frac{q_3L + 2\pi^2}{\sqrt{q_3L^2\left[1 - \frac{16}{3}\pi b_1^2(a_1 - 3m_{22}b_1)\right] + 2\pi^2\left(1 - \frac{16}{3}\pi a_1 b_1^2\right)}}. \end{aligned} \tag{5.128}$$

When $a_1 = b_1 = a$, (5.128) reduces to (5.127). We can see in these four modes, two of them are exactly the same and one is equal to the unperturbed mode. Therefore there are only three disparate curves as shown in figure 5.11.

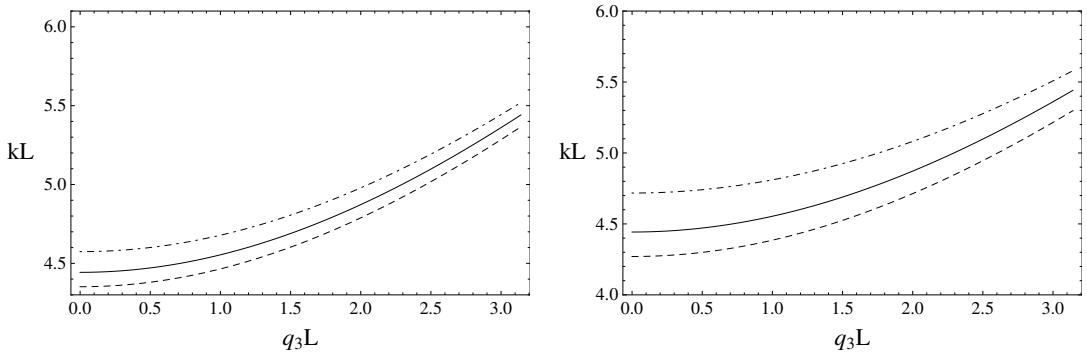

Figure 5.11: The perturbation of the first four-pole mode along MR for the simple cubic lattice. Dashed curves: two equal perturbed modes, solid curves: unperturbed mode and one perturbed mode, dot-dashed curves: the fourth perturbed mode. Left: sphere, right: prolate spheroid.

Chapter 6

Three-dimensional multiple resonant scattering

In this chapter, we consider the acoustic wave scattering by a strip of arrays of spheres or arbitrary shape scatterers using the methods of matched asymptotic expansions and multiple scales. We first consider the case of arrays of spheres, then generalise it to arbitrary shape scatterers, where the Green's identity must be used twice in order to obtain the integral on the scatterer. Finally, numerical results for the transmission wave intensity are given to make comparisons for different shapes of scatterers.

The three-dimensional problem of multiple scattering by doubly periodic planar arrays of bounded obstacles was first considered by Twersky [93, 94, 95], which followed his earlier work about the acoustic scattering by an infinite linear array of identical obstacles [92]. Twersky obtained approximate solutions for small scatterers or low frequencies but didn't give any numerical results. Achenbach and Kitahara [2] used the boundary integral equation method to consider the elastic wave scattering by a layer of doubly periodic array of spherical cavities in an infinite elastic solid. The same method is then used to obtain the dispersion relation for the propagation of harmonic waves in an elastic solid containing a three-dimensional array of regularly spaced spherical cavities [3], which adopted the results in their earlier work [2]. The elastic wave scattering by periodic structures of spherical objects was also considered using the multiple scattering theory (or KKR approach) by taking into account the full vector character [54]. Before this, the multiple scattering theory has been developed for three-dimensional electromagnetic

wave scattering to calculate the band structure of photonic crystals [99]. A layer multiple scattering theory of electromagnetic waves was also successfully implemented [63, 85] to calculate the transmission and reflection coefficients for a slab of periodically arranged spheres. Thompson and Linton [87] considered the guided acoustic wave propagating along one- and two-dimensional arrays of rigid spheres to study the existence of the surface modes numerically.

As in the two-dimensional case, we first derive the envelope equations in infinite three-dimensional arrays and then apply them to a strip of arrays of scatterers. The strip is assumed to be finite in one direction and infinite in other directions. As the scattered wave from one scatterer is of higher order of the small parameter compared with the incident wave and the scattered wave would not be weak any more over a large number of cylinders, the strip width must be large enough to make the resonance occur. This makes it possible to consider this problem in an infinite array first and then apply the results to approximate those in finite arrays. The size of the scatterer is still assumed to be smaller than both the wavelength and the array periodicity. Both matched asymptotic expansions and multiple scales are used to obtained the envelope equations. Numerical results are given to compare the transmission wave intensity for different shapes of scatterers.

6.1 Sphere

We consider the diffraction of plane acoustic waves by an infinite three-dimensional array of spheres. The global Cartesian coordinates (x, y, z) is used with origin O at the centre of one of the spheres. Similarly with the two-dimensional case, we assume the Bloch wave vector be $\boldsymbol{\beta}_1$ (the incident wavenumber), another wave in the direction of $\boldsymbol{\beta}_m$ is said to be resonantly scattered if $\boldsymbol{\beta}_m$ and $\boldsymbol{\beta}_1$ are related to a reciprocal lattice vector $\mathbf{K}_m$ by the Bragg condition

$$\boldsymbol{\beta}_m = \boldsymbol{\beta}_1 + \mathbf{K}_m, \tag{6.1}$$

where $\beta_m = |\boldsymbol{\beta}_m|$ is all the same for any m and we define $\beta = |\boldsymbol{\beta}_m|$. If more than one wave is resonantly scattered, any two resonated wave vectors are related by

$$\boldsymbol{\beta}_n = \boldsymbol{\beta}_m + \mathbf{K}_n - \mathbf{K}_m. \tag{6.2}$$

If the array is infinite, the solution is require to satisfy the Bloch theorem

$$\Phi(\mathbf{r}+\mathbf{R}_j) = \mathrm{e}^{\mathrm{i}\boldsymbol{\beta}_m^T\mathbf{R}_j}\Phi(\mathbf{r}), \tag{6.3}$$

where $\mathbf{r} = (x, y, z)^T$ and $\mathbf{R}_j$ is the jth lattice point given by (5.35). Let $(r_j, \theta_j, \varphi_j)$ be defined as the local spherical coordinate centred at lattice node j. The global spherical coordinates with the global origin at O are denoted by (r, θ, φ) Then the position of any point in space is

$$\mathbf{r} = \mathbf{R}_j + \mathbf{r}_j. \tag{6.4}$$

For a given lattice and scattering configuration found by Ewald construction described in chapter 4, we shall derive the equations coupling the envelopes of the incident and $M-1$ resonantly scattered waves.

First of all, the velocity potential Φ must satisfy the wave equation

$$\frac{\partial^2\Phi}{\partial t^2} - c^2\nabla^2\Phi = 0, \tag{6.5}$$

everywhere in the medium, where ∇ is the gradient operator. On the boundary of the spheres, the normal flux must vanish

$$\frac{\partial\Phi}{\partial r_j} = 0,\ r_j = |\mathbf{r}-\mathbf{R}_j| = a,\ \text{for all } j. \tag{6.6}$$

We now add the assumption that the sphere radius a is much smaller than the typical wave length $2\pi/\beta$ so that

$$\epsilon_1 = \beta a \ll 1. \tag{6.7}$$

From section 5.1, the field scattered from a single sphere is order ϵ_1^3 compared to the incident wave, then the accumulated effects over N spheres becomes of order one when N is order $1/\epsilon_1^3$, i.e. over the distance of order $1/\beta\epsilon_1^3$. It then follows that strong reflection evolves over the dimensionless length scale $\beta(x, y, z)$ of order $1/\epsilon_1^3$. This suggests the asymptotic method of multiple scales is applicable. For the outer field we introduce fast and slow variables

$$x,\ y,\ z,\ t;\ X = \epsilon_1^3 x,\ Y = \epsilon_1^3 y,\ Z = \epsilon_1^3 z,\ T = \epsilon_1^3 t, \tag{6.8}$$

so that $x,\ y,\ z,\ t$ describe the fast motion characterised by the length and time scales of $1/\beta,\ 1/\omega$, while $X,\ Y,\ Z,\ T$ describe the slow variation of the envelope. To use the

method of matched asymptotic expansions, each lattice cell is divided into two overlapping regions, an outer region at distances $r_j \gg a$ and an inner region within distances $r_j \ll \beta^{-1}$. In the inner region a scaled coordinate $\rho = r_j/a$ is used. As the boundary-value problem is homogeneous, the leading order outer solution may be taken as strictly order one in ϵ_1, then we expand the outer solution as follows

$$\Phi = Re\{[\Phi_0 + \epsilon_1^3 \Phi_3 + O(\epsilon_1^6)]\mathrm{e}^{-\mathrm{i}\omega t}\}, \tag{6.9}$$

where Φ_0 and Φ_3 are functions of (x, y, z, X, Y, Z, T) and ω is the frequency associated with β (i.e. $\omega = \beta c$). Substituting (6.9) into the wave equation (6.5) and collecting like terms of order one and order ϵ_1^3, we obtain the perturbation equations for the outer potentials Φ_0 and Φ_3. At the first order, the outer velocity potential Φ_0 is governed by

$$\nabla^2 \Phi_0 = -\frac{\omega^2}{c^2}\Phi_0, \tag{6.10}$$

and also satisfy the Bloch theorem (6.3) on the short scale. The first order solution is formally the sum of all mutually resonant progressive waves

$$\Phi_0 = \sum_{m=1}^{M} A_m(X, Y, Z, T)\psi_m(x, y, z), \tag{6.11}$$

$$\Phi_0(\mathbf{r} + \mathbf{R}_j) = \mathrm{e}^{\mathrm{i}\boldsymbol{\beta}_m^T \mathbf{R}_j}\Phi_0(\mathbf{r}),\ m = 1, 2, \ldots, M, \tag{6.12}$$

where

$$\psi_m(x, y, z) = \mathrm{e}^{\mathrm{i}\boldsymbol{\beta}_m^T \mathbf{r}} = 4\pi \sum_{\nu=0}^{\infty} \mathrm{i}^\nu j_\nu(\beta r) \sum_{\mu=-\nu}^{\nu} Y_\nu^\mu(\hat{\mathbf{r}}) Y_\nu^\mu(\hat{\boldsymbol{\beta}}_m)^*. \tag{6.13}$$

For the second order outer solution Φ_3

$$\nabla^2 \Phi_3 + \frac{\omega^2}{c^2}\Phi_3 = -2\overline{\nabla} \cdot \nabla\Phi_0 - \frac{2\mathrm{i}\omega}{c^2}\frac{\partial \Phi_0}{\partial T}, \tag{6.14}$$

$$\Phi_3(\mathbf{r} + \mathbf{R}_j) = \mathrm{e}^{\mathrm{i}\boldsymbol{\beta}_m^T \mathbf{R}_j}\Phi_3(\mathbf{r}),\ m = 1,\ 2,\ \ldots, M. \tag{6.15}$$

In (6.14), $\overline{\nabla}$ denotes the gradient operator with respect to the slow variables X, Y and Z.

From the solution form of the leading order problem (6.11) and (6.13), the inner

expansion of the leading-order outer solution is

$$\Phi_0^{(0,1)} = \sum_{h=1}^{M} A_h 4\pi \left\{ j_0(kr) Y_0^0(\hat{\mathbf{r}}) Y_0^0(\hat{\boldsymbol{\beta}}_h)^* + \mathrm{i} j_1(\beta r) \sum_{\mu=-1}^{1} Y_1^\mu(\hat{\mathbf{r}}) Y_1^\mu(\hat{\boldsymbol{\beta}}_h)^* \right\}$$
$$= \sum_{h=1}^{M} A_h \left\{ 1 + \frac{4\pi}{3} \mathrm{i}\epsilon\rho \sum_{\mu=-1}^{1} Y_1^\mu(\hat{\mathbf{r}}) Y_1^\mu(\hat{\boldsymbol{\beta}}_h)^* \right\} \tag{6.16}$$

Therefore, to match with the outer solution Φ_0, the inner solution ϕ has the form (suggested by results in chapter 5)

$$\phi^{(1)} = B_0 + \epsilon_1 \left[B_1 + \left(2\rho + \frac{1}{\rho^2} \right) (u_1^{-1}, u_1^0, u_1^1) \begin{pmatrix} Y_1^{-1}(\hat{\mathbf{r}}) \\ Y_1^0(\hat{\mathbf{r}}) \\ Y_1^1(\hat{\mathbf{r}}) \end{pmatrix} \right], \tag{6.17}$$

where $\rho = r_j/a$ is the inner coordinate.

For each $m = 1, \ldots, M$, we are going to apply Green's identity to ψ_m^* and the solution in one cell C excluding the sphere S: C_s, where ψ_m^* denotes the complex conjugate of the plane waves ψ_m defined in (6.13). The solution in this cell is expressed as a composite expansion that is valid everywhere in the cell. As we know, the inner solution is only valid in the immediate vicinity of the scatterer and the outer solution is only valid in the outer region far from each scatterer. To find a solution that is valid everywhere in the whole region, we need to do some work to the inner and outer solutions. One of the methods may be called additive composition. Since the inner expansion and the outer expansion have a common region of validity, the composite expansion can be constructed by subtracting the part they are in common, so that it is not counted twice [102, page 94]. We denote the composite expansion by ξ and take

$$\xi = \Phi^{(3)} + \phi^{(1)} - \phi^{(1,3)}. \tag{6.18}$$

Then the Green's identity is now used for ξ and ψ_m^* on C_s

$$\iiint_{C_s} \left(\xi \nabla^2 \psi_m^* - \psi_m^* \nabla^2 \xi \right) dv = \iint_{\partial C_s} \left(\xi \frac{\partial \psi_m^*}{\partial n} - \psi_m^* \frac{\partial \xi}{\partial n} \right) ds, \tag{6.19}$$

Then omitting the higher order term and noting that every $\psi_m^*,\ m = 1, \ldots, M$ satisfies the Helmholtz equation and $\phi^{(1)} - \phi^{(1,3)} = 0$ by the inner solution (6.17), the left hand side of Green's identity becomes

$$LHS(6.19) = \iiint_{C_s} \left(\Phi^{(3)} \nabla^2 \psi_m^* - \psi_m^* \nabla^2 \Phi^{(3)} \right) dv.$$

Using the governing equations for the first and second order outer solutions (6.10) and (6.14) and dropping terms of order higher than ϵ_1^3

$$\begin{aligned}
LHS(6.19) &= \iiint_{C_s} \left(\Phi_0 \nabla^2 \psi_m^* - \psi_m^* \nabla^2 \Phi_0\right) dv + \epsilon_1^3 \iiint_{C_s} \left(\Phi_3 \nabla^2 \psi_m^* - \psi_m^* \nabla^2 \Phi_3\right) dv \\
&= \iiint_{C_s} \left[\Phi_0(-\beta^2 \psi_m^*) - \psi_m^* \left(-\frac{\omega^2}{c^2}\Phi_0\right)\right] dv \\
&+ \epsilon_1^3 \iiint_{C_s} \left[-\Phi_3 \beta^2 \psi_m^* - \psi_m^*(-2\overline{\nabla} \cdot \nabla \Phi_0 - \frac{\omega^2}{c^2}\Phi_3 - \frac{2\mathrm{i}\omega}{c^2}\frac{\partial \Phi_0}{\partial T})\right] dv \\
&= \epsilon_1^3 \iiint_{C_s} \left(2\psi_m^* \overline{\nabla} \cdot \nabla \Phi_0 + \frac{2\mathrm{i}\omega}{c^2}\psi_m^* \frac{\partial \Phi_0}{\partial T}\right) dv \\
&= \epsilon_1^3 \left(2\mathrm{i} \sum_{h=1}^{M} \overline{\nabla} A_h \cdot \boldsymbol{\beta}_h + \frac{2\mathrm{i}\omega}{c^2} \sum_{h=1}^{M} \frac{\partial A_h}{\partial T}\right) \iiint_{C_s} \mathrm{e}^{\mathrm{i}(\boldsymbol{\beta}_h - \boldsymbol{\beta}_m)^T \mathbf{r}} dv \\
&= \epsilon_1^3 \sum_{h=1}^{M} \left(\frac{2\mathrm{i}\omega}{c^2}\frac{\partial A_h}{\partial T} + 2\mathrm{i}\overline{\nabla} A_h \cdot \boldsymbol{\beta}_h\right) \iiint_{C_s} \mathrm{e}^{\mathrm{i}(\boldsymbol{\beta}_h - \boldsymbol{\beta}_m)^T \mathbf{r}} dv. \qquad (6.20)
\end{aligned}$$

The volume of a sphere V_s is much smaller than that of one cell V_c, therefore the volume of the cell C excluding the sphere S is: $V_{cs} = V_c - 4\pi a^3/3 = V_c[1 + O(\epsilon_1^3)] \approx V_c$. Therefore the integral in (6.20) can be approximated by

$$\begin{aligned}
\iiint_{C_s} \mathrm{e}^{\mathrm{i}(\boldsymbol{\beta}_h - \boldsymbol{\beta}_m)^T \mathbf{r}} dv &= \iiint_{V_c} \mathrm{e}^{\mathrm{i}(\boldsymbol{\beta}_h - \boldsymbol{\beta}_m)^T \mathbf{r}} dv + O(\epsilon_1^3) V_c \\
&= \delta_{hm} V_c + O(\epsilon_1^3) V_c. \qquad (6.21)
\end{aligned}$$

Substituting (6.21) into (6.20) and dropping terms of order higher than ϵ_1^3, we get

$$LHS(6.19) = \epsilon_1^3 \frac{2\mathrm{i}\omega}{c^2} V_c \left(\frac{\partial A_m}{\partial T} + \frac{c^2}{\omega}\overline{\nabla} A_m \cdot \boldsymbol{\beta}_m\right). \qquad (6.22)$$

On the sphere $r_j = a$, we have

$$\psi_m^*|_{r_j=a} = \mathrm{e}^{\mathrm{i}\boldsymbol{\beta}_m^T \mathbf{r}}|_{r=a} = \mathrm{e}^{-\mathrm{i}\boldsymbol{\beta}_m^T \mathbf{R}_j} \mathrm{e}^{-\mathrm{i}\beta a \cos\alpha}, \qquad (6.23)$$

$$\left.\frac{\partial \psi_m^*}{\partial r}\right|_{r_j=a} = -\mathrm{i}\beta \cos\alpha \ \mathrm{e}^{-\mathrm{i}\boldsymbol{\beta}_m^T \mathbf{R}_j} \mathrm{e}^{-\mathrm{i}\beta a \cos\alpha}, \qquad (6.24)$$

where $\cos\alpha = \sin\tau_m \sin\theta \cos(\gamma_m - \varphi) + \cos\tau_m \cos\theta$. Therefore, noting that the normal flux on the sphere vanishes and the contribution from the outer boundaries of the primary

cell vanishes by the Bloch theorem

$$
\begin{aligned}
&RHS(6.19)\\
&= \iint_{\partial S} \left(\phi^{(1)} \frac{\partial \psi_m^*}{\partial n} - \psi_m^* \frac{\partial \phi^{(1)}}{\partial n} \right) ds \\
&= - \iint_{\partial S} \phi^{(1)} \frac{\partial \psi_m^*}{\partial r} ds \\
&= - \int_0^{2\pi} \int_0^{\pi} \phi^{(1)} \frac{\partial \psi_m^*}{\partial r} a^2 \sin\theta d\theta d\varphi \\
&= - \int_0^{2\pi} \int_0^{\pi} \left\{ B_0 + \epsilon_1 \left[B_1 + \left(2\rho + \frac{1}{\rho^2} \right) (u_1^{-1}, u_1^0, u_1^1) \begin{pmatrix} Y_1^{-1}(\hat{\mathbf{r}}) \\ Y_1^0(\hat{\mathbf{r}}) \\ Y_1^1(\hat{\mathbf{r}}) \end{pmatrix} \right] \right\} \\
&\qquad\qquad \mathrm{e}^{-\mathrm{i}\boldsymbol{\beta}_m^T \mathbf{R}_j} \Big[-\mathrm{i}\beta\cos\alpha \Big] \Big[1 - \mathrm{i}\epsilon_1 \cos\alpha + 1 + \frac{1}{2}\mathrm{i}^2 \epsilon_1^2 \cos^2\alpha + O(\epsilon_1^3) \Big] a^2 \sin\theta d\theta d\varphi \\
&= -\epsilon_1^3 \mathrm{e}^{-\mathrm{i}\boldsymbol{\beta}_m^T \mathbf{R}_j} \left[-\frac{4\pi}{3\beta} B_0 - \frac{4\pi\mathrm{i}}{\beta} (u_1^{-1}, u_1^0, u_1^1) \begin{pmatrix} Y_1^{-1}(\hat{\boldsymbol{\beta}}_m) \\ Y_1^0(\hat{\boldsymbol{\beta}}_m) \\ Y_1^1(\hat{\boldsymbol{\beta}}_m) \end{pmatrix} \right] + O(\epsilon_1^4). \qquad (6.25)
\end{aligned}
$$

To get B_0 and $\mathbf{u}_1 = (u_1^{-1}, u_1^0, u_1^1)$, we need to do the matching between the inner solution (6.17) and the outer solution (6.16). By the matching rule $\Phi^{(0,1)} \equiv \phi^{(1,0)}$, we have

$$
B_0 = \sum_{h=1}^{M} A_h \mathrm{e}^{\mathrm{i}\boldsymbol{\beta}_h^T \mathbf{R}_j}, \qquad (6.26)
$$

$$
(u_1^{-1}, u_1^0, u_1^1) = \mathrm{i} \sum_{h=1}^{M} A_h \mathrm{e}^{\mathrm{i}\boldsymbol{\beta}_h^T \mathbf{R}_j} \frac{2\pi}{3} \mathrm{i} \left(Y_1^{-1}(\hat{\boldsymbol{\beta}}_h)^*, Y_1^0(\hat{\boldsymbol{\beta}}_h)^*, Y_1^1(\hat{\boldsymbol{\beta}}_h)^* \right). \qquad (6.27)
$$

Therefore

$$RHS(6.19) = -\epsilon_1^3 \mathrm{e}^{-\mathrm{i}\boldsymbol{\beta}_m^T \mathbf{R}_j} \sum_{h=1}^{M} A_h \mathrm{e}^{\mathrm{i}\boldsymbol{\beta}_h^T \mathbf{R}_j} \times \left[-\frac{4\pi}{3\beta} + \frac{8\pi^2}{3\beta} \left(Y_1^{-1}(\hat{\boldsymbol{\beta}}_h)^*, Y_1^0(\hat{\boldsymbol{\beta}}_h)^*, Y_1^1(\hat{\boldsymbol{\beta}}_h)^* \right) \begin{pmatrix} Y_1^{-1}(\hat{\boldsymbol{\beta}}_m) \\ Y_1^0(\hat{\boldsymbol{\beta}}_m) \\ Y_1^1(\hat{\boldsymbol{\beta}}_m) \end{pmatrix} \right]$$

$$= -\epsilon_1^3 \sum_{h=1}^{M} A_h \frac{4\pi}{\beta} \left[-\frac{1}{3} + \frac{2\pi}{3} \left(Y_1^{-1}(\hat{\boldsymbol{\beta}}_h)^*, Y_1^0(\hat{\boldsymbol{\beta}}_h)^*, Y_1^1(\hat{\boldsymbol{\beta}}_h)^* \right) \begin{pmatrix} Y_1^{-1}(\hat{\boldsymbol{\beta}}_m) \\ Y_1^0(\hat{\boldsymbol{\beta}}_m) \\ Y_1^1(\hat{\boldsymbol{\beta}}_m) \end{pmatrix} \right] \tag{6.28}$$

Then, by the results of left hand side (6.22) and right hand side (6.28), we obtain

$$\frac{\partial A_m}{\partial T} + \mathbf{C}_g^{(m)} \cdot \overline{\nabla} A_m = \frac{1}{2} \mathrm{i}\Omega_0 \sum_{h=1}^{M} A_h \left[-\frac{1}{3} + \frac{2\pi}{3} \left(Y_1^{-1}(\hat{\boldsymbol{\beta}}_h)^*, Y_1^0(\hat{\boldsymbol{\beta}}_h)^*, Y_1^1(\hat{\boldsymbol{\beta}}_h)^* \right) \begin{pmatrix} Y_1^{-1}(\hat{\boldsymbol{\beta}}_m) \\ Y_1^0(\hat{\boldsymbol{\beta}}_m) \\ Y_1^1(\hat{\boldsymbol{\beta}}_m) \end{pmatrix} \right], \tag{6.29}$$

where $m = 1, \ldots, M$ and

$$\mathbf{C}_g^{(m)} = \frac{c^2 \boldsymbol{\beta}_m}{\omega} = \frac{c\boldsymbol{\beta}_m}{\beta}, \quad \Omega_0 = \frac{4\pi c}{\beta^2 V_c}. \tag{6.30}$$

Outside the strip, the envelope equations reduce to

$$\frac{\partial A_m}{\partial T} + \mathbf{C}_g^{(m)} \cdot \overline{\nabla} A_m = 0, \ m = 1, \ldots, M. \tag{6.31}$$

Let us multiply both sides of equation (6.29) by A_m^* and adding the resulting equation with its complex conjugate. After summation over m, we obtain

$$\sum_{m=1}^{M} \left(\frac{\partial |A_m|^2}{\partial T} + \mathbf{C}_g^{(m)} \cdot \overline{\nabla} |A_m|^2 \right) = \frac{\Omega_0}{2} \sum_{m=1}^{M} \sum_{h=1}^{M} \left[-\frac{1}{3} + \frac{2\pi}{3} \left(Y_1^{-1}(\hat{\boldsymbol{\beta}}_h)^*, Y_1^0(\hat{\boldsymbol{\beta}}_h)^*, Y_1^1(\hat{\boldsymbol{\beta}}_h)^* \right) \begin{pmatrix} Y_1^{-1}(\hat{\boldsymbol{\beta}}_m) \\ Y_1^0(\hat{\boldsymbol{\beta}}_m) \\ Y_1^1(\hat{\boldsymbol{\beta}}_m) \end{pmatrix} \right] (\mathrm{i}A_h A_m^* - \mathrm{i}A_h^* A_m). \tag{6.32}$$

By changing the second term in the last parentheses on the right from $A_h^* A_m$ to $A_m^* A_h$, the double series is unaltered, hence must be zero, yielding

$$\frac{\partial}{\partial T}\sum_{m=1}^{M}|A_m|^2+\sum_{m=1}^{M}(\mathbf{C}_g^{(m)}\cdot\overline{\nabla}|A_m|^2)=0. \tag{6.33}$$

Thus the total energy is conserved in the array.

6.2 Arbitrary shape scatterers

6.2.1 Formulation

When the scatterers are of arbitrary shape, it is difficult to perform the integration over the scatterer when using Green's identity to obtain the envelope equations. To overcome this, we will use Green's identity again in the inner region. By the results of infinite array (5.77) and (5.80), the form of the inner solution is

$$\begin{aligned}\phi^{(2)} =&B_0+\nu_{11}(\epsilon_1)B_{11}+\epsilon_1\left\{B_1+(u_1^{-1},u_1^0,u_1^1)\left[\rho\begin{pmatrix}Y_1^{-1}(\hat{\mathbf{r}})\\Y_1^0(\hat{\mathbf{r}})\\Y_1^1(\hat{\mathbf{r}})\end{pmatrix}+\chi_1(\hat{\mathbf{r}})\right]\right\}\\&+\epsilon_1\left\{\nu_{11}(\epsilon_1)(u_{11}^{-1},u_{11}^0,u_{11}^1)\left[\rho\begin{pmatrix}Y_1^{-1}(\hat{\mathbf{r}})\\Y_1^0(\hat{\mathbf{r}})\\Y_1^1(\hat{\mathbf{r}})\end{pmatrix}+\chi_1(\hat{\mathbf{r}})\right]\right\}+\mu_{21}(\epsilon_1)B_{21}\\&+\epsilon_1^2\left\{B_0\left[-\frac{1}{6}\rho^2+\Gamma(\rho,\theta,\varphi)\right]+B_2+(u_2^{-1},u_2^0,u_2^1)\left[\rho\begin{pmatrix}Y_1^{-1}(\hat{\mathbf{r}})\\Y_1^0(\hat{\mathbf{r}})\\Y_1^1(\hat{\mathbf{r}})\end{pmatrix}+\chi_1(\hat{\mathbf{r}})\right]\right.\\&\left.+(v_2^{-2},v_2^{-1},v_2^0,v_2^1,v_2^2)\left[\rho^2\begin{pmatrix}Y_2^{-2}(\hat{\mathbf{r}})\\Y_2^{-1}(\hat{\mathbf{r}})\\Y_2^0(\hat{\mathbf{r}})\\Y_2^1(\hat{\mathbf{r}})\\Y_2^2(\hat{\mathbf{r}})\end{pmatrix}+\chi_2(\hat{\mathbf{r}})\right]+\cdots\right\}\end{aligned} \tag{6.34}$$

where Γ is a harmonic function introduced to compensate for the flux across the scatterer S that is induced by the term involving $1/6$, and $\chi_2(\hat{\mathbf{r}})=o(1)$ as $\rho\to\infty$. As with the

two-dimensional case, the ellipsis denotes those eigenfunctions that will be needed to match with the extra terms in the outer solution Φ_3 that arise from the right hand side of (6.14). By (5.85),

$$\Gamma(\rho,\theta,\varphi)+\frac{V_s}{4\pi a^3}\frac{1}{\rho}\to 0,\ \text{as } \rho\to\infty, \tag{6.35}$$

and by the definition of the dipole matrix (5.68)

$$\chi_1-\frac{\mathbf{M}}{\rho^2}\begin{pmatrix}Y_1^{-1}(\hat{\mathbf{r}})\\ Y_1^0(\hat{\mathbf{r}})\\ Y_1^1(\hat{\mathbf{r}})\end{pmatrix}=o(\rho^{-2})\ \text{ as }\ \rho\to\infty, \tag{6.36}$$

where $\mathbf{M}$ is the dipole matrix determined by the shape of the scatter [8, page 121].

Similar to the case of spheres, Green's identity is going to be used in the cell C excluding the scatterer S, C_s, to obtain the envelope equations. We first define the composite solution ξ (here the inner solution up to order ϵ_1^2 is needed) in a cell

$$\xi=\Phi^{(3)}+\phi^{(2)}-\phi^{(2,3)}. \tag{6.37}$$

Then by the inner solution up to order ϵ_1^2 in the previous chapter (5.77), (5.80) and (5.86), we have

$$\phi^{(2)}-\phi^{(2,3)}=\epsilon_1^2\left[\frac{1}{\rho^2}(u_2^{-1},u_2^0,u_2^1)\begin{pmatrix}Y_1^{-1}(\hat{\mathbf{r}})\\ Y_1^0(\hat{\mathbf{r}})\\ Y_1^1(\hat{\mathbf{r}})\end{pmatrix}+\frac{1}{\rho^3}\sum_{\mu=-2}^{2}v_2^\mu Y_2^\mu(\hat{\mathbf{r}})\right]. \tag{6.38}$$

Now apply Green's identity to the conjugate of the plane waves ψ_m^* and the composite solution ξ in the entire cell excluding the scatterer C_s

$$\iiint_{C_s}(\xi\nabla^2\psi_m^*-\psi_m^*\nabla^2\xi)dv=\iint_{\partial C_s}\left(\xi\frac{\partial\psi_m^*}{\partial n}-\psi_m^*\frac{\partial\xi}{\partial n}\right)ds, \tag{6.39}$$

where the integration on the right hand side includes the integration over the scatterer and the integration over the outer boundaries of the primary cell which vanishes by the Bloch condition; thus Green's identity becomes

$$\iiint_{C_s}(\xi\nabla^2\psi_m^*-\psi_m^*\nabla^2\xi)dv=\iint_{\partial S}\left(\phi^{(2)}\frac{\partial\psi_m^*}{\partial n}-\psi_m^*\frac{\partial\phi^{(2)}}{\partial n}\right)ds. \tag{6.40}$$

Because the scatterer is now arbitrary shape, it is difficult to obtain the integration on the scatterer directly. What we can do is to use Green's identity to ψ_m^* and the inner

solution ϕ in the inner region C_ρ to get an approximation by the integration on the outer 'boundary' of the inner region. We denote the outer 'boundary' of the inner region by a sphere surface ∂S^* centred within the scatterer in the cell C as $\rho \to \infty$. Before using Green's identity, we expand ψ_m^*,

$$\begin{aligned}\psi_m^* &= \mathrm{e}^{-\mathrm{i}\boldsymbol{\beta}_m^T\cdot\mathbf{r}} \\ &= 1 - \mathrm{i}\epsilon_1\rho\cos\alpha - \frac{1}{2}\epsilon_1^2\rho^2\cos^2\alpha + \frac{1}{6}\mathrm{i}\epsilon_1^3\rho^3\cos^3\alpha + \frac{1}{12}\epsilon_1^4\rho^4\cos^4\alpha + O(\epsilon_1^5) \\ &:= \hat{\psi}_m^* + O(\epsilon_1^5). \end{aligned} \tag{6.41}$$

That's because the expansion of ψ_m^* is only valid when ρ is strictly order one, i.e. near the scatterer, so we cannot use this expansion in Green's identity which involves the whole inner region including $\rho \to \infty$. This expansion makes the omitted terms higher order. Then we have

$$\begin{aligned}\nabla^2\hat{\psi}_m^* &= \nabla^2\left[1 - \mathrm{i}\epsilon_1\rho\cos\alpha - \frac{1}{2}\epsilon_1^2\rho^2\cos^2\alpha + \frac{1}{6}\mathrm{i}\epsilon_1^3\rho^3\cos^3\alpha + \frac{1}{12}\epsilon_1^4\rho^4\cos^4\alpha\right] \\ &= -\epsilon_1^2 + \mathrm{i}\epsilon_1^3\rho\cos\alpha + \epsilon^4\rho^2\cos^2\alpha. \end{aligned} \tag{6.42}$$

Now we apply Green's identity to the truncated function $\hat{\psi}_m^*$ and the inner solution up to order ϵ_1^2 over the inner region C_ρ

$$\iiint_{C_\rho}(\phi^{(2)}\nabla^2\hat{\psi}_m^* - \hat{\psi}_m^*\nabla^2\phi^{(2))})dv = \iint_{\partial C_\rho}\left(\phi^{(2)}\frac{\partial\hat{\psi}_m^*}{\partial n} - \hat{\psi}_m^*\frac{\partial\phi^{(2)}}{\partial n}\right)ds, \tag{6.43}$$

where the boundary of the inner region including the surface of the scatterer and the outer boundary ∂S^*

$$\partial C_\rho = \partial S + \partial S^*.$$

In the inner coordinates, the Helmholtz equation becomes

$$\nabla_\rho^2\phi + \epsilon_1^2\phi = 0. \tag{6.44}$$

The inner solution takes the form

$$\phi = \phi_0 + \epsilon_1\phi_1 + \epsilon_1^2\phi_2 + O(\epsilon^3) \tag{6.45}$$

then substituting for (6.45) in (6.44) and collecting the like power terms we obtain

$$\nabla_\rho^2\phi_0 = 0, \quad \nabla_\rho^2\phi_1 = 0, \quad \nabla_\rho^2\phi_2 = -\phi_0, \tag{6.46}$$

Therefore

$$
\begin{aligned}
&LHS(6.43)\\
&= \iiint_{C_\rho} \Big\{ \big(\phi_0 + \epsilon_1\phi_1 + \epsilon_1^2\phi_2\big)\big(-\epsilon_1^2 + \mathrm{i}\epsilon_1^3\rho\cos\alpha + \epsilon_1^4\rho^2\cos^2\alpha\big)\\
&\qquad - \big(1 - \mathrm{i}\epsilon_1\rho\cos\alpha - \frac{1}{2}\epsilon_1^2\rho^2\cos^2\alpha + \frac{1}{6}\mathrm{i}\epsilon_1^3\rho^3\cos^3\alpha\big)(-\epsilon_1^2)\\
&\qquad \big(\phi_0 + \epsilon_1\phi_1 + \epsilon_1^2\phi_2\big)\Big\} dv = O(\epsilon_1^4),
\end{aligned} \tag{6.47}
$$

which gives

$$
\iint_{\partial S} \phi^{(2)}\frac{\hat{\psi}_m^*}{\partial n} - \hat{\psi}_m^*\frac{\partial\phi^{(2)}}{\partial n}ds = -\iint_{\partial S^*} \phi^{(2)}\frac{\hat{\psi}_m^*}{\partial n} - \hat{\psi}_m^*\frac{\partial\phi^{(2)}}{\partial n}ds + O(\epsilon_1^4). \tag{6.48}
$$

Substituting for ϕ and $\hat{\psi}_m^*$ with (6.34) and (6.41) respectively in (6.48)

$$
\begin{aligned}
RHS(6.48) =& -\int_0^{2\pi}\int_0^{\pi}\left[\phi^{(2)}\frac{\hat{\psi}_m^*}{\partial\rho} - \hat{\psi}_m^*\frac{\partial\phi^{(2)}}{\partial\rho}\right]\rho r\sin\theta d\theta d\varphi + O(\epsilon_1^4)\\
=& \pi\frac{\epsilon_1^3}{\beta}\left[B_0\frac{V_s}{\pi a^3} + 4\mathrm{i}(u_1^{-1}, u_1^0, u_1^1)\mathbf{M}\begin{pmatrix} Y_1^{-1}(\hat{\boldsymbol{\beta}}_m)\\ Y_1^0(\hat{\boldsymbol{\beta}}_m)\\ Y_1^1(\hat{\boldsymbol{\beta}}_m)\end{pmatrix}\right] + O(\epsilon_1^4).
\end{aligned} \tag{6.49}
$$

Therefore, by (6.40), (6.48) and (6.49)

$$
\begin{aligned}
&\iiint_{C_s} (\xi\nabla^2\psi_m^* - \psi_m^*\nabla^2\xi)dv\\
&\qquad = \mathrm{e}^{-\mathrm{i}\boldsymbol{\beta}_m^T\cdot\mathbf{R}_j}\pi\frac{\epsilon_1^3}{\beta}\left[B_0\frac{V_s}{\pi a^3} + 4\mathrm{i}(u_1^{-1}, u_1^0, u_1^1)\mathbf{M}\begin{pmatrix} Y_1^{-1}(\hat{\boldsymbol{\beta}}_m)\\ Y_1^0(\hat{\boldsymbol{\beta}}_m)\\ Y_1^1(\hat{\boldsymbol{\beta}}_m)\end{pmatrix}\right] + O(\epsilon_1^3).
\end{aligned} \tag{6.50}
$$

By result from the sphere (6.22), we have

$$
\iiint_{C_s} (\xi\nabla^2\psi_m^* - \psi_m^*\nabla^2\xi)dv = \epsilon_1^3\frac{2\mathrm{i}\omega}{c^2}V_c\left(\frac{\partial A_m}{\partial T} + \frac{c^2}{\omega}\overline{\nabla}.A_m\cdot\boldsymbol{\beta}_m\right). \tag{6.51}
$$

Thus, by (6.50) and (6.51)

$$
\begin{aligned}
&\epsilon_1^3\frac{2\mathrm{i}\omega}{c^2}V_c\left(\frac{\partial A_m}{\partial T} + \frac{c^2}{\omega}\overline{\nabla}A_m\cdot\boldsymbol{\beta}_m\right)\\
&\qquad = \mathrm{e}^{-\mathrm{i}\boldsymbol{\beta}_m^T\cdot\mathbf{R}_j}\pi\frac{\epsilon_1^3}{\beta}\left[B_0\frac{V_s}{\pi a^3} + 4\mathrm{i}(u_1^{-1}, u_1^0, u_1^1)\mathbf{M}\begin{pmatrix} Y_1^{-1}(\hat{\boldsymbol{\beta}}_m)\\ Y_1^0(\hat{\boldsymbol{\beta}}_m)\\ Y_1^1(\hat{\boldsymbol{\beta}}_m)\end{pmatrix}\right] + O(\epsilon_1^4),
\end{aligned} \tag{6.52}
$$

which is

$$\frac{\partial A_m}{\partial T} + \frac{c^2}{\omega}\overline{\nabla} A_m \cdot \boldsymbol{\beta}_m$$
$$= \frac{\pi c^2}{2\beta \mathrm{i}\omega V_c} \mathrm{e}^{-\mathrm{i}\boldsymbol{\beta}_m^T \cdot \mathbf{R}_j} \pi \left[B_0 \frac{V_s}{\pi a^3} + 4\mathrm{i}(u_1^{-1}, u_1^0, u_1^1)\mathbf{M} \begin{pmatrix} Y_1^{-1}(\hat{\boldsymbol{\beta}}_m) \\ Y_1^0(\hat{\boldsymbol{\beta}}_m) \\ Y_1^1(\hat{\boldsymbol{\beta}}_m) \end{pmatrix} \right] + O(\epsilon_1^4). \quad (6.53)$$

By the matching between outer solution (6.16) and inner solution (6.34)

$$B_0 = \sum_{h=1}^{M} A_h \mathrm{e}^{-\mathrm{i}\boldsymbol{\beta}_m^T \cdot \mathbf{R}_j}, \quad (6.54)$$

$$(u_1^{-1}, u_1^0, u_1^1) = \sum_{h=1}^{M} A_h \mathrm{e}^{\mathrm{i}\boldsymbol{\beta}_h^T \mathbf{R}_j} \frac{4\pi}{3} \mathrm{i} \left(Y_1^{-1}(\hat{\boldsymbol{\beta}}_h)^*, Y_1^0(\hat{\boldsymbol{\beta}}_h)^*, Y_1^1(\hat{\boldsymbol{\beta}}_h)^* \right). \quad (6.55)$$

Now we have the envelope equations

$$\frac{\partial A_m}{\partial T} + \mathbf{C}_g^{(m)} \cdot \overline{\nabla} A_m$$
$$= -\frac{1}{2}\mathrm{i}\Omega_0 \sum_{h=1}^{M} A_h \left[\frac{V_s}{4\pi a^3} - \frac{4\pi}{3} \left(Y_1^{-1}(\hat{\boldsymbol{\beta}}_h)^*, Y_1^0(\hat{\boldsymbol{\beta}}_h)^*, Y_1^1(\hat{\boldsymbol{\beta}}_h)^* \right) \mathbf{M} \begin{pmatrix} Y_1^{-1}(\hat{\boldsymbol{\beta}}_m) \\ Y_1^0(\hat{\boldsymbol{\beta}}_m) \\ Y_1^1(\hat{\boldsymbol{\beta}}_m) \end{pmatrix} \right], \quad (6.56)$$

for all $m = 1, 2, \ldots, M$, where $\mathbf{C}_g^{(m)}$ and Ω_0 are given by (6.30).

If we multiply both sides of equation (6.56) by A_m^* (the conjugate of A_m) and add the resulting equation with its complex conjugate. After summation over m, we obtain

$$\sum_{m=1}^{M} \left(\frac{\partial A_m}{\partial T} + \mathbf{C}_g^{(m)} \cdot \overline{\nabla} A_m \right)$$
$$= -\frac{\Omega_0}{2} \sum_{m=1}^{M} \sum_{h=1}^{M} \left[\frac{V_s}{4\pi a^3} - \frac{4\pi}{3} \left(Y_1^{-1}(\hat{\boldsymbol{\beta}}_h)^*, Y_1^0(\hat{\boldsymbol{\beta}}_h)^*, Y_1^1(\hat{\boldsymbol{\beta}}_h)^* \right) \mathbf{M} \begin{pmatrix} Y_1^{-1}(\hat{\boldsymbol{\beta}}_m) \\ Y_1^0(\hat{\boldsymbol{\beta}}_m) \\ Y_1^1(\hat{\boldsymbol{\beta}}_m) \end{pmatrix} \right]$$
$$\times (\mathrm{i}A_h A_m^* - \mathrm{i}A_h^* A_m). \quad (6.57)$$

By changing the second term in the last parentheses on the right from $A_h^* A_m$ to $A_m^* A_h$, the double series is unaltered, hence must be zero, yielding

$$\frac{\partial}{\partial T} \sum_{m=1}^{M} |A_m|^2 + \sum_{m=1}^{M} (\mathbf{C}_g^{(m)} \cdot \overline{\nabla} |A_m|^2) = 0. \quad (6.58)$$

Thus the total energy is conserved in the array.

When the scatterers are sphere, the volume $V_s = 4\pi a^3/3$, and the matrix of dipole coefficients $\mathbf{M}$ is obtained in the infinite array (5.97)

$$\mathbf{M} = \begin{pmatrix} \frac{1}{2} & 0 & 0 \\ 0 & \frac{1}{2} & 0 \\ 0 & 0 & \frac{1}{2} \end{pmatrix}, \tag{6.59}$$

therefore the envelope equations become

$$\begin{aligned} &\frac{\partial A_m}{\partial T} + \mathbf{C}_g^{(m)} \cdot \overline{\nabla} A_m \\ &\qquad = \frac{1}{2}\mathrm{i}\Omega_0 \sum_{h=1}^{M} A_h \left[-\frac{1}{3} + \frac{2\pi}{3} \left(Y_1^{-1}(\hat{\boldsymbol{\beta}}_h)^*, Y_1^0(\hat{\boldsymbol{\beta}}_h)^*, Y_1^1(\hat{\boldsymbol{\beta}}_h)^* \right) \begin{pmatrix} Y_1^{-1}(\hat{\boldsymbol{\beta}}_m) \\ Y_1^0(\hat{\boldsymbol{\beta}}_m) \\ Y_1^1(\hat{\boldsymbol{\beta}}_m) \end{pmatrix} \right], \end{aligned} \tag{6.60}$$

which is in agreement with the results of scattering by an array of sphere (6.29).

If the array is infinite, the amplitude doesn't depend on the space variation, thus there is only time variation. If we search the solution in the form of $A_m(T) = a_m \mathrm{e}^{-\mathrm{i}\Omega T}$, the envelope equations become

$$\Omega a_m = \frac{2\pi c}{\beta^2 V_c} \sum_{h=1}^{M} a_h \left[\frac{V_s}{4\pi a^3} - \frac{4\pi}{3} \left(Y_1^{-1}(\hat{\boldsymbol{\beta}}_h)^*, Y_1^0(\hat{\boldsymbol{\beta}}_h)^*, Y_1^1(\hat{\boldsymbol{\beta}}_h)^* \right) \mathbf{M} \begin{pmatrix} Y_1^{-1}(\hat{\boldsymbol{\beta}}_m) \\ Y_1^0(\hat{\boldsymbol{\beta}}_m) \\ Y_1^1(\hat{\boldsymbol{\beta}}_m) \end{pmatrix} \right], \tag{6.61}$$

where $\Omega = \mathcal{K}c$. $\mathcal{K}$ is the detuning of the wavenumber and the detuned wavenumber $k = \beta + \epsilon_1^3 \mathcal{K}$, and the detuned frequency $\omega' = kc = \omega + \epsilon_1^3 \Omega$. The envelope equations (6.61) should be consistent with results obtained in infinite array (5.91)

$$\delta_m U_m = \frac{4\pi L^2}{k V_c} \sum_{h=1}^{M} U_h \left[\frac{V_s}{4\pi a^3} - \frac{4\pi}{3} \left(Y_1^{-1}(\hat{\boldsymbol{\beta}}_h)^*, Y_1^0(\hat{\boldsymbol{\beta}}_h)^*, Y_1^1(\hat{\boldsymbol{\beta}}_h)^* \right) \mathbf{M} \begin{pmatrix} Y_1^{-1}(\hat{\boldsymbol{\beta}}_h) \\ Y_1^0(\hat{\boldsymbol{\beta}}_h) \\ Y_1^1(\hat{\boldsymbol{\beta}}_h) \end{pmatrix} \right], \tag{6.62}$$

where

$$\delta_m = \frac{(k^2 - \beta_m^2)L^2}{k^3 a^3} = \frac{(k+\beta)(k-\beta)L^2}{k^3 a^3}, \text{ with } \beta_m = \beta.$$

Equations (6.61) and (6.62) define the same eigenvalue problem, therefore we have

$$\delta_m = \frac{2\beta^2 L^2}{kc}\Omega = \frac{2\beta^2(k-\beta)L^2}{k\epsilon_1^3} = \frac{2(k-\beta)L^2}{k\beta a^3} \approx \frac{(k+\beta)(k-\beta)L^2}{k^3 a^3}, \tag{6.63}$$

on a first approximation in the limit $k \to \beta$.

6.2.2 Numerical results

We now apply the system to a three-dimensional strip of scatterers occupying $0 \leq x \leq d$. A train of plane incident acoustic waves arrives from the left hand side of the array. Let the width d of the strip be of order $1/\epsilon_1^3$ in the x direction (that is to make sure the array width is big enough for the resonance to occur) and the length be infinite in both of $\pm y$ and $\pm z$ directions, see figure 6.1, where we only draw the scatterers on the visible surfaces of the cuboid.

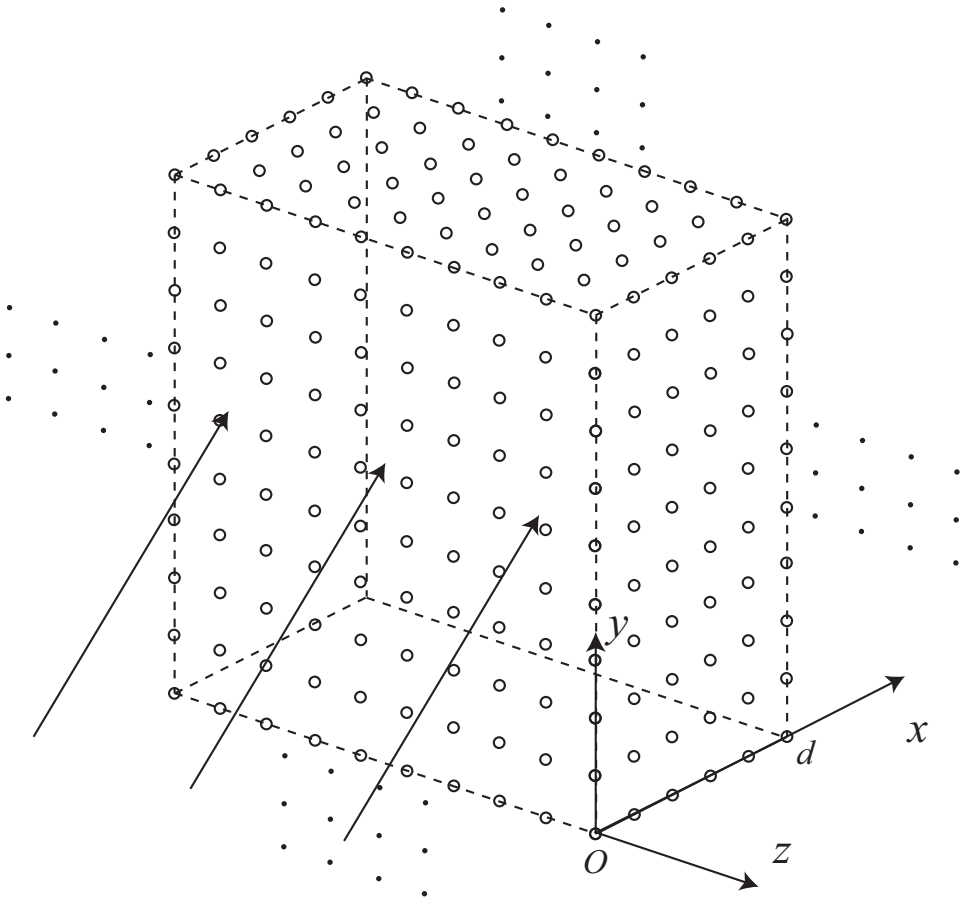

Figure 6.1: Strip

Write the wave potentials in the three zones (left side, right side and in the strip) in

the form of

$$\Phi_0 = \sum_{m=1}^{M} A_m(X,Y,Z,T)\mathrm{e}^{\mathrm{i}\boldsymbol{\beta}_m^T\mathbf{r}}, \tag{6.64}$$

where

$$A_m = \begin{cases} A_m^-, & X < 0, \\ A_m, & 0 \leqslant X \leqslant D, \\ A_m^+, & X > D, \end{cases} \tag{6.65}$$

with $D = \epsilon_1^2 d$. Note that, with $\boldsymbol{\beta}_m = \beta \begin{pmatrix} \sin\tau_m \cos\gamma_m \\ \sin\tau_m \sin\gamma_m \\ \cos\tau_m \end{pmatrix}$,

$$\mathrm{e}^{\mathrm{i}\boldsymbol{\beta}_m^T\mathbf{r}} = \mathrm{e}^{\mathrm{i}\beta(x\sin\tau_m\cos\gamma_m + y\sin\tau_m\sin\gamma_m + z\cos\tau_m)}, \tag{6.66}$$

where τ_m is the angle between $\boldsymbol{\beta}_m$ and z-axis, γ_m is the angle between the projection of $\boldsymbol{\beta}_m$ on $x-y$ plane and x-axis. With the presence of the scatterers in the strip, the incident plane waves $\mathrm{e}^{\mathrm{i}\boldsymbol{\beta}_m^T\mathbf{r}}$ will be perturbed. We choose a small perturbation (the detuning) of frequency of the incident wave and write

$$A_1^-(X,Y,Z,T) = A_0\mathrm{e}^{\mathrm{i}(\mathcal{K}\sin\tau_1\cos\gamma_1 X + \mathcal{K}\sin\tau_1\sin\gamma_1 Y + \mathcal{K}\cos\tau_1 Z - \Omega T)}, \tag{6.67}$$

where $\mathcal{K}$ is the detuning of the wavenumber and Ω is the detuning of the frequency, related by $\mathcal{K} = \Omega/c$. By the continuity conditions at $X = 0, D$, the y and z dependence must be the same in every component of the solution. Thus, look for solutions in the form

$$\begin{pmatrix} A_m^-(X,Y,Z,T) \\ A_m(X,Y,Z,T) \\ A_m^+(X,Y,Z,T) \end{pmatrix} = A_0 \begin{pmatrix} B_m^-(X) \\ B_m(X) \\ B_m^+(X) \end{pmatrix} \mathrm{e}^{\mathrm{i}(\mathcal{K}\sin\tau_1\sin\gamma_1 Y + \mathcal{K}\cos\tau_1 Z - \Omega T)}, \ m = 1,2,\ldots,M. \tag{6.68}$$

Along the edges of the strip, the dynamic pressure $-\mathrm{i}\omega\Phi_0$ and the normal velocity $\partial\Phi_0/\partial x$ must be continuous,

$$\sum_{m=1}^{M} A_m^-(0,Y,Z,T)\mathrm{e}^{\mathrm{i}\boldsymbol{\beta}_m^T\mathbf{r}} = \sum_{m=1}^{M} A_m(0,Y,Z,T)\mathrm{e}^{\mathrm{i}\boldsymbol{\beta}_m^T\mathbf{r}}, \tag{6.69}$$

$$\sum_{m=1}^{M} A_m(D,Y,Z,T)\mathrm{e}^{\mathrm{i}\boldsymbol{\beta}_m^T\mathbf{r}} = \sum_{m=1}^{M} A_m^+(D,Y,Z,T)\mathrm{e}^{\mathrm{i}\boldsymbol{\beta}_m^T\mathbf{r}}, \tag{6.70}$$

$$\frac{\partial}{\partial x}\sum_{m=1}^{M} A_m^-(X,Y,Z,T)\mathrm{e}^{\mathrm{i}\boldsymbol{\beta}_m^T\mathbf{r}}\bigg|_{X=0} = \frac{\partial}{\partial x}\sum_{m=1}^{M} A_m(X,Y,Z,T)\mathrm{e}^{\mathrm{i}\boldsymbol{\beta}_m^T\mathbf{r}}\bigg|_{X=0}, \tag{6.71}$$

$$\frac{\partial}{\partial x}\sum_{m=1}^{M} A_m(X,Y,Z,T)\mathrm{e}^{\mathrm{i}\boldsymbol{\beta}_m^T\mathbf{r}}\bigg|_{X=D} = \frac{\partial}{\partial x}\sum_{m=1}^{M} A_m^+(X,Y,Z,T)\mathrm{e}^{\mathrm{i}\boldsymbol{\beta}_m^T\mathbf{r}}\bigg|_{X=D}, \tag{6.72}$$

which lead to

$$\sum_{m=1}^{M}(B_m^-(0)-B_m(0))\mathrm{e}^{\mathrm{i}\beta(y\sin\tau_m\sin\gamma_m+z\cos\tau_m)} = 0, \tag{6.73}$$

$$\sum_{m=1}^{M}(B_m^-(D)-B_m(D))\mathrm{e}^{\mathrm{i}\frac{\beta D}{\epsilon_1^3}\sin\tau_m\cos\gamma_m}\mathrm{e}^{\mathrm{i}\beta(y\sin\tau_m\sin\gamma_m+z\cos\tau_m)} = 0, \tag{6.74}$$

and

$$\sum_{m=1}^{M}(B_m^-(0)-B_m(0))\mathrm{i}\beta\sin\tau_m\cos\gamma_m\mathrm{e}^{\mathrm{i}\beta(y\sin\tau_m\sin\gamma_m+z\cos\tau_m)} = O(\epsilon_1^3), \tag{6.75}$$

$$\sum_{m=1}^{M}(B_m^-(D)-B_m(D))\mathrm{i}\beta\sin\tau_m\cos\gamma_m\mathrm{e}^{\mathrm{i}\frac{\beta D}{\epsilon_1^3}\sin\tau_m\cos\gamma_m}\mathrm{e}^{\mathrm{i}\beta(y\sin\tau_m\sin\gamma_m+z\cos\tau_m)} = O(\epsilon_1^3). \tag{6.76}$$

Then using the orthogonality of the trigonometric functions, we obtain

$$\begin{aligned} B_m^-(0) &= B_m(0), \quad m=1,2,\ldots,M. \\ B_m(D) &= B_m^+(D), \quad m=1,2,\ldots,M. \end{aligned} \tag{6.77}$$

Note the incident wave vector is $\boldsymbol{\beta}_1 = \beta(\sin\tau_1\cos\gamma_1, \sin\tau_1\sin\gamma_1, \cos\tau_1)^T$, so the direction of the incident wave is determined by two angles τ_1 and γ_1. Without loss of generality we limit γ_1 to be $0 < \gamma_1 < \pi/2$. From the definition of the spherical coordinates, $0 \le \tau_1 \le \pi$. Arrange the components so that

$$\cos\gamma_m > 0 \quad \text{for} \quad m \in \{1,2,\ldots,M^+\} \equiv Z_1,$$

and

$$\cos\gamma_m < 0 \quad \text{for} \quad m \in \{M^+ + 1, M^+ + 2, \ldots, M\} \equiv Z_2.$$

In the field without scatterers $X < 0$, the only forward propagating wave is the incident wave so that

$$B_m^-(X) = 0, \quad m \in Z_1 \setminus \{1\}. \tag{6.78}$$

In the field $X > D$, there are no backward propagating waves so that

$$B_m^+(X) = 0, \quad m \in Z_2. \tag{6.79}$$

Now we are going to derive the envelope equations in and out of the strip in forms of $B_m^-(X), B_m(X), B_m^+(X)$. The governing equations in the strip and the outside the strip are given by (6.60) and (6.31) respectively. Outside the strip, from (6.68) and the the envelope equations (6.31), we have

$$\frac{dB_m^\pm}{dX} = \mathrm{i}\mathcal{K}\frac{1 - \sin\tau_1 \sin\gamma_1 \sin\tau_m \sin\gamma_m - \cos\tau_1 \cos\tau_m}{\sin\tau_m \cos\gamma_m} B_m^\pm, \quad m = 1, 2, \ldots, M. \tag{6.80}$$

Thus

$$B_m^\pm(X) = b_m^\pm \mathrm{e}^{\mathrm{i}\mathcal{K}_m X}, \tag{6.81}$$

where

$$\mathcal{K}_m = \frac{1 - \sin\tau_1 \sin\gamma_1 \sin\tau_m \sin\gamma_m - \cos\tau_1 \cos\tau_m}{\sin\tau_m \cos\gamma_m}\mathcal{K}, \quad m = 1, 2, \ldots, M.$$

Inside the strip, from (6.68), the envelope equations (6.56) become

$$\begin{aligned}\frac{dB_m}{dX} =& \frac{\mathrm{i}\Omega_0}{C_g \sin\tau_m \cos\gamma_m}\Bigg\{\frac{\Omega}{\Omega_0}(1 - \sin\tau_1 \sin\gamma_1 \sin\tau_m \sin\gamma_m - \cos\tau_1 \cos\tau_m)B_m \\ &+ \frac{1}{2}\sum_{h=1}^{M} B_h \left[\frac{4\pi}{3}\left(Y_1^{-1}(\hat{\boldsymbol{\beta}}_h)^*, Y_1^0(\hat{\boldsymbol{\beta}}_h)^*, Y_1^1(\hat{\boldsymbol{\beta}}_h)^*\right)\mathbf{M}\begin{pmatrix} Y_1^{-1}(\hat{\boldsymbol{\beta}}_m) \\ Y_1^0(\hat{\boldsymbol{\beta}}_m) \\ Y_1^1(\hat{\boldsymbol{\beta}}_m)\end{pmatrix}\right] - \frac{V_s}{4\pi a^3}\Bigg\},\end{aligned} \tag{6.82}$$

which is

$$\frac{d}{dX}\begin{pmatrix} B_1 \\ B_2 \\ \vdots \\ B_M\end{pmatrix} = \frac{\mathrm{i}\Omega_0}{C_g}\mathbf{F}\begin{pmatrix} B_1 \\ B_2 \\ \vdots \\ B_M\end{pmatrix}, \tag{6.83}$$

where the elements of the matrix $\mathbf{F}$ are

$$\begin{aligned}F_{ii} =& \frac{1}{\sin\tau_i \cos\gamma_i}\Bigg[\frac{\Omega}{\Omega_0}(1 - \sin\tau_1 \sin\gamma_1 \sin\tau_i \sin\gamma_i - \cos\tau_1 \cos\tau_i) \\ &+ \frac{2\pi}{3}\left(Y_1^{-1}(\hat{\boldsymbol{\beta}}_i)^*, Y_1^0(\hat{\boldsymbol{\beta}}_i)^*, Y_1^1(\hat{\boldsymbol{\beta}}_i)^*\right)\mathbf{M}\begin{pmatrix} Y_1^{-1}(\hat{\boldsymbol{\beta}}_i) \\ Y_1^0(\hat{\boldsymbol{\beta}}_i) \\ Y_1^1(\hat{\boldsymbol{\beta}}_i)\end{pmatrix} - \frac{V_s}{8\pi a^3}\Bigg],\end{aligned} \tag{6.84}$$

$$F_{ij} = \frac{1}{\sin\tau_i \cos\gamma_i} \left[\frac{2\pi}{3} \left(Y_1^{-1}(\hat{\boldsymbol{\beta}}_j)^*, Y_1^0(\hat{\boldsymbol{\beta}}_j)^*, Y_1^1(\hat{\boldsymbol{\beta}}_j)^* \right) \mathbf{M} \begin{pmatrix} Y_1^{-1}(\hat{\boldsymbol{\beta}}_i) \\ Y_1^0(\hat{\boldsymbol{\beta}}_i) \\ Y_1^1(\hat{\boldsymbol{\beta}}_i) \end{pmatrix} - \frac{V_s}{8\pi a^3} \right],$$

$$i, j = 1, 2, \ldots, M. \quad (6.85)$$

Here we only consider the case that none of the eigenvalues are equal to each other. In this case, the general solution of the linear system (4.87) is of the form

$$\begin{aligned} \mathbf{B} &= (B_1, B_2, \ldots, B_M)^T \\ &= C_1 \mathbf{V}^{(1)} \mathrm{e}^{\mathrm{i}\lambda_1 \Omega_0 X/C_g} + C_2 \mathbf{V}^{(2)} \mathrm{e}^{\mathrm{i}\lambda_2 \Omega_0 X/C_g} + \ldots + C_M \mathbf{V}^{(M)} \mathrm{e}^{\mathrm{i}\lambda_M \Omega_0 X/C_g}, \end{aligned} \quad (6.86)$$

where $\mathbf{V}^{(j)}$ is eigenvectors corresponding to eigenvalue λ_j, $j = 1, 2, \ldots, M$. The unknown coefficients $C_1, C_2, \ldots, C_M$ will be determined by the boundary conditions (6.78) and (6.79). The properties of this solution form depend on whether the eigenvalues of matrix $\mathbf{F}$ are real or complex, and the forms of the eigenvalues depend on the sign of the discriminant of the characteristic equation, which is, for example,

$$\lambda^2 - (F_{11} + F_{22})\lambda + (F_{11}F_{22} - F_{12}F_{21}) = 0, \text{ for } M = 2, \quad (6.87)$$

and

$$\lambda^3 + \alpha_2 \lambda^2 + \alpha_1 \lambda + \alpha_0 = 0, \text{ for } M = 3, \quad (6.88)$$

where

$$\alpha_2 = -(F_{11} + F_{22} + F_{33}), \quad (6.89)$$

$$\alpha_1 = \det \begin{pmatrix} F_{11} & F_{12} \\ F_{21} & F_{22} \end{pmatrix} + \det \begin{pmatrix} F_{11} & F_{13} \\ F_{31} & F_{33} \end{pmatrix} + \det \begin{pmatrix} F_{22} & F_{23} \\ F_{32} & F_{33} \end{pmatrix}, \quad (6.90)$$

$$\alpha_0 = -\det(\mathbf{F}). \quad (6.91)$$

The discriminants are

$$\Delta_2 = (F_{11} + F_{22})^2 - 4(F_{11}F_{22} - F_{12}F_{21}), \text{ for } M = 2, \quad (6.92)$$

$$\Delta_3 = 4\alpha_1^3 - \alpha_1^2\alpha_2^2 + 4\alpha_0\alpha_2^3 - 18\alpha_0\alpha_1\alpha_2 + 27\alpha_0^2, \text{ for } M = 3. \quad (6.93)$$

The discriminant Δ is a function of the detuning of the frequency Ω/Ω_0, which is contained in F_{ij}. For example, when $\Delta_3 < 0$, one of the eigenvalues is real and the other two are complex. Therefore one of the eigensolutions (6.86) is oscillatory in X with constant amplitude. The remaining two are oscillatory with exponentially decaying or growing amplitude. When $\Delta_3 > 0$, all the eigenvalues are real and all the waves in the array will oscillate in X with constant amplitudes.

Next, we will consider and compare the primary wave intensity $|B_1(X)|^2$ for three types of scatterers, where the primary wave is the continuation of the incident wave in the array. We always assume the length of the axis of the scatterer in x direction is a, the length of the axis in y direction is b, and the length of the axis in z direction is c. Given a length l, we take the typical size of the three types of scatterers as follows

1. Sphere: $a = b = c = l$.

2. Prolate spheroid: $a = 2l,\ b = c = l$.

3. Oblate spheroid: $a = l,\ b = c = 2l$.

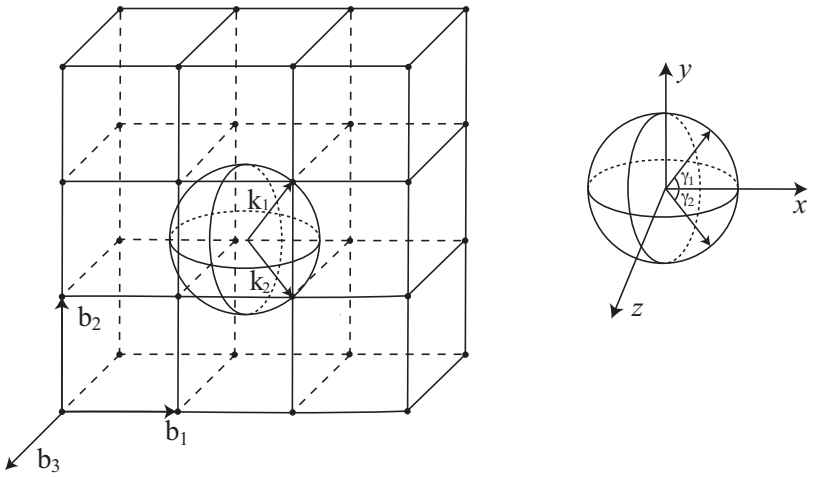

Figure 6.2: $M = 2$, forward scattering by a simple cubic lattice.

The matrix of the dipole coefficient is given by (5.97), which is related to the added mass coefficients by (5.98). For a sphere, the added mass coefficients are [65, page 144]

$$a_{11} = a_{22} = a_{33} = \rho V_s/2,\ a_{ij} = 0,\ i \neq j. \tag{6.94}$$

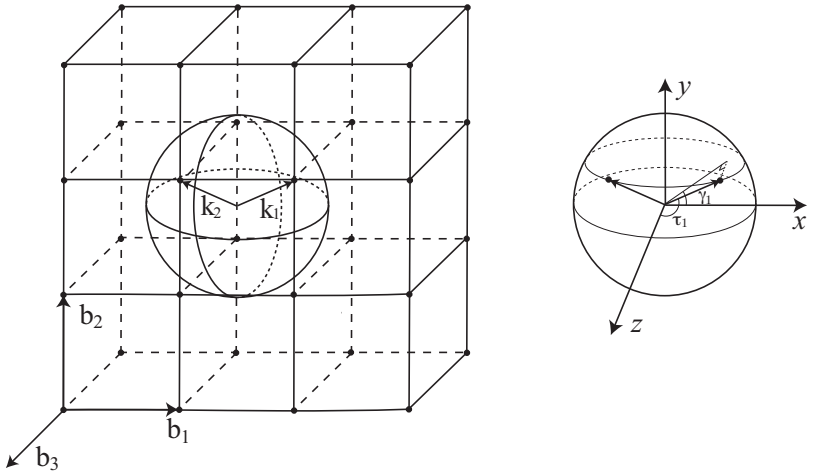

Figure 6.3: $M = 2$, backward scattering by a simple cubic lattice.

For a spheroid, the added mass coefficients are [32, page 153]

$$a_{11} = \frac{\alpha_0}{2 - \alpha_0} \frac{4}{3} \pi \rho a_1 b_1^2, \tag{6.95}$$

$$a_{22} = a_{33} = \frac{\beta_0}{2 - \beta_0} \frac{4}{3} \pi \rho a_1 b_1^2, \tag{6.96}$$

where for a prolate spheroid

$$\alpha_0 = -\frac{2b^2 \left[\sqrt{a^2 - b^2} - a \ \text{arccosh} \left(\frac{a}{b} \right) \right]}{(a^2 - b^2)^{3/2}}, \tag{6.97}$$

$$\beta_0 = \gamma_0 = \frac{a \left[a\sqrt{a^2 - b^2} - b^2 \ \text{arccosh} \left(\frac{a}{b} \right) \right]}{(a^2 - b^2)^{3/2}}, \tag{6.98}$$

and for an oblate spheroid

$$\alpha_0 = \frac{2b^2 \left[\sqrt{b^2 - a^2} - a \ \arccos \left(\frac{a}{b} \right) \right]}{(b^2 - a^2)^{3/2}}, \tag{6.99}$$

$$\beta_0 = \gamma_0 = -\frac{a \left[a\sqrt{b^2 - a^2} + b^2 \ \arccos \left(\frac{a}{b} \right) \right]}{(b^2 - a^2)^{3/2}}. \tag{6.100}$$

In the following results for these three types of scatterers, we use l as the dimensionless parameter, and the small parameter $\epsilon_1 = kl$.

Without loss of generality, we limit the angle of the incident wave with x-axis to be in $(0, \pi/2)$. If we define the positive direction of x-axis as forward and the negative direction of x-axis as backward, then when $M = 2$, there are two types of scattering,

forward scattering and backward scattering. For examples, we take the following data for numerical calculations

$$\text{Forward scattering}: \tau_1 = \tau_2 = \pi/2, \gamma_1 = \pi/3, \gamma_2 = -\pi/3. \quad \text{See figure 6.2.}$$

$$\text{Backward scattering}: \tau_1 = \tau_2 = \pi/3, \gamma_1 = \pi/6, \gamma_2 = 5\pi/6. \quad \text{See figure 6.3.}$$

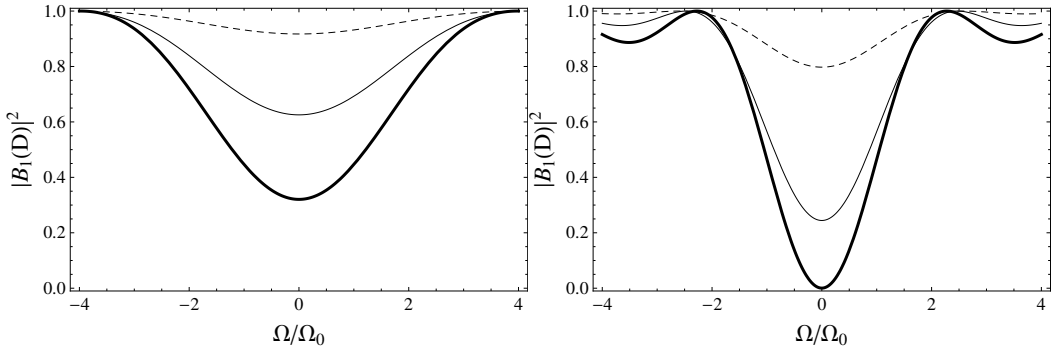

Figure 6.4: M=2, forward scattering. Comparison of the transmission wave intensity $|B_1(D)|^2$ over the detuning Ω/Ω_0. Left: $\Omega_0 D/C_g = 0.5$. Right: $\Omega_0 D/C_g = 0.8$. Dashed line: sphere, solid line: prolate spheroid, thick solid line: oblate spheroid.

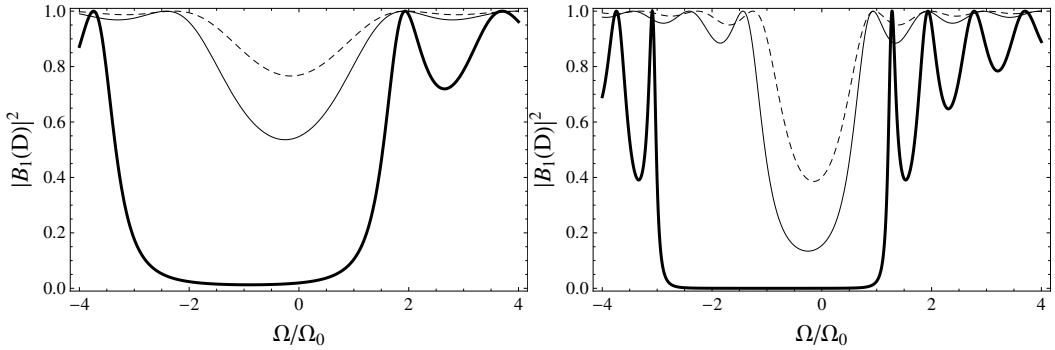

Figure 6.5: M=2, backward scattering. Comparison of the transmission wave intensity $|B_1(D)|^2$ over the detuning Ω/Ω_0. Left: $\Omega_0 D/C_g = 2$. Right: $\Omega_0 D/C_g = 4$. Dashed line: sphere, solid line: prolate spheroid, thick solid line: oblate spheroid.

In figure 6.4 we plot the primary wave (the continuity of the incident wave in the array) intensity on the right edge of the strip $|B_1(L)|^2$ against the detuning Ω/Ω_0 for forward scattering and strip widths $\Omega_0 D/C_g = 0.5$ and $\Omega_0 D/C_g = 0.8$. As we can see, the oblate spheroid array is most efficient in blocking the primary wave while the sphere is the least efficient one, which is because the oblate spheroid has the biggest volume and the sphere has the smallest volume by the scatterer size we use. The same situation happens for the backward scattering, which is shown in figure 6.5.

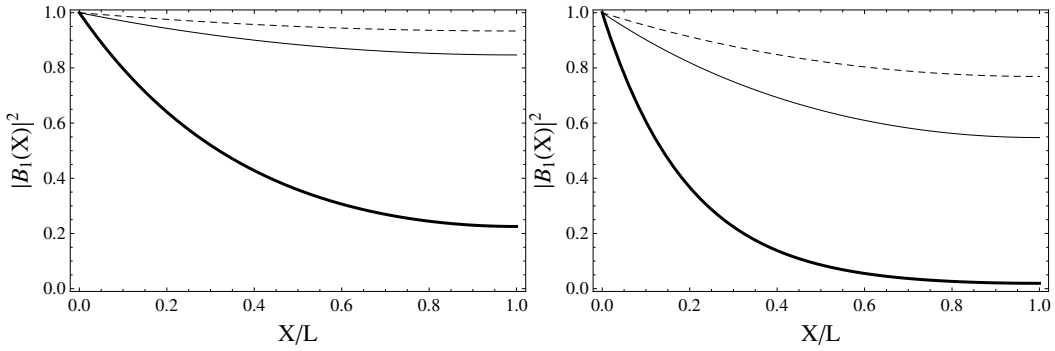

Figure 6.6: M=2, backward scattering. Comparison of the primary wave intensity $|B_1(X)|^2$ across the strip when $\Omega/\Omega_0 = 0$, which lies in the stop band. Left: $\Omega_0 D/C_g = 1$, right: $\Omega_0 D/C_g = 2$. Dashed line: sphere, solid line: prolate spheroid, thick solid line: oblate spheroid.

In the case of the backward scattering, there is a region of detuning which makes eigenvalues be complex conjugate. In this region, the solutions for the primary wave $B_1(X)$ and scattered wave $B_2(X)$ are oscillatory with exponential decaying or growing amplitude. We define this region as the stop band. In figure 6.6 we compare the primary wave intensity $|B_1(X)|^2$ across the strip for scattering configuration in figure 6.3 when the detuning $\Omega/\Omega_0 = 0$. From 6.6, we can see the primary wave intensity for sphere array decays most slowly and it decays fastest for oblate spheroid array. When the strip width is increased to 2, the primary wave intensity decays to nearly zero for oblate spheroid array at the right edge and it decays more slowly for the other two scatterers. When the strip width is large enough, the primary wave intensities of all three types of scatterers will decay to nearly zero at the exit edge of the strip.

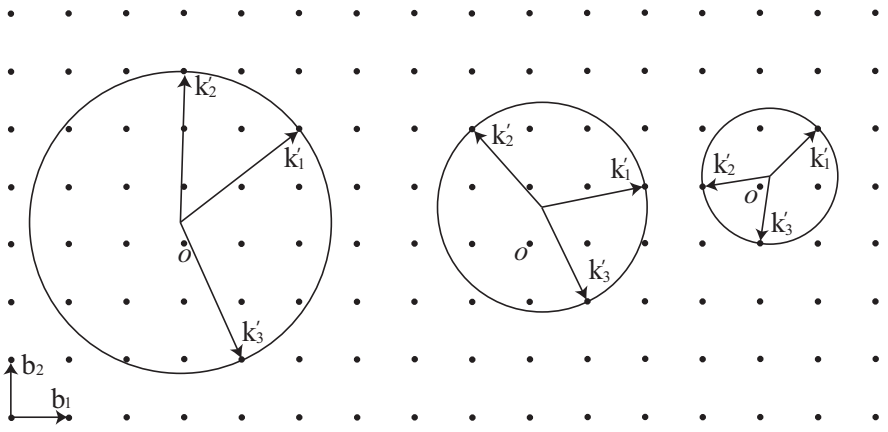

Figure 6.7: $M = 3$, the projections of the wave vectors in $x - y$ plane. Left: forward-forward scattering, middle: forward-backward scattering, right: backward-backward scattering.

Next we consider the case of $M = 3$, i.e. two resonantly scattered waves in the array. Three types of scattering are possible. In figure 6.7 we give the projections of the wave vectors in $x-y$ plane, which are denoted by dashed symbols. The strip array we consider is a simple cubic array.

1. Type I (forward-forward): both resonated waves propagate forward as shown in the left hand diagram of figure 6.7. $\mathbf{k}_1' = (2, 2, 0)$, $\mathbf{k}_2' = (0, 3, 0)$, $\mathbf{k}_3' = (1, -2, 0)$, the scatterer centre in primary cell is $(-1/18, 7/18, -1/4)$. $\tau_1 = \tau_2 = \tau_3 = \cos^{-1}(9/\sqrt{8921}) \approx 84.53°$, $\gamma_1 = \tan^{-1}(29/37) \approx 38.09°$, $\gamma_2 = \tan^{-1}(47) \approx 88.78°$, $\gamma_3 = \tan^{-1}(-43/19) \approx 66.16°$.

2. Type II (forward-backward): one resonated wave is reflected and another one propagates forward as shown in the middle diagram of figure 6.7. $\mathbf{k}_1' = (2, 1, 0)$, $\mathbf{k}_2' = (-1, 2, 0)$, $\mathbf{k}_3' = (1, -1, 0)$, the scatterer centre in primary cell is $(3/14, 9/14, 5/4)$. $\tau_1 = \tau_2 = \tau_3 = \cos^{-1}(-7/3\sqrt{17}) \approx 124.47°$, $\gamma_1 = \tan^{-1}(1/5) \approx 11.31°$, $\gamma_2 = \pi + \tan^{-19/17}(47) \approx 131.82°$, $\gamma_3 = \tan^{-1}(-23/11) \approx -64.44°$.

3. Type III (backward-backward): Both resonated waves are reflected, therefore propagate backward as shown in the right hand diagram of figure 6.7. $\mathbf{k}_1' = (1, 1, 0)$, $\mathbf{k}_2' = (-1, 0, 0)$, $\mathbf{k}_3' = (0, -1, 0)$, the scatterer centre in primary cell is $(1/6, 1/6, 0)$. $\tau_1 = \tau_2 = \tau_3 = \pi/2$, $\gamma_1 = \tan^{-1}(1) = \pi/4$, $\gamma_2 = -\pi + \tan^{-1}(1/7) \approx -171.87°$, $\gamma_3 = -\pi + \tan^{-1}(7) \approx -98.13°$.

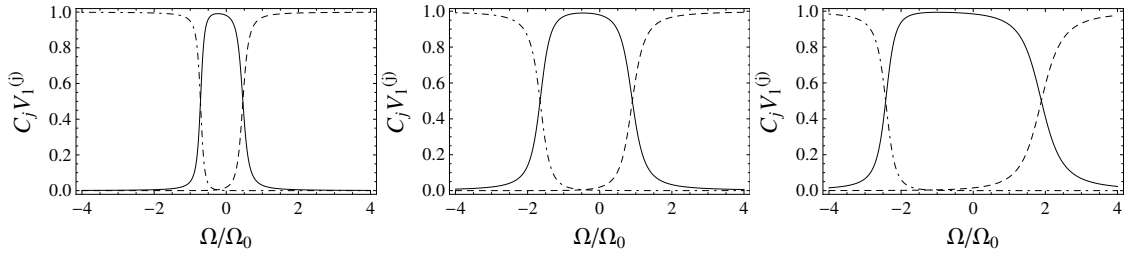

Figure 6.8: Three coefficients of the primary wave in type I scattering. Left: sphere, middle: prolate spheroid, right: oblate spheroid. Dashed line: $C_1V_1^{(1)}$, solid line: $C_2V_1^{(2)}$, dot-dashed line: $C_3V_1^{(3)}$.

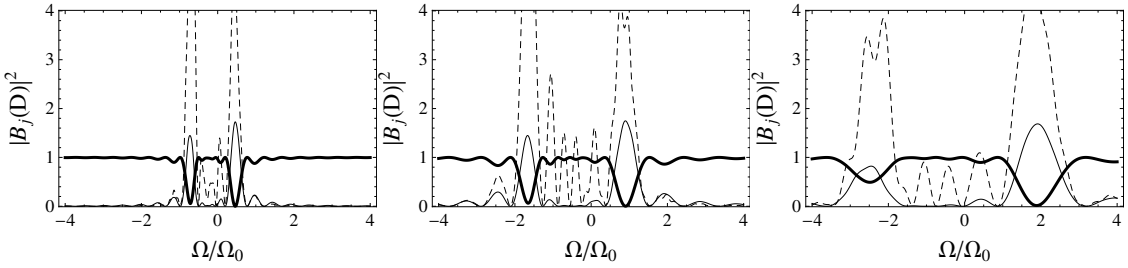

Figure 6.9: Dependence of wave intensities for type I scattering on the detuning frequency Ω/Ω_0. Left: sphere, $\Omega_0 D/C_g = 4$; middle: prolate spheroid, $\Omega_0 D/C_g = 2$; right: oblate spheroid, $\Omega_0 D/C_g = 1$. Thick solid line: $|B_1(D)|^2$, dashed line: $|B_2(D)|^2$, thin solid line: $|B_3(D)|^2$.

When $M = 3$, the general solutions of equation (6.82) inside the strip have the form (6.86)

$$\begin{aligned}\mathbf{B}(X) &= (B_1(X), B_2(X), B_3(X))^T \\ &= C_1\mathbf{V}^{(1)}\mathrm{e}^{\mathrm{i}\lambda_1\Omega_0 X/C_g} + C_2\mathbf{V}^{(2)}\mathrm{e}^{\mathrm{i}\lambda_2\Omega_0 X/C_g} + C_3\mathbf{V}^{(3)}\mathrm{e}^{\mathrm{i}\lambda_3\Omega_0 X/C_g}, \end{aligned} \tag{6.101}$$

where λ_j and $\mathbf{V}^{(j)}$, $j = 1, 2, 3$ are the eigenvalues and the corresponding eigenvectors of matrix $\mathbf{F}$, respectively. The coefficients C_j, $j = 1, 2, 3$ will be determined by boundary conditions at the edge of the cylinder strip. Here we only consider the case that none of the eigenvalues is equal to each other. In figure 6.8 we give the three coefficients of the primary wave in type I scattering shown in the left hand diagram of figure 6.7. In figure 6.9 we give the dependence of wave intensities in the array for type I scattering on the detuning frequency Ω/Ω_0. If we compare figure 6.8 with 6.9, we find the primary wave intensity $|B_1(X)|^2$ has valleys where two of the three primary wave coefficients are nearly equal. For example, in the left hand diagram of 6.8, at $\Omega/\Omega_0 \approx 0.46$, the coefficients $C_1V_1^{(1)}$ and $C_2V_1^{(2)}$ cross each other and nearly equal to 0.5. On the other hand, the other coefficient $C_3V_1^{(3)}$ is nearly zero. Therefore, the primary wave $B_1(X)$ is

dominant by the first two eigenvectors; its intensity can be approximated by

$$\begin{aligned} |B_1(X)|^2 &\sim |C_1 V_1^{(1)} \mathrm{e}^{\mathrm{i}\lambda_1 \Omega_0 X/C_g} + C_2 V_1^{(2)} \mathrm{e}^{\mathrm{i}\lambda_2 \Omega_0 X/C_g}|^2 \\ &\sim \frac{1}{4}\left|1 + \mathrm{e}^{\mathrm{i}(\lambda_1-\lambda_2)\Omega_0 X/C_g}\right|^2 \\ &= \cos^2 \frac{(\lambda_1-\lambda_2)\Omega_0 X}{C_g}. \end{aligned} \tag{6.102}$$

Therefore the minimum transmission intensity occurs around

$$\begin{aligned} \frac{\Omega_0 X}{C_g} &= \frac{(2n+1)\pi}{|\lambda_1-\lambda_2|},\ n = 1, 2, \ldots \\ &\approx 3.45, 10.34, 17.28, \ldots. \end{aligned} \tag{6.103}$$

In the left hand diagram of figure 6.8, the strip width we use is $\Omega_0 D/C_g = 4$, which is near the minimum primary wave intensity occurring point $\Omega_0 D/C_g = 3.45$. We can see the minimum primary wave intensity of this strip width is quite close to zero.

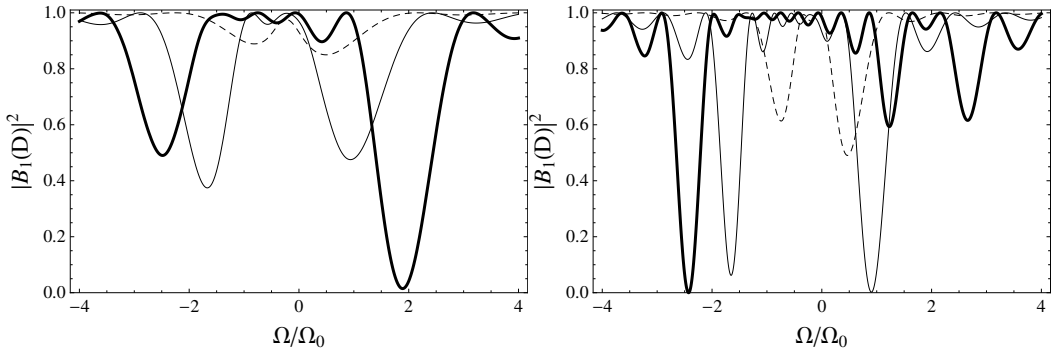

Figure 6.10: M=3. Comparison of the transmitted wave intensity for type I on the exit edge of the strip $|B_1(D)|^2$ over the detuning. Left: $\Omega_0 D/C_g = 1$. Right: $\Omega_0 D/C_g = 2$. Dashed line: sphere, solid line: prolate spheroid, thick solid line: oblate spheroid.

In figure 6.10, we compare the transmitted wave intensity $|B_1(D)|^2$ for type I scattering on the exit edge of the strip against the detuning. We can see that for same strip width, the oblate spheroid array blocks most energy and the sphere array blocks least energy.

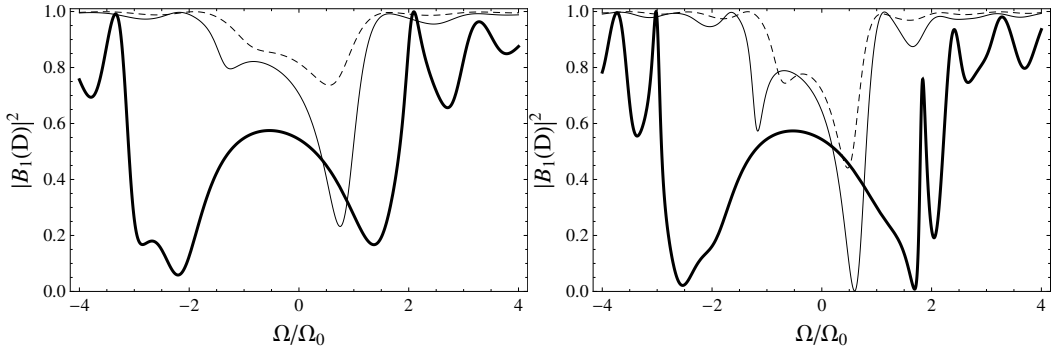

Figure 6.11: M=3. Comparison of the transmitted wave intensity for type II on the exit edge of the strip $|B_1(D)|^2$ over the detuning. Left: $\Omega_0 D/C_g = 2$. Right: $\Omega_0 D/C_g = 3$. Dashed line: sphere, solid line: prolate spheroid, thick solid line: oblate spheroid.

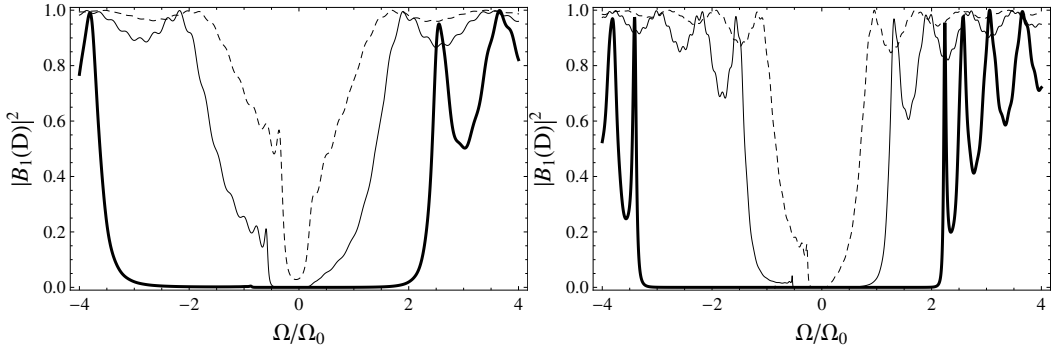

Figure 6.12: M=3. Comparison of the transmitted wave intensity for type III on the exit edge of the strip $|B_1(D)|^2$ over the detuning. Left: $\Omega_0 D/C_g = 2$. Right: $\Omega_0 D/C_g = 4$. Dashed line: sphere, solid line: prolate spheroid, thick solid line: oblate spheroid.

For type II forward-backward scattering and type III backward-backward scattering, two of the three eigenvalues are conjugate complex for some region of detuning (the stop band). In figure 6.11 and 6.12, we compare the transmitted wave intensity $|B_1(D)|^2$ on the right edge of the strip against the detuning Ω/Ω_0 and we can see the stop bands are always widest for oblate spheroid array. Thus the oblate spheroid array is the most efficient scatterer in blocking the incident wave and most energy is transferred into scattered energy when the detuning lies in the stop band.

Chapter 7

Conclusions

7.1 Summary

Methods of matched asymptotic expansions and multiple scales were used to consider acoustic or elastic wave propagations through both infinite and finite (only finite in one direction) periodic arrays.

For the infinite arrays, elastic wave propagation through doubly-periodic arrays of cavity cylinders and acoustic wave propagation through triply-periodic arrays of arbitrary shape scatterers were considered. Wave potentials satisfy the Helmholtz equations given that the waves are time-harmonic. The scatterer size was assumed to be small compared to both the wavelength and the length scale of the array periodicity, but there was no restriction on the sizes between the latter two. This allows us to investigate the phenomena associated with the periodicity, such as band gaps. The main idea we used is to obtain perturbations of the quasi-periodic plane wave solutions that exist in the absence of the scatterers. In the elastic case, we need to take account of the coupling between shear and dilatational waves that arises from the boundary conditions. A notable feature of the matched asymptotic expansions was that certain eigenfunctions must be included in the inner solution ahead of any obvious need for them. Explicit expressions for the frequencies were obtained that showed how the mode frequencies depended on the Bloch vector, the geometry, and the Lamé constants for the medium. Perturbed dispersion relations were then given to show the appearance of the local band gaps when the scatterer size was increased from zero. In the elastic case, results were also given to

illustrate the appearance of local band gaps, the splitting and crossing of double modes, and switching between dilatational and shear modes for square and hexagonal lattices. In the acoustic case, the scatterers can be arbitrary shape. Results were given for simple cubic lattice and body-centred cubic lattice to compare the perturbed dispersion relations for spherical and prolate spheroidal scatterers. It was shown that the size of the local band gaps were always bigger for prolate spheroid array than for sphere array, which is because the prolate spheroid had bigger volume than the sphere for the sizes we chose.

For the finite arrays, we considered the multiple resonant scattering by a large width strip of arrays of scatterers. The strip had finite width in only one direction and infinite in other directions. As in the case of infinite arrays, the scatterers are cavity cylinders for the two-dimensional elastic case and can be arbitrary shape for three-dimensional acoustic case. As the strip width must be large enough to make the resonance occur, we first derived the envelope equations for an infinite array with the help of the results of the infinite arrays and the method of multiple scales. The envelope equations were then applied to a finite array to investigate how waves propagate in the array. We compared the transmission wave intensities for different shape scatterers for the acoustic case. It was shown that the transmission wave intensities not only depended on the shape of the scatterer, the strip width and detuning of the frequency but also the incident angle. For the elastic case, we applied the envelope equations to an elastic strip with an array of cavity cylinders bounded by acoustic media on both sides.

7.2 Future work

The immediate future work is to consider the elastic wave propagation through infinite and finite three-dimensional arrays of spheres using the matched asymptotic expansions (multiple scales should also be used when the array is finite in one direction). Another possible work is the wave propagation through arrays of Dirichlet scatterers. Moreover, elastic wave scattering by other shape scatterers, such as elliptical cylinders in two-dimensional and spheroids in three-dimensional are quite possible to be solved by these methods using the elliptical cylindrical coordinates or spheroidal coordinates system. Another possibility would be the electromagnetic waves propagate through various arrays: two-dimensional and three-dimensional, infinite and finite etc.

Bibliography

[1] Abramowitz, M. and Stegun, I. A., *Handbook of Mathematical Functions*, National Bureau of Standards, 1964. 34

[2] Achenbach, J. D. and Kitahara, M., *Reflection and transmission of an obliquely incident wave by an array of spherical cavities*, J. Acoust. Soc. Am., **80**(4), 1209-1214, 1986. 152

[3] Achenbach, J. D. and Kitahara, M., *Harmonic waves in a solid with a periodic distribution of spherical cavities*, J. Acoust. Soc. Am., **81**(3), 595-598, 1987. 152

[4] Anderson, V. C., *Sound scattering from a fluid sphere*, J. Acoust. Soc. Am., **22**(4), 1950. 123

[5] Andrianov, I. V., Bolshakov, V. I., Danishevs'kyy, V. V. and Weichert, D., *Higher order asymptotic homogenisation and wave propagation in periodic composite materials*, Proc. R. Soc. Lond. A, **464**, 1181-1201, 2008. 16

[6] Ashcroft, N. W. and Mermin, N. D., *Solid State Physics*, Saunders College, 1976. 46, 124

[7] Bao, K. D, McPhedran, R. C., Nicorovici, N. A., Poulton, C. G. and Botten, L. C., *The electromagnetic modes and homogenisation for a cubic lattice of spheres*, Physica B, **279**, 162-163, 2000. 124

[8] Batchelor, G. K., 1967, *An Introduction to Fluid Dynamics*, Cambridge University Press. 78, 136, 161

[9] Billingham, J., and King, A. C., *Wave Motion*, Cambridge University Press, 2000. 6, 11, 12

[10] Brekhovskikh, L. M., *Waves in Layered Media*, Academic Press, 1960. 117

[11] Burke, J. E. and Twersky, V., *On scattering of waves by the infinite grating of elliptic cylinders*. IEEE Trans. Antennas Propag., **14**, 465-480, 1966. 67

[12] Cai, L. W., *Evaluation of layered multiple-scattering method for antiplane shear wave scattering from gratings*, J. Acoust. Soc. Am., **120**(1), 49-61, 2006. 70

[13] Craster, R. V., Kaplunov, J. & Pichugin, A. V., *High-frequency homogenisation for periodic media*, Proc. R. Soc. Lond. A, **466**, 2341-2362, 2010. 17

[14] Crighton, D. G. and Leppington, F. G., *Singular perturbation methods in acoustics: diffraction by a plate of finite thickness*, Proc. R. Soc. Lond. A, **335**, 313-339, 1973. 23, 24

[15] Crighton, D. G., Dowling, A. P., Ffowcs Williams, J. E., Heckl, M. and Leppington, F. G., *Modern Methods in Analytical Acoustics*, Springer, 1992. 21, 68, 123

[16] Datta, S. K., *A self-consistent approach to multiple scattering by elastic ellipsoidal inclusions*, ASME J. Appl. Mech., **44**(4), 657-662, 1977. 2, 17

[17] Datta, S. K., *Diffraction of plane elastic waves by ellipsoidal inclusions*, J. Acoust. Soc. Am., **61**(6), 1432-1437, 1977. 2, 16

[18] Davis, J. L., *Wave Propagation in Solids and Fluids*, Springer-Verlag, 1988. 10

[19] Dowling, J. P., *Photonic & Sonic Band-Gap and Metamaterial Bibliography.* Available online at: http://phys.lsu.edu/∼jdowling/pbgbib.html, 2008. 1

[20] Erbaş, B. and Abrahams, I. D., *Scattering of sound waves by an infinite grating composed of rigid plates*, Wave Motion, **44**, 282-303, 2007. 67

[21] Evans, D. V. and Shipway, B. B., *A continuum model for multi-column structures in waves*, Proceedings of the 15th International Workshop on Water Waves and Floating Bodies, held in Caesarea, Israel, 27 February-1 March 2000, 47-50. 1, 144

[22] Faran, J. J. JR., *Sound scattering by solid cylinders and spheres*, J. Acoust. Soc. Am., **23**(4), 405-418, 1951. 123

[23] García-Pablos, D., Sigalas, M., Montero de Espinosa, F. R., Torres, M., Kafesaki, M. and García, N., *Theory and experiments on elastic band gaps*, Phys. Rev. Lett., **84**, 4349-4352, 2000. 1

[24] Guenneau, S. and Movchan, A. B., *Analysis of elastic band structures for oblique incidence*, Arch. Rational Mech. Anal., **171**, 129-150, 2004. 16

[25] Guenneau, S. and Movchan, A. B., *Elastic waves in arrays of elliptic inclusions*, Z. Kristallogr., **220**, 906-911, 2005. 16

[26] Guenneau, S., Poulton, C. G. and Movchan, A. B., *Oblique propagation of electromagnetic and elastic waves for an array of cylindrical fibres*, Proc. R. Soc. Lond. A, **459**, 2215-2263, 2003. 16

[27] Heathershaw, A. D., *Seabed-wave resonance and sand bar growth*, Nature, **296**, 343-345, 1982. 68

[28] Hills, N. L. and Karp, S. N., *Semi-infinite diffraction gratings–I*, Comm. Pure Appl. Maths., **18**, 203-233, 1965. 69

[29] Hills, N. L., *Semi-infinite diffraction gratings. II. Inward resonance*, Comm. Pure Appl. Maths., **18**, 389-395, 1965. 69

[30] Huang, W., Wang, Y.J. and Rokhlin, S. I., *Oblique Scattering of an elastic wave from a multilayered cylinder in a solid. Transfer matrix approach*, J. Acoust. Soc. Am., **99**(5), 2742-2754,1996. 8

[31] Ivanov, V. P., *Plane-wave diffraction by an N-layer grating*, Sov. Phys. Acoust., **17**(2), 202-207, 1971. 67

[32] Lamb, H., *Hydrodynamics*, Sixth Edition, Dover Publications, New York, 1945. 142, 172

[33] Leiko, A. G. and Mayatskii, V. I., *Diffraction of plane sound waves by an infinite grating of perfectly compliant cylinders*, Sov. Phys. Acoust., **20**(3), 256-258, 1974. 67

[34] Leiko, A. G. and Mayatskii, V. I., *Diffraction of a plane sound wave by an infinite grating of perfectly rigid elliptical cylinders*, Sov. Phys. Acoust., **20**(4), 389-390, 1975. 67

[35] Kafesaki, M. and Economou, E. N., *Multiple-scattering theory for three-dimensional periodic acoustic composites*, Physical Review B, **60**(17), 11993-12001, 1999. 1, 124

[36] Kagemoto, H., Murai, M., Saito, M., Molin, B. and Malenica, Š, *Experimental and theoretical analysis of the wave decay along a long array of vertical cylinders*, J. Fluid Mech., **456**, 113-135, 2002. 68

[37] Kalhor, H. A. and Ilyas, M., *Scattering of plane electromagnetic waves by a grating of conducting cylinders embedded in a dielectric slab over a ground plane*, IEEE Trans. Antennas Propag., **AP-30**(4), 576-579, 1982. 67

[38] Kashiwagi, M., *Hydrodynamic interactions among a great number of columns supporting a very large flexible structure*, J. Fluids and Structures, **14**, 1013-1034, 2000. 68

[39] Krynkin, A. and McIver, P., *Approximations to wave propagation through a lattice of Dirichlet scatterers*, Waves in Random and Complex Media, **19**(2), 347-365, 2009. 17

[40] Kushwaha, M. S. and Djafari-Rouhani, B., *Complete acoustic stop bands for cubic arrays of spherical liquid balloons*, J. Appl. Phys., **80**(6), 3191-3195, 1996. 124

[41] Kushwaha, M. S., Djafari-Rouhani, B., Dobrzynski, L. and Vasseur, J. O., *Sonic stop-bands for cubic arrays of rigid inclusions in air*, Eur. Phys. J. B, **3**, 155-161, 1998. 124

[42] Kushwaha, M. S. and Halevi, P., *Stop bands for cubic arrays of spherical balloons*, J. Acoust. Soc. Am., **101**(1), 619-622, 1997. 124

[43] Kuang, W. M., Hou, Z. L., Liu, Y. Y. and Li, H., *The band gaps of cubic phononic crystals with different shapes of scatterers*, J. Phys. D: Appl. Phys., **39**, 2067-2071,2006. 124

[44] Lakhtakia, A., Varadan, V. V. and Varadan, V. K., *Reflection characteristics of an elastic slab containing a periodic array of elastic cylinders: SH wave analysis*, J. Acoust. Soc. Am., **80**(1), 311-316, 1986. 69

[45] Lakhtakia, A., Varadan, V. V. and Varadan, V. K., *Reflection characteristics of an elastic slab containing a periodic array of circular elastic cylinders: P and SV wave analysis*, J. Acoust. Soc. Am., **83**(4), 1267-1275, 1988. 69

[46] Lewis, T. S. and Kraft, D. W., *Scattering of long-wavelength elastic waves by a cylindrical obstacle in a solid*, J. Appl. Phys., **47**(4), 1265-1269, 1976. 15

[47] Lewis, T. S., Kraft, D. W. and Hom, N., *Scattering of elastic waves by a cylindrical cavity in a solid*, J. Appl. Phys., **47**(5), 1795-1798, 1976. 15

[48] Li, Y. and Mei, C. C., *Bragg scattering by a line array of small cylinders in a waveguide. Part 1. Linear aspects*, J. Fluid Mech., **583**, 161-187, 2007. 68

[49] Li, Y. and Mei, C. C., *Multiple resonant scattering of water waves by a two-dimensional array of vertical cylinders: Linear aspects*, Physical Review E, **76**, 016302, 2007. 3, 4, 5, 68, 77, 102

[50] Linton, C. M., *Lattice sums for the Helmholtz equation*, SIAM Review, **52**(4), 630-674, 2010. 131, 132

[51] Linton, C. M. and Martin, P. A., *Semi-infinite arrays of isotropic point scatterers. A unified approch*, SIAM J. Appl. Math., **64**(3), 1035-1056, 2004. 69

[52] Linton, C. M., Porter, R. and Thompson, I., *Scattering by a semi-infinite periodic array and the excitation of surface waves*, SIAM J. Appl. Math., **67**(5), 1233-1258, 2007. 69

[53] Linton, C. M. and McIver, P., *Handbook of Mathematical Techniques of Wave/Structure Interactions*, Chapman&Hall/CRC, 2001. 69

[54] Liu, Z., Chan, C. T., Sheng, P, Goertzen, A. L. and Page, J. H., *Elastic wave scattering by periodic structures of spherical objects: Theory and experiment*, Physical Review B, **62**(4), 2446-2457, 2000. 1, 152

[55] Martin, P., *Multiple scattering*, Cambridge University Press, 2006. 18, 131, 135

[56] Mei, C. C., *Resonant reflection of surface waves by periodic sandbars*, J. Fluid Mech., **152**, 315-335, 1985. 68

[57] Mei, J., Liu, Z., Shi, J. and Tian, D., *Theory for elastic wave scattering by a two-dimensional periodical array of cylinders: An ideal approach for band-structure calculations*, Physical Review B, **67**, 245107, 2003. 16

[58] McIver, P., *Water-wave propagation through an infinite array of cylindrical structures*, J. Fluid Mech., **424**, 101-125, 2000. 68

[59] McIver, P., *Wave interaction with arrays of structures*, Applied Ocean Research, **24**, 121-126, 2002. 68

[60] McIver, P., *Approximations to wave propagation through doubly-periodic arrays of scatterers*, Waves in Random and Complex Media, **17**(4), 439-453, 2007. 2, 16, 74, 78, 83, 84, 144

[61] Millar, R. F., *Plane wave spectra in grating theory. III. Scattering by a semi-infinite grating of identical cylinders*, Can. J. Phys., **42**, 1149-1184, 1964. 69

[62] Miles, J. W., *On Rayleigh scattering by a grating*, Wave Motion, **4**, 285-292, 1982. 67

[63] Modinos, A., *Scattering of electromagnetic waves by a plane of spheres-Formalism*, Physica, **141A**, 575-588, 1987. 153

[64] Morse, P. M., *Vibration and Sound*, McGraw-Hill Book Company, New York, 1948, 2nd edition. 128

[65] Newman, J. N., *Marine Hydrodynamics*, Cambridge, Massachusetts: MIT Press, 1967. 89, 141, 142, 171

[66] Nicorovici, N. A. and McPhedran, R. C., *Propagation of electromagnetic waves in periodic lattices of spheres: Green's function and lattice sums*, Physical Review B, **51**(1), 690-702, 1995. 124

[67] Nicorovici, N. A. and McPhedran, R. C., *Photonic band gaps for arrays of perfectly conducting cylinders*, Physical Review E, **52**(1), 1135-1145, 1995. 16

[68] Nishimoto, M. and Ikuno, H., *Analysis of electromagnetic wave diffraction by a semi-infinite strip grating and evaluation of end-effects*, Progress in Electromagnetics Research, **23**, 39-58, 1999. 69

[69] Nishimoto, M. and Ikuno, H., *Space-wavenumber analysis of field scattered from a semi-infinite strip grating*, Electrical Engineering in Japan, **132**, 1-8, 2000. 69

[70] Pao, Y. H. and Mow, C. C., *Scattering of plane compressional waves by a spherical obstacle*, J. Appl. Phys., **34**(3), 493-499, 1963. 123

[71] Pao, Y. H. and Mow, C. C., *Diffraction of Elastic Waves and Dynamic Stress Concentrations*, Crane, Russack, New York, 1973. 20

[72] Parnell, W. J. and Abrahams, I. D., *Dynamic homogenisation in periodic fibre reinforced media. Quasi-static limi for SH waves*, Wave Motion, **43**, 474-498, 2006. 16

[73] Parnell, W. J. and Abrahams, I. D., *Homogenization for wave propagation in periodic fibre-reinforced media with complex microstructure. I–Theory*, J. Mech. Phys. Solids, **56**, 2521-2540, 2008. 16

[74] Parnell, W. J. and Grimal, Q., *The influence of mesoscale porosity on cortical bone anisotropy. Investigations via asymptotic homogenisation*, J. R. Soc. Interface, **6**, 97-109, 2009. 16

[75] Platts, S. B., Movchan, N. V., McPhedran, R. C. and Movchan, A. B., *Transmission and Polarization of elastic waves in irregular structures*, J. Eng. Mater. Technol., **125**(1), 2-6, 2003. 70

[76] Porter, R. and Evans, D. V., *Wave scattering by periodic arrays of breakwaters*, Wave Motion, **23**, 95-120, 1996. 67

[77] Poulton, C. G., Movchan, A. B., McPhedran, R. C., Nicorovici, N. A. and Antipov, Y. A., *Eigenvalue problems for doubly periodic elastic structures and phononic band gaps*, Proc. R. Soc. Lond. A, **456**, 2543-2559, 2000. 1, 4, 16, 30, 34, 35, 39, 65

[78] Psarobas, I. E. and Sigalas, M. M., *Elastic band gaps in a fcc lattice of mercury spheres in aluminum*, Physical Review B, **66**, 052302, 2002. 124

[79] Lord Rayleigh (Strutt, J. W.), *On the electromagnetic theory of light*, Philos. Mag., **12**, 81-101, 1881. 68, 70

[80] Lord Rayleigh (Strutt, J. W.), *The Theory of Sound*, Dover Publications, New York, 1945. 67, 123

[81] Robert, S., Conoir, J.-M. and Franklin, H., *Propagation of elastic waves through two-dimensional lattices of cylindrical empty or water-filled inclusions in an aluminum matrix*, Ultrasonics, **45**, 178-187, 2006. 70

[82] Scarpetta, E. and Sumbatyan, M. A., *On wave propagation in elastic solids with a doubly-periodic array of cracks*, Wave Motion, **25**, 61-72, 1997. 69

[83] Sigalas, M. and Economou, E. N., *Elastic and acoustic wave band structure*, J. Sound and Vibration, **158**(2), 377-382, 1992. 124

[84] Sigalas, M. and Economou, E. N., *Band structure of elastic waves in two dimensional systems*, Solid State Commun., **86**, 141-143, 1993. 1

[85] Stefanou, N., Karathanos, V. and Modinos, A., *Scattering of electromagnetic waves by periodic structures*, J. Phys.: Condens. Matter, **4**, 7389-7400, 1992. 153

[86] Tabaei, A. and Mei, C. C., *Viscous effects on Bragg scattering of water waves by an array of piles*, Physical Review E, **79**, 026314, 2009. 68

[87] Thompson, I. and Linton, C. M., *Guided surface waves on one- and two-dimensional arrays of spheres*, SIAM J. Appl. Math., **70**(8), 2975-2995, 2010. 153

[88] Twersky, V., *Multiple scattering of radiation by an arbitrary configuration of parallel cylinders*, J. Acoust. Soc. Am., **24**(1), 42-46, 1952. 67

[89] Twersky, V., *Multiple scattering of radiation by an arbitrary planar configuration of parallel cylinders and by two parallel cylinders*, J. Appl. Phys., **23**(4), 407-414, 1952. 67

[90] Twersky, V., *On the multiple scattering theory of the finite grating and the wood anomalies*, J. Appl. Phys. **23**(10), 1099-1118, 1952. 67

[91] Twersky, V., *On the scattering of waves by an infinite grating*, IEEE Trans. Antennas Propag., **4**, 330-345, 1956. 67

[92] Twersky, V., *Multiple scattering of sound by a periodic line of obstacles*. J. Acoust. Soc. Am., **53**(1), 96-112, 1973. 152

[93] Twersky, V., *Multiple scattering of waves by the doubly periodic planar array of obstacles*, J. Appl. Phys., **16**(3), 633-643, 1975. 152

[94] Twersky, V., *Lattice sums and scattering coefficients for the rectangular planar array*, J. Appl. Phys., **16**(3), 644-657, 1975. 152

[95] Twersky, V., *Low frequency coupling in the planar rectangular lattice*, J. Appl. Phys., **16**(3), 658-666, 1975. 152

[96] Tymis, N. and Thompson, I., *Low-frequency scattering by a semi-infinite lattice of cylinders*, Q. J. Mechanics Appl. Math. Published online on 25th March 2011. 69

[97] Wang, Y. Z., Li, F. M., Kishimoto, K., Wang, Y. S. and Huang, W. H., *Wave band gaps in three-dimensional periodic piezoelectric structures*, Mechanics Research Communication, **36**, 461-468, 2009. 124

[98] Wang, Y. Z., Li, F. M., Kishimoto, K., Wang, Y. S. and Huang, W. H., *Band gaps of elastic waves in three-dimensional piezoelectric phononic crystals with initial stress*, European Journal of Mechanics A/Solids, **29**, 182-189, 2010. 124

[99] Wang, X., Zhang, X.-G., Yu, Q. and Harmon, B. N., *Multiple-scattering theory for electromagnetic waves*, Physical Review B, **47**(8), 4161-4167, 1993. 153

[100] Waterman, P. C., *Scattering by dielectric obstacles*, Alta Freq., **38**(Special), 348-352, 1969. 69

[101] White, R.M., *Elastic wave scattering at a cylindrical discontinuity in a Solid*, J. Acoust. Soc. Am., **30**(8), 771-785, 1958. 15

[102] Van Dyke, M., *Perturbation Methods in Fluid Mechanics*, Academic Press, 1964. 2, 75, 156

[103] Vasseur, J. O., Djafari-Rouhani, B., Dobrzynski, L., Kushwaha, M. S. and Halevi, P., *Complete acoustic band gaps in periodic reinforced composite materials: the carbon/epoxy composite and some metallic systems*, J. Phys.: Condens. Matter, **6**, 8759-8770, 1994. 16

[104] Ying, C. F. and Truell, R., *Scattering of a plane longitudinal wave by a spherical obstacle in a isotropically elastic solid*, J. Appl. Phys., **27**(9), 1086-1097, 1956. 123

[105] Zalipaev, V. V., Movchan, A. B., Poulton, C. G. and McPhedran, R. C., *Elastic waves and homogenisation in oblique periodic structures*, Proc. R. Soc. Lond. A, **458**, 1887-1912, 2002. 1, 4, 16, 30, 35, 39, 40, 65